COMBINED ABSORPTION POWER AND REFRIGERATION SYSTEMS DRIVEN BY LOW AND MID-GRADE HEAT SOURCES.

Dereje Sendeku Ayou

Dipòsit Legal: T 993-2015

Dereje Sendeku Ayou

COMBINED ABSORPTION POWER AND REFRIGERATION SYSTEMS DRIVEN BY LOW AND MID-GRADE HEAT SOURCES

DOCTORAL THESIS

Supervised by

Prof. Dr. Alberto Coronas

Dr. Joan Carles Bruno

Department of Mechanical Engineering

UNIVERSITAT ROVIRA I VIRGILI

Tarragona, November 2014

UNIVERSITAT
ROVIRA I VIRGILI
DEPARTAMENT D'ENGINYERIA MECÀNICA
Escola Tècnica Superior d'Enginyeria Química (ETSEQ).
Avgda Paisos Catalans, 26 ; 43007 Tarragona (Spain)

WE STATE that the present study, entitled "Combined Absorption Power and Refrigeration Systems driven by Low and Mid-Grade Heat Sources", presented by Dereje Sendeku Ayou for the award of the degree of Doctor, has been carried out under our supervision at the Department of Mechanical Engineering of this university, and that it fulfils all the requirements to be eligible for the International Doctorate Award.

Tarragona, October 13, 2014

Doctoral Thesis Supervisors

Dr. Alberto Coronas

Dr. Joan Carles Bruno

This thesis is dedicated to my beloved mother, "W/ro Abeba Abebe".

Acknowledgements

I wish to express my deepest gratitude to my supervisor Prof. Dr. Alberto Coronas, for giving me the opportunity to join the CREVER research group, the world of absorption refrigeration systems. I am very much thankful for his guidance. Surely, I would like to extend my sincere appreciation to my co-supervisor Dr. Joan Carles Bruno, who helped me so much throughout the doctoral program.

I would like to sincerely express my deepest appreciation and profound gratitude to Prof. Dr. R. Saravanan for his support and kindness. I had a great time sharing ideas with him.

Many thanks to Prof. Dr. D. Yogi Goswami and Prof. Dr. Elias Etefanakos for their help, discussions and valuable comments during my research stay in their group CERC-Clean Energy Research Center at the University of South Florida. I also acknowledge all the members of CERC group.

I gratefully acknowledge the financial support received from AGAUR (Catalan Government) for the pre-doctoral fellowship (FI-DGR 2011) and the Universitat Rovira i Virgili for funding my research stay in the United States. The financial support of the NARILAR Project (Grant Number 269321) for my research visit at the Indian Institute of Technology Madras-IITM, Chennai (India) is also acknowledged.

I would like also to thank Dr. Jesús López Villada, Dr. Daniel Salavera and Dr. Iván Andrés Montero who contributed in many ways to realize this thesis. Thank you all my Ethiopian friends in Tarragona for all the good times we had together. I would also like to thank all the current and previous members of CREVER group for their support and friendship.

Finally, my special heartfelt thanks goes to my beloved mother, brothers and sisters for their unconditional love and support.

Abstract

Energy-efficient and renewable energy technologies are two major technical frontiers to address the current global energy-related challenges which include energy supply uncertainty, rising price of fuels and adverse environmental impact. Air-conditioning, refrigeration and electricity are useful forms of energy products, usually produced using separate energy conversion technologies. Most end-users need at least dual energy products: typical example could be building's applications where space air-conditioning and electricity for various purposes are in need. The combined production of electricity (decentralized) and cold using efficient thermally-driven energy conversion systems are one of the suitable technological solution to address the current global energy-related challenges.

It is the focus of this PhD thesis through the use of new class of absorption cycles and systems for efficient conversion of low and mid-grade thermal energy sources into useful energy products: mechanical (or electrical) energy, air-conditioning, refrigeration and cold-storage. To achieve this aim, first combined absorption cycles proposed in the literature for the co-production of power and cold were reviewed. The concept of combined absorption cycles were explained in terms of idealized energy conversion systems to describe it within the larger context of all the thermodynamic possibilities. The dual-output nature of these cycles makes it difficult to evaluate their performance so that various performance criteria used in the literature were presented and discussed. Ammonia/water mixture is the most commonly used working fluid in these types of systems. Accordingly, its property database sources were reviewed and its influence on cycle performance analysis was evaluated. Other ammonia based mixtures (ammonia/$LiNO_3$ and ammonia/NaSCN) are used in these types of systems in order to avoid the rectification process in ammonia/water based systems. Information on their thermophysical properties of these mixtures are limited and the available sources were reviewed.

In this thesis, several new combined absorption cycle configurations were proposed for the simultaneous and/or alternative production of mechanical power and cold by using low and mid-grade heat sources (< 300 °C). These new classes of absorption cycle architectures were designed by modifying ammonia/water absorption refrigeration cycles. Their performances were analysed and discussed from the energetic and exergetic viewpoints. Further, the cycles were modified to improve their performance and to extend their operational working range through the introduction of pressure devices and other working fluid mixtures. The pressure devices include mechanical compressor and vapour ejector.

Since the work developing expansion device is the most crucial component in such types of combined absorption cycles, a semi-empirical model for a scroll expander (Sanden TRSA05) using ammonia (and ammonia/water mixture with high concentration of ammonia) as working fluid was developed. The adjustable parameters of the model were acquired using experimental data obtained in a test bench and was validated with the experimental data. This model is able to estimate the main outputs with good accuracy. It was scaled-up to estimate the performance of other scroll expanders (Sanden TRSA09 and TRSA12), with higher swept volume, in the same family series. This semi-empirical model was integrated into a combined absorption cycle global model for the purpose of representing the performance of the work developing device in the cycle.

Finally, a Solar Absorption Power and Cooling System (SAPCS) was developed using TRNSYS software as simulation tool. It is used to demonstrate a representative case for the integration of combined absorption cycles with solar thermal plant. Therefore, two combined absorption cycle configurations (Goswami cycle and basic single-stage combined absorption cycle using ammonia/water, ammonia/$LiNO_3$ and ammonia/NaSCN working fluid mixtures) were integrated with three solar thermal collectors (ETC, LFC, PTC) based solar thermal plants. First, a new component in TRNSYS was created for the combined absorption cycles by using the correlations obtained from the data generated using the thermodynamic model of the combined absorption cycles. A complete analysis of the proposed SAPCS was performed for a specific case located in Sevilla (Spain).

Keywords: *Combined absorption cycle, Mechanical power, Modelling, Refrigeration and Scroll expander.*

Contributions by the Author

Articles in Peer-Reviewed Scientific Journals

- **D.S. Ayou**, J.C. Bruno and A. Coronas. Steady-state operational degrees of freedom in absorption chillers and heat pumps: Methodology and case study. *International Journal of Refrigeration, 35(6): 1570-1582, 2012.*

- **D.S. Ayou**, J.C. Bruno, R. Saravanan and A. Coronas. An overview of combined absorption power and cooling cycles. *Renewable and Sustainable Energy Reviews, 21(May): 728-748, 2013.*

- **D.S. Ayou**, R. Saravanan, J.C. Bruno and A. Coronas. Analysis and simulation of modified ammonia/water absorption cycle for power and cooling applications. *International Journal of Low-Carbon Technologies, 8(suppl 1): i19-i26, 2013.*

- **D.S. Ayou**, J.C. Bruno and A. Coronas. New Power and Cooling Absorption Cycles. *International Journal of Thermal and Environmental Engineering, Volume 5(2): 135-143, 2013.*

- J. López-Villada, **D.S. Ayou**, J.C. Bruno and A. Coronas. Modelling, simulation and analysis of solar absorption power-cooling systems. *International Journal of Refrigeration, 39(March): 125-136, 2014.*

- L.C. Mendoza, **D.S. Ayou**, J. Navarro-Esbrí, J.C. Bruno and A. Coronas. Small capacity absorption systems for cooling and power with a scroll expander and ammonia based working fluids. *Applied Thermal Engineering, 72(2): 258-265, 2014.*

- **D.S. Ayou**, J.C. Bruno and A. Coronas. Combined Absorption Power and Refrigeration Cycles using Low- and Mid-Grade Heat Sources. *American Society of Heating,*

Refrigerating and Air-Conditioning Engineers (ASHRAE) Journal. Reference no. RSCH-00136-2014 to the HVAC&R Research ***(under review)***.

- **D.S. Ayou**, J.C. Bruno and A. Coronas. A single-stage combined absorption power and refrigeration cycle with an integrated compression booster: Part-I (Mechanical Compression). *Energy Journal* ***(manuscript in preparation)***.

- **D.S. Ayou**, R. Saravanan, J.C. Bruno and A. Coronas. A single-stage combined absorption power and refrigeration cycle with an integrated compression booster: Part-II (Vapour Ejector). *Energy Journal* ***(manuscript in preparation)***.

Papers in Congresses, Conferences, Seminars and Workshops

- **D.S. Ayou**, R. Saravanan, J.C. Bruno and A. Coronas. Analysis and simulation of modified ammonia-water absorption cycle for power and cooling applications. *6^{th} Heat Powered Cycles Conference, Alkmaar, Netherlands, 10-12 September, 2012. (Oral presentation)*

- **D.S. Ayou**, J.C. Bruno, D. Salavera, R. Saravanan and A. Coronas. New working fluids for a combined power and cooling cycle. *6^{th} Heat Powered Cycles Conference, Alkmaar, Netherlands, 10-12 September, 2012. (Oral presentation)*

- **D.S. Ayou**, F. Asfand, J.C. Bruno and A. Coronas. A hybrid single-stage absorption refrigeration cycle with new working mixtures for refrigeration and power generation. *4^{th} Jordanian IIR International Conference on Refrigeration and Air Conditioning, Amman, Jordan, 10-12 September, 2012. (Oral presentation)*

- J. López-Villada, I.A. Montero, L.C. Mendoza, **D.S. Ayou**, J.C. Bruno and A. Coronas. Modelling, simulation and analysis of solar absorption power-cooling systems. *Eurosun International Conference on Solar Heating, Cooling and Buildings, Rijeka, Croatia, 18-20 September, 2012. (Poster presentation)*

- **D.S. Ayou**, L.C. Mendoza, J.C. Bruno and A. Coronas. Solar power/refrigeration absorption systems. *The Second International Conference on Energy and Sustainable Development, Adrar, Algeria, 19-20 February, 2013. (Oral presentation)*

- **D.S. Ayou**, J.C. Bruno and A. Coronas. Single-stage absorption cooling and power cycle with an integrated compression booster. *International Workshop on New Working Fluids for Absorption Heat Pumps and Refrigeration Systems (EUROTHERM Seminar No 100), Tarragona, Spain, 22-23 July, 2013. (Oral presentation)*

- F. Asfand, **D.S. Ayou**, J.C. Bruno and A. Coronas. Effect of ammonia-water mixture property methods on absorption cycle calculations using Aspen Plus. *International Workshop on New Working Fluids for Absorption Heat Pumps and Refrigeration Systems (EUROTHERM Seminar No 100), Tarragona, Spain, 22-23 July, 2013. (Poster presentation)*

- L.C. Mendoza, **D.S. Ayou**, J.C. Bruno and A. Coronas. Small capacity absorption systems for cooling and power with a scroll expander and ammonia based working fluids. *International Symposium on Innovative Materials for Processes in Energy Systems-IMPRES2013, Fukuoka, Japan, 4-6 September, 2013. (Oral presentation)*

- L.C. Mendoza, **D.S. Ayou**, J.C. Bruno, J. Navarro-Esbrí and A. Coronas. Scroll expander configurations for small capacity absorption power and cooling cycles. ASME-*2nd International Seminar on ORC Power System, Rotterdam, Netherlands, 7-8 October, 2013. (Oral presentation)*

- **D.S. Ayou**, J.C. Bruno, D.Y. Goswami and A. Coronas. Integration of scroll-expanders into combined absorption cycles for power and refrigeration applications. *In proceedings of the International Sorption Heat Pump Conference ISHPC 2014, Maryland, USA, March 31 - April 2, 2014. (Oral presentation)*

- **D.S. Ayou**, J.C. Bruno and A. Coronas. Combined absorption power and refrigeration cycles using low- and mid-grade heat sources. *In proceedings of the International Sorption Heat Pump Conference ISHPC 2014, Maryland, USA, March 31 - April 2, 2014. (Oral presentation)*

- **D.S. Ayou**, J.C. Bruno and A. Coronas. Configurations, performance and working fluids for new absorption power and cooling cycles. *VII Congreso Ibérico y V Congreso Iberoamericano de Ciencias y Técnicas del Frío (CYTEF-2014), Tarragona, Spain, 18-19 June, 2014. (Oral presentation)*

Other Contributions

Article in Peer-Reviewed Scientific Journal

- **D.S. Ayou**, M.R. Currás, D. Salavera, J. García, J.C. Bruno and A. Coronas. Performance analysis of absorption heat transformer cycles using ionic liquids based on imidazolium cation as absorbents with 2,2,2-trifluoroethanol as refrigerant. *Energy Conversion and Management, 84(August): 512-523, 2014.*

Papers in Congresses, Conferences, Seminars and Workshops

- D. Martínez-Maradiaga, **D.S. Ayou**, J.C. Bruno and A. Coronas. Integrated approach for the treatment of steady-state operational data of absorption chillers and heat pumps. *International Sorption Heat Pump Conference (ISHPC11), Padua, Italy, 28-29 April, 2011. (Oral presentation)*

- **D.S. Ayou**, J.C. Bruno and A. Coronas. Systematic selection of operational variables for the modelling and optimization of absorption chillers and heat pumps. *Third International Conference on Applied Energy, Perugia, Italy, 16-18 May, 2011. (Oral presentation)*

- **D.S. Ayou**, D. Salavera, T. Altamash, J. García and A. Coronas. Analysis of a Single-effect absorption refrigeration cycle with 2,2,2-trifluoroethanol (TFE) + 1-butyle-3-methylimidazolium tetrafluoroborate ([bmim][BF4]). *ILSEPT 2011: 1st International Conference on Ionic Liquids in Separation and Purification Technology, Sitges, Spain, 4-7 September, 2011. (Poster presentation)*

- D. Martínez-Maradiaga, **D.S. Ayou**, J. Ortiga, J.C. Bruno and A. Coronas. A new methodology for operational data treatment, monitoring and performance analysis of absorption chillers. *4th International Conference Solar Air-Conditioning, Larnaca, Cyprus, 12-14 October, 2011. (Poster presentation)*

- **D.S. Ayou**, D. Salavera, M.R. Currás, J. García, J.C. Bruno and A. Coronas. Performance analysis of a single-effect absorption cooling cycle with 2,2,2-trifluoroethanal + 1-ethyl-3-methylimidazolium tetrafluoroborate system. *In Proceedings of the Inter-*

national Workshop on Ionic Liquids-Seeds for New Engineering Application, Lisbon, Portugal, 2-3 February, 2012. (Oral presentation)

- **D.S. Ayou**, M.R Currás, D. Salavera, J. García, J.C. Bruno and A. Coronas. Performance analysis of absorption heat transformers using ionic liquids with 2,2,2-trifluoroethanal as working fluid pairs. *In Proceedings of the International Workshop on Ionic Liquids-Seeds for New Engineering Application, Lisbon, Portugal, 2-3 February, 2012. (Poster presentation)*

- S.K. Swarnkar, G. Venkatarathnam, **D.S. Ayou**, J.C. Bruno and A. Coronas. A review on absorption heat pumps and chillers using ionic liquids as absorbent. *In Proceedings of the International Workshop on Ionic Liquids-Seeds for New Engineering Application, Lisbon, Portugal, 2-3 February, 2012. (Oral presentation)*

- D. Martínez-Maradiaga, **D.S. Ayou**, J. Ortiga, J.C. Bruno and A. Coronas. Reconciliación de datos y detección de errores sistemáticos en sistemas de refrigeración por absorción. *VI Congreso Ibérico y IV Congreso Iberoamericano de Ciencias y Técnicas del Frío (CYTEF-2012), Madrid, Spain, 22-24 February, 2012. (Oral presentation)*

- **D.S. Ayou**, J.C. Bruno and A. Coronas. Absorption heat pumps working with ionic liquids. *5^{th} Congress on Ionic Liquids, Algarve, Portugal, 21-25 April, 2013. (Oral presentation)*

- **D.S. Ayou**, J.C. Bruno and A. Coronas. Present status of the research in absorption technology using ionic liquids. *2^{nd} International Workshop on "Ionic Liquids: Alternative Benign Materials for Renewable Energy and its Applications", Pune, India, 16-17 January, 2013. (Oral presentation)*

Participation in Projects

- SOLEF - Absorption Systems for Simultaneous Refrigeration & Power driven by Thermal Solar Energy or Waste Heat. Spanish Ministry of Science and Innovation. Reference: ENE2009-14177. Duration: 2010-2012. Principal Investigator: Alberto Coronas.

- AHP2 - Development of New Working Fluids, Components and Configurations for High Performance Absorption Heat Pumps. Reference: DPI2012-38841-C02-01. Duration: 3 years, Start Date: 01/01/2013. Principal Investigator: Alberto Coronas.

- NARILAR - New working fluids based on natural refrigerants and ionic liquids for absorption refrigeration. Project (Pirses-GA-2010FP7) of the People-2010-IRSES Program - Marie Curie Action. Duration: 01/04/2011 to 31/03/2015. Principal Investigator in CREVER: Alberto Coronas.

Contents

Contents

List of Figures

List of Tables

Nomenclature

ABS : Absorber

APC : Absorption power cycle

ARC : Absorption refrigeration cycle

CAC : Combined absorption cycle

CAS : Combined absorption system

CON : Condenser

COP : Coefficient of performance [-]

DES : Desorber

EVA : Evaporator

Ex : Exergy

EXP : Expander

f : Thermodynamic quality weight factor [-]

GAX : Generator absorber heat exchanger

HX : Heat exchanger

MIX : Mass flow stream mixer

REC : Rectifier

REV : Refrigerant expansion Valve

RSC : Refrigerant sub-cooler

SAPCS : Solar absorption power-cooling system

SEV : Solution expension valve

SF : Solar fraction

SH : Superheater

SHX : Solution heat exchanger

SP : Solution pump

SPL : Mass flow stream splitter

SR : Split ratio

SSAPRC-2D : Single-stage combined absorption power and refrigeration cycle with two desorber

SSAPRC-COM : Single-stage combined absorption power and refrigeration cycle with mechanical compression

SSAPRC-EJE : Single-stage combined absorption power and refrigeration cycle with vapour ejector

SSAPRC-P : Single-stage combined absorption power and refrigeration cycle with parallel flow arrangement

SSAPRC-S : Single-stage combined absorption power and refrigeration cycle with series flow arrangement

TSAPRC-S : Two-stage combined absorption power and refrigeration cycle with series flow arrangement

Chapter 1

Introduction and Thesis Objectives

Energy-efficient and renewable energy technologies are two major technical frontiers to address the current global energy challenges. These challenges include energy supply uncertainty, rising price of fuels and adverse environmental impact. Further, fossil fuels have major share on the global energy supply mix: it is more than 80% of global energy consumption [1]. Forecasts of global energy consumption based on the current government policies and technological developments indicate a highly probable continuation of this fossil fuel dependency (see Fig. 1.1). This energy supply trend is not in favour to meet the obligations for climate change protection and sustainable energy supply acts set by national and international bodies.

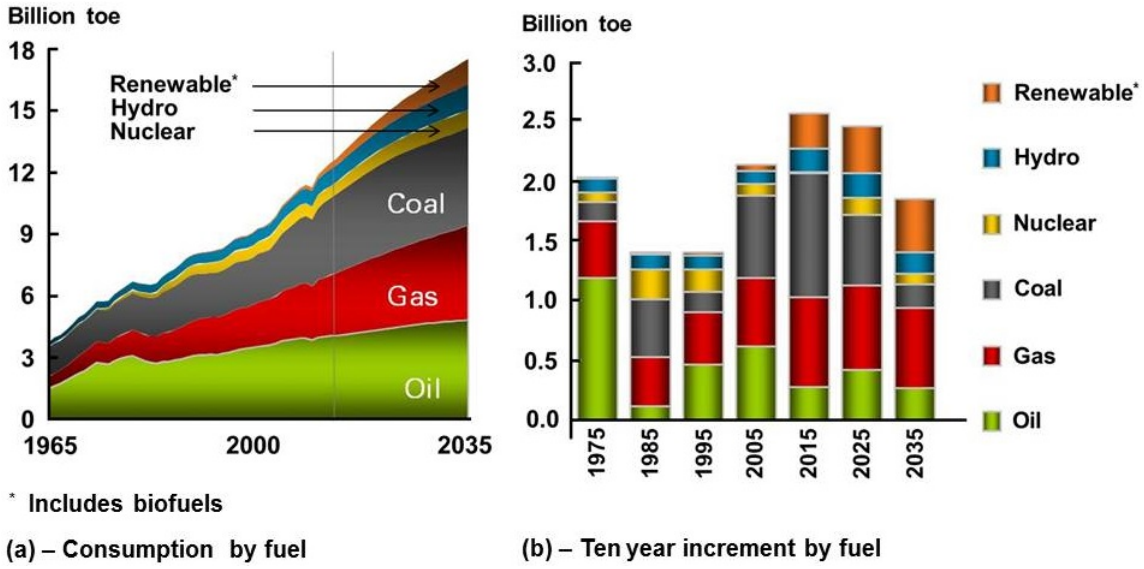

Figure 1.1: Global primary energy consumption trends [2].

Air-conditioning, refrigeration and electricity are useful forms of energy products, usually produced using separate energy conversion technologies. Most end-users need at least dual energy products: a typical example could be building applications where space air-conditioning and electricity (for various purposes) are needed. In many countries, air-conditioning systems are one of the dominating energy consumers. And, these energy consumptions are increasing due to enhanced indoor air comfort requirements, architectural tendency and global climate change.

In air-conditioning sector the dominant technology is electrically driven compression chillers. In most regions, their operation causes high peak loads during the summer. The driving electrical power is mainly obtained from central electric utilities (in MW scale). Furthermore, according to the world bank report in 2010 over 20% of the world's population lacks access to electricity [3] and providing electricity to these peoples is a difficult and enduring challenge for today's generation. In regions with dispersed communities, far from the main grid or no electricity provider at all (e.g. in some areas of developing countries), supplying electricity using centralized electric grid infrastructure is a costly option. Communities in these areas may depend on distributed mini-power generating systems like petroleum-based generators or renewable sources (such as solar, wind, biomass, geothermal and mini hydro-power) technologies if they are available and cost effective.

The combined production of electricity (decentralized) and cold using efficient thermally-driven energy conversion systems could be one of a suitable technological solution to address the aforementioned energy related challenges. It is the focus of this study through the use of new thermodynamic concepts and systems for efficient conversion of low and mid-grade thermal energy sources into useful energy products: electricity, air-conditioning, refrigeration and cold-storage.

The first aim of this chapter is to give an overview on the different thermal energy sources. The second aim is to give a review on the state-of-the-art of the different technologies that can deliver electrical (or mechanical) energy and cold separately by using low and mid-grade heat sources. The current options for the co/tri-generation of cooling, heating and power may also quickly be viewed from technical and performance perspectives. Finally, general and specific objectives of the thesis are described with a brief introduction to the topics discussed in the following chapters.

1.1 Thermal Energy Sources

Solar thermal, geothermal, biomass and waste heat from various thermal processes are abundantly available energy resources. These sensible thermal resources through the use of efficient technologies have promising potential for conversion to highly valuable energy products. Consequently, the burning of fossil fuels and the emission of greenhouse gases can be reduced significantly. They can also be used to meet the power needs of remote areas, where centralized power supply is not available or too expensive to deliver it.

1.1.1 Solar thermal energy

The earth upper atmosphere receives a tremendous amount of radiation energy from the sun: it is about 174 PW (1 PW = 10^{12} kW) [4].

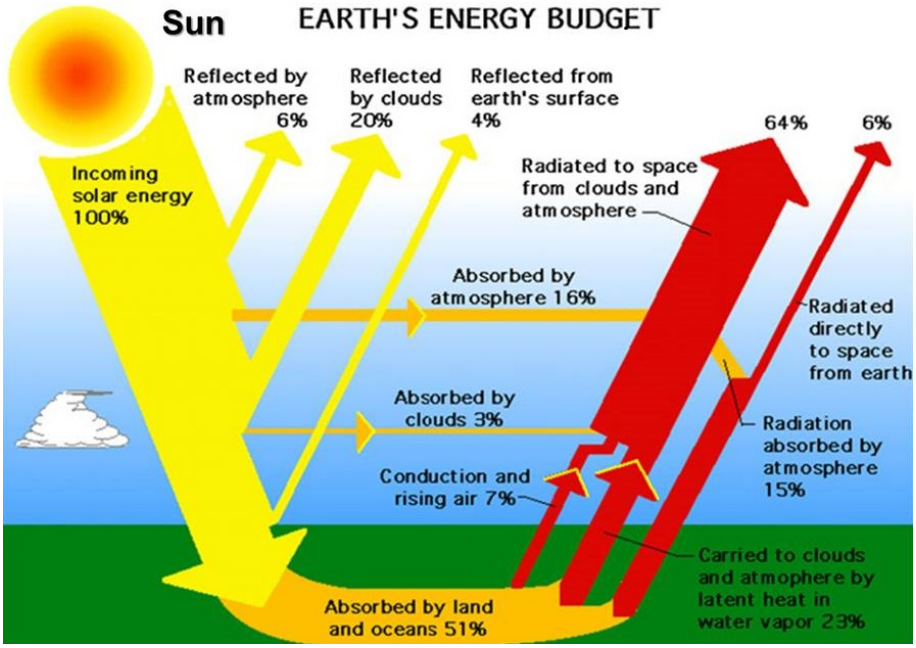

Figure 1.2: Breakdown of incoming solar radiation energy [4].

When it arrives the earth's surface around 45% of the energy is absorbed and reflected by the atmosphere and clouds as shown in Fig. 1.2. However, the total amount of solar energy available on the earth surface is still an enormous amount, for instance it is estimated that the amount of solar energy that falls on the earth's surface in 40 minutes equals the total annual energy consumption of all mankind. Fig. 1.3 shows the potential of solar energy at a global scale [5]. Solar energy needs to be collected and stored efficiently because

of its low density and intermittent nature. Thus, solar thermal collectors and thermal storage systems are the main components of a solar thermal system. Simply, solar thermal collectors are special kind of heat exchangers that converts solar radiation energy into heat and then transport it by using heat transfer fluids (e.g. air, water/steam and thermal oil) [6]. Thermal energy storage systems are coupled with solar thermal collectors, especially in concentrating solar thermal power plants, in order to store thermal energy that can be used later to drive the power plant's heat engine.

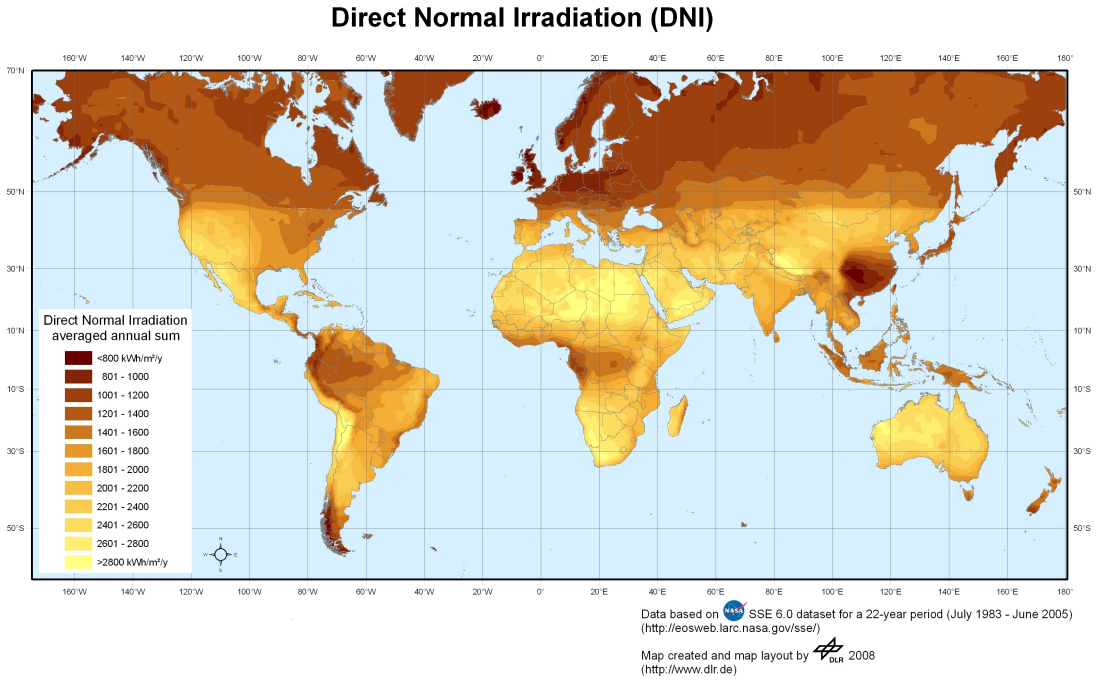

Figure 1.3: Global annual direct normal irradiation in kWh/m^2/year [5].

Two types of solar thermal collectors are available in the market: stationary/non-concentrating and concentrating. A stationary collector has the same area for intercepting and absorbing solar radiation [6]. Sun-tracking concentrating solar collectors usually have reflective or refractive mirrors/lens to intercept and focus the sun's beam of radiation to a smaller receiving area, thereby increasing the radiation flux.

A comprehensive list of solar thermal collectors available in the market are shown in Table 1.1. Except the two-axes tracking solar thermal collectors-namely parabolic dish and heliostat field collectors, all the other collectors produce heat in the range of temperatures between 40 °C and 400 °C.

Table 1.1: Different type of solar thermal collectors ([6]-[8]).

Collector type (motion)	Absorber type	Concentration ratio	Temperature range [°C]
Flat plate collector (Stationary)	Flat	1	40–80
Evacuated tube collector (Stationary)	Flat	1	70–120
Compound parabolic collector	Tubular		
(Stationary)		1–10	60–200
(Single-axis tracking)		10–15	60–300
Linear Fresnel reflector (Single-axis tracking)	Tubular	10–40	50–300
Parabolic trough collector (Single-axis tracking)	Tubular	15–45	50–400
Cylindrical trough collector (Single-axis tracking)	Tubular	10–50	60–300
Parabolic dish collector (Two-axes tracking)	Point	100–1000	150–1500
Heliostat field collector (Two-axes tracking)	Point	150–1500	300–2000

1.1.1.1 Stationary collectors

This group of collectors do not use any mechanisms to track the sun and are fixed to their position. They can produce thermal energy at temperatures up to 200 °C. Flat Plate Collectors (FPCs), Evacuated Tube Collectors (ETCs) and Compound Parabolic Collectors (CPCs) with concentration ratio between 1 and 10 are belonging to this group of solar thermal collectors.

In the non-concentrating type of collectors, the collector area (i.e. the area that intercepts the solar radiation) is the same as the absorber area. It is a part of the collector that absorbs the radiation and converts it into heat. There are many possible flat-plate type collector designs, but, in general all consist of: a flat plate absorber which intercepts and absorbs the solar radiation; a transparent cover(s) to allow solar radiation but reduces heat loss from the absorber; a heat transfer fluid to collect heat from the absorber; and a heat insulated

back cover. FPCs are generally designed to prevent heat losses to the surrounding. It is the simplest and cheapest collector technology for conversion of solar energy into heat. ETCs have less heat loss and perform better at relatively high temperatures. They are typically made in a glass tube design, i.e. a metallic absorber inserted in an evacuated glass tube. Fig. 1.4 shows the schematic diagrams of stationary solar thermal collectors: FPC and ETC.

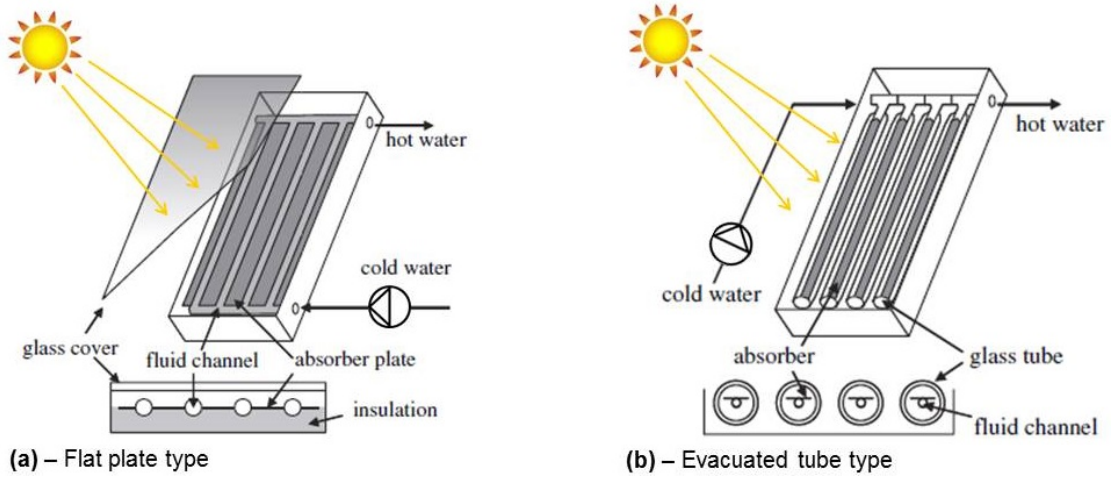

Figure 1.4: Schematic diagram of stationary solar thermal collectors (adapted from [9]).

1.1.1.2 Concentrating collectors

Basically, there are five types of solar thermal collector technologies falling in this category which includes: the one-axis tracking Parabolic Trough Collector (PTC), Linear Fresnel Reflector (LFR) and Cylindrical Trough Collector (CTC); and the two-axes tracking Parabolic Dish Collector (PDC) and Heliostat Field Collector (HFC) technologies.

Parabolic trough solar collectors are the most advanced and matured technology compared with the other concentrating technologies. It is mainly due to considerable know-how regarding the technology and quite large number of small commercial industries have been available to manufacture and market these collectors. Spain and the United States are the two leading countries in installing concentrating solar thermal power technologies. And, most of these installations (about 71%) are based on PTC technology [4].

A typical parabolic trough solar thermal collector and its operation is shown in Fig. 1.5. A PTC consists of a set of parabolic mirrors made of reflective material, a long tubular black receiver which is covered by a glass tube to reduce the heat losses. PTCs are able

to concentrate the solar radiation flux 30 to 80 times, heating the heat transfer fluid up to 400 °C [6]. When it is used for electrical power production, the heat transfer fluid circulate through the PTC solar field and power block, where the fluid's heat is used to drive the heat engine coupled with an electric generator. One of the world largest and oldest electric power plant, in Mojave Desert California, is based on this PTC technology: part of the collector field at Kramer Junction is shown in Fig. 1.6.

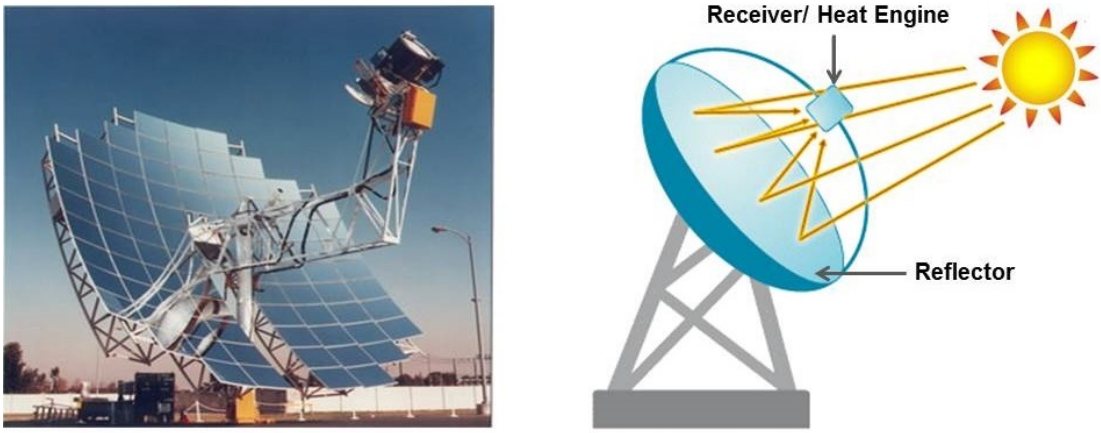

Figure 1.5: Parabolic trough solar collector technology.

Figure 1.6: Photo of PTC field at Kramer Junction in Mojave Desert (California, the United States).

The Linear Fresnel Reflector (LFR) technology uses modular flat reflectors (mirrors) to focus the sun rays onto a long elevated thermal receiver which is mounted on a linear tower. The receiver consists of a tube through which a heat transfer fluid, usually water, flows and collect the heat produced by the concentrated sun rays on the receiver in a form of saturated steam or superheated steam. Then, it can be used either for electric power production, industrial process heat or solar thermal cooling applications. Puerto Errado 2 Thermosolar Power Plant (shown in Fig. 1.7) located in Murcia, Spain, is the world's largest commercial solar thermal power plant (peak power output of 30 MWel) based on LFR technology. It produces 50 million kWh of clean electricity per year which is equivalent to providing electricity to around 12,000 Spanish households [10]. The operating temperature of the collector field is around 270 °C.

A Parabolic Dish Collector (PDC) is a point-focus collector mounted on a two-axes tracking mechanism to follow the sun more accurately. A PDC is made of a parabolic-shaped dish concentrator that reflects solar radiation onto a receiver mounted at the focal point (see Fig. 1.8 (b)). The receiver is a set of absorber tube bundle to collect and transfer the heat to the heat-engine, power block, usually attached to the receiver, absorber, or in some cases to a central heat-engine. When the receiver and heat-engine are integrated together, the same fluid usually hydrogen or helium are used as heat transferring fluid as well as working fluid for the heat-engine cycle. The temperature of the heat transfer fluid can reach above 1500 °C. The Stirling and Brayton cycle engines are the most common type of heat-engine cycles applied in parabolic dish power generating systems.

Individual dishes are limited to a few amount of power output (usually between 10 kWel and 50 kWel) mainly due to aerodynamic constraints like wind forces: it can deform the surface of the concentrator. Such type of collector technology is successfully demonstrated in several projects; a typical example could be the US department of energy Solar Total Energy Project (STEP) in Shenandoah, Georgia between 1982 and 1989. It was the world's first and largest solar thermal cogeneration project having an industrial application: it used solar energy to provide electricity and process heat to a nearby knitwear factory as well as low-pressure steam to run the air-conditioning system of the factory.

Figure 1.7: LFR collector field at Puerto Errado 2 Thermosolar power plant in Calasparra (Murcia, Spain) [10].

The Heliostat Field Collector (HFC), often called central receiver collector system, is a technology that consists of a number of nearly-flat mirrors called heliostats that collect and concentrate solar radiation onto a central receiver mounted on a tower (Fig. 1.9). It absorbs the concentrated sunlight and transfers its energy to a heat transfer fluid. The heat transfer system of HFC based power plant comprises pipes, pumps and valves which directs the transfer fluid in a closed loop between the receiver, thermal storage and power block sub-systems.

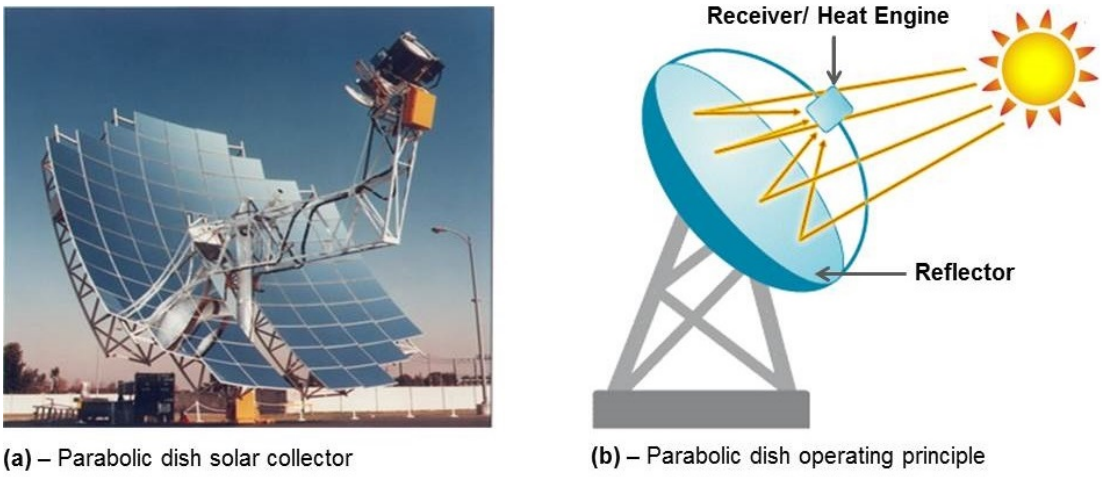

Figure 1.8: Parabolic dish solar collector system.

The HFCs have several advantages including high collecting and conversion, into electricity, efficiencies. It can be integrated with fossil fuels based existing power plants. They can store thermal energy conveniently. Therefore, HFCs are more suitable for utility scale power plants (more than 10 MWel). The largest HFC technology based power plant in

the world is in Mojave Desert (southern California, the United States) shown in Fig. 1.10 and it is in operation since 2013 [11]. The plant has a capacity to generate 392 MW of clean electricity which is enough to provide electricity for 94,000 average US homes. The potential and possible applications of geothermal energy, biomass energy and waste heat sources from various thermal processes are briefly described in the next subsections.

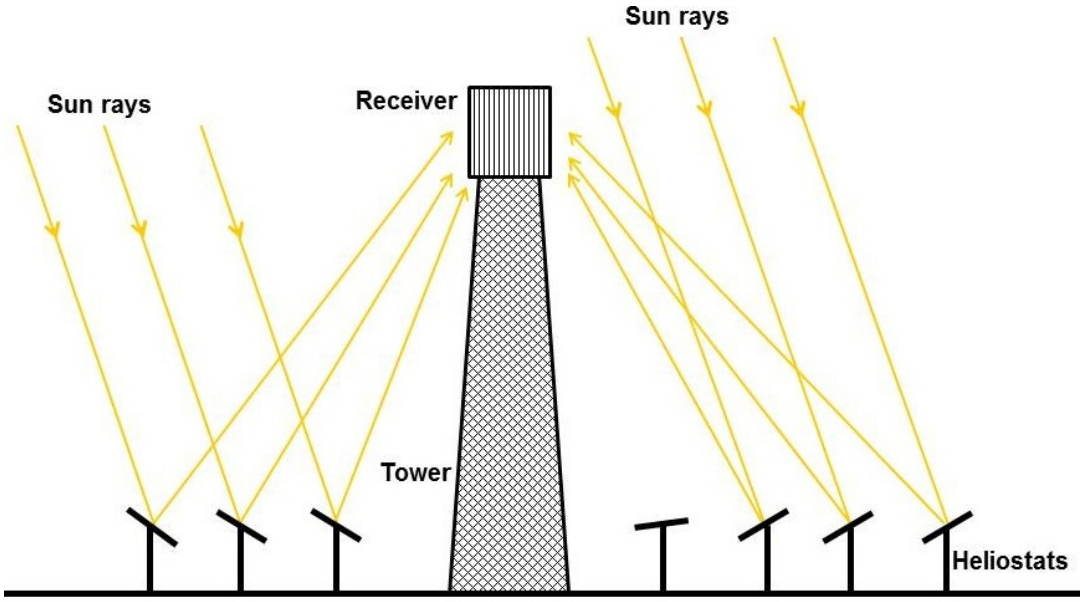

Figure 1.9: Schematic diagram of Heliostat Field Collector system.

1.1.2 Geothermal energy

Geothermal energy is a clean and sustainable thermal energy source from the earth. Unlike other renewable energy sources (e.g. solar and wind), it does not show intermittent nature. And, geothermal energy is utilized in several applications such as district space heating and cooling for commercial and residential buildings, electricity production and several industrial process applications including drying, process heating, chemical extraction, etc.

Four types of geothermal power plants are available in the world for electricity production: dry steam, flash, binary and flash/binary combined power plants. In dry steam power plants, a steam produced by the well of geothermal reservoir is used directly to drive a steam turbine coupled with electric generator. In the case of flash power plants, hot water at pressure (heated using geothermal resources) is flashed in a vessel and separated into steam and hot water (called “brine”).

Figure 1.10: Photo of Ivanpah solar power facility using central collector system ([11]).

The steam is then used to drive the turbine for electrical power production whereas the liquid brine is injected back into the geothermal reservoir. For effective utilization of geothermal resources below 150 °C, power plants based on organic Rankine cycle technologies are often used and it is called Binary Power Plant. In these plants, geothermal brine heats the organic fluid in the power block through a heat exchanger to generate the vapour that drives the turbine for electrical power production. After being used, the geothermal brine is injected back into the reservoir.

Other type of commercially available technology is the flash/binary combined cycle. It uses a combination of both flash and binary plants in order to take the advantages of both technologies. In this type of plant, the portion of the geothermal water which "flashes" to steam under reduced pressure is first converted to electricity with a back pressure steam turbine and the low-pressure steam exiting the back pressure turbine is condensed in a binary system. Recently, new technologies like the Kalina Cycle Technology for converting geothermal resources into electricity are also emerging and it will be discussed later in detail in section 1.2. The geothermal based electrical power production around the world for the year 2010 is about 10.9 GW and the forecast of 2015 is about 19.8 GW as shown in Fig. 1.11: (a) and (b) respectively.

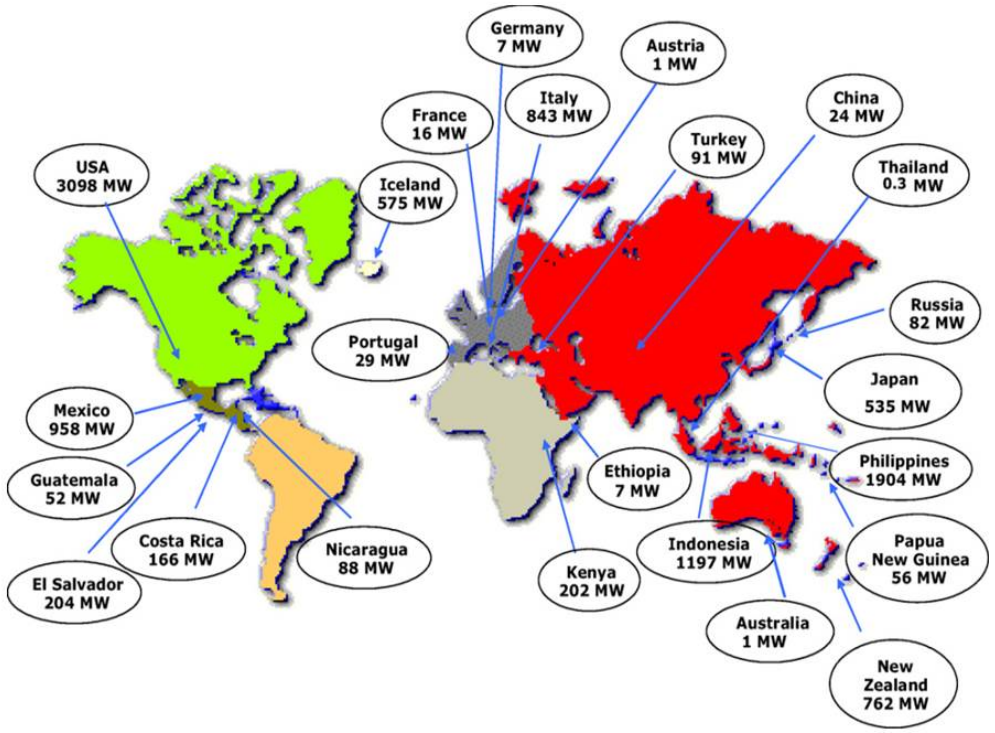

(a) – Installed capacity in 2010

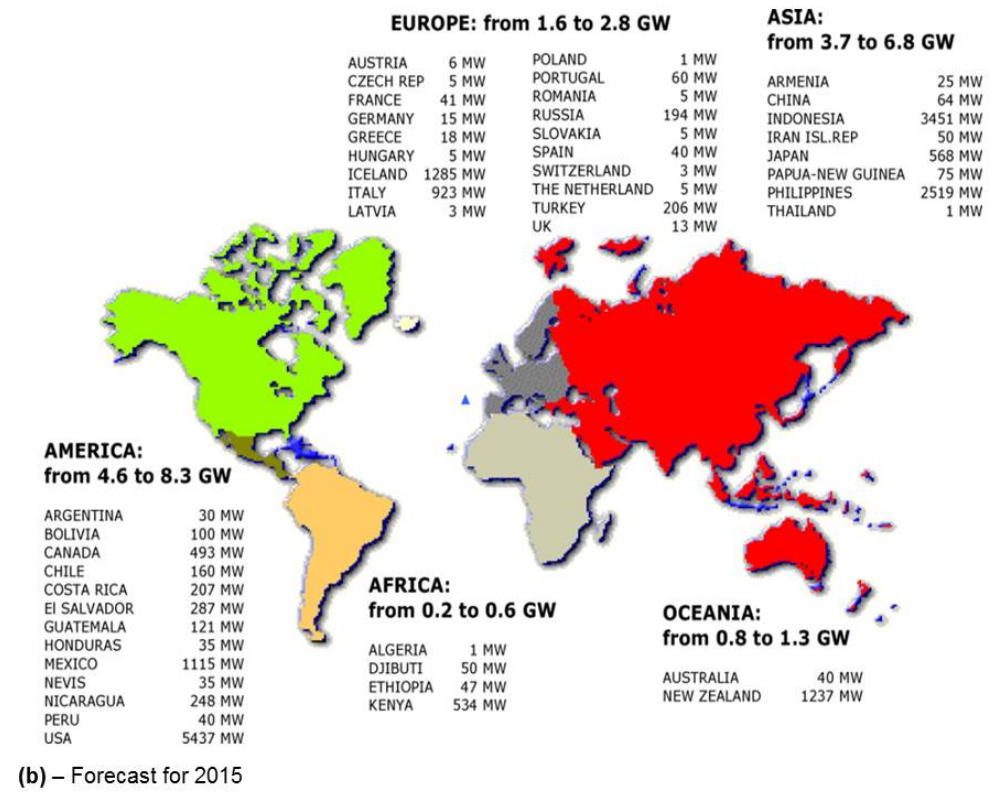

(b) – Forecast for 2015

Figure 1.11: Worldwide geothermal power generating capacity: (a) - Installed capacity in 2010; (b) - Forecast of installed capacity in 2015 [12].

1.1.3 Biomass energy

According to the International Energy Agency (IEA), biomass refers to the biodegradable portion of products, waste and residues from agriculture which includes vegetable and animal substances, forestry and related industries, as well as biodegradable fraction of industrial and municipal waste [13]. Unlike fossil fuel, biomass is considered as renewable energy source since it requires short time to replace, via photosynthesis, what is used as energy source. As a consequence, there are no net CO_2 emissions over the time frame of a cycle of biomass usage as energy source. In this sense biomass is the only renewable energy source that releases CO_2 while in use.

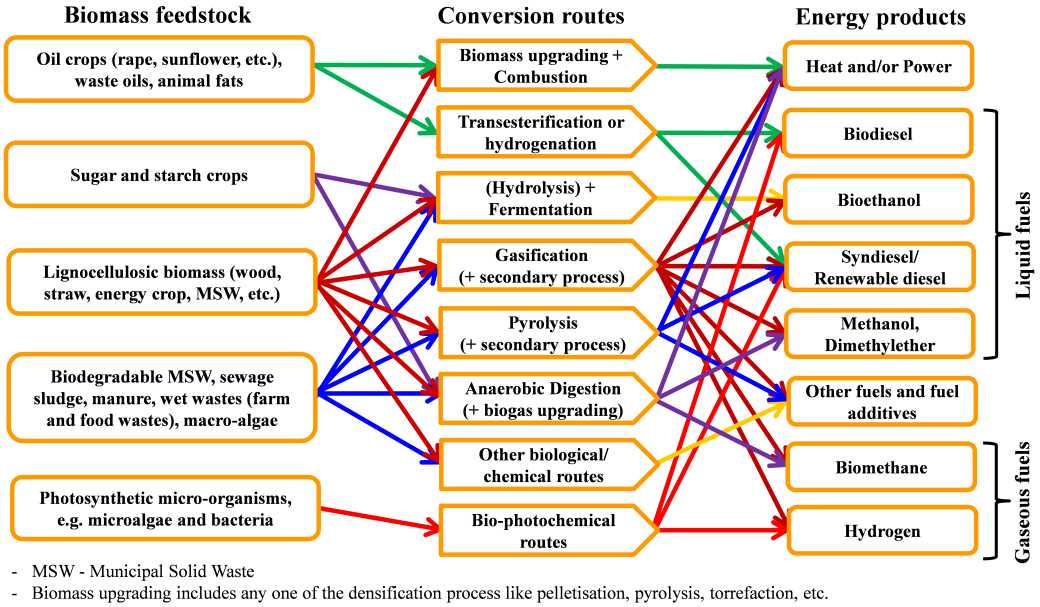

Figure 1.12: Schematic view of the wide variety of biomass conversion routes [13].

In 2009, biomass accounts approximately 10% of global annual energy supply which is around 50 EJ (1 EJ = 10^{18} J). It is mostly consumed in less developed countries by using inefficient ways like open fires or simple cookstoves that have considerable negative impact on human health because of smoke pollution. Electrical power production from biomass has been increasing steadily since 2000. In 2010, a total of 280 TWh (terawatt-hours) of electricity equivalent to 1.5% world electricity production was produced globally by using biomass resources. And also, 8 EJ of biomass for heat were used in the industrial sector. At present, forestry, agricultural and municipal residues, and wastes are the main feedstocks for the production of electricity and heat from biomass. And also, a very small share of

sugar, grain, and vegetable oil crops are used as feedstocks for production of liquid biofuels.

There is a significant potential to expand biomass use by tapping the large volume of unused residues and wastes. There are many bioenergy (i.e. energy from biomass) routes, as depicted in Fig. 1.12, which can be followed to convert raw biomass feedstock into final useful energy products. Several conversion technologies have been developed which are adapted to the different physical nature and chemical composition of the feed stock as well as the energy product required (heat, power and transport fuel). Biomass feedstock upgrading technologies such as pelletisation, torrefaction, and pyrolysis are being developed to convert bulky biomass into denser and more efficient for transportation, storage and convenient use in subsequent conversion processes.

1.1.4 Waste heat

Thermal waste is one of an unavoidable requirements of many processes in industries and power plants. With proper technological solutions, it can be the largest sources of low-cost and clean energy source to produce useful energy products. Many energy-intensive industries like iron and steel, bricks, ceramic and cement industries produce large amount of unused heat, which is cooled off with expensive cooling units or directly exhausted to the environment resulting thermal pollution. Therefore, suitable waste heat recovery measures can contribute to the reduction of CO_2 emissions by reducing fossil fuels consumption and to the reduction of the energy costs of industrial plants.

Mostly, waste heat sources are classified based on their temperature levels and one typical classification could be as: low-grade waste heat ($<$ 100 °C), mid-grade (100 °C - 400 °C) and high-grade ($>$ 400 °C) [14]. The waste heat flow characteristics are strongly dependent on the heat source nature and upstream thermal processes. Its characteristics includes, for instance, flue gas composition, dust load, contamination of water, steam quality and corrosion. The amount and quality, measured by its temperature level, of available waste heat depends on the thermal/industrial process upstream the heat recovery system. Hence, significant amount of fluctuations are possible at night, weekend and season. Therefore, the design of optimized waste heat recovery systems require detailed evaluation and analysis of the available waste heat sources as well as potential useful applications within or outside the source (e.g. district heating or cooling systems).

The next section describes technologies available for the conversion of thermal energy at low and mid-grade temperatures below 300 °C into power and cold.

1.2 Technologies for Power and Cold Productions

The steam Rankine cycle, Brayton cycle (for very high temperatures) and combined power cycle (Brayton cycle-topping cycle and steam Rankine cycle-bottoming cycle) are more efficient for conversion into power of heat sources at a temperature higher than 300 °C. As mentioned previously, low and mid-grade heat sources ($<$ 300 °C) are abundantly available: for instance, from stationary and low-concentrating solar collectors, geothermal sources, biomass sources and waste heat from various thermal processes. These sensible heat sources through the use of efficient and reliable technologies have promising potential for conversion to highly valuable energy products: electricity, air-conditioning and refrigeration. The conventional power plants, however, depend on power cycles, e.g. steam Rankine cycle, and have technical limitations to convert these thermal energy resources effectively.

Furthermore, the conventional vapour compression cooling technology uses high grade energy inputs in the form of electricity or mechanical power to drive its vapour compression stage. The driving power is obtained mostly by burning fossil fuels in power plants. In this section, an overview of the available technologies for the separate production of power and cold using heat sources at temperatures below 300 °C are presented.

1.2.1 Power production

1.2.1.1 Organic Rankine Cycle (ORC) technology

In principle, the ORC is similar to the conventional Rankine cycle with the main difference being the working fluid which is a low-boiling temperature organic fluid instead of water. Accordingly, several new features are observed in ORC systems that are mainly attributed to the nature of the organic working fluid employed in the cycle. It is one of the promising technologies for electrical (or mechanical) power production from heat sources at temperatures below 300 °C. The cycle architecture of the ORC system is relatively simpler than the steam Rankine cycle. In this cycle, the driving heat addition processes - preheating, vaporization and/or superheating can be done in a single heat exchanging unit [15].

The cycle variations common to steam Rankine cycle such as reheating and turbine bleeding are not necessary to ORC systems [15]. However, internal heat recuperation between the turbine (in general any mechanical work developing expansion device) exhaust and pump outlet are often included to recover heat and as a consequence improve the energetic performance of the system.

The schematic diagram of the ORC system with internal heat recuperator is illustrated in Fig. 1.13. The working fluid is pumped to the evaporator where it is heated to boiling, and then the generated vapour passed through an expander to develop the mechanical work that drives the coupled electric generator. After internal heat recuperation, the exhaust of the expander is condensed to liquid in the condenser by rejecting heat to the cooling medium. Finally, the liquid condensate is pumped back to the evaporator via the recuperator to complete the cycle.

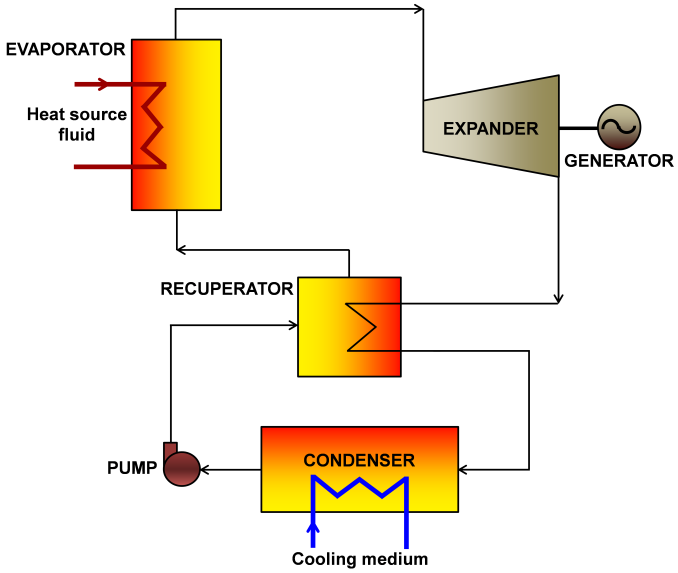

Figure 1.13: Schematic diagram of Organic Rankine Cycle with internal recuperator.

Recently, the selection of a suitable working fluid for ORC systems is a focus of interest in the scientific community ([15]-[21]). It is a critical issue because depending on the application and heat source characteristics, the working fluid must have optimal thermophysical properties and also meet other requirements including thermal stability, environmental regulations, safety, material compatibility, availability and cost. In this regards, several pure organic fluids have been studied for their use in the ORC systems: it includes refrigerants like R134a, R245fa, isobutane, n-pentane and others ([16]-[21]).

Mixtures of organic fluids are also suggested for ORC systems in order to reduce the irreversibilities associated with the sensible heat addition and rejection processes in the cycle ([22],[23]). Another option also suggested and analysed by many to reduce the irreversibilities of the heat addition process is supercritical heating [24]. For working fluids with relatively low critical pressure and temperature, the fluid can be compressed to its critical pressure and then heated to supercritical state which is followed by expansion process to develop the mechanical work. Thus, better thermal match is achieved in the heat addition process resulting higher thermal efficiency.

In vapour power cycles, another important aspect that must be considered during the selection of working fluid is the behaviour of its vapour saturation curve. The characteristic of the vapour saturation curve affects the fluid applicability, cycle efficiency, components type and layout. Accordingly, the fluids are classified into three groups by considering the slope of their vapour saturation curve on the T-s diagram. A wet fluid (e.g. water, ammonia and R134a) has a negative slope; a dry fluid (e.g. R245fa and n-pentane) has a positive slope; and an isentropic fluid has infinitely large slopes (e.g. R11). Mostly, organic fluids are either dry or isentropic thus do not need any superheating. Since the enthalpy drop across the expander and cycle pressure ratios are relatively small compared to the conventional steam Rankine-power plants, ORC systems typically require a single-expander resulting a simple and economical system (both in capital and maintenance costs).

The development of power plants based on ORC has received much attention after the oil crises of the 1970s. Since then several ORC system manufacturers have been entered in to the world market. The ORC technology is a matured technology for effective utilization of geothermal resources, biomass and waste heat recovery. At present, a few commercial solar ORC power plants are available: a typical example could be the 1 MWel solar ORC plant in Arizona, the United States [25]. The ORC market is well developed for the MW electrical power production range and recently it is rising rapidly for power production ranges between 0.2 MWel and 2 MWel. The major ORC manufactures present in the world today provides ORC technological solution at different ranges of electrical power outputs by using heat sources at various temperature levels; and are shown in Table 1.2. Moreover, lower capacity power blocks (in few kW scales) are still at the proof-of-concept stage development mainly due to the lack of appropriate power developing expanders [26].

Up to now, there is no supercritical ORC system in operation. Nonetheless, it has been suggested strongly in the literature due to its higher thermal efficiency and simplicity than problematic multiple-pressures boiling options. Supercritical Rankine cycle using zeotropic mixture working fluids are also focus of recent interest for conversion of thermal energy sources at low and mid-temperature levels into electrical or mechanical power.

Table 1.2: List of the main organic Rankine cycle manufactures worldwide ([15],[17]).

Manufacturer (Country)	Heat source temperature [°C]	Working fluid	Type of heat source
Cryostar (France)	100–400	R245fa, R134a	Geothermal and Waste heat
TRI-O-GEN (Netherlands)	> 350	Toluene	Waste heat
GMK (Germany)	120–350	GL-160®	Geothermal, Biomass and Waste heat
Adoratec/Maxxtec (Germany)	300	OMTS	Biomass
ORMAT (USA)	150–300	n-pentane and others	Solar, Geothermal and Waste heat
Turboden (Italy)	100–300	OMTS, Solkatherm	Geothermal, Biomass and Waste heat
GE Power & Water (USA)	> 115 < 240	R245fa	Solar, Biomass and Waste heat
Eneftech (Switzerland)	120–200	n/a	Solar, Biomass, Geothermal, and Waste heat
LTi REEnergy (Germany)	> 160	n/a	Waste heat
Bosch KWK (Germany)	120–150	R245fa	Waste heat
Turboden PureCycle (USA)	91–149	R245fa	Geothermal and Waste heat
Pratt & Whitney Power Systems (USA)	91–149	R245fa	Solar, Geothermal, Biomass and Waste heat
Barber Nichols (USA)	> 115	n/a	Geothermal and Waste heat
GE CleanCycle (USA)	> 121	R245fa	Waste heat
FREEPOWER (England)	> 110	n/a	Solar, Geothermal, Biomass and Waste heat
Opcon (Sweden)	< 120	Ammonia*	Waste heat
Infinity Turbine (USA)	< 90	R134a	Geothermal and Waste heat
	90–120	R245fa	Waste heat
Electratherm (USA)	> 93	R245fa	Solar and Waste heat

OMTS - Octamethyltrisiloxane; GL-160® is GMK (Germany) patented working fluid;
n/a - not available; * - Inherently, it should not be an ORC working fluid. However, because of its similarity with ORC working fluid it is included.

1.2.1.2 Kalina cycle technology

The use of multi-component mixtures instead of pure fluids, e.g. steam in conventional Rankine cycle or organic fluid in ORC systems, as working fluid produces a better thermal match between the sensible heat source (and also heat sink) and working fluid. As a consequence, there are less thermodynamic irreversibilities during the heat supply and rejection processes, which increases the cycle efficiency. In absorption power cycles, the multi-component working fluid mixture is only partially boiled in a boiler and the remaining liquid can be used to absorb vapour in the absorber coming from the expander (turbine) outlet. This means, then, that the turbine back pressure is reduced not by the condensation process instead by absorption-condensation. The varying temperature, at constant pressure, of the multi-component working fluid during the heat addition processes also reduces the effect of the thermal pinch in the boiler.

The most commonly studied mixture for absorption power systems is ammonia/water (NH_3/H_2O). However, it should be pointed out that other multi-component mixtures have the same benefit and can also be used ([27]-[29]). Maloney and Robertson were among the first to study an NH_3/H_2O based absorption power cycle [30] and found that it had no significant thermodynamic advantages over the steam-Rankine cycle configuration in the thermal boundary conditions considered. Fig. 1.14 shows the schematic flow diagram of the Maloney and Robertson absorption power cycle.

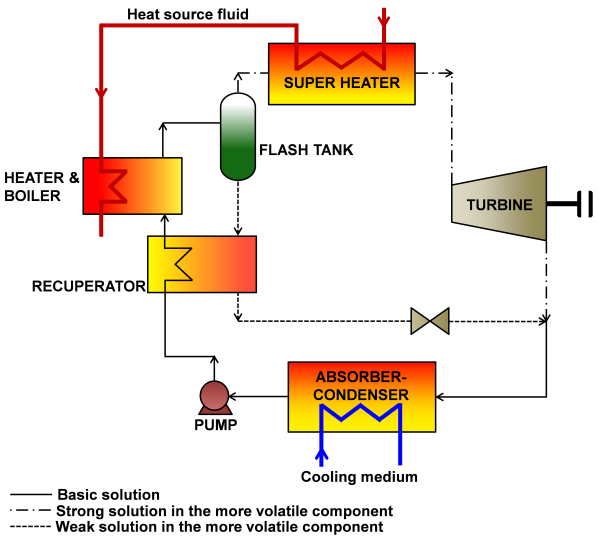

Figure 1.14: The Maloney and Robertson power cycle [30].

They did not consider the fact that NH_3/H_2O mixtures can have lower temperature pinch points in counter flow heat exchangers. The condensation process took place at a variable temperature and resulted in a higher turbine back pressure than of the conventional steam Rankine cycle. This had a negative effect on power production and consequently on cycle efficiency. Further, the NH_3/H_2O property database source used at that time was limited and may had shortcoming on the results of their cycle analysis.

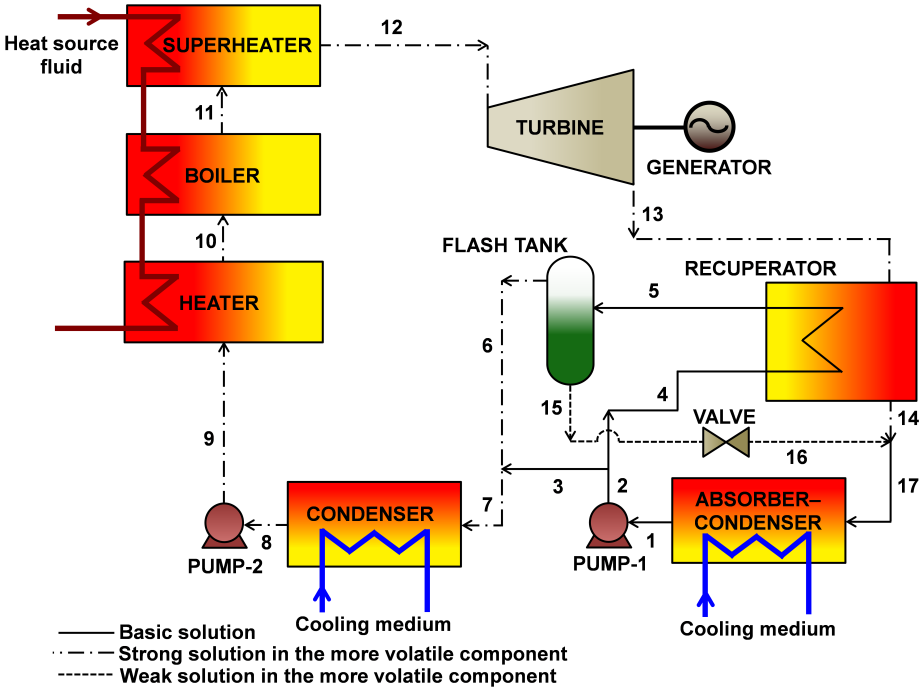

Figure 1.15: Kalina power cycle proposed by A.I. Kalina (1983, [32]).

In the early 1980s, Dr. Alexander I. Kalina proposed and patented an NH_3/H_2O based absorption power cycle ([31]-[33]) that has some differences, in cycle configuration, with respect to the one studied by Maloney and Robertson. In this cycle (see Fig. 1.15) a basic NH_3/H_2O solution (state 1) is pumped to an intermediate pressure (state 2) and then split into two streams (state 3 and 4); about 80% of the basic solution passes to a flash tank (separator) after it recovers heat (state 4-5) from the turbine exhaust. The recovered heat partially boils the basic solution and then separated into strong, in NH_3, vapour solution and weak, in NH_3, liquid solution in the flash tank (state 6 and 15, respectively). The vapour stream (state 6) mix with the other 20% basic solution (state 3) by passed the separator. A second condenser is added to condense the combined stream (state 7); it

adds an extra degree of freedom to operate the separator at lower pressure than the boiler (turbine inlet) pressure. Accordingly, less energy is required to boil the basic solution. The condensate (state 8) is pumped to the boiler pressure and then heated (states 9-10), vaporized (states 10-11) and superheated (states 11-12) before entering the turbine. After generating mechanical power, the expanded vapour passes through the recuperator to recover heat from it (states 13-14). And, then, mix with the weak solution coming from the separator (state 16) to regenerate the basic solution through an absorption-condensation process (states 17-1). The condenser and absorber-condenser units reject their heat to the external cooling medium.

Similar to Rankine cycle which has several design options to implement in power plants that include reheat, regenerative heating, supercritical pressure, etc., Kalina cycle also has many special design configurations comprising a family of unique Kalina Cycle Systems (KCSs) ([31]-[43]). Each KCS in the family of designs has specific applications and is identified by a unique system number as illustrated in Table 1.3.

Table 1.3: Different Kalina cycle configurations and their applications.

System designation	Application	Reference
	For mid and high-temperature heat sources applications	
KCS 1	Bottoming cycle for small power plants ($<$ 20 MWel) (about 8 MWel from the bottoming cycle)	[33]
KCS 3	High temperature geothermal and industrial waste heat	[35]
KCS 4	Cogeneration systems	[35]
KCS 5	Direct-fired plants (using coal and other solid fuels)	[35]
KCS 5n	High temperature gas-cooled nuclear reactor (similar to KCS 5) apart from the water loop since the heat source is relatively lower than obtained from combustion system	[34]
KCS 6	Bottoming cycle for Gas turbine-based combined cycles (More suitable for large capacity power plants: $>$ 20 MWel)	[37]
KCS 7 & 8	Direct fired and Bottoming cycle split cycles, respectively	[34]
KCS 9	Retrofit subsystem for existing plant	[34]
	For low-temperature heat sources applications	
KCS 2	Geothermal utilization ($<$ 190 °C)	[35]
KCS 11	Heat sources (between 121 °C – 204 °C) conversion into electricity	[39]
KCS 12	Low-temperature geothermal applications	[34]
KCS 34	Combined power and district heating applications (for heat source temperatures below 121 °C)	[41]
KCS 34g	Small size power plants using heat sources less than 121 °C	[41]

Fig. 1.16 shows the three basic cycle configuration designs for using low-temperature heat sources (originally designed for the utilization of geothermal resources). It may be used with a combined heat and power plant (at the Industriepark Hoechst site in Frankfurt am Main, Germany) to improve the overall efficiency of the plant [42]. The production of electrical energy using absorption cycles of the Kalina type has a promising future and there are already a few power plants with a capacity range up to 8.6 MWel [44] and several countries have demonstration sites (Japan, Germany and Iceland) [42]. The most common commercially available Kalina Cycle® Technology power plants are given in Table 1.4.

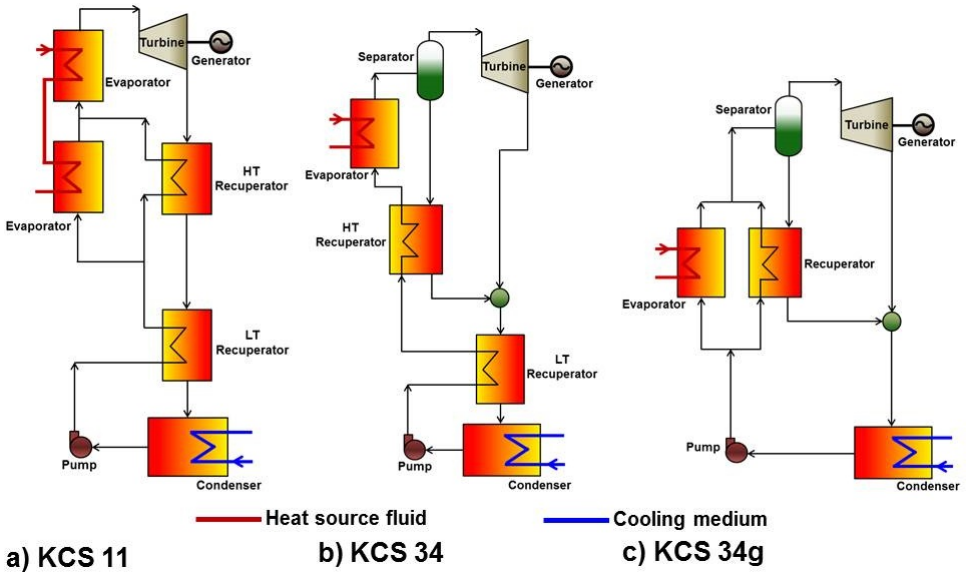

Figure 1.16: Kalina Cycle Systems for using low-temperature heat sources [43].

Table 1.4: Kalina Cycle® Power plants in operation worldwide ([42],[44]).

Project name (Country)	Starting year	Heat source type	Power output [kW]
Canoga Park* (USA)	1992	Exhaust of gas turbine (515 °C)	6500
Fukuoka* (Japan)	1998	Waste heat - incineration plant	4500
Sumitomo Metals (Japan)	1999	Waste heat (from Steel mill)	3500
Husavik (Iceland)	2000	Geothermal brine (at 120 °C)	2000
Fuji Oil (Japan)	2006	Waste heat (from Oil refinery)	4000
Unterhaching (Germany)	2009	Geothermal brine (at 124 °C)	3400
Bruchsal (Germany)	2009	Geothermal brine	600
Tibet* (Tibet)	2009	Geothermal brine	50
Shanghai World Expo (China)	2010	Solar thermal	50
Taiwan* (Taiwan)	2010	Geothermal brine	50
Khairpur Cement Plant (Pakistan)	2013	Waste heat (Gas and air from kiln)	8600
Star Cement Plant (UAE)	2013	Waste heat (Hot air from kiln)	4750

*Demonstration plants operated for fixed periods (up to 5 years)

1.2.2 Cold production

From the thermally-activated technologies for cold production (see Fig. 1.17), sorption cooling technologies, in particular absorption chillers, are the dominant sector in the market. Sorption is a process by which one substance takes up or holds another. Desorption, also called generation, is the reverse of sorption process. In both processes, the mass transfer phenomena accompanied by heat transfer (take place with the environment) and they are inherently irreversible. In sorption processes, a pair of substances are involved. The substance with lower boiling temperature is called sorbate (which act as a refrigerant) and the other is sorbent. Heat is evolved during sorption process while heat should be supplied to drive out the sorbate from the sorbent (desorption process). Thus, with the right combination of these processes, thermal energy can be converted directly to refrigeration (cooling effect) [45].

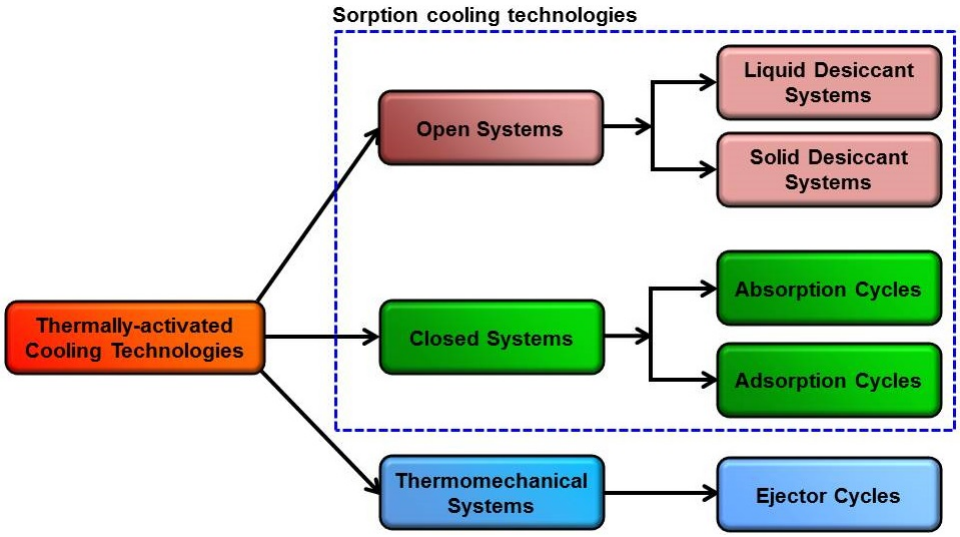

Figure 1.17: Main thermally-activated cooling technology options.

The main difference between sorption and the conventional cooling technologies is in their refrigerant vapour compression stage. The former uses thermal energy to drive the system whereas the later uses high grade energy in the form of electricity (or mechanical work). Hence, the vapour compression stage/process in sorption technology is often called as "thermal compression". Sorption cooling technologies are classified according to sorbent type (liquid or solid) and also on whether the entire process is performed in a closed (absorption and adsorption cooling cycles) or open (liquid and solid desiccant cooling systems)

environment. Absorption is a process in which a substance in one phase is incorporated into another substance of a different phase (e.g. vapour being absorbed by a liquid); adsorption refers to the use of a solid surface to adhere or bond ions and molecules of another substance [45]. Desiccation is a process where the sorbent, desiccant which is either liquid or solid, absorbs the moisture (water vapour) from humid airstream [45].

1.2.2.1 Absorption chillers

The development of absorption refrigeration machines begins between the late 1700's and early 1800's when Edmond Carré developed an absorption machine using water and sulfuric acid as a working pair [46]. However, it had two major problems: corrosion and leakage of air into the system. Later in 1859, his brother Ferdinand Carré developed and demonstrated for the first time an NH_3/H_2O based absorption refrigerator and received French and US patents for his invention (in 1859 and 1860, respectively). It was a bases for early age developments of absorption refrigeration machines used for ice making and food storage [46].

A commercially successful absorption refrigerator was introduced by a Swedish company "AB Electrolux", 1926-1950, and in the United States by "Servel" which was able to brought refrigerators to millions of homes. Both companies were used the patented inventions of two Swedish engineering students (were at that time): Carl G. Munters and Baltzar von Platen. However, the production of these refrigerators was stopped in the 1950s, mainly, due to the introduction of high performance mechanical vapour compression refrigerators in the market. After World War II, large capacity single-effect absorption chillers that uses water/lithium bromide (H_2O/LiBr) solution as working pair was introduced for industrial applications. A few years later, indirect fired double-effect H_2O/LiBr absorption chiller was entered in the market by the Japanese company "Kawaski". Then, in 1970s Trane Company introduced the first mass-produced steam-fired double-effect H_2O/LiBr absorption chiller in the US market. Since then, several factors including the oil crisis in the 1973 and the development of more efficient mechanical compression chillers declined the sales of absorption chillers in the US market.

Recent decades have showed a worldwide interest on absorption chillers, in fact to all thermally-activated cooling technologies, due to their inherent potential to utilize renew-

able energy sources and waste heat recovery. Absorption chillers are designed based on various cycle configuration options in order to meet different operating conditions and applications. A single-stage, single-effect, absorption cycle (see Fig. 1.18) is the basic configuration used under normal operating conditions and it is also a building block for other advanced cycle configurations. A half-effect and compressor/absorption hybrid cycles can be used under lower evaporation temperatures, higher absorber and condenser temperatures or lower desorber activation temperatures ([46],[47]).

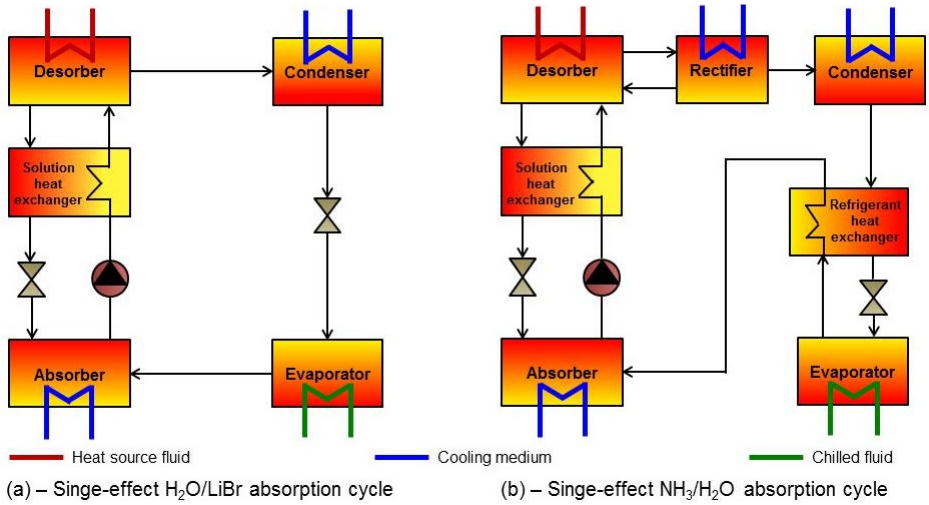

Figure 1.18: Single-stage absorption refrigeration cycle.

For an efficient utilization of relatively high temperature heat sources, multi-stage (multi-effect) absorption cycles and Generator Absorber heat eXchanger (GAX) cycles can be employed ([48]-[50]). There are different types of advanced, multi-effect and GAX, cycle configuration possibilities to improve the energetic efficiency (measured by the coefficient of performance, COP) of absorption chillers. Some of these configurations are depicted in Fig. 1.19 ([51],[52]). For cooling applications, the COP is defined as the ratio of the cooling effect ($\dot{Q}_{cold}$) to the driving heat input ($\dot{Q}_{input}$): $COP = \dot{Q}_{cold}/\dot{Q}_{input}$. Typical COP values and driving heat source temperature ranges for several types of absorption chiller cycles are presented in Table 1.5. At present, several absorption chiller manufactures are available in the world market (Table 1.6) that uses the conventional H_2O/LiBr and NH_3/H_2O, and other working pairs. In 2013, Kawasaki Thermal Engineering Co., Ltd. announced the release of the world's most efficient double-effect H_2O/LiBr absorption chiller, about a COP of 1.51, shown in Fig. 1.20.

Table 1.5: Typical COP values for several types of absorption chiller cycles.

Type of Cycle	Working pair	Chilled fluid temperature [°C]	Heat source temperature range [°C]	COP [-]
Single-effect	$H_2O/LiBr$	5–10	80–110	0.6–0.75
	NH_3/H_2O	< 0	120–140	~ 0.5
Double-effect	$H_2O/LiBr$	5–10	120–170	1.1–1.3
Triple-effect	$H_2O/LiBr$	5–10	200–250	1.4–1.7
GAX	NH_3/H_2O	< 0	150–220	0.7–0.9
Half-effect	$H_2O/LiBr$	5–10	50–70	0.3–0.35

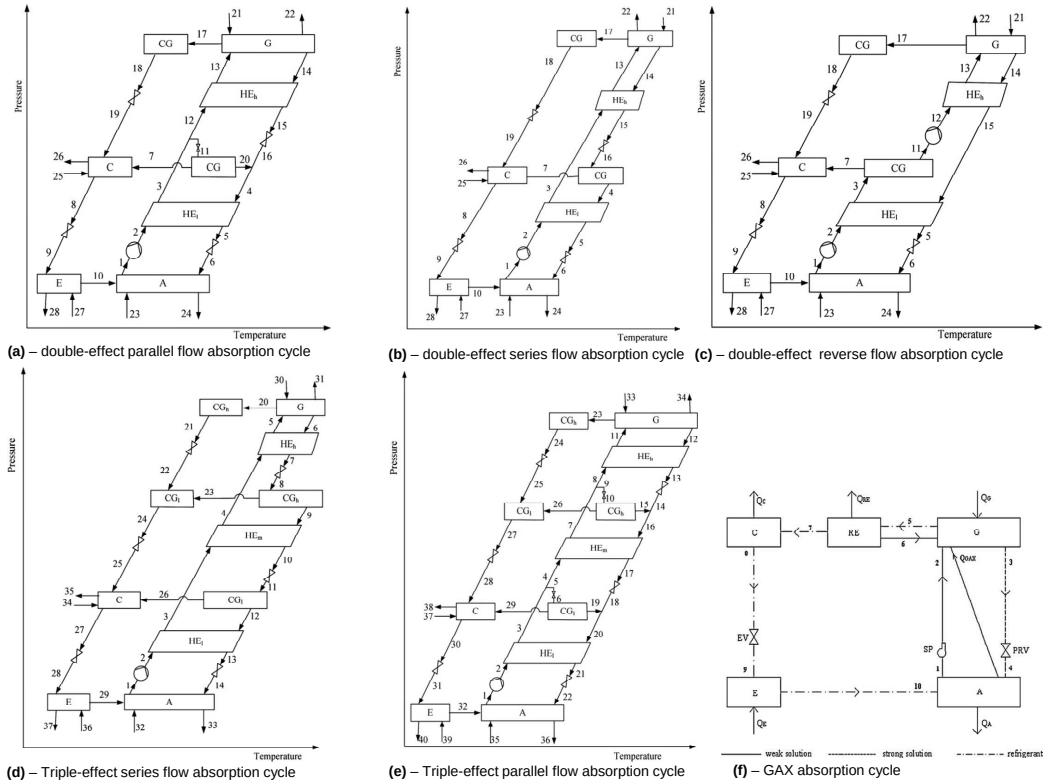

Figure 1.19: Different types of advanced absorption refrigeration cycles ([51],[52]).

This high performance was made possible due to innovative developments on fuel-saving technologies and high performance plate heat exchanger, high-efficiency heat exchanger tubes, exhaust gas heat exchanger, and two-stage evaporation/absorption structures [53]. In order to fulfil broad customers need (capacity range and operating conditions), the company lunched four types of this new 'effico' series absorption chiller with range of capacity between 281 kW to 3516 kW at different COP values (1.51, 1.41, 1.39 and 1.33).

Table 1.6: Different market available small-to-large capacity absorption chillers.

Supplier name (Country)	Capacity [kW]	Type of technology	Working pair	Website
AGO (Germany)	50–1000	SE (Ind.-fired)	NH_3/H_2O	www.ago.ag
Broad (China)	105–5272	SE (Ind.-fired)	H_2O/LiBr	www.broad.com
	150–23260	DE (Dir./Ind.-fired)		
Carrier (USA)	98–3587	SE (Ind.-fired)	H_2O/LiBr	www.commercial.carrier.com
	346.5–5303	DE (Dir./Ind.-fired)		
Climatewell (Sweden)	10 and 20	SE[1] (Ind.-fired)	H_2O/LiCl	www.climatewell.com
EAW (Germany)	15–200	SE (Dir./Ind.-fired)	H_2O/LiBr	www.eaw-energieanlagenbau.de
Entropie (France)	300–6000	SE (Ind.-fired)	H_2O/LiBr	www.entropie.com
Fischer Eco Solutions (Germany)	15–5000	SE (Ind.-fired)	H_2O/LiBr, Methanol/LiBr	www.fischer-group.com
Hitachi (Japan)	106–19690	DE (Dir./Ind.-fired)	H_2O/LiBr	www.hitachi-ap.com
Jiangsu Huineng (China)	11–380	SE, DE (Dir./Ind.-fired)	H_2O/LiBr	www.tynkt.com
Kawasaki (Japan)	141–2462	DE (Dir./Ind.-fired)	H_2O/LiBr	www.khi.co.jp
	563–1196	TE (Dir.-fired)		
LG (S. Korea)	98–3587	SE (Ind.-fired)	H_2O/LiBr	www.lge.com
	176–5275	DE (Dir./Ind.-fired)		
	258–3427	SE[2](Ind.-fired)		
Pink (Austria)	10, 12, 19	SE (Ind.-fired)	NH_3/H_2O	www.pink.co.at
Robur (Italy)	14–87.5	SE (Dir.-fired)	NH_3/H_2O	www.roburcorp.com
Sakura (Japan)	105–5272	SE (Ind.-fired)	H_2O/LiBr	www.sakura-aircon.com
	176–5272	DE (Dir./Ind.-fired)		
	264–4571	SE[2] (Ind.-fired)		
Shuangliang (China)	2901–1630	SE, DE (Dir./Ind.-fired)	H_2O/LiBr	www.shuangliang.com
SolarNext	17.5–105	SE (Ind.-fired)	H_2O/LiBr	www.solarnext.eu
(Germany)	>12	SE (Ind.-fired)	NH_3/H_2O	
Thermax (India)	175–3500[3]	SE (Ind.-fired)	H_2O/LiBr	www.thermaxindia.com
	35–14000[3]	SE, DE (Dir./Ind.-fired)		
Trane Company	392–4725	SE (Ind.-fired)	H_2O/LiBr	www.trane.com
(USA)	350–5775	DE (Dir./Ind.-fired)		
Yazaki (Japan)	17.5–175	SE (Ind.-fired)	H_2O/LiBr	www.yazaki-airconditioning.com
	105–703	DE (Dir.-fired)		
York (USA)	280–3150	SE (Ind.-fired)	H_2O/LiBr	www.johnsoncontrols.com
	703–2370	DE (Dir./Ind.-fired)		

[1] - With storage; [2] - Double-lift; [3] - Including custom built design units; Dir. - Direct; Ind. - Indirect; SE - Single-effect; DE - Double-effect; TE - Triple-effect

Kawasaki is also the first to launch the word's first triple-effect H_2O/LiBr absorption chiller with highest COP of 1.74 for capacity range of 563 kW to 1196 kW. Then, recently, Thermax-India designed and implemented the first solar air-conditioning technology using a triple-effect absorption chiller. This 100 kW demonstration project was made by integrating a triple-effect chiller with solar parabolic concentrators (collectors), both are developed by the company itself. The use of absorption chillers in countries like Japan,

China, South Korea and India has grown exponentially but their share still very far from the share of the conventional mechanical vapour compression cooling technologies. The drawbacks of absorption chillers which are mostly mentioned are heavy weight and large footprint, lower efficiency compared with conventional chillers, difficulty to understand the process, and, above all, the relatively high capital cost [49].

Figure 1.20: Kawasaki efficio series double-effect water/LiBr absorption chiller-heater.

1.2.2.2 Adsorption chillers

The discovery of adsorption process for cold production dates back to the 18^{th} century when Faraday, in 1848, used AgCl to adsorb ammonia and showed that cooling effect could be produced [54]. Then, later in 1920s G.E. Hulse produced adsorption refrigeration system using silica gel-SO_2 working pair and reached evaporation temperature of about -12 °C [55]. It was used for food storage applications on trains. Similar to absorption refrigerators, the demand of adsorption refrigerators also decreased due to the rapid development of mechanical vapour compression chillers. However, recently much attention is given to adsorption chiller technology as well [56].

A simple adsorption chiller consists of a solid adsorbent bed (adsorber), a condenser, an evaporator and an expansion valve. Its basic flow diagram is shown in Fig. 1.21 (a). The entire adsorption chiller process can be divided into two parts: adsorbent heating and desorption process; and the adsorption process. For adsorbent heating and desorption process, the valve between the adsorber and condenser is opened while the other valve is

closed. As a result, the refrigerant condenses in the condenser by rejecting heat to the cooling medium. After the desorption process, the adsorber is connected to the evaporator through the valve between the adsorber and the evaporator. Then, the adsorber cooling and adsorption process produces the cooling effect in the evaporator by evaporating the refrigerant. The cooling output of the basic system, shown in Fig. 1.21 (a), is intermittent in nature.

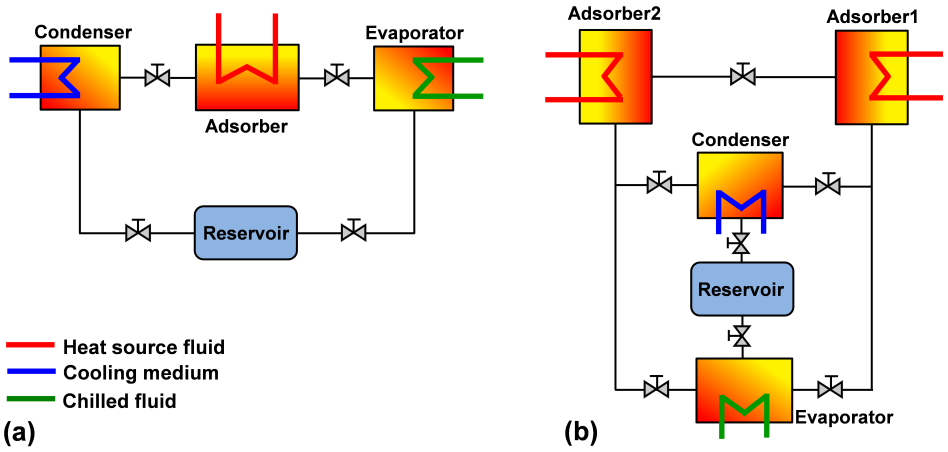

Figure 1.21: Schematic flow diagram of the conventional adsorption refrigeration systems: (a) - basic system; (b) - continuous system.

For continuous cold production, two adsorbers should be incorporated together in the system (see Fig. 1.21 (b)), in which one bed is heated during desorption process and the other one is cooled during the adsorption process. It is difficult to transport solid sorbent from one component to another, hence each of the adsorbent function alternatively as generator and adsorber. Since a mass recovery process could greatly improve the performance of an adsorption refrigeration system, the two adsorbers could be connected with a valve in order to have the mass recovery and then significant improvement on performance (higher COP) could be achieved. The most commonly used working pairs (refrigerant/adsorbent combination) in adsorption chillers are water/silica-gel, water/zeolite and methanol/activated carbon [57].

Adsorption chillers first appeared in the market, in 1986, by the Japanese company Nishiyodo Kuchouki, Co.Ltd [58]. This chiller is driven by a heat source temperature between 50 °C and 90 °C and capable of producing chilled water as low as 3 °C. The rated cooling capacity of the chiller is from 51 kW to 1000 kW. At a heat source temperature

of around 90 °C, a COP of 0.7 could be achieved. Nowadays, there are other adsorption chillers available in the market; specially for small capacity solar cooling applications [59]. The main challenges of this technology are low thermal conductivity and non-fluidity of the solid adsorbent which hinders internal heat recuperation, consequently it limits the effective utilization of the heat source. Another limitation often mentioned is the relative low cycle mass of the working pair: that means the adsorption capacity difference between adsorption phase and desorption phase is low [57].

1.2.2.3 Other technologies

Apart from absorption and adsorption cooling technologies, desiccant dehumidifier and cooling, and ejector cooling systems are other thermally-driven technologies that have been investigated by a number of researchers ([60]-[62]). Ejector cooling systems have been used for many years. However, they have much lower COP than sorption cooling technologies but offers advantages of simplicity and no moving mechanical parts. Therefore, considerable research efforts are undergoing to increase the ejector efficiency on design and off-design operating conditions, and also beside steam to use other natural refrigerants for low temperature applications (< 0 °C).

A desiccant dehumidifier removes the humidity (water vapour) from the incoming air-stream by using materials that draw and hold moisture. In order to achieve comfortable cooling, the sensible and latent parts of the cooling load should be handled simultaneously. A desiccant dehumidifier handles the latent cooling part of the load: to control humidity. Whereas the sensible cooling load can be handled either by an evaporator cooler or traditional air-conditioner. It means that, the desiccant dehumidifier always operate with chillers or conventional air-conditioning systems to provide comfortable cooling and to increase the overall system performance. There are two types of desiccant dehumidifiers which are distinguished by the type of desiccant material used in their system: solid and liquid desiccant dehumidifiers [60].

The desiccant materials must be regenerated using thermal energy sources. In solid-desiccant based systems, the air is brought into direct contact with the solid desiccant, which is commonly contained in a rotating wheel. One half of the wheel is exposed to the airstream while the other half is exposed to thermal heat source for regeneration.

Regarding the liquid desiccant-based systems, the airstream is brought into direct contact with the liquid desiccant which absorbs some moisture from the airstream. Solid desiccant dehumidifiers are usually used in HVAC systems whereas liquid desiccant dehumidifiers are more common in industrial and residential applications.

There are other alternative emerging technologies including magnetic cooling, thermoacoustic cooling, thermoelectric cooling (peltier cells), thermoeletric cooling which do not use directly thermal energy as a driving source but have considerable potential in the future for cold production. The physical principles and the current state-of-the-art of these technologies can be found elsewhere [64].

1.3 Combined Production of Useful Energy Products

Combined heat and power (CHP) systems are proven and reliable technologies that provide various technical, economic and environmental advantages compared with the separate production of useful heat and power (electrical or mechanical) ([66]-[69]). The conventional way to supply electricity and useful heat is to purchase electricity from the local central utility-scale power plants (if available) and produce useful heat by burning fuel in a boiler. A CHP system uses the waste heat rejected from the power generating unit (from the prime mover) to simultaneously produce electricity and useful heat (for various purposes like space heating, sanitary hot water and industrial process steam). In case of building applications, the CHP system performance (efficiency) and capability decreases significantly in hot climates particularly in summer months where heating demand is minimal. In general, CHP systems are more suitable and efficient for supplying a balanced and continuous heat and electricity demand profile all over the year, which is not the case in reality. A summer season is characterized by an increasing demand for cooling and air-conditioning due to large thermal loads and high levels of human thermal comfort requirements.

When a CHP system is coupled, through heat integration, with thermally-activated cooling systems the integrated system is called combined cooling, heating and power (CCHP) and often also called trigeneration system. It can be viewed as an extension of CHP system to produce triple-useful energy products (cold, heat and electrical/mechanical power) to the maximum or at least dual-outputs, depending on the need, from a single fuel or energy

source. A trigeneration system mainly comprises a power generation unit (prime mover coupled with electric generator), a heat recovery unit, a thermally-driven cooling unit, a heating unit and a control system. A typical trigeneration system with examples for its prime mover is illustrated schematically in Fig. 1.22.

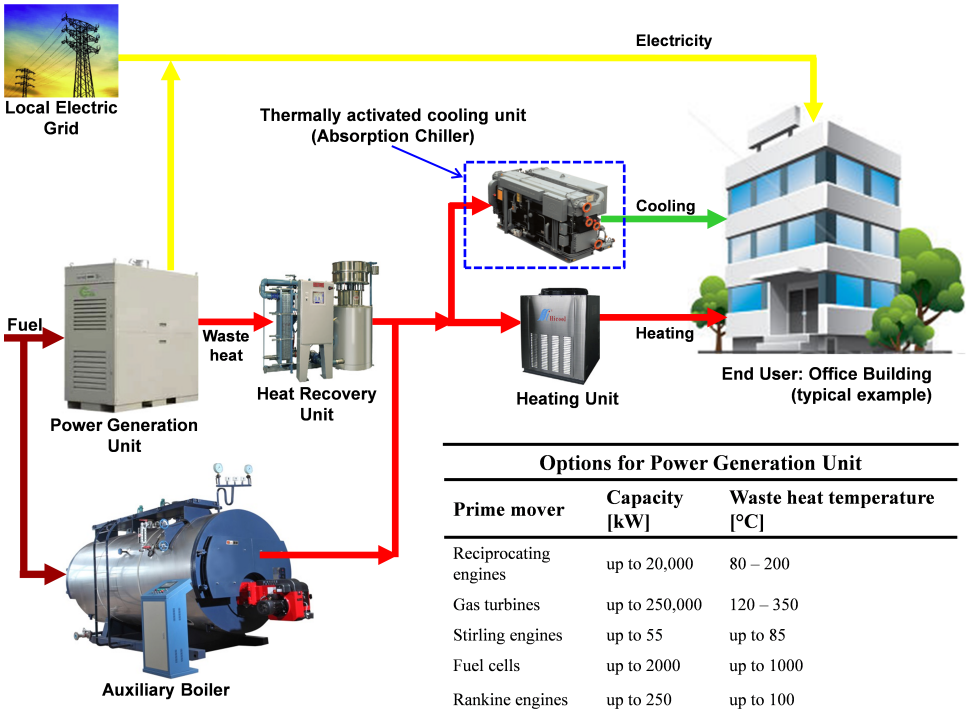

Options for Power Generation Unit

Prime mover	Capacity [kW]	Waste heat temperature [°C]
Reciprocating engines	up to 20,000	80 – 200
Gas turbines	up to 250,000	120 – 350
Stirling engines	up to 55	up to 85
Fuel cells	up to 2000	up to 1000
Rankine engines	up to 250	up to 100

Figure 1.22: A typical trigeneration system (Source of prime mover options: Ref. [69]).

Compared to the conventional way of separate useful energy production, a trigeneration system has several benefits including improvement on the overall energy production efficiency and other technical, socio-economic and environmental advantages. Theses benefits are described as follows [69].

- Flexibility to deliver multiple energy products: electricity, cooling and heating at variable ratios.
- Reduce primary energy consumption as well as thermal losses.
- Reduce operational costs.
- Improve energy supply reliability and energy sector security.
- Emission reduction: reduce greenhouse gas emissions and pollutants in many cases.

As mentioned above, the currently used systems for combined production of power and cold in order to get the benefits of combined productions of useful energy products from

a single energy source requires at least three or more separate sub-systems (units): power generation unit, waste heat recovery unit and thermally-driven cooling unit; mostly absorption chillers. As a consequence, two thermodynamic cycles are involved to govern their operation usually: power cycle and absorption refrigeration cycle. In most cases, the thermodynamic power cycle is driven by high temperature heat sources ($>$ 350 °C) obtained by burning fossil fuels like natural gas.

The use of absorption chillers is usually restricted to the summer season while in intermediate seasons they are only partially used. However, electrical power is required almost constantly throughout the year. A combined absorption system producing not only power as in the case of the Kalina Cycles but also cold could be adapted to the whole range of energy demand, from only power to only cold modes with intermediate operation modes that produce different ratios of each. Such kind of systems have several advantages, first they can produce dual-useful energy products using the same heat source at low or mid-grade temperature levels ($<$ 300 °C). Second, they have advantages from the technical and performance perspectives since they use a single thermodynamic cycle (absorption cycle) that means they also share components.

1.4 General and Specific Thesis Objectives

According to the review presented above the main purpose of this doctoral thesis is the development of new class of combined absorption systems, capable to produce power and refrigeration simultaneously and/or alternatively by utilizing a single thermal energy source available at low and medium temperatures below 300 °C. The combined absorption systems are suitable for applications characterized by micro, mini and small-scale power capacities. The capacity of the combined absorption systems is categorized according to the COGEN Europe "a guide to cogeneration": micro-scale under 20 kWel, mini-scale between 20 kWel and 500 kWel and everything under 1 MWel as small-scale capacity [70]. The core of these new systems, for the co-production of power and cold, should be the architecture of the absorption cycle configurations. These systems will help to reduce primary energy consumption, decrease capital and operation costs, and also reduce adverse environmental impact helping to advancement towards the NZEB (Net Zero Energy Building) concept.

In order to achieve the overall objective of the thesis, the following specific objectives are set:

- Theoretical analysis and discussion on the fundamentals of combined power and refrigeration absorption cycles. Study on the various performance criteria used in the literature for the energetic and exergetic performance evaluations of these types of dual purpose systems (cycles). Then, define performance indicators that account for the thermodynamic quality of the system's dual-outputs.
- Comprehensive review of combined absorption cycle configurations proposed in the literature for the co-production of mechanical power and cold.
- Review on the thermophysical properties relations of ammonia based working fluid pairs (NH_3/H_2O, $NH_3/LiNO_3$ and NH_3/NaSCN) and study on the influence of the thermodynamic property database source, for NH_3/H_2O mixture, for cycle performance analysis.
- Propose new absorption cycle configurations for the co-production of mechanical power and cold using low-grade heat sources (< 200 °C). And also, compare the energetic and exergetic performances of the cycles, first, with other combined absorption cycle in the literature and then with available technologies for separate production of mechanical power and cold.
- A basic single-stage combined absorption cycle modification using compression boosters, such as mechanical compressor and vapour ejector, to improve its performance and extend operational working range. And also, analyse the performance potential of non-conventional Ammonia/Salt mixtures ($NH_3/LiNO_3$ and NH_3/NaSCN) in combined absorption cycles.
- Propose new cycle configuration for the co-production of mechanical power and cold for the effective utilization of mid-grade heat sources (between 200 °C and 300 °C). And then, performance potential improvement using pressure recovery devices like vapour-liquid ejector.
- Develop a semi-empirical model for a scroll expander working with pure fluid (NH_3) and NH_3/H_2O mixtures. Furthermore, integration of scroll expander semi-empirical

model into combined absorption cycles global model to represent the performance of the work developing device in the cycles.

- Finally, develop and demonstrate representative case for the integration of combined absorption cycles with solar thermal plant for a specific location and application. Two representative cycle configurations (well-known Goswami cycle and basic single-stage combined absorption cycle using NH_3/H_2O, $NH_3/LiNO_3$ and NH_3/NaSCN working fluid mixtures for latent cooling output) are considered.

1.5 Thesis Structure

In the first chapter, overview of different thermal resources including solar, geothermal, bioenergy and waste heat were presented. Then, a review on the state-of-the-art of the different technologies for separate production of electrical (or mechanical) energy and cold were provided. Finally, the current options for the co/tri-generation of cooling, heating and power are briefly described from the technical and performance perspectives. It is then followed by the description of the general and specific objectives of the thesis. The remaining chapters of the thesis are organized as follows.

In Chapter 2, fundamentals of combined absorption power and refrigeration cycles are presented and discussed. Performance evaluation criteria that account for the thermodynamic quality of the useful dual-outputs of the cycle are defined and later used to evaluate the energetic and exergetic performance of the combined absorption cycles. Then, a literature review on various cycle configurations are provided including the well-known Goswami combined power/cooling cycle. Chapter 2 also presents a comprehensive review on the thermophysical properties of ammonia based working pairs (NH_3/H_2O, $NH_3/LiNO_3$ and NH_3/NaSCN) used to calculate the performance of the studied cycles and influence of NH_3/H_2O thermodynamic property database source on the cycle performance analysis is presented in detail.

Chapter 3 presents the energetic and exergetic performance analysis and operational characteristics of a new class of combined absorption cycles developed for the simultaneous and/or alternative production of mechanical power and cold by using low-grade heat sources (< 200 °C). This chapter also deals with the comparison of these new cycle config-

urations with the well-known Goswami combined power/cooling cycle at the same thermal boundary conditions. Finally, a comparison with technologies for the separate production of power and cold on the basis of driving input energy consumption is covered.

Chapter 4 deals with single-stage combined absorption cycle configuration modifications using compression boosters (mechanical compressor and vapour ejector) in order to improve cycle performance and extend its operational working ranges. Performance analysis of the combined absorption cycles, using non-conventional working fluid pairs (ammonia/salt mixtures: $NH_3/LiNO_3$ and $NH_3/NaSCN$) are also presented.

Chapter 5 is dedicated to the energetic and exergetic analysis of a new combined absorption cycle proposed for the co-production of mechanical power and cold for efficient utilization of mid-grade heat sources (between 200 °C and 300 °C). Effect of cycle modification, using pressure recovery devices like vapour-liquid ejector, on the performance improvement of the cycle is also presented.

In Chapter 6, a semi-empirical model for a scroll expander using pure fluid (NH_3) and NH_3/H_2O mixture (with high concentration of NH_3) as working fluid is developed and presented. This model is validated with experimental data obtained in a test bench and is able to estimate the main outputs (mass flow rate, shaft power and exhaust temperature) of the model with good accuracy. Then, it is scaled-up to estimate the performance of other scroll expanders with higher swept volume, in the same family series. Finally, this semi-empirical model is integrated into the combined absorption cycles global model for the purpose of representing the performance of the work developing expansion device in the cycles.

Chapter 7 deals with the integration of some of the proposed combined absorption cycles with solar thermal plants to cover the typical variable cooling and power demands of a building. To compare the configurations, the energetic and exergetic analysis of the solar absorption power and cooling system is performed for a specific case located in Sevilla (Spain) using TRNSYS software as simulation tool.

Finally, **Chapter 8** gives the general conclusions and future outlooks regarding the study reported in this thesis. The future outlooks are given in a way focusing on what has been missing or lacking in the course of study and provide suggestion for future research directions.

Chapter 2

Combined Absorption Power and Refrigeration Systems

Major parts of this chapter has been published in:

Renewable and Sustainable Energy Reviews, 21(May): 728-748, 2013. An overview of combined absorption power and cooling cycles by ***Dereje S. Ayou****, Joan Carles Bruno, Rajagopal Saravanan and Alberto Coronas.*

"This page intentionally left blank"

2.1 Introduction

In this chapter, a review of absorption cycles proposed in the literature for the co-production of power and refrigeration (cooling) is presented. The concept of combined absorption cycles is explained in terms of idealized energy conversion systems to describe it within the larger context of all the thermodynamic possibilities. The dual-output nature of these cycles makes it difficult to evaluate their performance so the various criteria used in the literature are presented and discussed. Ammonia/water mixture is the most commonly used working fluid in this type of systems and, accordingly, its property database sources are reviewed. Further, the influence of thermodynamic property database sources on cycle performance analysis is evaluated using a typical combined absorption cycle (Goswami cycle) configuration. Other ammonia based mixtures such as ammonia/$LiNO_3$ and ammonia/NaSCN can also be used in this type of systems in order to avoid the need for the rectification process in ammonia/water systems. The information on the thermophysical properties of these mixtures is limited and the available sources are reviewed.

2.2 Fundamentals of Combined Absorption Cycles

Absorption cycles are designed mainly for serving one particular purpose such as cooling (refrigeration cycles), heating (heat pumps) or power generation (i.e., Kalina cycles). In general, two or more independent flow streams exist in absorption cycle configurations. Hence, two or more useful purposes can be served simultaneously and/or alternatively using a new class of absorption cycle configuration architectures. The main advantages of these classes of absorption cycles, hereafter called combined absorption cycles, are their abilities to use a single heat source for producing multiple useful outputs. The outputs include electrical (or mechanical) power and cold at different temperature levels.

In this section the concept of combined absorption cycles suitable for co-production of power and cold is explained in terms of idealized energy conversion systems (cycles). They are described within the larger context of all the thermodynamic possibilities. An absorption refrigeration cycle can be regarded as, at least in a simplified way, a three-temperature-level heat conversion cycle (Fig. 2.1 (a)) that uses driving heat input ($\dot{Q}_2$) at high temperature (T_2), produce cold ($\dot{Q}_0$) at low temperature (T_0) and rejects heat ($\dot{Q}_1$)

at medium temperature (T_1).

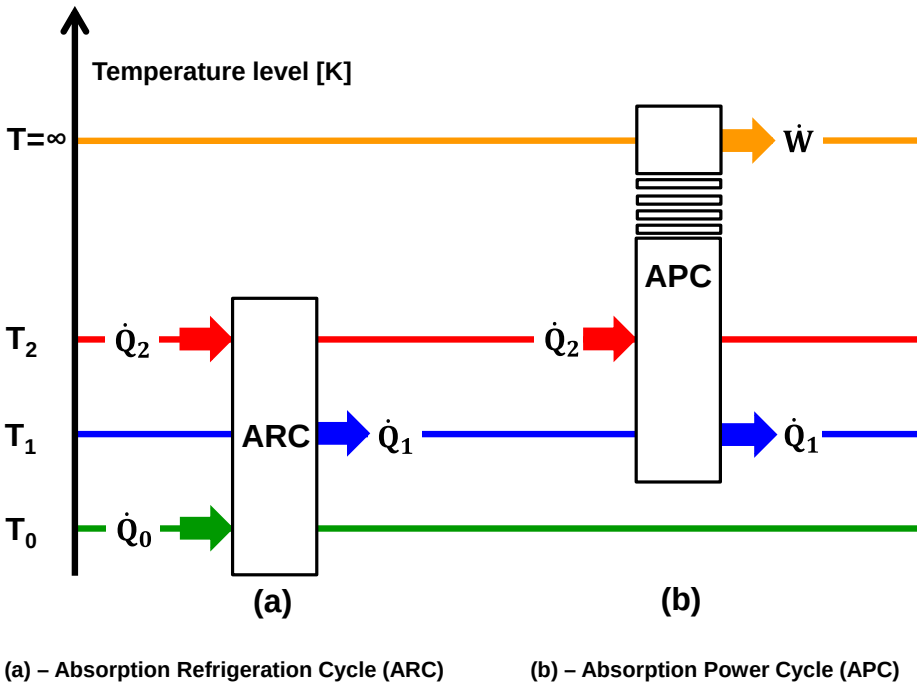

Figure 2.1: Generic thermally-driven cycles for separate production of power and cold.

Applying the first and second laws of thermodynamics for the cycle under reversible (ideal) condition:

$$\dot{Q}_2 + \dot{Q}_0 - \dot{Q}_1 = 0 \tag{2.2.1}$$

$$\frac{\dot{Q}_2}{T_2} + \frac{\dot{Q}_0}{T_0} - \frac{\dot{Q}_1}{T_1} = 0 \tag{2.2.2}$$

The refrigerator (chiller) efficiency to describe the quality of the conversion of heat into cold can be defined using the COP that for a reversible absorption chiller is:

$$COP_{rev} = \frac{\dot{Q}_0}{\dot{Q}_2} = \frac{T_0}{(T_1 - T_0)} \frac{(T_2 - T_1)}{T_2} \tag{2.2.3}$$

The expression in Eq. 2.2.3 is frequently referred as the Carnot COP[1] for cold production. The COP of an absorption chiller is lower than the Carnot COP since it accounts for both the internal and external irreversibilities.

[1] Thermodynamic limit for cycles operating between isothermal heat source and sink.

The efficiency of a reversible thermal power cycle, like the simplified absorption power cycle shown in Fig. 2.1 (b), can be defined as

$$\eta_{rev} = \frac{\dot{W}}{\dot{Q}_2} = \frac{(T_2 - T_1)}{T_2} \tag{2.2.4}$$

and combining with Eq. 2.2.3:

$$COP_{rev} = \frac{T_0}{(T_1 - T_0)} \eta_{rev} \tag{2.2.5}$$

Comparing Eqs. 2.2.3 and 2.2.4 under similar thermal boundary conditions, it can be seen that the reversible power cycle efficiency (Eq. 2.2.4) has to be multiplied by the factor $T_0/(T_1 - T_0)$, which is typically in the order of 10 [71]. This means that with similar low temperature heat sources significantly more cold is produced (mostly about ten times as much, as it is illustrated in Fig. 2.2 for typical operating conditions) than mechanical/electrical energy.

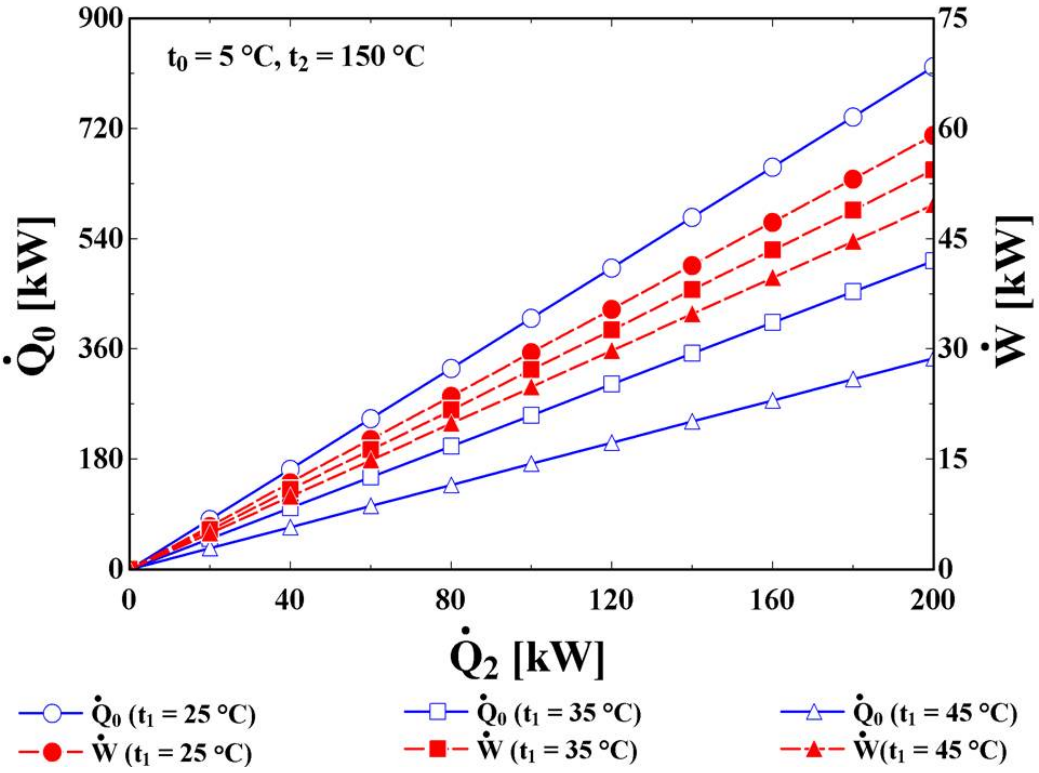

Figure 2.2: Power and cold production using separate ideal absorption power and refrigeration cycles (APC and ARC, respectively, in Fig. 2.1).

2.2.1 Combined power and cold

In a Combined Absorption System (CAS) (see Fig. 2.3), the driving heat input ($\dot{Q}_2$) is now the energy that is required to drive both the power and cold production processes.

$$\dot{Q}_2 = \dot{Q}_{2,power} + \dot{Q}_{2,cold} \tag{2.2.6}$$

being $\dot{Q}_{2,power}$ and $\dot{Q}_{2,cold}$ the heat required for the production of power and cold respectively, and $\dot{Q}_2$ the total amount of provided heat. In this case, two independent parameters are needed to describe the energetic performance of the combined absorption system since we have two useful outputs: the electrical/thermal efficiency ($\dot{W}/\dot{Q}_2$) and the cooling COP ($\dot{Q}_0/\dot{Q}_2$), or one of these plus the power-to-cold ratio ($\dot{W}/\dot{Q}_0$). Accordingly the following equations are obtained. For reversible power and cooling processes:

$$\eta_{rev} = \frac{\dot{W}}{\dot{Q}_{2,power}} = \frac{(T_2 - T_1)}{T_2} \tag{2.2.7}$$

$$COP_{rev} = \frac{\dot{Q}_0}{\dot{Q}_{2,cold}} = \frac{T_0}{(T_1 - T_0)} \frac{(T_2 - T_1)}{T_2} \tag{2.2.8}$$

By combining Eqs. 2.2.6 to 2.2.8, the following expressions for the performance parameters are obtained:

$$\frac{\dot{Q}_0}{\dot{Q}_2} = \frac{((T_2 - T_1)/T_2)(T_0/(T_1 - T_0))}{1 + (T_0/(T_1 - T_0))(\dot{W}/\dot{Q}_0)} = \frac{COP_{rev}}{1 + (T_0/(T_1 - T_0))(\dot{W}/\dot{Q}_0)} \tag{2.2.9}$$

$$\frac{\dot{W}}{\dot{Q}_2} = \frac{(T_2 - T_1)/T_2}{1 + ((T_1 - T_0)/T_0)(\dot{Q}_0/\dot{W})} = \frac{\eta_{rev}}{1 + ((T_1 - T_0)/T_0)(\dot{Q}_0/\dot{W})} \tag{2.2.10}$$

It can be seen that when power production is zero in Eq. 2.2.9 or the cold output is zero in Eq. 2.2.10 the problem reduces to the simple separate production of power and cold.

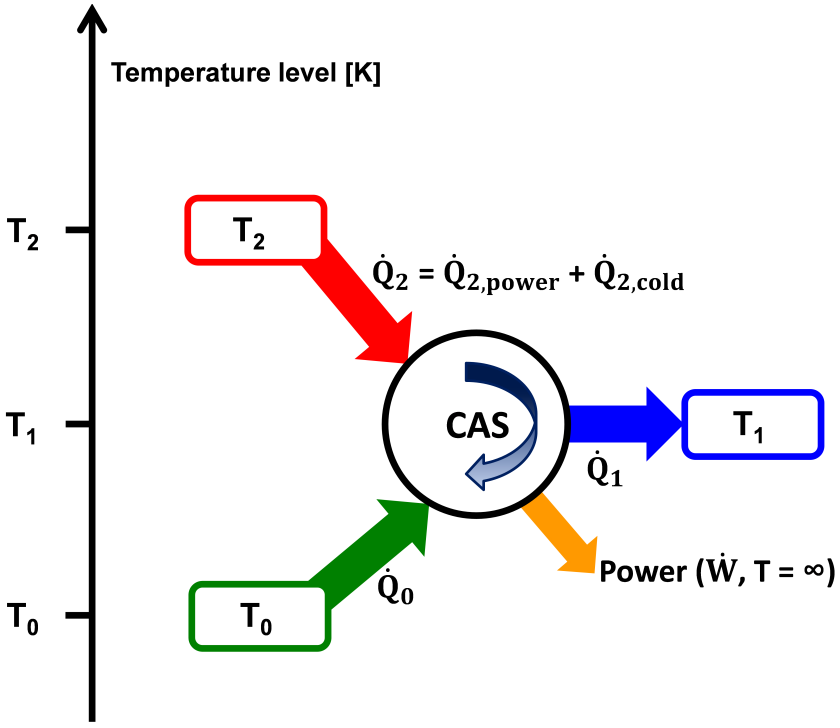

Figure 2.3: Diagram of combined absorption system (CAS) for co-production of power and cold from a heat source.

One of the main limitations of the aforementioned simplified analysis is that the heat flows are assumed at fixed temperature levels. In fact in most scenarios, there is a temperature glide in the heat supply as well as heat rejection processes. A typical example could be the use of sensible driving heat sources (mostly in liquid/gas form), chilled fluid, and cooling water/air as a heat rejection medium. Furthermore, temperature glide is an inherent feature of absorption and desorption processes in absorption cycles due to the presence of multi-component working fluid in the system [72]. Therefore, the most realistic approach to represent the thermodynamic limits of absorption refrigeration and power cycles is by using a reversible cycle with non-isothermal heat addition and rejection processes: that means the appropriate reversible cycle for such types of systems is the Lorenz refrigerator and heat-engine. A T-S diagram of a Lorenz cycle with its processes description is illustrated in Fig. 2.4.

The efficiency of the Lorenz cycle (heat-engine) is defined as

$$\eta_{Lorenz} = \frac{\dot{W}}{\dot{Q}_2} = \frac{\int_b^c TdS - \int_a^d TdS}{\int_b^c TdS} \tag{2.2.11}$$

It is relatively more complex and tedious to calculate the efficiency of the Lorenz heat-engine using Eq. 2.2.11. As a consequence, conceptual simplification is often applied in the efficiency expressions of the Lorenz cycle. First, the cycle is considered as an "equivalent Carnot cycle" operations between two thermodynamic mean temperature levels that corresponds to the constant heat source and sink temperatures of the equivalent Carnot cycle. Then, these thermodynamic mean temperatures (also called entropic average temperatures: $\hat{T}_1$ and $\hat{T}_2$) are defined as follows.

$$\hat{T}_1 = \frac{\int_a^d T dS}{S_d - S_a} \quad and \quad \hat{T}_2 = \frac{\int_b^c T dS}{S_c - S_b} \tag{2.2.12}$$

The entropic average temperatures can also be defined as the ratio of enthalpy difference to entropy difference: $\hat{T}_1 = \frac{h_d - h_a}{s_d - s_a}$ and $\hat{T}_2 = \frac{h_c - h_b}{s_c - s_b}$. Further, for constant specific heat capacity fluids, the entropic average temperatures can be expressed only in terms of temperatures as $\hat{T}_1 = \frac{(T_d - T_a)}{Ln(T_d/T_a)}$ and $\hat{T}_2 = \frac{(T_c - T_b)}{Ln(T_c/T_b)}$.

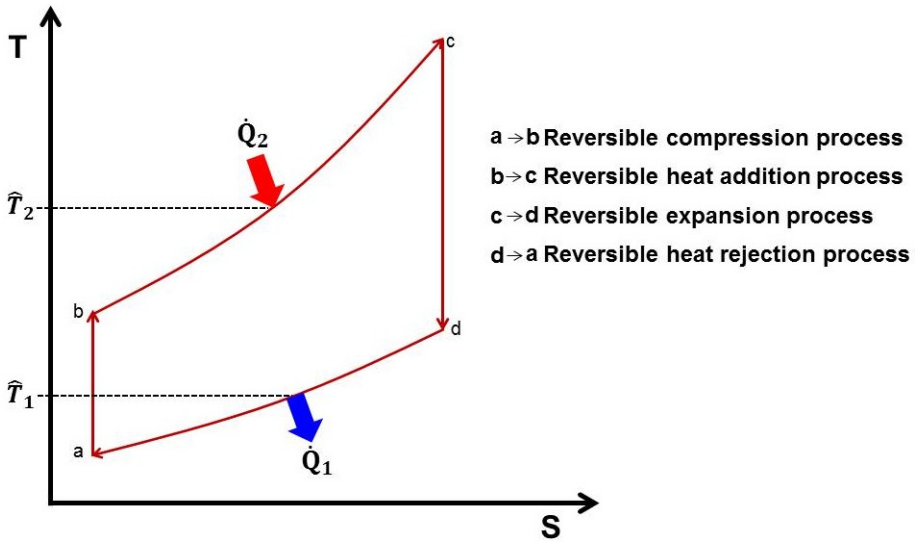

Figure 2.4: Reversible system with non-isothermal heat addition and rejection processes (Lorenz cycle).

Finally, the above expressions for the performance parameters of reversible chillers, power plants and combined absorption systems can also be applied effectively when they are interacting with varying temperature heat sources and sink by replacing the temperatures (T_2, T_0 and T_1) by the corresponding thermodynamic mean temperatures of non-isothermal heat sources and sink ($\hat{T}_2$, $\hat{T}_0$ and $\hat{T}_1$ respectively).

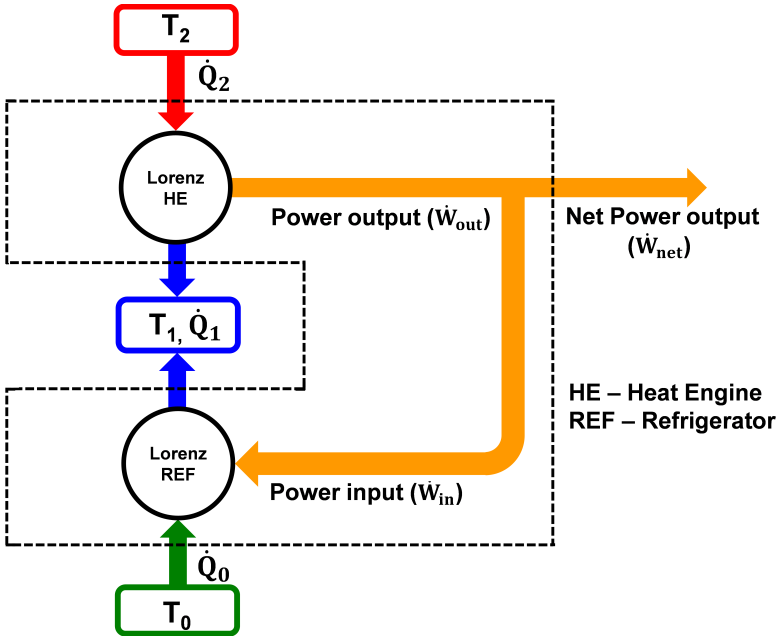

Figure 2.5: Schematic diagram of cascaded Lorenz heat engine and refrigerator cycles.

There are two essential objectives when evaluating the performance of a system: one is to choose the parameters that lead to the best system performance; and the other is to compare the system with other energy conversion options [73]. Energy (first law), exergy and second law-based criteria are often used to assess the performance of energy conversion systems [73]. Since there are two different kinds of simultaneous useful outputs (power and cold), the quality of the cold output of the cycle needs to be determined in order to define its energetic and exergetic efficiency. To apply the conventional definition of second law efficiency for a combined absorption cycle, a suitable reversible cycle must first be defined.

As explained before, for cycles with variable temperature heat addition and rejection processes, the corresponding reversible cycle should be the Lorenz cycle type [73]. For the same thermal boundary condition a cascaded Lorenz heat-engine and refrigerator (shown in Fig. 2.5) can define an ideal combined absorption cycle.

2.2.2 Performance evaluation criteria: performance indicators

The useful outputs of the combined absorption cycles are different on their energy (thermodynamic) quality: mechanical power and cold (refrigeration) which are not akin to add them in the definition of cycle efficiencies. When the cold output of the combined absorption cycle is weighted by a factor, *f*, to account for its thermodynamic quality:

- The energetic (first law) efficiency (η_I):

$$\eta_I = \frac{\dot{W} + f\dot{Q}_0}{\dot{Q}_2} \tag{2.2.13}$$

- Exergetic efficiency (η_{ex}):

$$\eta_{ex} = \frac{\dot{W} + f\dot{Q}_0}{\Delta\dot{E}x_{hs}} \tag{2.2.14}$$

Since a sensible heat source provides the driving heat of the cycle, the denominator in Eq. 2.2.14 is the change in exergy of the heat source fluid. In the literature, different weight factors (f) for the cold produced by the combined absorption cycle are often used in the above efficiency expressions and in other similar efficiency expressions as well. The different cases are illustrated below:

Case I. In this case, the general form of the basic concept to measure the performance of the energy conversion systems used to define the first law efficiency of energy conversion systems as useful output per driving input. Accordingly, the energy (first law) efficiency of the combined absorption cycle is defined by adding the two different outputs (power and cold) directly as useful output of the system. In this case, the factor f in Eq. 2.2.13 is one ($f = 1$). In this type of first law efficiency definition, the quality of the cold obtained from the combined absorption cycle is not accounted for, resulting in the first law efficiency of the cycle being overestimated. In some cases it is closer to the thermodynamic limit of the first law efficiency or even exceeds it [73].

Case II. An appropriate and thermodynamically consistent way to account for the quality of the cold, in first law and exergy efficiency definitions, produced by the combined absorption cycle is to replace the cold output of the cycle by the exergy ($\dot{E}x_{cold}$) associated with the cooling effect. This is equivalent to replacing the cold output by the minimum possible work required to produce it, which means that the cold output is weighted by the reciprocal of the reversible refrigeration cycle COP ($f = {}^1/_{COP_{rev}}$). Efficiency expressions based on this weight factor can be used to compare the thermodynamically consistent performance of the combined absorption cycle with other combined power and cold producing options. However, in this case the cold output is not realistically weighted because the actual (real)

work input required to produce the same cooling effect is quit high due to the internal and external irreversibilities inherent in real refrigeration cycle processes.

Case III. In order to weight the cold output of a combined absorption cycle realistically, the cold output must be weighted by a practically achievable cooling COP ($COP_{practical}$) or dividing the exergy of the cold ($\dot{E}x_{cold}$) by a reasonable second law efficiency for a refrigeration system ($\eta_{II,ref}$). On the basis of this factor the first law and exergy efficiencies of the combined absorption cycle also referred to by Vijayaraghavan and Goswami [73] as effective efficiencies defined as:

$$\eta_{I,eff} = \frac{\dot{W} + \dot{Q}_0/COP_{practical}}{\dot{Q}_2} = \frac{\dot{W} + \dot{E}x_{cold}/\eta_{II,ref}}{\dot{Q}_2} \tag{2.2.15}$$

$$\eta_{ex,eff} = \frac{\dot{W} + \dot{Q}_0/COP_{practical}}{\Delta\dot{E}x_{hs}} = \frac{\dot{W} + \dot{E}x_{cold}/\eta_{II,ref}}{\Delta\dot{E}x_{hs}} \tag{2.2.16}$$

In some cases the combined absorption cycle operates in such a way that the output of the cycle is only power. Eqs. 2.2.15 and 2.2.16 can be used to compare the performance of a cycle that produces both power and one that produces only power.

For an identical cold-to-power ratio (r) in the combined absorption cycle and the corresponding reversible cascaded cycle, second law efficiency (η_{II}) using a weight factor f for the cold, which is dependent on the thermal boundary conditions (Case II):

$$\eta_{II} = \frac{\eta_I}{\eta_{Lorenz}[1 + (r(f - 1/COP_{Lorenz})/1 + r/COP_{Lorenz})]} \tag{2.2.17}$$

It is a measure of the energetic performance of the combined absorption system with respect to its corresponding reversible system (cascaded Lorenz heat-engine and refrigerator, as illustrated in Fig. 2.5).

The results of the idealised performance parameters presented in the present section are independent of the working fluid properties. However, the efficiency, design and operational characteristics (such as the temperature and pressure working ranges) of real (irreversible) cycles are determined to a larger extent by the properties of the working fluid which causes various internal irreversibilities and the method used to calculate its thermodynamic properties also has a significant effect (see section below).

2.3 Ammonia based Working Fluid Mixtures

Many thermodynamic cycles have been used with such finite (sensible) sources as solar thermal, geothermal and waste heat to produce power using a pure component working fluid. In these cycles more than half of the driving heat transfer occurs during the boiling process. Since the boiler operates at essentially constant pressure, the temperature is also constant during the boiling of the working fluid. This results in a mismatch between the temperature profile of the heat source and the working fluid. Consequently, there is significant exergy destruction during the process of heat addition in the boiler.

One of the methods that can be used to reduce this exergy destruction (or irreversibility) is to use multi-pressure boiling. The other option is to use non-azeotropic mixtures as a working fluid (e.g. ammonia/water) in a Kalina cycle. Non-azeotropic mixtures have variable boiling temperatures during a boiling process at constant pressure, which means that they provide a good thermal match with the sensible heat source [74].

2.3.1 Ammonia/water (NH_3/H_2O) mixture

Ammonia/water is the most extensively used binary mixture in absorption power cycles and combined absorption cycles. In power cycles, it has shown that it can provide higher thermal efficiencies than the conventional Rankine cycle with steam as a working fluid in different thermal boundary conditions ([75]-[86]). The correlations for the thermodynamic properties of NH_3/H_2O mixtures play a vital role in calculating the performance of the cycles. Most of the correlations that have been proposed ([87]-[98]) were developed for pressures and temperatures that are lower than those commonly found in conventional power cycles. Table 2.1 shows the correlations that have been used in the literature to analyse NH_3/H_2O absorption cycles with their pressure and temperature application ranges. The theoretical bases of the correlations are also presented in Table 2.1.

To improve the cycle efficiency operating at high temperatures and pressures, relevant data needs to be provided for regions beyond those covered by the present data. Combined absorption systems that use the NH_3/H_2O mixture as working fluid can only be designed if accurate thermodynamic properties data of the mixtures is available over a wide range of T, p, X, including near and supercritical regions. Thorin et al. [100] compared the correlations

developed by various sources ([87]-[90]). The difference in saturation temperature for the different correlations is as high as 20%, and the difference in saturation enthalpy 100% when the pressure is 20 MPa.

Nowarski and Friend [101] presented an application of the "one-fluid extended corresponding states method" for calculating the thermodynamic surface of the NH_3/H_2O mixture. The results show a strong temperature and composition dependence of both interaction parameters for the liquid, as well as for the vapour phase. Formulating the binary interaction parameters as functions of temperature and composition significantly improves the accuracy of density and pressure predictions at saturated conditions. The authors also evaluated the statistical quality of the method using the data available on the thermophysical properties of the mixture.

The influence of various correlations for predicting thermophysical properties on determining the size of heat exchangers is reported by Thorin [102]. Different correlations for predicting the thermodynamic and transport properties give differences in the individual heat exchanger area of up to 24% and 10%, respectively. For the total heat exchanger area, the influence of the various correlations for the thermodynamic properties is 7% but for the transport properties it is not larger than 3%. A difference in the total heat exchanger area of 7% predicted by the thermodynamic properties would probably be less than 2% of the total cost of the process equipment.

Table 2.1: NH_3/H_2O mixture property correlations range available in the literature.

Reference	**Correlation basis**	**Application range**	
		Pressure [bar]	**Temperature [°C]**
El-Sayed and Tribus [87]	EoS and Gibbs excess energy	0.1–110	27–499
Ibrahim and Klein [88]	Extension of Ziegler and Trepp model using measured data from [99]	0.2–110	−43–327
Park [89]	Based on the law of corresponding states	up to 200	up to 377
Stecco and Desideri [90]	EoS and Gibbs excess energy	up to 115	n/a
Smolen et al. [91]	Cubic EoS	up to 34	20–140
Moshfeghian et al. [92]	Cubic EoS and Group contribution theory	up to 35	up to 121
Ziegler and Trepp [93]	EoS and Gibbs excess energy	up to 50	up to 227
Ikegami et al. [94]	Benedict–Webb–Rubin EoS	up to 25	up to 107
Friend et al. [95]	Based on the law of corresponding states	up to 35	up to 177
Patek and Klomfar [96]	Empirical polynomial correlations	up to 20	up to 200
Tillner-Roth and Friend [97]	Complete thermodynamic model based on the Helmholtz free energy equilibrium equations	up to 400	n/a
Xu and Goswami [98]	Gibbs free energy method for mixture properties and empirical T_{bubble} and T_{dew} equations for vapour-liquid equilibrium	0.2–110	−43 to 327

EoS - Equations of State; T_{bubble} - Bubble point temperature; T_{dew} - Dew point temperature; n/a - not available.

Mejbri and Bellagi [103] formulated and compared three different approaches to model the thermodynamic properties of the NH_3/H_2O mixture. They are an empirical Gibbs free energy model, a semi-empirical approach based on the Patel-Teja cubic equation of state and a theoretical approach based on the PC-SAFT (Perturbed Chain Statistical Associating Fluid Theory) equation of state. The Gibbs free energy model is the most flexible and can describe the thermodynamic surface of the ammonia/water mixture up to 80 bar and 227 °C. It is used for medium temperatures and pressures, while the PC-SAFT equation of state is recommended for very high temperatures and pressures.

The PVTx properties of the NH_3/H_2O mixture have been measured by Polikhronidi et al. [104] in the near and supercritical regions using a high-temperature, high-pressure, constant-volume adiabatic calorimeter-piezometer, along 40 liquid and vapour isochores between 120.03 kg/m^3 and 727.75 kg/m^3, at temperatures between 28 °C and 36 °C and at pressures up to 28 MPa. Temperatures and densities at the liquid-gas phase transition curve, dew- and bubble-pressure points, and the critical parameters for the mixture were obtained using two different methods: namely, quasi-static thermograms and isochoric (P-T) break-point techniques. The derived and the measured values of the critical parameters such as temperature, pressure and density were found to be in close agreement.

Since the boiling point difference between ammonia ("normal" boiling point: −33.34 °C) and water ("normal" boiling point: 99.98 °C) is relatively low, purification of the vapour stream of NH_3/H_2O absorption cycle is necessary for cold production. Without purification (rectification), water accumulates in the evaporator and reduces the performance of the system. Therefore, a rectifier is required in the NH_3/H_2O absorption cycle designed for cold production in order to ensure the level of purity of the refrigerant NH_3 vapour stream (usually no lower than 99.8%) [105].

2.3.2 Ammonia/Salt ($LiNO_3$ or NaSCN) binary mixtures

Other ammonia based alternative working fluids, such as $NH_3/LiNO_3$ and NH_3/NaSCN, can also be used in combined absorption system (as well as absorption power and refrigeration systems). Since there is a very high boiling point difference between ammonia and inorganic salts like $LiNO_3$ and NaSCN, pure NH_3 vapour is generated during the boiling of the mixtures. Thus, there is no need of rectifier for absorption systems based on these

mixtures. The $LiNO_3$ and NaSCN also offer the advantages of high solubility in NH_3 and no risk of corrosion on materials like steel [106].

The information available on the thermophysical properties of $NH_3/LiNO_3$ and NH_3/NaSCN mixtures is limited ([107]-[113]) and is described briefly below.

2.3.2.1 $NH_3/LiNO_3$ mixture

Aggarwal and Agarwal [107] reported the experimental thermodynamic property data of $NH_3/LiNO_3$ mixtures over a temperature range of -25 °C to 156 °C and pressure up to 2.2 MPa. A composition range from 0 to 70% of $LiNO_3$ mass fraction was considered. Based on the measured vapour-liquid equilibria data, a p-T-X correlation were developed by the authors. They also presented other properties like enthalpy of solution, latent heat of vaporization, integral and differential heat of solutions in the form of tabular and graphical forms. Infante Ferreira [108] presented comprehensive property correlations for the thermophysical properties of $NH_3/LiNO_3$ mixtures in a form suitable for the modelling and simulation of absorption cycles. These correlations are obtained by fitting experimental data, available at that time, collected by the author. The properties include vapour pressure of the mixture, viscosities of solution, densities, thermal conductivities, heat of solution, heat capacities and solution enthalpies.

Libotean et al. (2007 and 2008) ([109],[110]) measured and correlated properties of $NH_3/LiNO_3$ mixtures necessary for the design and thermodynamic evaluation of absorption refrigeration systems. The measured properties include vapour pressure, density, dynamic viscosity and solution heat capacity. The vapour pressure was measured for a temperature range from 20 °C to 80 °C with an NH_3 mass fraction between 20% and 60%. For the other properties, a temperature and composition range of 20 °C to 80 °C and 35% to 65%, respectively, at a constant pressure of 1.8 MPa were considered. Recently, new enthalpy and entropy correlations were developed by Garousi Farshi et al. [111] using the experimental data of $NH_3/LiNO_3$ mixture reported by Libotean et al. ([109],[110]). According to the authors, these correlations are able to predicate the properties of the $NH_3/LiNO_3$ mixture with a maximum error of 2% in the range of temperature between 10 °C and 160 °C and NH_3 mass fraction ranging from 10% to 100%.

2.3.2.2 NH_3/NaSCN mixture

Rogdakis and Antonopoulos [112] presented the thermodynamic properties of NH_3/NaSCN mixtures and they used a nomograph to report the behaviour of the mixture in a compact form that allows also direct estimation of its main characteristics. Chaudhari et al. [113] measured and correlated several thermophysical properties of NH_3/NaSCN mixtures as a function of temperature and composition. It includes density (from −3.8 °C to 77.8 °C at 3.0 MPa), dynamic viscosity (−3.4 °C to 77.8 °C at 3.0 MPa), isobaric heat capacity (31.0 °C to 91.0 °C at 3.0 MPa) and vapour-liquid equilibria data (from −20.0 °C to 120.0 °C). All properties were measured in a range of NH_3 mass fraction from 35% to 90%. The developed correlations were compared with values reported in the literature. Infante Ferreira [108] also presented property correlations of NH_3/NaSCN mixture fitted from experimental data. Analogues to $NH_3/LiNO_3$ mixture, Garousi Farshi et al. [111] also developed new correlations for the enthalpy and entropy of the solution in the range of temperature between 0 °C and 160 °C for an ammonia mass fraction from 30% to 100% with a maximum error of 2%.

The property correlations of $NH_3/LiNO_3$ and NH_3/NaSCN mixtures necessary for the performance evaluations of the combined absorption cycles and used in the subsequent Chapters are provided elsewhere ([109],[110] and [113]).

Ternary working fluid mixtures have also been suggested to overcome some of the drawbacks of the commonly used NH_3/H_2O mixtures as well as the non-conventional $NH_3/LiNO_3$ mixtures. Typical representatives of ternary working fluid mixtures considered in the literature are $NH_3/(H_2O + LiBr)$, $NH_3/(H_2O + LiNO_3)$ and $NH_3/(H_2O + X^+OH^-$, hydroxide) [106]. The addition of salts in NH_3/H_2O mixtures, reduces the amount of water in the vapour generated by boiling the mixture, so less rectification (or no rectification at all) are required. The $NH_3/(H_2O + LiNO_3)$ ternary mixtures have higher heat transfer coefficient and lower viscosity than binary $NH_3/LiNO_3$ mixtures which can improves the performance of the absorption system. However, the boiling temperature of the ternary $NH_3/(H_2O + LiNO_3)$ mixtures is higher than binary $NH_3/LiNO_3$ mixtures.

2.4 Combined Absorption Cycle Configurations: A review

Combined power and refrigeration cycles can use the waste heat rejected from the power cycle to run a coupled heat fired refrigeration cycle (see the block diagram in Fig. 2.6 (a)), such as an absorption refrigeration cycle, in which two cycles are combined to produce power and cold ([114],[115]).

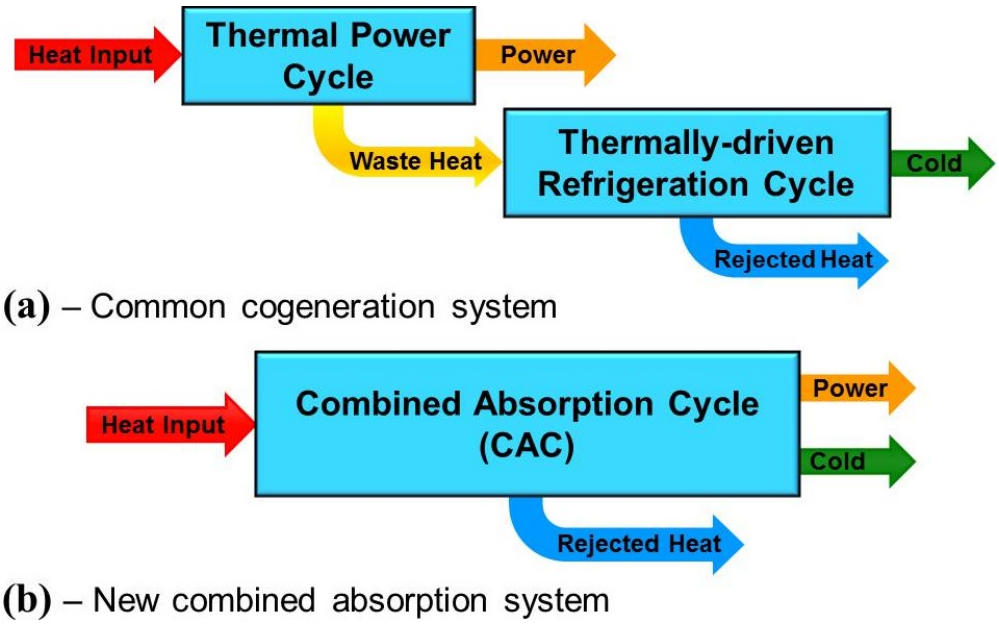

Figure 2.6: Options for combined production of power and refrigeration (cooling).

As mentioned in Chapter 1, such type of cycles are not covered in this study. Moreover, cycles producing power and cooling (and/or heating) using the same thermodynamic cycle without involving absorption process are also beyond the scope of this review section ([116],[117]). In the literature, simultaneous production of power and refrigeration (cooling) is described by several terminologies such as cogeneration, combined production/generation, dual-function, etc. In the sections following, they serve the same purpose.

A unique feature of the combined absorption cycle proposed by Goswami ([118],[119]) is that power and refrigeration (cooling) are simultaneously produced in the same loop. In all his studies Goswami used a binary mixture of ammonia and water, or some organic fluid mixtures, as working fluid [28]. Other NH_3/H_2O cycle configurations have been proposed by various researchers also for the production of power and cold from the same cycle but using different loops. Fig. 2.6 (b) shows the block diagram of combined absorption cycle.

This section focuses on the theoretical and experimental work of Goswami and co-workers and other configurations for producing power and cold with the same cycle proposed by several authors.

2.4.1 Goswami cycle

The Goswami cycle (see Fig. 2.7) basically operates in the following way. A mixture of ammonia and water, known as a basic solution, is pumped from the absorber (state 1) to high pressure (state 2) via the solution pump. It is then split into two streams (states 2A and 2B) which, after recovering heat (states 13 and 14), mixes and enter the desorber (state 3) which is called a boiler by Goswami and co-workers.

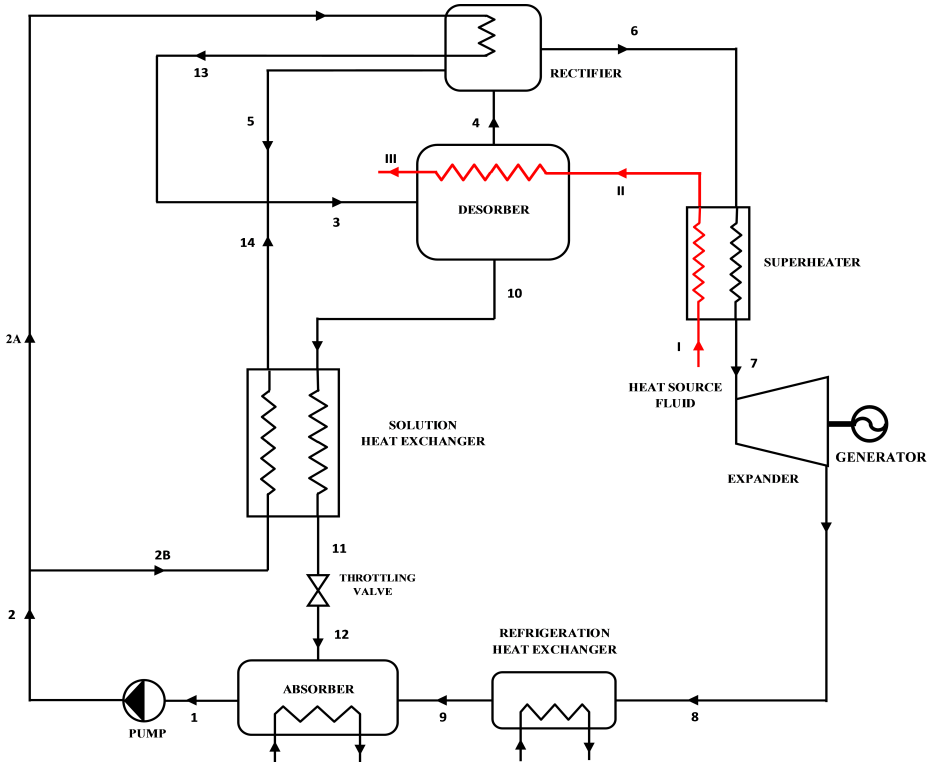

Figure 2.7: Schematic diagram of the Goswami cycle with internally cooled rectifier.

The mixture is partially boiled in the desorber to produce a vapour rich in ammonia (state 4) and a hot weak-in ammonia liquid solution (state 10). A rectifier is used to increase the concentration of ammonia in the vapour, from the desorber, by partially condensing water out of it. The resulting purified vapour (state 6) is superheated (state 7) and then expanded in the expander to produce power. Expanding the vapour (states 7-8)

below the ambient temperature can simultaneously provide power and cold. The cooling effect is obtained by sensible heating of the expander (turbine) exhaust (states 8-9). The weak liquid solution throttles back to the absorber after passing through a solution heat exchanger to recover heat from it (states 10-12). The vapour (state 9) and weak solution (state 12) are used to regenerate the basic solution in the absorber (state 1) and reject the heat from the cycle. In Fig .2.7, the condensed liquid from the rectifier (state 5) is also mixed with the basic solution after recovering heat. Alternatively, it can be re-circulated into the desorber ([120]-[122]) or throttled back to be mixed with the weak solution [123].

The cycle can use waste heat, or solar thermal and geothermal energy, etc. as the source of heat. It can also work as a bottoming cycle for conventional power cycles. The cooling part of the cycle (i.e. the refrigeration heat exchanger, states 8-9) functions because the working fluid is a binary mixture (NH_3/H_2O) and, at constant pressure, the condensing temperature of an ammonia-rich vapour can be significantly lower than the saturation temperature of a lower concentration NH_3/H_2O mixture. To expand the vapour to low temperature in the expander requires a vapour with a high NH_3 concentration and low temperatures at the expander inlet, which does not favour power production. Obviously, superheating of the rectified vapour increases the power production. But, it degrades cold production. Since Goswami proposed the combined absorption cycle, a number of studies have been made on such aspects as parametric analysis, optimization of the cycle, refrigeration output at very low temperatures, and cycle modification for improving resource utilisation to mention just a few. These studies are reviewed below.

Goswami and Xu [120] conducted a parametric analysis to study the effect of the cycle parameters on the performance of the cycle. Application of low heat-source temperatures below 200 °C is one of the characteristics of this cycle. Since it uses the expander exhaust vapour stream by means of a cooler that transfers sensible heat from the chiller water, the cooling output is relatively small. They also reported a procedure for optimising the operating conditions of the cycle for thermal performance [122]. Under optimum conditions for a heat source temperature of 87 °C, both power and refrigeration outputs were achieved. At a source temperature of 167 °C, optimum conditions do not provide any refrigeration output. However, under non-optimum operating conditions a refrigeration output was also possible for the same heat source temperature.

Lu and Goswami [121] focused on the refrigeration part of the total output of the Goswami cycle at low refrigeration temperatures. The performance of the combined cycle was determined at a wide range of low refrigeration temperatures and for a heat source temperature of 87 °C. At each refrigeration temperature, the cycle was optimised for maximum second law efficiency using the Generalized Reduced Gradient (GRG) algorithm. The authors defined the second law efficiency as the ratio of the useful energy output from the cycle to the exergy consumption of the cycle. Based on the type of weight factor used for the refrigeration output, two different second law efficiency definitions were used in the optimisation process. In the denominator of Eq. 2.4.1, the change in exergy of the heat source was calculated assuming that the heat source fluid is recirculated in a closed loop as in the case of a solar thermal system. However, in Eq. 2.4.2 the heat source fluid is assumed to be discharged to the ambient after the heat has been transferred to the working fluid. Lu and Goswami gave the two second law efficiencies as:

$$\eta_{II} = \frac{(\dot{W}_{net} + \dot{Q}_0/COP_{rev})}{\dot{m}_{hs}[(h_{hs}^{in} - h_{hs}^{out}) - T_0(s_{hs}^{in} - s_{hs}^{out})]} \tag{2.4.1}$$

and

$$\eta_{II} = \frac{(\dot{W}_{net} + \dot{Q}_0)}{\dot{m}_{hs}[(h_{hs}^{in} - h_0) - T_0(s_{hs}^{in} - s_0)]} \tag{2.4.2}$$

where η_{II} is the second law efficiency, $\dot{W}_{net}$ is the net power output, $\dot{Q}_0$ is the refrigeration output, COP_{rev} is the coefficient of performance for a reversible (ideal) refrigeration cycle, $\dot{m}_{hs}$ is the mass flow rate of the heat source fluid, h_{hs}^{in} and h_{hs}^{out} are the inlet and outlet specific enthalpy of the heat source fluid, s_{hs}^{in} and s_{hs}^{out} are the inlet and outlet specific entropy of the heat source fluid, h_0 and s_0 are the specific enthalpy and entropy of the heat source fluid at ambient temperature, and T_0 is the ambient temperature.

In the first definition, Eq. 2.4.1, the weight factor used is the reciprocal of the ideal COP ($f = 1/COP_{rev}$) which greatly undervalues the refrigeration output. For the second definition, Eq. 2.4.2, equal weight were given to the thermodynamic quality of both power and refrigeration output ($f = 1$). The refrigeration temperature was as low as −68 °C. The first law efficiency (where $f = 1$) and second law efficiency, based on Eq. 2.4.1, increased initially and then decreased with the refrigeration temperature. At a refrigeration temperature of −28 °C, the first and second law efficiency values reached a maximum of

17.4% and 63.7%, respectively. The trend was similar for the turbine inlet pressure, mass fraction of ammonia in the absorber and the refrigeration output of the cycle with the refrigeration temperature using a $^1/_{COP_{rev}}$ weight factor for the refrigeration output in the second law efficiency definition. When Eq. 2.4.2 is maximized, both first and second law efficiencies drop as the refrigeration temperature decreases.

In order to obtain a simultaneous cooling output a compromise between the work and cooling production exists. For instance, some rectification is needed to produce cooling particularly for a reasonable heat rejection (absorber) temperature such as 35 °C [123]. However, rectification decreases work production because less energy is available (low temperature) and the vapour mass flow rate is lower at the expander inlet. Thus, a new coefficient of performance (effective COP), specific to the Goswami cycle, was proposed to relate the amount of cooling produced with the potential work lost for the combined operation ([123],[124]). The proposed formulation by Sadrameli and Goswami [124] takes the form:

$$COP_{effective} = \frac{Q_{cold}}{W_{work/opt} - W_{w/cold}} \tag{2.4.3}$$

where $COP_{effective}$ is the effective coefficient of performance, Q_{cold} is the cooling heat transfer, $W_{work/opt}$ is ideal work production (optimised using the first law efficiency for work output only by giving no value for cooling) and $W_{w/cold}$ is network output from the cycle in dual-output mode. To optimize this trade-off, a thermodynamic analysis has been carried out using the equation oriented (EO) mode in ASPEN Plus 12.1 [125]. The optimization results confirmed that the conditions for the optimum cooling production are unfavourable for power production. The agreement between the simulation and the experimental results [126] proved that the model developed was accurate. Martin and Goswami [123] evaluated how effective the Goswami cycle was at producing cooling by introducing the effective COP as a new parameter and, therefore, optimizing the gain in the amount of cooling. The maximum overall effective COP of the combined cycle was found to be nearly 1.1 when compared with a work optimised system, which means that for each unit of cooling produced nearly an equal amount of work is generated.

Demirkaya et al. [127] presented a parametric analysis for a Goswami cycle using the ChemCAD process simulator [128]. They studied the performances of the cycle for a wide

range of boiler pressures and basic solution ammonia concentrations, and the effects of the sink for rectification cooling, both internal and external, on the cycle output. Using an external source for rectification cooling, is obtained an effective first law and exergy efficiency of 3% - 5% and 18% - 28% respectively, with a 50% - 75% turbine efficiency and, for a boiler and rectifier temperature of 83.4 °C and 41.7 °C, respectively. The effective first law and exergy efficiency could be increased to 3.5 - 5.5% and 22 - 33%, respectively, for the same turbine efficiency of 50% - 75% by using internally cooled rectifier. The authors claimed that even though the first law efficiency was low, low grade energy (below 100 °C) could be converted into power and refrigeration.

Xu et al. [129] presented a parametric analysis of a Goswami cycle. The simulation studies on this cycle show that the combined cycle achieves a high thermal efficiency of about 23.5% for a heat source temperature of 137 °C, which is higher than the efficiency of the conventional steam power cycle for the same operating conditions. In addition, a system designed to produce 2 MW of electrical power using the cycle will produce more than 700 kW of refrigeration. Using flat-plate or low-concentration solar thermal collectors in this cycle reduced the cost of a solar thermal power plant by 43% in the year 2000.

Pouraghaie et al. [130] optimized the Goswami cycle studied by Xu et al. [129] by varying such design variables as turbine inlet pressure, superheater and condenser temperature. The turbine work, cooling capacity and thermal efficiency of the cycle were first thermodynamically modelled so that the objective functions could be determined. Finally, the Pareto-based optimization approach was used to find the best possible combination of cycle outputs known as Pareto fronts. The results revealed that two extreme points in the Pareto included those of single-objective optimization results and, therefore, provided more choices for optimal output designs.

A second law analysis was made by Vidal et al. [131] of a combined power and refrigeration cycle proposed by Goswami [132]. The Redlich-Kwong-Soave equation of state was used to calculate the thermodynamic properties of the NH_3/H_2O mixture in the cycle simulation. Both reversible and irreversible cycles were simulated so that the effect of irreversibilities on each component could be studied. The exergy effectiveness was about 53% and 51% for the irreversible cycles when the heat source temperatures were 125 °C and 150 °C, respectively. Even though the amount of cooling produced was lower than the

amount of power, the second law analysis of the combined cycle shows that both power and cooling can be produced using low-temperature heat sources even for irreversible cycles.

Hasan et al. [132] analysed a combined power and refrigeration cycle proposed by Goswami ([118]-[120]) using the first and second laws of thermodynamics. They studied its performance for a heat source temperature range of 57 °C to 197 °C provided by low- and medium-temperature solar collectors. The net work output and refrigeration of the cycle, as a percentage of heat input was 16.9% and 1.26%, respectively, giving a first law efficiency of 16.9%. In the first law efficiency definition in Eq. 2.2.13, the exergy of the cooling effect was used to evaluate the contribution of the cooling output (where $f = {}^{1}/_{COP_{rev}}$). The thermodynamic performance of the cycle was optimised for maximum second law efficiency which, according to the definition provided by Eq. 2.2.17, was 65.8% and obtained at a heat source temperature of 147 °C. Exergy analysis was performed to determine the losses in the components of the cycle. About 44% of the total irreversibility occurred in the absorber, while the heat recovery in the rectifier and solution heat exchanger accounted for 16% and 24% of the total irreversibility, respectively. Irreversibility in the boiler was high at very low heat source temperatures but dropped at higher temperatures.

Vijayaraghavan and Goswami [133] performed optimisation studies on a Goswami cycle for maximum second law efficiency (known as Resource Utilization Efficiency (RUE)). They performed exergy analysis and the cycle configuration was modified accordingly using a distillation stage (with two different configurations: namely, configuration 1 and 2 (see Figs. 2.8 and 2.9, respectively)) to improve the RUE.

In the first configuration, a heat source fluid was used for the distillation, while in the second a condensing mixture of weak solution and vapour was used. The first configuration had a slightly higher RUE than the second at lower heat source temperatures. The first law efficiency was also higher at optimised RUE conditions. The authors used first law efficiency based on Eq. 2.2.13 with $f = {}^{1}/_{COP_{rev}}$ and also the effective first law efficiency described in Eq. 2.2.15. The efficiency improved by more than 25% in the modified configurations (configurations 1 and 2). A detailed description of the simulation and optimisation process for the cycle configurations (basic Goswami cycle, modified configurations 1 and 2) can be found elsewhere [134]. The cycle was optimised using a commercially available program called GRG2, which is one of the variations of the GRG algorithm [135].

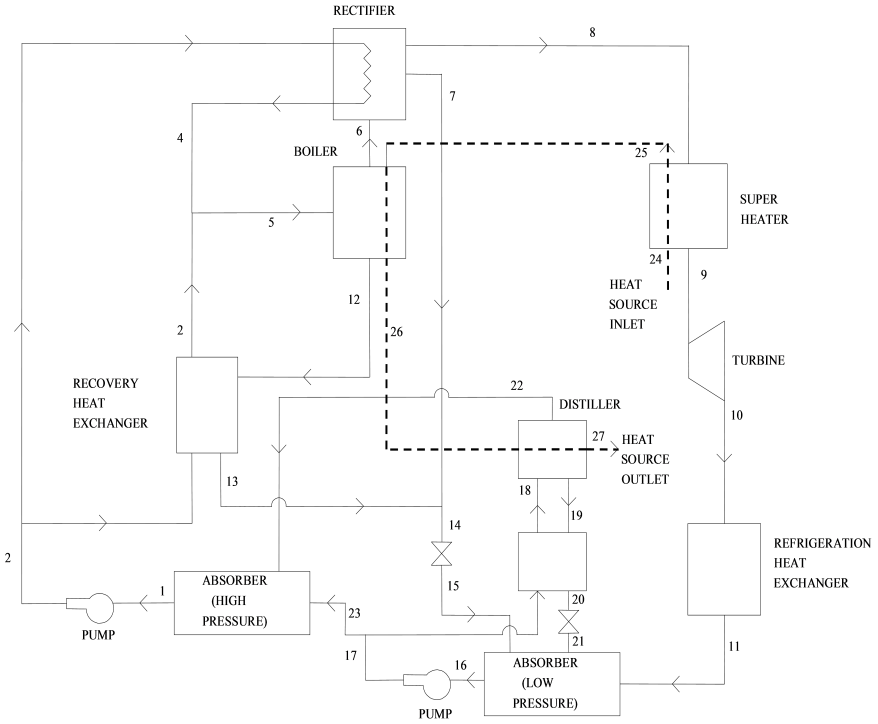

Figure 2.8: Schematic diagram of modified combined absorption power and cooling cycle - Configuration 1 of Vijayaraghavan and Goswami [133].

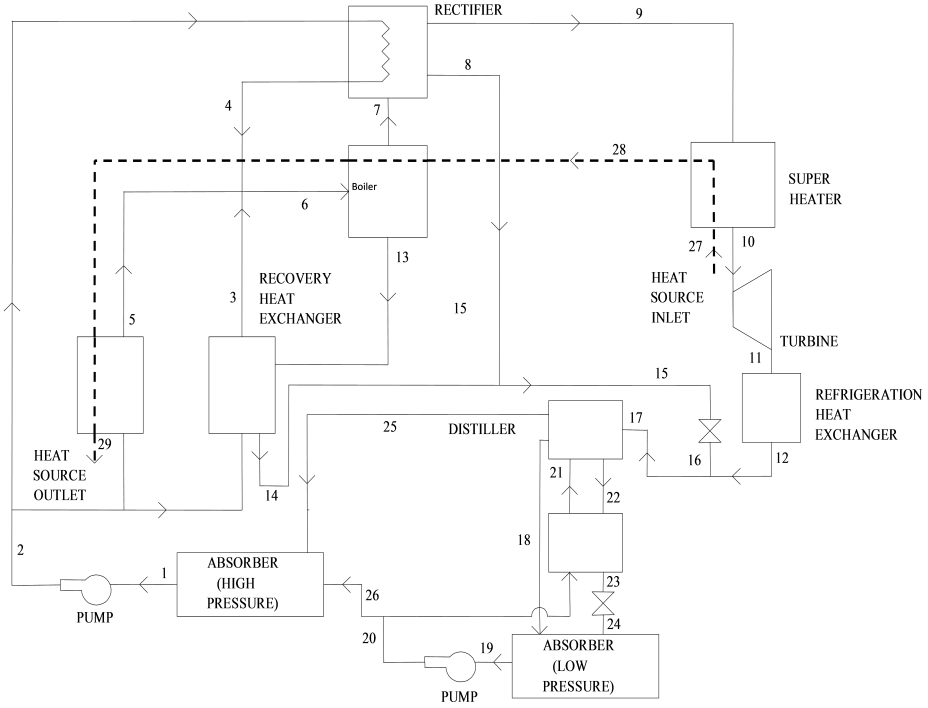

Figure 2.9: Schematic diagram of modified combined absorption power and cooling cycle - Configuration 2 of Vijayaraghavan and Goswami [133].

Since the Goswami cycle can operate as a bottoming cycle as well as an independent combined power and cooling cycle, Zare et al. [136] carried out a detailed thermodynamic analysis, parametric study, and optimization using the waste heat from a gas turbine-modular helium reactor (GT-MHR) to drive the Goswami cycle. The GT-MHR cycle consists of a compressor, a turbine, a helium reactor, a recuperator and a pre-cooler. They optimized both the combined cogeneration (GT-MHR cycle + Goswami cycle) cycle and GT-MHR power cycle based on the energy utilization (first law) and second law efficiencies. The authors showed that, the power generation and the energy utilization and second law efficiencies of the combined cogeneration cycle were increased with an increase in the turbine inlet temperature. The energy utilization and second law efficiencies of the combined cogeneration cycle were about 9 - 15% and 4 - 10% higher than those of the GT-MHR power cycle, respectively at nearly optimum conditions. The parametric study revealed that there is an optimum compressor pressure ratio that maximizes the energy utilization and second law efficiencies of the cycles. At the maximum energy utilization and second law efficiencies the optimum compressor pressure ratio was found slightly higher for the combined cogeneration cycle, which is a disadvantage from economics viewpoint. But, the helium mass flow rate in the combined cogeneration cycle was significantly lower than that in the GT-MHR cycle which can be considered as an advantage economically. Moreover, the size of the combined (GT-MHR cycle + Goswami cycle) cycle components is reduced. They also analysed the exergy losses in the different components of the cycles and their results showed that when the GTM-MHR cycle is combined with the Goswami cycle, the exergy losses in the compressor and the turbine increases whereas the exergy losses in the pre-cooler and in the recuperator decrease. The former is due to higher optimum pressure in the combined cogeneration cycle and the latter is due to several reasons such as: a lower temperature difference between the streams, reduced helium mass flow rate, and heat recovery in the boiler and in the superheater of the combined cogeneration cycle.

The Goswami cycle was also investigated and optimized from the economic point of view [137] using the genetic algorithm method for conducting the optimization process. Considering a practical range of decision variables, the performance of the cycle was assessed to find out their effects on the thermal and exergy efficiencies as well as on the unit cost of the cycle products (power and cooling). The authors obtained results that show the sum

of the unit costs of the products for the cost optimal design is reduced by around 18.6% and 25.9% as compared to that of the thermal efficiency and exergy efficiency optimal designs, respectively. Since the product cost is very low for the cost optimal design case in comparison with other optimal cases (i.e. thermodynamic optimal design cases), they concluded that the cost optimal case is the most promising one at the operating conditions considered in their study. Their result also shows, for each \$3/ton increase in unit cost of the heat source (steam) used, the unit cost of output power and cooling is increased by around \$7.6/GJ and \$15 - 19/GJ, respectively.

Demirkaya et al. [138], performed a multi-objective thermodynamic optimization study on the Goswami cycle by applying multi-objective genetic algorithms. The net work output, cooling capacity, effective first law, and exergy efficiencies of the cycle were considered as objective functions in their Pareto approach optimization of the Goswami cycle. In their study, two case scenarios were analysed. In the first case, the cycle is evaluated as it is a bottoming cycle and in the second case, as it is used as a top cycle that can utilize energy resources such as solar thermal or geothermal sources as well as waste heat. The optimization is carried out by varying selected design variables as basic solution concentration (between 0.2 - 0.65 ammonia mass fractions), rectifier temperature, and boiler temperature and pressure. The boiler temperature is varied between 70 °C - 150 °C and 150 °C - 250 °C for the first and second cases considered in the optimization processes, respectively. In the first case (as a bottom cycle), the results of the multi-objective optimization of the four objective functions showed that there is no conflict between net work output and exergy efficiency, and improving one results in the improvement of the other one. The maximum values of work and exergy efficiency were attained at the maximum boiler temperature. In the second case (top cycle), the authors showed that there is no conflict between network output, effective first, and exergy efficiencies. The optimal point attained at the maximum boiler temperature and minimum basic solution concentration.

According to the research of Padilla et al. [139], the cost of solar power plants which works normally with Rankine cycles can be reduced by improving the efficiency of the thermodynamic cycle employed in the power plant. The authors proposed a combined Rankine-Goswami cycle (GRC) to improve the efficiency of the power plant, the Goswami cycle with NH_3/H_2O mixture as a working fluid being the bottoming cycle. Using a

parabolic trough solar thermal plant with a capacity range of 40 MW to 50 MW, the performance of the combined GRC under full load conditions and with three different boiler exit case scenarios was investigated in order to analyse the effects of the ammonia mass fraction, condenser pressure and rectifier concentration on the net power output, cooling, and effective efficiency.

The three cases considered are: first case (case R) - the ammonia vapour leaving the boiler is rectified and then expanded in the turbine without superheating; second case (R+S) - in this case a superheater is included in the cycle configuration in order to superheat the rectified vapour before entering the turbine for expansion; the third final case (base case, B) - no superheater or rectification process is used (i.e. the vapour leaving the boiler goes directly for expansion without being superheated or rectified). They found out that as the condenser pressure increases (between 0.2 bar to 9 bar), the net work output goes up to a maximum value (57 MW) and then decreases for the case R and case (R+S). However, for the base case (B) as the condenser pressure increases the net power output increases too with the highest net work output value of 85 MW. For the range of condenser pressure between 3.5 bar and 9.0 bar, the cooling capacity of the cycle configuration with a rectifier (case R) is highly sensitive to the ammonia mass fraction. For base case (B), the first law efficiency values were in the range of 29.4% - 36.7% while that for cases R and R+S in the range of 19.2% - 33.3%.

2.4.2 Other ammonia/water cycle configurations

Using NH_3/H_2O as the working fluid, several researchers have proposed new cycle configurations for dual-function (electrical/mechanical power and cold production). These cycles are reviewed in this subsection.

Erickson et al. [140] proposed an NH_3/H_2O absorption cycle configuration that produces power and refrigeration interchangeable (Fig. 2.10). The dual-function absorption cycle is capable of converting low temperature (< 300 °C) sensible heat into power and refrigeration. Fig. 2.10 shows a simplified flow schematic of the cycle. It consists of a heat recovery unit, desorber, recuperator, absorber, turbine with electric generator, condenser and evaporator.

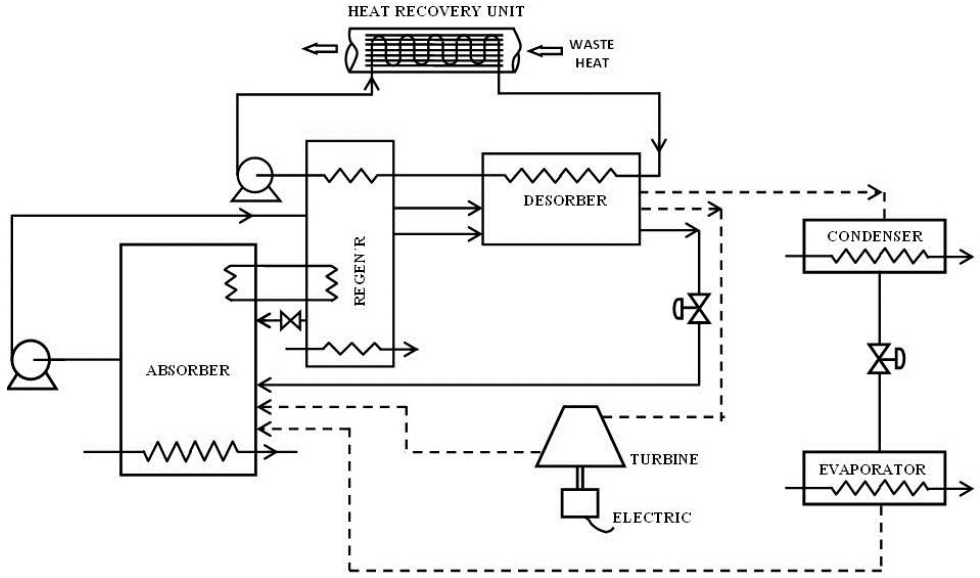

Figure 2.10: Flow schematic of the dual-function absorption cycle of Erickson et al. [140].

Zhang et al. [141] proposed a new NH_3/H_2O system (see Fig. 2.11) for the cogeneration of power and refrigeration. The system operates in a parallel combined mode with an NH_3/H_2O Rankine cycle and an NH_3/H_2O absorption refrigeration cycle, interconnected by absorption, separation and heat transfer processes. The authors found that the cycle has a good thermal performance with energy and exergy efficiencies of 25% and 50.9%, respectively, for the base case considered. The comparison between the cycle and the separate generation of power and refrigeration showed that the new cycle has the advantage that it consumes less energy (21.6% less). Wang et al. [142] studied the performance of a combined refrigeration and power cycle (Fig. 2.12), driven by waste heat but which can be heated by any heat source (e.g. solar energy, geothermal heat or an exhaust flue gas from a gas turbine). This cycle configuration is a modification of the cycle proposed by Zhang et al. [141]. The major difference between the two cycles is that the feed pump and condenser have been removed before and after the turbine in the cycle proposed, which makes the cycle simpler and less costly. A detailed parametric analysis was carried out to study the effect of such parameters as heat source temperature, refrigeration temperature, ambient temperature, turbine inlet pressure and basic solution ammonia mass fraction on the performance of the combined (dual-function) cycle. The authors optimised the thermal parameters in the cycle using the exergy efficiency as an objective function and the genetic algorithm method. The optimised exergy efficiency was 43% for a given condition.

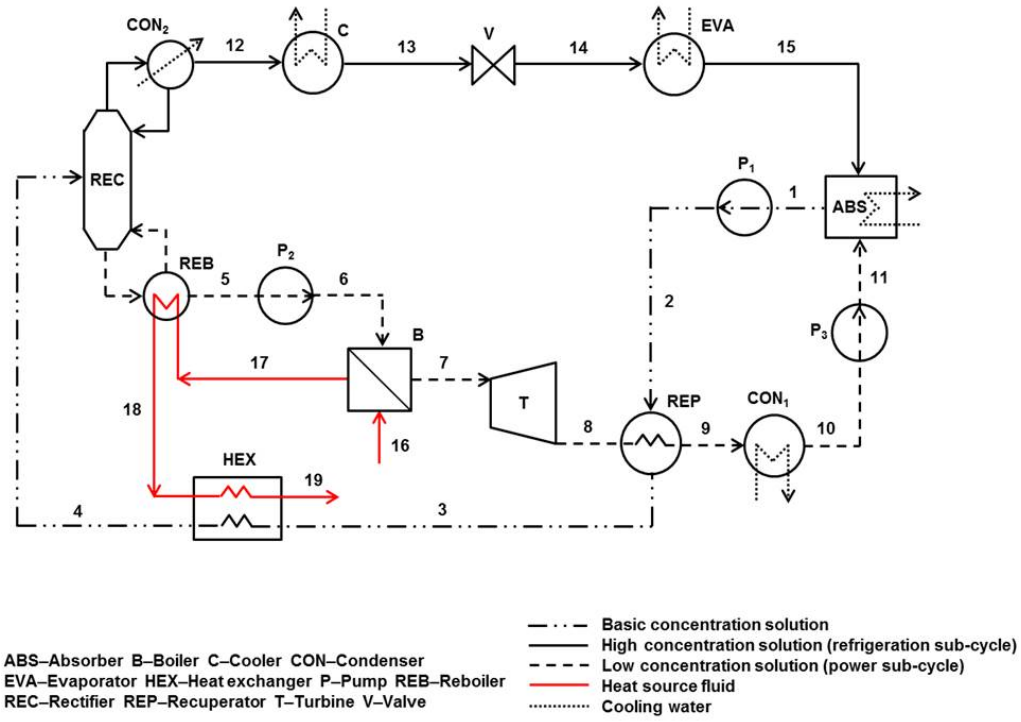

Figure 2.11: Schematic diagram for the cogeneration cycle of Zhang et al. [141].

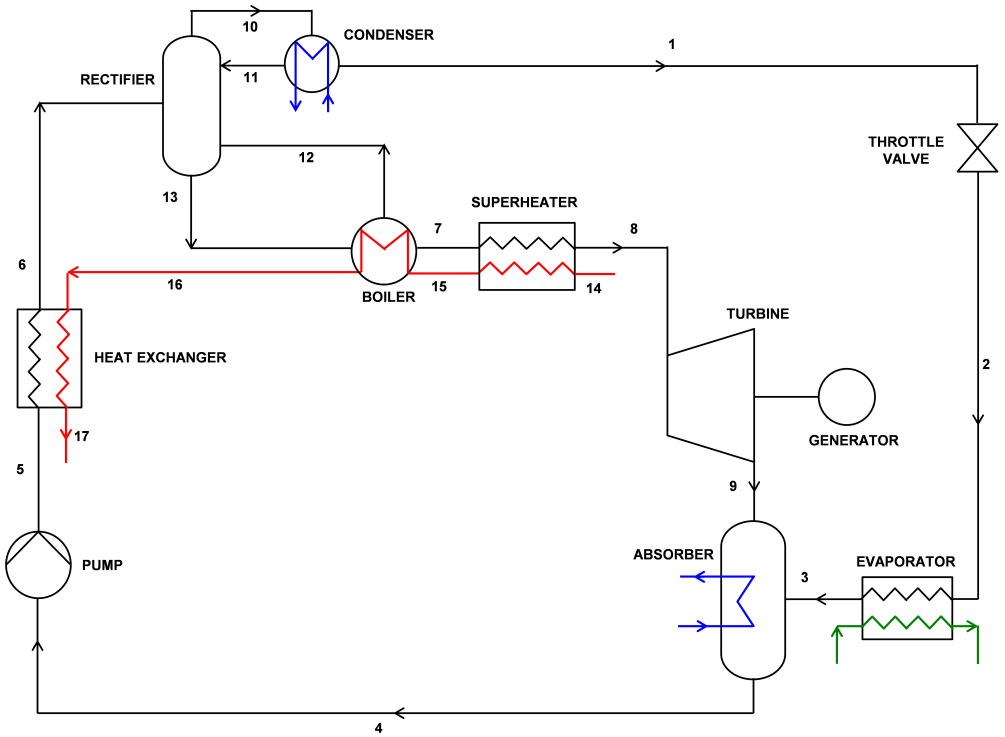

Figure 2.12: Schematic diagram of combined power-refrigeration cycle of Wang et al. [142].

A new combined power and ejector-absorption refrigeration cycle that can be operated by solar, geothermal and industrial waste heat has been proposed by Wang et al. [143]. The proposed cycle (Fig. 2.13) originated from the cycle developed by Wang et al. [142] introduces an ejector between the rectifier and the condenser. The high-pressure ammonia-rich vapour from the rectifier is used as the primary flow entering the ejector, and entrains low-pressure ammonia-rich vapour from the evaporator. As a result of introducing the ejector, the refrigeration capacity can be increased without significantly increasing the capacities of the rectifier and absorber. For instance, in comparison with the cycle in Ref.[142] the refrigeration capacity of the cycle with the ejector increased by 9.5% under the same conditions. Thus, the combined cycle can improve the cycle performance without greatly increasing the complexity of the system. Such parameters as heat source temperature, condenser temperature, evaporator temperature, turbine inlet pressure, turbine inlet temperature, and basic solution ammonia concentration have significant effects on the net power output, refrigeration output and exergy efficiency of the combined cycle.

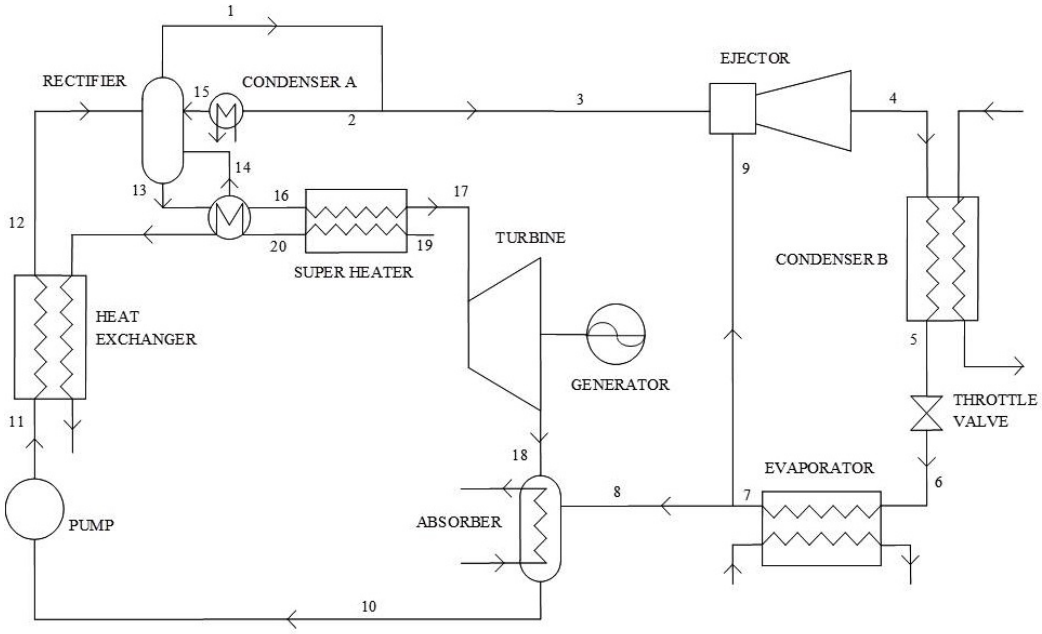

Figure 2.13: Schematic diagram of the combined power and ejector absorption refrigeration cycle proposed by Wang et al. [143].

Liu and Zhang [144] proposed a novel NH_3/H_2O combined cycle for the cogeneration of power and refrigeration. As shown in Fig. 2.14, a splitting/absorption unit was introduced into the combination of an NH_3/H_2O Rankine sub-cycle and an ammonia refrigeration

sub-cycle. The condenser in the Rankine cycle was replaced by an absorber. In this configuration, the basic solution of NH_3/H_2O is separated into a high concentration ammonia vapour and a relatively weak solution liquid in a device that operates like a distillation column. The modifications increased the ammonia mass fraction in the heat addition process and reduced it in the absorption-condensation process. The performance of the cycle was evaluated by exergy efficiency and found to be 58% for the base case studied. The cogeneration unit used nearly 18% less energy than the conventional separate system of power generation (a steam Rankine cycle) and refrigeration (an NH_3/H_2O absorption refrigeration cycle). The authors also suggested that there is an optimum pair of two split fractions: namely, SF1 (the ratio of the mass flow rate of the basic concentration solution split to heat exchanger 1 to the total mass flow rate of the basic concentration solution) and SF2 (the ratio of the mass flow rate of the high concentration solution split to absorber 1 to the total mass flow rate of the high concentration solution from the cooler) at which the exergy efficiency was maximum.

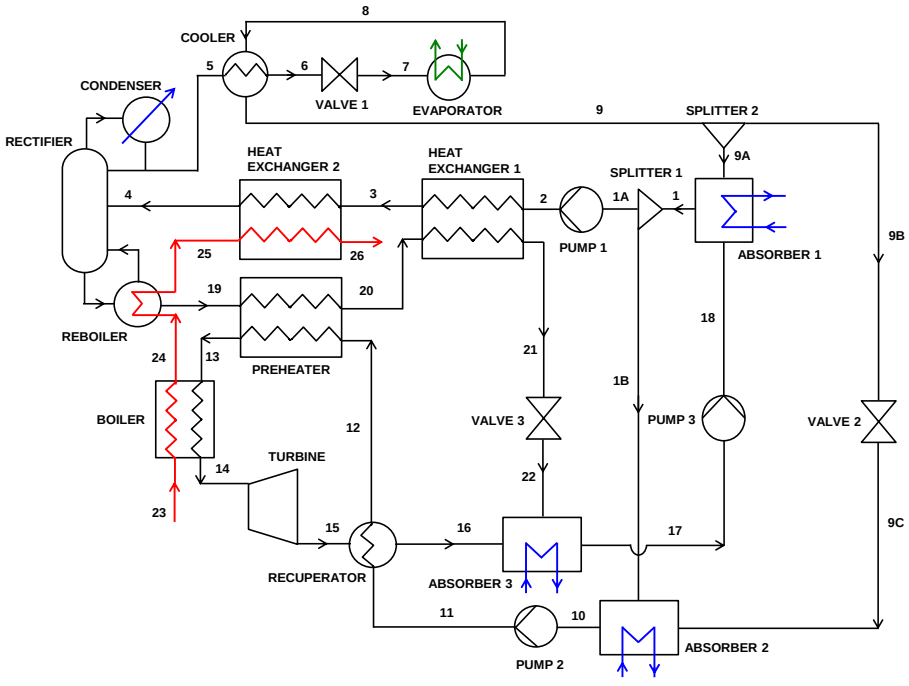

Figure 2.14: Flow sheet of the combined power/refrigeration cycle of Liu and Zhang [144].

Zheng et al. [145] proposed a combined power and cooling system (see Fig. 2.15) in which the flash tank or separator in the Kalina cycle was replaced by a rectifier to enhance

the separation process and to obtain an additional higher purity stream of ammonia for cooling. In order to produce a larger refrigeration output, the fluid should go through a phase change in the cooler. The proposed cycle requires two absorbers and was modelled with the process simulator Aspen Plus. A condenser and an evaporator were introduced between the rectifier and the second absorber. With these modifications, the cycle can simultaneously provide refrigeration and generate power. The overall thermal efficiency and exergy efficiency of the proposed cycle were found to be 24.2% and 37.3%, respectively. The addition of refrigeration as a useful output not only improves the cycle performance, but expands the application flexibility of the system.

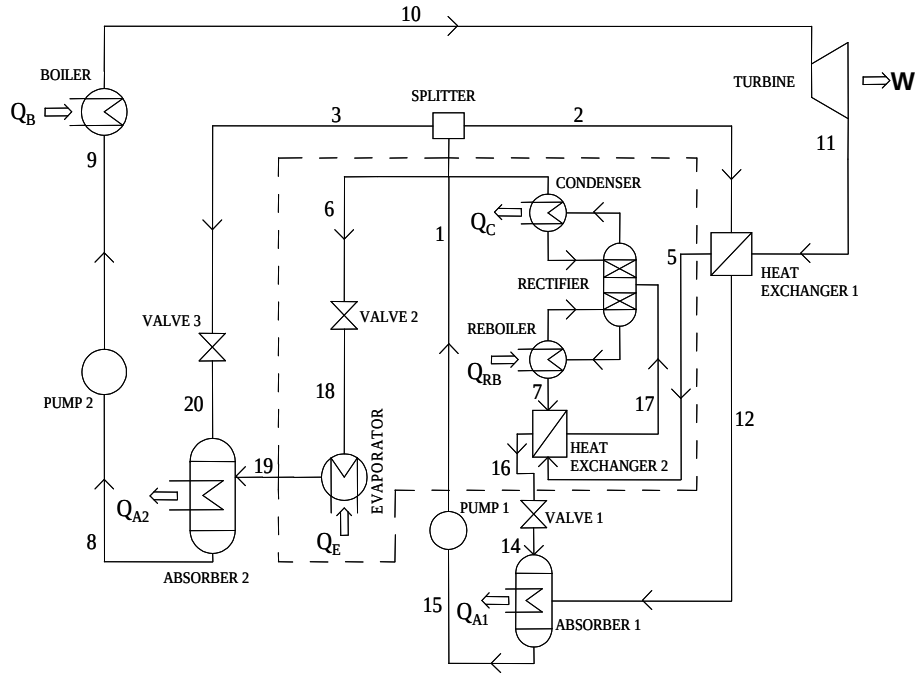

Figure 2.15: Absorption combined power/cooling cycle flow scheme of Zheng et al. [145].

Zhang and Lior [146] suggested that, by adding a rectifier, the liquid NH_3/H_2O stream could be evaporated and superheated in the reboiler at the bottom of the rectification column and later expanded in the turbine (see Fig. 2.16). The authors developed three different configurations: namely, parallel, series and compound cogeneration cycle configurations for the integration of refrigeration and power generation systems with a single heat source using NH_3/H_2O as the working fluid. The heat source fluid used was air. In the configurations analysed, the energy and exergy efficiencies were found to be 26% to

28% and 55% to 60%, respectively, at a heat input temperature of 450 °C. The parallel cycle configuration shown in Fig. 2.16 had the highest refrigeration-to-power ratio (0.37), while the compound configuration had the lowest (0.25). For a constant flow rate of the heating fluid, the compound configuration produced 9% and 11% more power, and 28% and 11% less refrigeration, respectively, than the parallel and series cycle configurations. When the heat source used was exhaust from the gas turbine plants, the total plant energy efficiency increased to 57%. These cycles have resulted in a potential high capital investment. Moreover, these cycles require high driving temperatures and therefore cannot be combined with solar energy for small- and medium-scale applications.

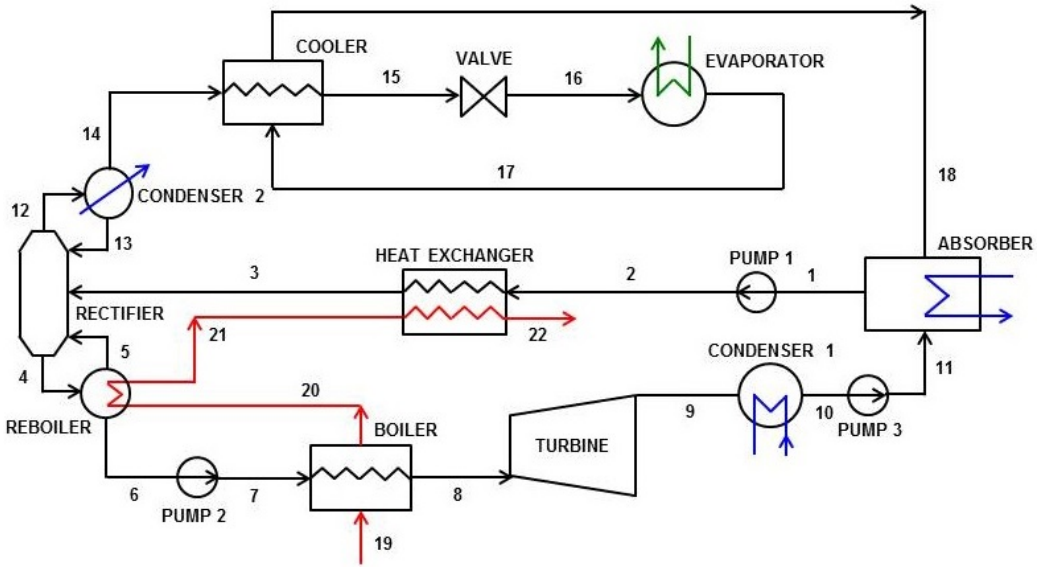

Figure 2.16: Flow sheet of the parallel power/refrigeration cycle of Zhang and Lior [146].

Zhang and Lior [147] proposed a new NH_3/H_2O system for the cogeneration of refrigeration and power. The plant is a parallel combination between an NH_3/H_2O Rankine cycle and an NH_3/H_2O absorption refrigeration cycle interconnected by absorption, separation and heat transfer processes. The authors investigated the effects of such key thermodynamic parameters as basic working solution concentration, the cooling water temperature, and turbine inlet parameters on both energy and exergy efficiencies. In the base case studied, the cycle has energy and exergy efficiencies of 27.7% and 55.7%, respectively. The cycle requires a high temperature (450 °C) at the superheater, which makes the cycle unfavourable for small- and medium-scale applications driven by low-grade thermal energy.

The Load-leveling Hyper Energy Converting and Utilization System (LHECUS) is a hybrid cycle which uses NH_3/H_2O as the working fluid in a combined power generation and refrigeration cycle developed by Kiani et al. [148]. The power generation cycle functions as a Kalina cycle and it is combined with an absorption refrigeration cycle as a bottoming cycle. Fig. 2.17 shows the flow diagram of the complete cycle configuration. LHECUS is designed to utilize the waste heat from industry to produce cooling and power simultaneously. The refrigeration effect can be either transported to end-use sectors by means of a Solution Transportation Absorption chiller (STA) driven by solution concentration difference or stored for demand load levelling.

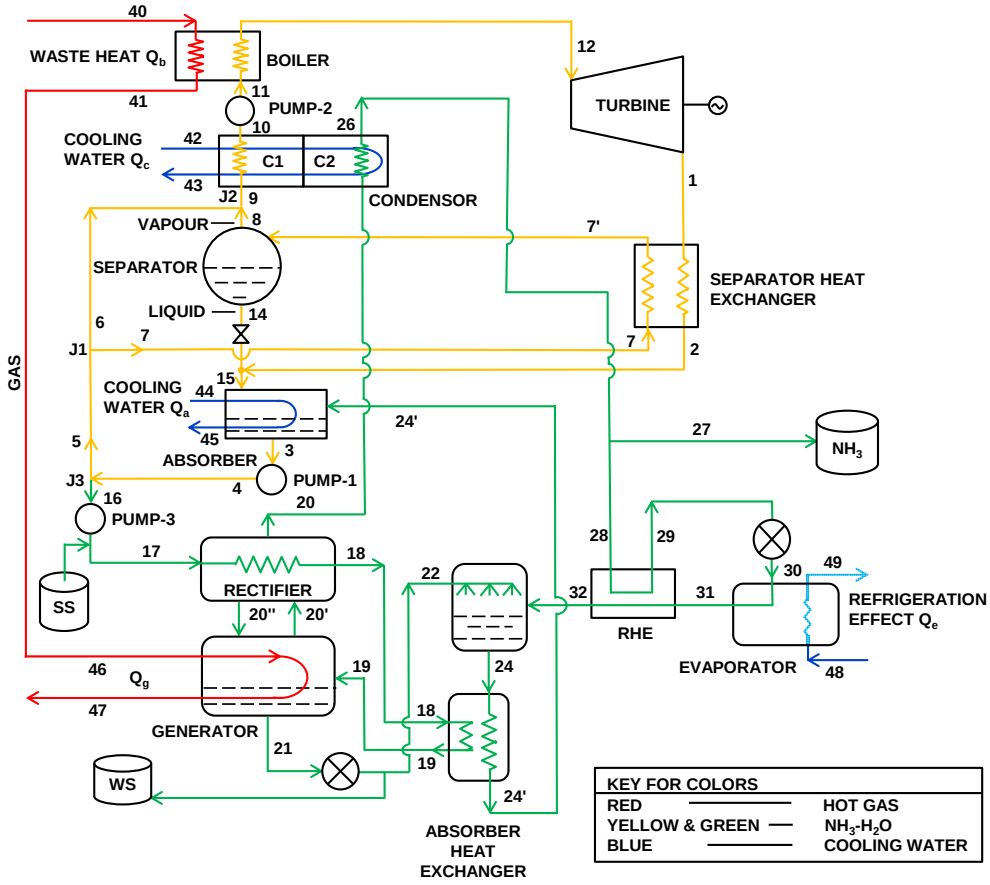

Figure 2.17: Flow diagram of the complete LHECUS cycle proposed by Kiani et al. [148].

A modified form of the basic absorption cooling cycle has been presented by Ziegler [71]. Fig. 2.18 shows a cooling and power cycle derived from a double-effect absorption system. It is estimated that with this cycle configuration 1.2 MW of cooling and 100 kW of power

can be produced from 1 MW of thermal energy when the system operates as a pure chiller and pure sorption power cycle, respectively. The main advantage of these configurations is that low-grade heat (such as solar energy or waste heat) can be used and the ratio between cold and power production can be adjusted.

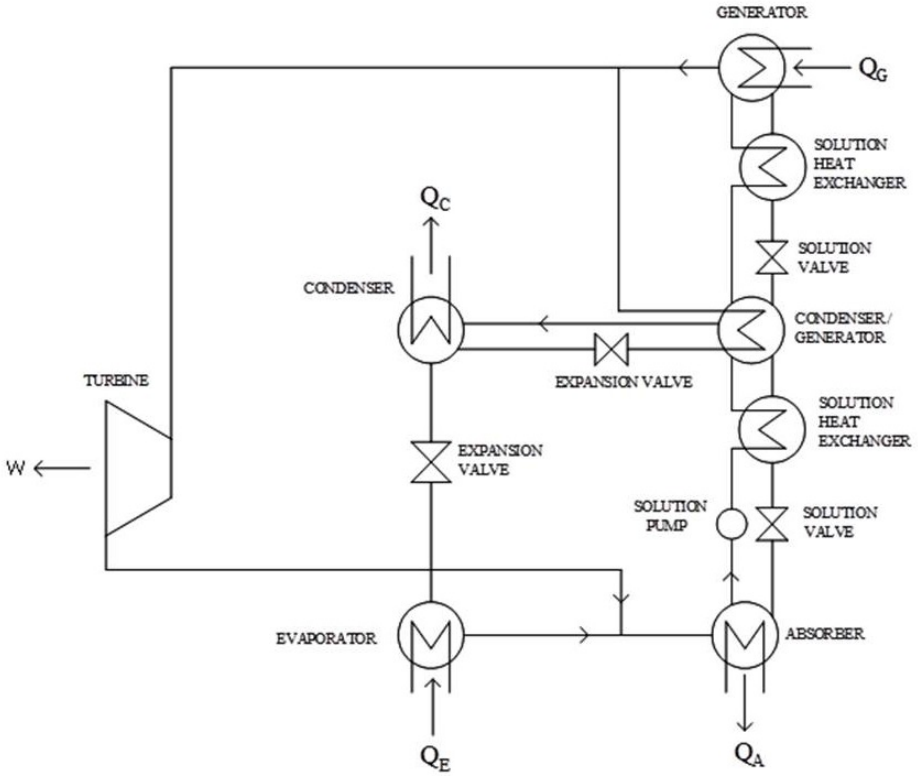

Figure 2.18: Double-effect absorption cooling-power cycle proposed by Ziegler [71].

As the GAX cycle has shown promising results in enhancing the performance of absorption cooling systems ([149],[150]), a new absorption cooling and power cycle has been proposed (Fig. 2.19) [151]. The GAX based power and cooling cycle is a modification of the simple absorption power and cooling cycle configuration. The thermodynamic analysis of the cycle was carried out for different generator, sink and evaporator temperatures. The split ratio was also varied in the analysis. It is defined as the ratio between the mass flow rates of the refrigerant flow through the power and cooling sub systems. The split factor of the cycle is also defined as the ratio of the mass flow rate of the refrigerant to the absorber to the mass flow rate of the refrigerant from the evaporator. The extent to which the COP and thermal efficiency of the GAX cycle configuration varied with respect to the split factor at a fixed split ratio (0.5) was studied for a constant heat source and sink

temperature. The optimum value for the split ratio was found to be 0.5 and the optimum split factor 0.8 - 0.9. At the optimum split ratio the cooling capacity and mechanical power output of the cycle was 225 kW and 80 kW, respectively, for generator, sink and evaporator temperatures of 150 °C, 35 °C and 0 °C. The combined thermal efficiency and COP in the optimum operating conditions were 35 - 45% and 0.35, respectively.

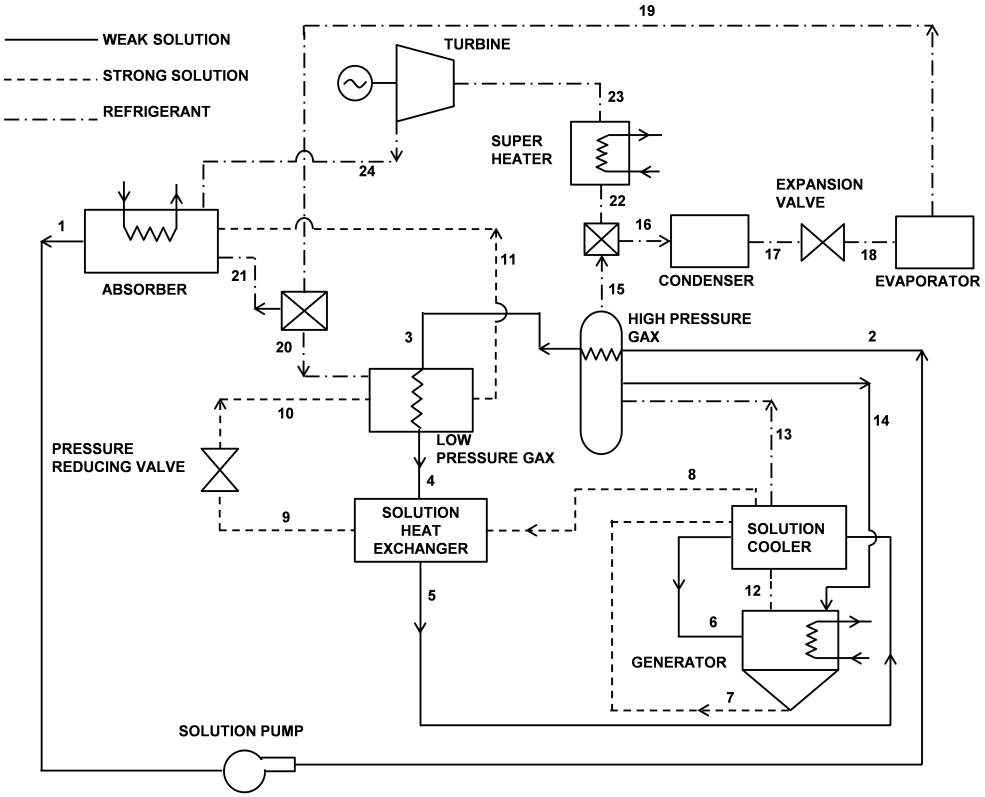

Figure 2.19: Schematic diagram of GAX based absorption cooling and power cycle [151].

The cycle configurations reviewed above are summarised in Table 2.2 with heat source inlet, sink and refrigeration temperatures. Other parameters such as turbine inlet and outlet temperatures and pressures are also given in Table 2.2. The performance parameters of the combined absorption cycle configurations such as power/cold ratio, and thermal (energy) and exergy efficiencies of the cycles are presented in Table 2.3.

Table 2.2: Operating condition for other ammonia/water combined absorption cycles found in the literature.

Reference	Cycle description	Temperature [°C]				Turbine Parameter	
		Heat source (Inlet)	Sink	Refrigeration	η_t [%]	Inlet/Outlet Pressure [bar]	Inlet/Outlet Temperature [°C]
Erickson et al. [140]	GAX + ARC	175	15[a]	n/a	75	25.1/5.2	155.0/61.7
Zhang et al. [141]	Rankine + ARC	465	30[a]	0.0	87	50.0/0.376	450.0/70.1
Wang et al. [142]	Rankine + ARC	300	20[b]	−5.0	85	25.0/1.194	285.0/96.9
Liu et al. [144]	Rankine + ARC	465	30[a]	−15.0	87	111.0/0.39	450.0/68.0
Zheng et al. [145]	Kalina + ARC	350[c] and 135[d]	35	−10.0	n.a	49.0/0.981	350/84.5
Zhang et al. [146]	Rankine + ARC	465	30[a]	−15.0[e]	87	51.0[f]/0.191[f], 152.5[g]/0.853[g]	450.0[f]/56.7[f], 450.0[g]/83.6[g]
						75.8[h]/0.191[h] and 0.4[h]	450.0[h]/56.6[h] and 66.8[h]
Wang et al. [143]	Rankine + Ejector-ARC	300	20[b]	−5.0	85	25.0/1.194	285.0/96.9
Kiani et al. [148]	Kalina + ARC	520	20[b]	7.0[i]	90	115.0/5.46	510.0/190.2
Zhang et al. [147]	Rankine + ARC	465	30[a]	−11.4[e]	87	52.4/0.242	450.0/61.3

ARC - Absorption Refrigeration Cycle; η_t- Isentropic turbine efficiency; [a]- External cooling water inlet temperature;
[b]- Ambient; [c]- Boiler input temperature; [d]- Reboiler input temperature; [e]- Evaporator outlet temperature;
n/a - not available; [f]- Parallel cogeneration system; [g]- Series connected cogeneration system (SF_1=0.4);
[h]- Compound configuration system (SF_2=0.72); [i]- External chilled water outlet temperature

Table 2.3: Efficiencies and power/cold ratio for different types of combined absorption cycle configurations.

Reference	Efficiency [%]		Power/ Cold ratio	Remark
	Thermal	Exergy		
Erickson et al. [140]	11.96	n/a	n/a	- Turbine power output, $\dot{W} = 1.77$ MWel - When $\dot{W} = 0$, refrigeration output $\dot{Q}_0 = 10.5$ MW
Zhang et al. [141]	25.00	50.90*/53.40**	4.00	For the base case considered; - Energy efficiency weighs both power and cooling equally ($f = 1$); - For exergy efficiency: $f = 1/COP_{rev}$(*); $f = 1/COP_{practical}$(**) and $\eta_{ref} = 40\%$
Wang et al. [142]	20.45	35.54	2.73	- For a particular operating condition; - For optimised condition: Power-to-cold ratio = 4.24 and $\eta_{ex} = 43\%$; - Thermal efficiency weighs both outputs equally ($f = 1$); - Exergy efficiency based on $f = 1/COP_{rev}$
Liu et al. [144]	n/a	57.60	3.62	- Performance parameters for the base case; - Exergy efficiency based on $f = 1/COP_{rev}$
Zheng et al. [145]	24.20	37.30	2.48	- Overall thermal efficiency weighs power and refrigeration effect equally ($f = 1$); - Exergy efficiency weighs the refrigeration output by factor $f = 1/COP_{rev}$
Zhang et al. [146]	28.20[a]/ 26.42[b]/27.92[c]	55.80[a]/54.12[b]/ 59.50[c]	2.70[a]/ 3.27[b]/ 4.08[c]	- Three cycle configurations analysed at the base case; - The energy efficiency equally weighs the power and refrigeration outputs ($f = 1$); - Exergy efficiency based on $f = 1/COP_{rev}$
Wang et al. [143]	20.97	35.77	2.49	- The performance parameters were for a particular operating condition; - Parametric analysis were done; - Thermal efficiency weighs both power and refrigeration output equally ($f = 1$); - Exergy efficiency based on $f = 1/COP_{rev}$
Kiani et al. [148]	30.0	n/a	n/a	- Maximum overall thermal efficiency of the hybrid cycle based on $f = 1/COP_{practical}$where $COP_{practical} = 2.48$
Zhang et al. [147]	27.70	55.70	2.99	- Performance parameters were determined for the base case; - Energy efficiency weighs the power and refrigeration outputs equally ($f = 1$); - Exergy efficiency based on $f = 1/COP_{rev}$
Jawahar et al. [151]	35.00 - 45.00	n/a	0.36***	- Maximum overall thermal efficiency of the combined cycle based on $f = 1$ - (***) - at $t_G = 150$ °C, $t_{sink} = 35$ °C, $t_E = 0$ °C, optimum split factor (0.8) and split ratio (0.5). - $COP = 0.35$ at the optimum condition

n/a - not available; η_{ref} - Second law efficiency of refrigeration
[a]Parallel cogeneration system;
[b]Series connected cogeneration system ($SF_1 = 0.4$)
[c]Compound configuration system ($SF_2 = 0.72$)

Experimental work on combined absorption systems available in the literature is very limited and will be presented in the next subsection.

2.4.3 Experimental studies

The experimental work published on the feasibility, operating conditions and processes involved in combined absorption systems is mainly based on the Goswami cycle configuration. The studies were made using the laboratory experimental setups at the University of Florida and then later at the University of South Florida, USA.

The Goswami cycle was theoretical and experimentally investigated by Tamm et al. ([152],[153]). The parametric studies revealed that the cycle can be optimized for first and second law efficiency as well as power and cooling output. The thermal efficiency, and the power and the cooling outputs decrease by 20.6%, 11.8% and 37.7% respectively when the real losses are considered in the analysis. The theoretical analysis showed that when the cycle is optimised for second law efficiency, it produces no refrigeration at high heat source temperatures, but it does have a refrigerating effect at low heat source temperatures. The experimental studies demonstrated the feasibility of a combined absorption cycle. The results of the experiments confirmed that the vapour production and absorption-condensation processes work well. The agreement between the theoretical and experimental results was found to be close (Fig. 2.20).

Martin [126] made an experimental study on the novel concept of producing power and cooling using low temperature (< 200 °C) thermal resources. The experimental setup developed by Martin was based on Tamm [154] but included a rectifier and a turbine to condition the vapour and to extract work from the fluid, respectively, with the aim of demonstrating the sub-ambient turbine exhaust conditions. The author concluded that with better expander performance, practical power and cooling production can be achieved with the proposed novel cycle configuration (Goswami cycle). Subsequently, Goel [155] studied the absorption and condensation process by modifying the rectifier column (increasing its diameter from 2 to 3 inches) and making the separator vessel smaller. The study proposed a new concept that enhances heat and mass transfer processes in a falling film absorber and considerably reduces the absorber size without having any effect on high vapour and coolant side pressure drops. After the experiments performed by Goel, all

the components in the set-up were moved to the University of South Florida, upgraded and replaced (including the work developing expansion device, which is replaced by scroll type expander) except the separator and the rectifier column [156]. The scroll expander isentropic efficiency was between 30% - 50%, and the expander performed better when the vapour was superheated [156].

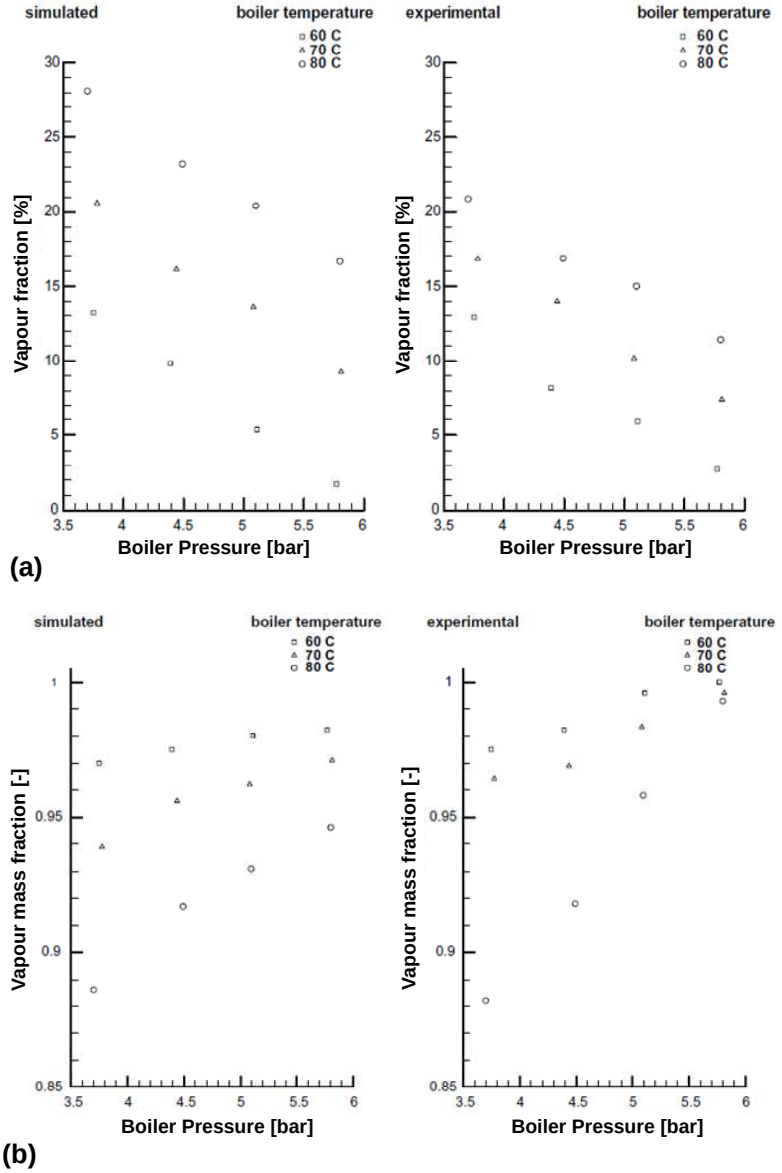

Figure 2.20: (a) - Vapour fraction; (b) - Vapour mass fraction for various boiler temperatures and pressures [152].

Recently, Han et al. [157] built an experimental test rig for a combined refrigeration/power system with NH_3/H_2O mixture in order to investigate the dual functioning of the system under absorption refrigeration and absorption power modes. The authors

do not use an actual expander instead they simulate the expansion process in the power generating subsystem by throttling and heat transfer processes using a throttle valve and vapour heat exchanger in their experimental test rig. They claimed that there is no efficient expander available in the market for a few kilowatts capacity experimental prototypes.

2.5 Thermodynamic Property Database Influence on Cycle Performance Analysis

As already stated (in section 3.2.1), there are several property database sources for NH_3/H_2O mixture in the literature. Thus, to demonstrate the influence of the NH_3/H_2O database source on the analysis of a combined absorption cycle, a well-known combined absorption cycle (Goswami cycle) was selected and analysed using four property database sources available in the literature ([88],[97], and [127]). The input parameters and the model main assumptions considered in the analysis of the Goswami cycle illustrated in Fig. 2.7 are shown in Table 2.4.

Table 2.4: Input parameters and assumptions considered for cycle analysis (Fig. 2.7).

Parameter	**Value**
Reference temperature [°C]	17.0
Desorber temperature [°C]	125.0
Desorber pressure [bar]	20.5
Absorber pressure [bar]	1.5
Basic solution concentration [ammonia mass fraction]	0.43
Rectifier temperature [°C]	108.5
Expander isentropic efficiency [%]	85
Pump isentropic efficiency [%]	80
Second law efficiency of refrigeration [%]	30
Minimum temperature difference for each heat exchanger [°C]	5.0
Mass flow rate of basic solution [basis for calculation, kg/s]	1.0

The cycle simulation was conducted under the following conditions:

- Steady-state steady flow operation;
- Thermal and pressure losses were neglected;
- Throttling valve was isenthalpic;

- Saturated basic solution stream leaving the absorber at the absorber pressure;
- Saturated liquid and vapour streams leaving the desorber are at the desorber temperature and pressure;
- No superheater was considered;
- Saturated liquid and vapour streams leaving the rectifier are at the rectifier temperature and pressure;
- Water was used as a chilled fluid in the refrigeration heat exchanger (cooler).

The results of the cycle calculations are presented in Table 2.5. The turbine power shows a relative difference of about 16.4%, from the lowest 44.0 kW (I) to the highest 52.6 kW (IV). In the other cycle components, relative differences between the highest and lowest values of heat duty were about 16.4%, 16.4% and 30.8% for boiler, absorber and sensible heat exchanger (cooler), respectively. The relative difference between the highest and lowest value of pump power consumption was about 9.4%. The reason for these discrepancies is that different property databases (equation of states) were used in the analysis.

Table 2.5: Effect of NH_3/H_2O mixture database on cycle parameters calculation.

Cycle Parameter	**Ammonia/water database**			
	(I)	**(II)**	**(III)**	**(IV)**
Turbine power [kW]	44.00	47.81	47.96	52.60
Pump power [kW]	2.78	3.07	3.00	3.00
Boiler heat duty [kW]	271.70	294.00	321.44	324.50
Absorber heat duty [kW]	233.90	252.00	279.81	277.0
Cooling load [kW]	3.35	2.77	3.85	4.00
Cold/Power ratio, R	0.081	0.062	0.086	0.081
Effective first law efficiency [%] (using Eq. 2.2.15)	15.1	15.2	14.0	15.3

(I) - Ibrahim and Klein [88]; (II) - Tillner-Roth and Friend [97]; (III) - PSRK equation of state and Latent-heat H model used [127]; and (IV) - SRK equation of state used [127].

Hence, the appropriate thermophysical property data need to be used to analyse combined absorption systems and care must be taken to avoid confusion when projections based on different databases are used. Of the sources analysed, the property data correlation evaluated by Tillner-Roth and Friend [97] seems to predict the experimental values with reasonable accuracy. NIST REFPROP 9 [158] includes the correlation proposed by

Tillner-Roth and Friend [97] to predict the NH_3/H_2O mixture properties. The combination of experimental uncertainties and database deviations may makes it difficult to interpret energy and mass balance calculations performed in cycle analysis.

2.6 Conclusions

A wide variety of combined absorption cycle configurations has been studied and reported in the literature for the co-production of power and cooling (refrigeration). The literature on the combined absorption cycles has found that greater importance is given to power output than refrigeration. It is concluded that two general types of cycles have been identified: those producing cold using sensible heat (mainly the Goswami cycle) and those based on latent heat (mainly hybrid Rankine and absorption refrigeration cycles). The working fluid that has been proposed for a combined absorption cycle (except a few case were organic fluid mixtures are used) is a binary mixture of NH_3/H_2O, which is environmentally friendly. This working pair requires rectification of the vapour stream in the cold producing loop of the combined absorption cycles: sensible cooling output in the case of Goswami cycle and latent cooling output in the other combined absorption cycles.

This chapter has presented a review of the existing combined absorption cycles. Some of the configurations are simple modifications of the Kalina absorption power cycle that produce cooling as a sub product. In some cases these cycles are very complex and have a high number of splits and components. The most suitable combined absorption systems for effective utilization of low and mid-grade heat sources such as from stationary or low-concentration solar thermal collectors seem to be those derived directly from such absorption chiller cycles as single or double-effect cycles or advanced GAX cycles. They are more suitable for solar applications in buildings which are characterised by small-to-medium power and cooling demands.

The dual-output nature of combined absorption systems needs care during the system performance evaluations in particular for its energetic performance evaluation. At least two independent parameters are required to evaluate the energetic performance of the combined absorption systems: effective first law efficiency and power/cold ratio.

Chapter 3

Low-Grade Heat Driven Combined Absorption Cycles

Parts of this chapter has been published in:

- *International Journal of Low-Carbon Technologies, 8(suppl 1), i19–i26, 2013. Published by Oxford University Press. Analysis and simulation of modified ammonia/water absorption cycle for power and cooling applications by* ***Dereje S. Ayou****, Rajagopal Saravanan, Joan Carles Bruno and Alberto Coronas.*
- *And some parts are under review process in: American Society of Heating, Refrigerating and Air-Conditioning Engineers (ASHRAE) Journal. Reference no. RSCH-00136-2014 to the HVAC&R Research. Combined Absorption Power and Refrigeration Cycles using Low- and Mid-Grade Heat Sources by* ***Dereje S. Ayou****, Joan Carles Bruno and Alberto Coronas.*

"This page intentionally left blank"

3.1 Introduction

Several combined absorption cycles are proposed and analysed for the simultaneous and/or alternative production of power and cold by utilizing low-grade heat sources (< 200 °C). These new classes of absorption cycles are designed by modifying a basic NH_3/H_2O absorption refrigeration cycle. This chapter discusses the performance analysis of these cycles from energetic and exergetic viewpoints, and also provides operating characteristics and process descriptions of the cycles. Finally, their performances are compared with each other and with the well-know Goswami combined power/cooling cycle at the same thermal boundary conditions. The performance of a representative combined absorption cycle, from the proposed new class of combined absorption cycles, is also compared with available technologies for separate production of power and cold.

3.2 Single-Stage Combined Absorption Cycles for Power and Refrigeration Applications

Basically, these new classes of combined absorption cycles are derived from a single-stage (single-effect) absorption refrigeration cycle by incorporating additional heat and/or mass exchanging components, mass flow stream splitter(s), mixer(s), and power sub-cycle that include mechanical work developing device, hereafter referred as expander, and superheater. Because of the inclusion of the power sub-cycle these new class of absorption cycles are capable of producing dual useful energy products: mechanical or electrical (by coupling electric generator) power and cold at different temperature levels.

Three different types of cycle configuration architectures are presented in this chapter:

- Single-Stage combined Absorption Power and Refrigeration Cycle with Parallel flow arrangement (SSAPRC-P),
- Single-Stage combined Absorption Power and Refrigeration Cycle with two Desorbers (SSAPRC-2D), and
- Single-Stage combined Absorption Power and Refrigeration Cycle with Series flow arrangement (SSAPRC-S).

Analogues to the well-known Goswami combined power/cooling cycle, application of low-grade heat sources below 200 °C is one of the main characteristics of these cycle configurations. Their main difference with respect to the Goswami cycle is on the nature of the cold output production: on the new cycles latent cooling output whereas on Goswami cycle-sensible cooling output.

The process description, operating characteristics and performance analysis of the proposed combined absorption cycles (SSAPRC-P, SSAPRC-2D and SSAPRC-S) are provided in the next sections. First, the thermodynamic modelling approach followed to simulate the thermodynamic performance and operating conditions of the combined absorption cycles is introduced and described in detail below.

3.2.1 Absorption cycle modelling

The physical-mathematical models for the proposed combined absorption cycles (SSAPRC-P, SSAPRC-2D and SSAPRC-S) have been developed. These models are used to evaluate the cycle's thermodynamic performance from the energetic and exergetic viewpoints; and also later to compare their performance with each other and other commonly employed options for separate production of power and cold. The models are based on mass and energy conservation laws, exergy balance, model assumptions and thermodynamic properties of the working fluid pair (NH_3/H_2O mixture) and external heat transferring fluid circuits. Each component (unit) in the cycle is treated as a control volume with inlet and outlet mass flow streams, heat transfer and work interactions with its surroundings. The surrounding may refer to other adjoining units in the cycle or external heat transferring fluid circuits such as chilled fluid, heat sink medium or driving heat source fluid streams. The operation of the cycle is limited to a steady-state steady flow condition.

The generic equations based on mass and energy conservation laws for each unit of the cycle can be expressed as follows:

Global mass balance:

$$\sum_{i \in IN(u)} \dot{m}_i - \sum_{i \in OUT(u)} \dot{m}_i = 0, \tag{3.2.1}$$

where $\dot{m}_i$ is the mass flow rate of stream i and it can be either an inlet or outlet stream.

Therefore, IN(u) denotes the set of inlet mass flow rate streams of the component u, whereas OUT(u) indicates the set of outlet mass flow streams.

Species (ammonia) mass balance:

$$\sum_{i \in IN(u)} z_i \dot{m}_i - \sum_{i \in OUT(u)} z_i \dot{m}_i = 0, \tag{3.2.2}$$

where z_i is ammonia mass fraction of stream i.

Energy balance:

$$\sum_{i \in IN(u)} h_i \dot{m}_i - \sum_{i \in OUT(u)} h_i \dot{m}_i + \dot{Q}_u - \dot{W}_u = 0, \tag{3.2.3}$$

where h_i is the specific enthalpy of stream i. The heat and work flow rates that could be into or out of the control volume are $\dot{Q}_u$ and $\dot{W}_u$ respectively. Heat flows into a unit and work developed by a unit are taken as positive in Eq. 3.2.3.

When dealing with energy balance, we refer to the applications of first law of thermodynamics, it consider all forms of energy are equally convertible from one form to another, and it focuses on the quantity of energy (i.e. amount of heat or work) but not on its thermodynamic quality. The heat duty and work developed (or consumed) by the units of the combined absorption cycle are calculated according to the first law of thermodynamics. This approach is concerned only with energy conservation, and consequently it does not provide sufficient information how efficiently the available heat source is utilized and also cannot show how or where thermodynamic inefficiencies (irreversibilities) occur in the cycle ([159],[160]). Therefore, the exergy analysis, based on first and second law of thermodynamics, is applied to define a proper performance criteria and to determine the irreversibilities associated with each unit of the cycle. It also helps to identify the components in which the main inefficiencies (exergy destructions) occur; thus it shows the direction for further improvements of the system.

Exergy of a system (or control volume) is defined as the maximum amount of useful work obtainable from a system when it is brought from its thermodynamic state to one in equilibrium with a pre-defined environmental state. A system which is in equilibrium with its reference environment state has zero exergy and it is said to be in a dead state [160].

In general, exergy can be transferred by accompanying mass flow, heat flow and work transfer. Exergy transfer associated with mass flow is expressed in terms of four constituting parts: physical (thermo-mechanical) exergy, kinetic exergy, potential exergy and chemical exergy [160]. However, the kinetic and potential exergies are usually neglected in absorption system analysis ([85],[131],[162]). Since there is no departure of chemical species from the cycle to the environment (for closed cycle) and no chemical reactions involved, the chemical exergy is considered zero ([85],[131]). Exergetic analysis of complex thermodynamic cycle like combined absorption cycles can be performed by analysing each unit of the cycle separately. For a generic steady-state steady flow process, the exergy balance for a unit can be expressed as:

$$\sum_{i \in IN(u)} ex_i \dot{m}_i - \sum_{i \in OUT(u)} ex_i \dot{m}_i + \tau_u \dot{Q}_u - \dot{W}_u = \dot{E}x_{D,u}, \tag{3.2.4}$$

where ex_i is specific physical exergy associated with the mass flow stream i. The specific physical exergy (ex) is calculated by the general expression:

$$ex_i = (h_i - h_0) - T_0(s_i - s_0), \tag{3.2.5}$$

where T_0 is the exergy reference environment temperature. h_0 and s_0 are the specific enthalpy and entropy at the exergy reference environment condition ($p_0 = 101.325$ kPa, $t_0 = 25$ °C and $z_0 = 0.5$ are taken in this work). Note that other researchers consider different values for the reference ammonia mass fraction as well as for the reference temperature to calculate the physical exergy of the streams ([85],[163]). However, its effect is insignificant for the overall exergy analysis of the system. The first two terms in the left of the exergy balance (Eq. 3.2.4) represent the exergy flow associated with entering and leaving mass flows. Then, the next term $\tau_u \dot{Q}_u$ (thermal exergy, where $\tau_u = 1 - \frac{T_0}{\hat{T}_u}$ is the Carnot equivalent factor or exergetic temperature factor according to Dincer and Rosen [160]) represents the exergy transfer accompanied by the heat flow. The exergy transfer associated with shaft and electrical work transfers is equal to the work transfer itself ($\dot{W}_u$) [160]. $\hat{T}_u$ is an entropic average temperature to represent the equivalent uniform temperature at which a non-isothermal heat addition or removal process of a unit takes place.

The $\dot{E}x_{D,u}$ in Eq. 3.2.4 represents the exergy destruction rate, irreversibility rate, of a unit (u). According to Gouy-Stodola relation ([159],[160]), the exergy destruction rate is related to the entropy generation rate ($\dot{S}_{gen,u}$) of the unit as follows:

$$\dot{E}x_{D,u} = T_0 \dot{S}_{gen,u} \tag{3.2.6}$$

The total exergy destruction rate $\dot{E}x_{D,total}$ can be determined from the sum of individual unit exergy destruction rates. A non-dimensional exergy destruction of each unit can be defined as the ratio between the exergy destruction of a unit to the total exergy destruction of the system: $\dot{E}x_{D,u}/\dot{E}x_{D,total}$ [164].

The following main assumptions were made to develop the thermodynamic models and conduct the simulation of the combined absorption cycles: SSAPRC-P, SSAPRC-2D and SSAPRC-S configurations.

- Pressure drops and thermal losses in the components and pipes are neglected.
- Potential and kinetic energy effects are also neglected.
- A minimum vapour mass fraction (dryness) at the exit of expander is set at 90%.
- Liquid solutions leaving the absorber and generator are saturated at the absorber and generator temperatures and evaporator and condenser pressures, respectively.
- The liquid and vapour leaving the rectifier are saturated and the composition (ammonia mass fraction) of the liquid is identical to the strong, in ammonia, solution entering the desorber.
- The degree of purification in the rectifier is specified by an ammonia mass fraction of 0.998.
- A constant isentropic efficiency is set for the solution pump as 80%.
- A fixed isentropic efficiency is considered for the expander, except to a few specific cases were isentropic expansion process is consider for some parametric studies.
- A constant effectiveness value for solution heat exchanger (80%) and refrigerant subcooler (80%) is considered.

- Saturated liquid solution leaving the condenser whereas partial vaporisation is allowed in the evaporator for maintaining an acceptable internal temperature glide across the evaporator.
- The solution and refrigerant expansion valves are adiabatic (isenthalpic).
- Water is used as a heat rejection, heat sink, medium for the absorber and condenser.
- Minimum approach temperature difference for the absorber, condenser, desorber, evaporator and superheater is set at 5 °C.
- Ethylene glycol/water mixture ($<$ 3 °C) and water ($>$ 3 °C) are used as secondary heat transfer fluid (chilled fluid) for the cold production.
- Hot water at pressure ($<$ 150 °C) and "BP Transcal N" thermal oil (from 150 °C to 200 °C) are considered as external heat supplying fluid circuits.

The energetic performance of the combined absorption cycle is evaluated using effective first law efficiency, according to the definition and explanation provided in Chapter 2, and the power/cold ratio R.

Effective first law efficiency ($\eta_{I,eff}$):

$$\eta_{I,eff} = \frac{\dot{W}_{net} + \frac{\dot{E}x_{cold}}{\eta_{II,ref}}}{\dot{Q}_{in}}, \tag{3.2.7}$$

where $\dot{W}_{net}$ is the mechanical power output from the expander ($\dot{W}_{exp}$), reduced by the mechanical power consumption of the solution pump ($\dot{W}_{sp}$). $\eta_{II,ref}$ is a typical second law efficiency for mechanical vapour compression refrigeration cycle (equal to 30% in this study) [73]. $\dot{Q}_{in}$ is the driving heat input: it is the sum of desorber(s) and superheater heat duties.

In Eq. 3.2.7, the exergy of the cold output $\dot{E}x_{cold}$ is calculated as the exergy change of the chilled fluid in order to account the external irreversibility associated with the cold transfer ($\dot{Q}_{cold}$) and given as follows [127]:

$$\dot{E}x_{cold} = \dot{m}_{cf}[(h_{cf,in} - h_{cf,out}) - T_0(s_{cf,in} - s_{cf,out})], \tag{3.2.8}$$

where $\dot{m}_{cf}$ is the chilled fluid mass flow rate. $h_{cf,in}$ and $h_{cf,out}$ are the specific enthalpies at the inlet and outlet of the chilled fluid. $s_{cf,in}$ and $s_{cf,out}$ are the specific entropies at the inlet and outlet of the chilled fluid.

Exergy efficiency (η_{ex}):

$$\eta_{ex} = \frac{\dot{W}_{net} + \dot{E}x_{cold}}{\Delta \dot{E}x_{hs}} \tag{3.2.9}$$

Effective exergy efficiency ($\eta_{ex,eff}$):

$$\eta_{ex,eff} = \frac{\dot{W}_{net} + \frac{\dot{E}x_{cold}}{\eta_{II,ref}}}{\Delta \dot{E}x_{hs}} \tag{3.2.10}$$

The denominator in Eqs. 3.2.9 and 3.2.10 refers to the change in exergy of the driving sensible heat source fluid.

The thermodynamic properties of the working fluid pair (NH_3/H_2O mixture) employed in the cycle and water used as external heat transferring fluid are obtained using the correlations from Tillner-Roth and Friend (1998) [97] and Wagner and Pruss [165], respectively. The thermodynamic property correlations for "BP Transcal N" thermal oil and ethylene glycol/water mixture used in the cycle's simulation are obtained from the data available elsewhere ([166],[167]).

3.3 Single-Stage Combined Absorption Power and Refrigeration Cycle with Parallel flow arrangement (SSAPRC-P)

As stated above, there are several combined absorption cycles for the simultaneous and/or alternative production of power and cold. One kind of this type of absorption cycles that can be driven by low-temperature heat sources is depicted in Fig. 3.1. This cycle configuration is a modification of a dual pressure levels single-effect NH_3/H_2O absorption refrigeration cycle [48] by splitting of the vapour generated, by using external driving heat input, in the desorber into two sub-vapour streams that follows the power and refrigeration sub-cycles. It is done by inserting a mass flow stream splitter at the exit of the desorber.

Then, a power sub-cycle components (expander and superheater) are introduced in parallel with the refrigeration sub-cycle. This cycle configuration (SSAPRC-P) basically operates at similar thermal boundary conditions (driving heat source fluid, heat rejection medium and chilled fluid inlet/outlet temperatures) typical for a single-effect NH_3/H_2O absorption refrigeration cycle.

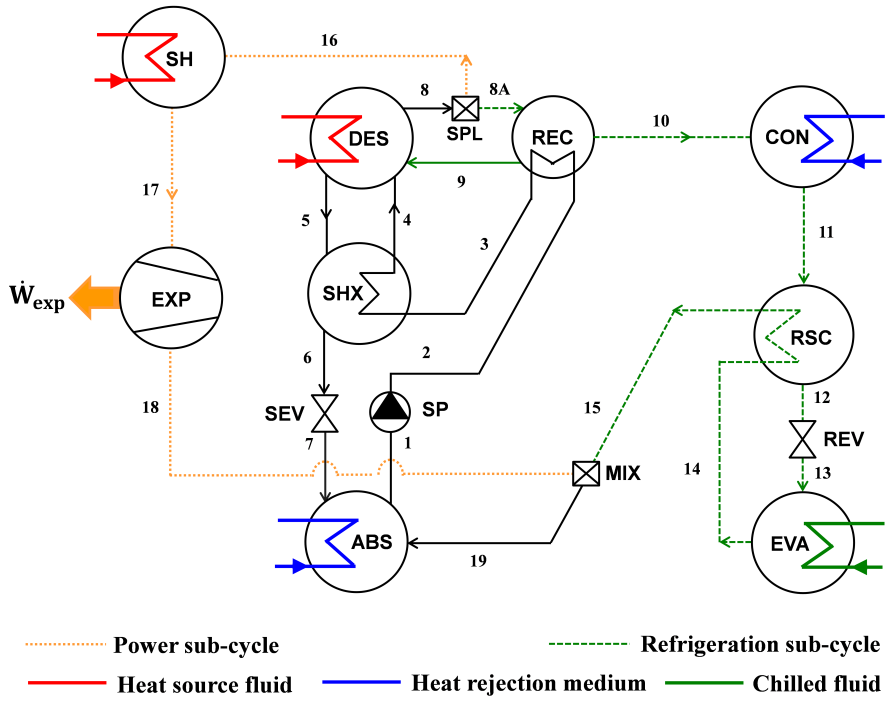

Figure 3.1: Schematic diagram of single-stage combined absorption cycle with parallel flow arrangement (SSAPRC-P).

3.3.1 Process description of SSAPRC-P

In the desorber (DES) ammonia vapour (state 8) is generated using external driving heat input $\dot{Q}_{des}$ at a temperature up to t_{des} (t_5 in Fig. 3.1). This vapour splits into two parts by a mass flow stream splitter (SPL) that follows the power sub-cycle (states 16-17-18) and refrigeration sub-cycle (states 8A-9-10-11-12-13-14-15) processes. The vapour contains traces of water due to the relatively low boiling temperature difference between the absorbent (H_2O) and refrigerant (NH_3). Since high degree of purification is required in the refrigeration sub-cycle, the vapour passes through a rectifier (REC) where the water is condensed in heat exchange with the rectifier cooling medium (internally cooled rectifier is used in this configuration: basic NH_3/H_2O solution as a rectifier heat rejection medium).

The reflux liquid, state 9, returns to the desorber. The rectified vapour (state 10) is liquefied in the condenser (CON, states 10-11) at high (desorber) pressure by rejecting heat $\dot{Q}_{con}$ to the heat rejection medium (ultimately to the ambient). It is then throttled in the refrigerant expansion valve (REV, states 12-13) to low (evaporator) pressure and then evaporated in the evaporator (EVA, states 13-14) by absorbing heat $\dot{Q}_{eva}$ from the space being refrigerated (cooled). A small quantity is not vaporized due to the water content, about 0.1%, of the stream entering the evaporator. A refrigerant sub-cooler (RSC) is added in the refrigeration sub-cycle. It is used to vaporize the remaining liquid from the evaporator and also it reduces the enthalpy of the stream at the evaporator inlet (state 13) through internal heat recuperation. This effect increases the refrigeration capacity and consequently the cycle performance improves.

The vapour stream that follows the power sub-cycle is first superheated by an external driving heat input $\dot{Q}_{sh}$ in the superheater (SH, states 16-17) up to a temperature t_{sh} (t_{17} in Fig. 3.1) and then expanded through an expander (EXP, states 17-18) in order to develop the mechanical power $\dot{W}_{exp}$. After expansion, the vapour stream is mixed with the other vapour stream (state 15) from the refrigeration sub-cycle by using a mass flow stream mixer (MIX). Then, the mixed vapour (state 19) is absorbed by the weak, in ammonia, solution from the desorber which then leaves the absorber as strong, in ammonia, solution at t_{abs} (t_1 in Fig. 3.1). The heat of absorption $\dot{Q}_{abs}$ is rejected to the cooling medium: mostly the same heat rejection (cooling) medium is used for the absorber and condenser.

The strong solution from the absorber is first pre-heated in the rectifier (REC, states 2-3) and then in solution heat exchanger (SHX, states 3-4) before it enters to the desorber for the desorption process. The weak solution leaves the desorber (state 5) at t_{des} (t_5 in Fig. 3.1) cools down in the solution heat exchanger (states 5-6) and throttled to the low pressure by solution expansion valve (SEV, states 6-7) into the absorber. To overcome the pressure difference and to circulate the solution in the cycle a solution pump (SP, states 1-2) is introduced in the cycle. The power consumption of the solution pump, $\dot{W}_{sp}$, is covered from the power developed by the expander.

Fig. 3.2 shows the SSAPRC-P on a pressure-temperature-concentration diagram. It has to be noted that the pressure at state 16 and 17 are at the same pressure (p_{high}) and state 18 is at low pressure (p_{low}). In this diagram (Fig. 3.2), states at equilibrium (saturated

vapour or liquid streams) are represented correctly otherwise only two intensive variables of a state are correctly represented.

The main features of this cycle configuration is its ability to operate in three different modes of operation by directly controlling its vapour split ratio: only cold-mode, co-production mode and only power-mode. The co-production mode represents the simultaneous useful dual-outputs production with varying power/cold ratio (R) that can be controlled to follow the demand profile of the power and cold needs.

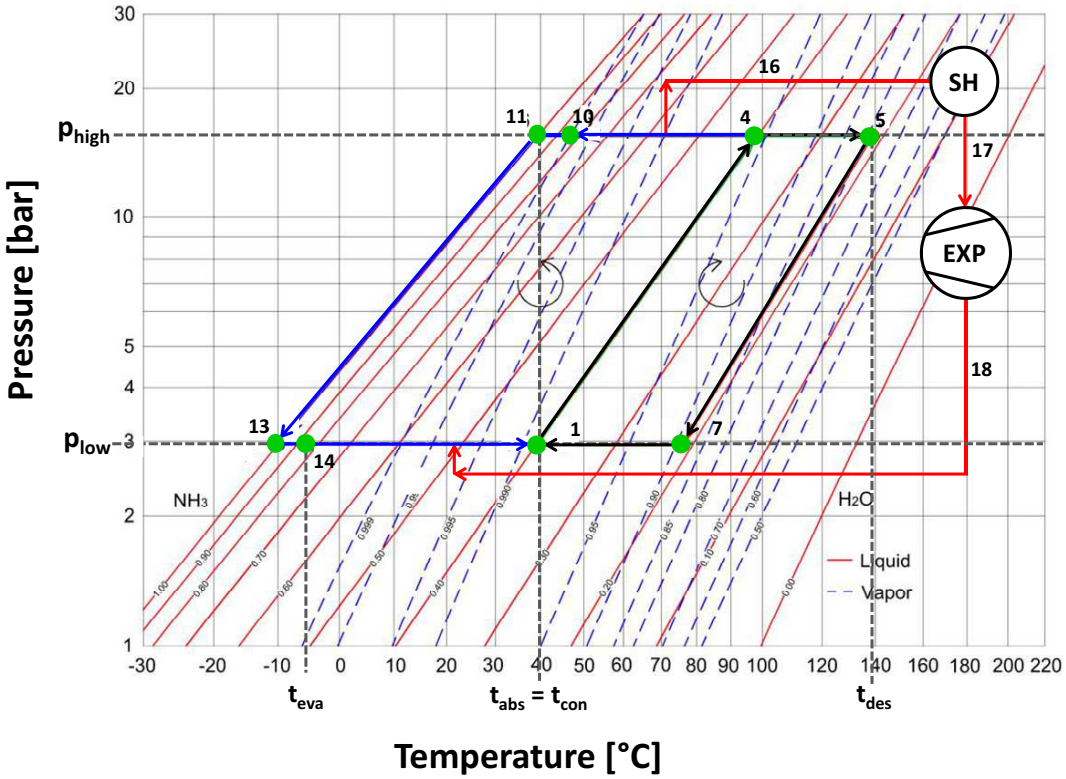

Figure 3.2: A single-stage combined absorption power and refrigeration cycle with parallel flow arrangement on P-T-x-y diagram of NH_3/H_2O mixture.

3.3.2 Operating characteristics and analysis of SSAPRC-P

The energetic and exergetic performance analysis of the SSAPRC-P has been performed for the cycle input operating conditions and design parameters provided in Table 3.1.

Table 3.1: Input operating conditions and design parameters for single-stage combined absorption cycle with parallel flow arrangement (SSAPRC-P, Fig. 3.1).

Input variable	Values
Typical chilled fluid inlet/outlet temperatures, $t_{cf,in}/t_{cf,out}$ [°C]	$8/3^a$, $12/7^b$, $16/11^c$ and $20/15^d$
Cooling water inlet/outlet temperatures, $t_{cw,in}/t_{cw,out}$ [°C]	27/32, 32/37, 37/42 and 42/47
(parallel flow arrangement for absorber and condenser)	
Vapour split ratio, SR [-]	0.6
(for co-production mode of operation)	
Isentropic efficiency of expander, η_{exp} [%]	85
Basic solution ammonia mass fraction, $\dot{m}_1$ [kg/s]	1.0

[a] Refrigeration applications (e.g. milk storage); [b] Space air-conditioning using Fan Coils;
[c,d] Space air-conditioning using Cooled Ceilings

A fixed split ratio ($SR = 0.6$) is considered to investigate the influence of the heat source inlet temperature on the cycle useful dual-outputs and efficiencies when the cycle operates on co-production mode at different operating conditions. The split ratio is defined as the ratio of the vapour mass flow rate that follows the power sub-cycle to the total amount of vapour generated by the desorber. The heat source fluid inlet temperature is varied between the minimum heat source temperature ($t_{hs,in,min}$, it corresponds to the desorber cut-off temperature) and 150 °C. The minimum heat source inlet temperature of SSAPRC-P is determined by the working fluid characteristics (NH_3/H_2O mixture), absorber, condenser, evaporator and superheater (if any) operating conditions and design parameters. The influence of the superheater operating condition for determining $t_{hs,in,min}$ is relatively low. The heat source fluid first enters into the superheater and then to the desorber. And, its mass flow rate is determined by minimising the heat capacity rates (product of specific heat capacity and mass flow rate) mismatch in the desorber. It means that the temperature difference between the hot and cold streams at the hot and cold end of the desorber are the same [159]: it is done by adjusting the outlet temperature of the heat source fluid.

A sensitivity analysis is carried out to investigate the effect of the driving heat source temperature on the cycle's dual-outputs, energetic and exergetic performances, and operational working range. When the heat source inlet temperature is varied all the other input variables are maintained at their respective values indicated in Table 3.1. The sensitivity of the cycle dual-outputs (mechanical power and cold) with respect to the variation of the heat source inlet temperature are illustrated in Fig. 3.3 for the co-production of mechan-

ical power and chilled water at typical representative temperatures for refrigeration and air-conditioning applications (3 °C, 7 °C, 11 °C and 15 °C).

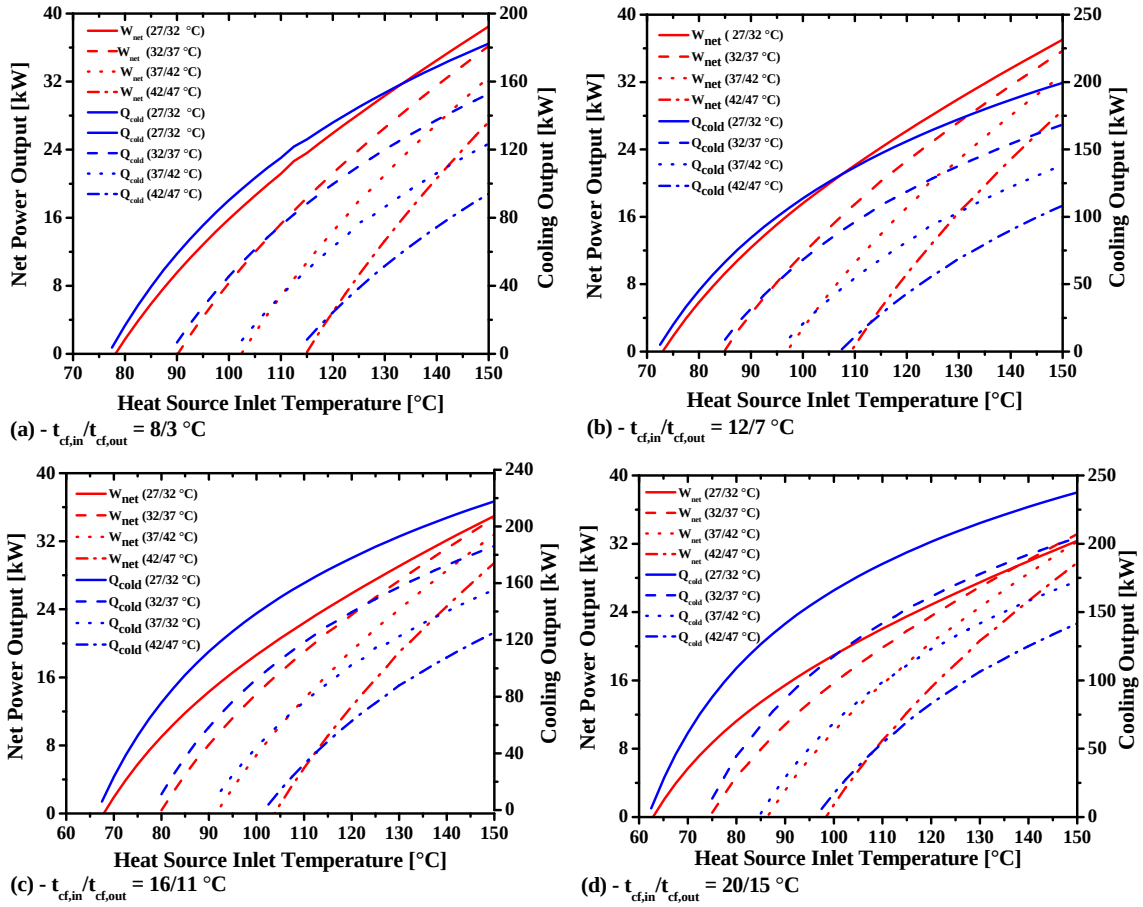

Figure 3.3: Effect of heat source inlet temperature on cycle useful outputs at several operating conditions for co-production of power and cold (SSAPRC-P).

A similar trend is observed for all the cases considered for the co-production of power and cold. As the heat sink inlet temperature (cooling water inlet temperature, $t_{cw,in}$) increases, the high pressure of the cycle increases as well, and also less ammonia vapour is absorbed in the absorber because the absorber temperature increases at constant pressure. The combined effect reduces the power and cold productions as the sink temperature increases at constant heat source and chilled fluid temperatures. Fig. 3.4 illustrates the variation of the effective first law and exergy efficiency of the cycle, with respect to the heat source inlet temperatures at several sink inlet temperatures (27 °C, 32 °C, 37 °C and 42 °C) and chilled fluid outlet temperatures (3 °C, 7 °C, 11 °C and 15 °C). As inferred from Fig. 3.4 when the heat source inlet temperature increases, the first law efficiency first also increases and

then it is flattened gradually. Thus, further increase in the heat source temperature has no gain on the effective first law efficiency of the cycle and essentially remains almost constant after certain heat source temperature value. The effective exergy efficiency of the cycle also shows an optimum value for each operating conditions considered in the sensitivity analysis. The cycle has maximum effective exergetic efficiency at lower sink temperatures and also as the chilled fluid outlet temperature increases, the effective exergy efficiency of the cycle decreases. It is mainly due to the work contribution of cold output of the cycle that increases as the chilled fluid temperature decreases.

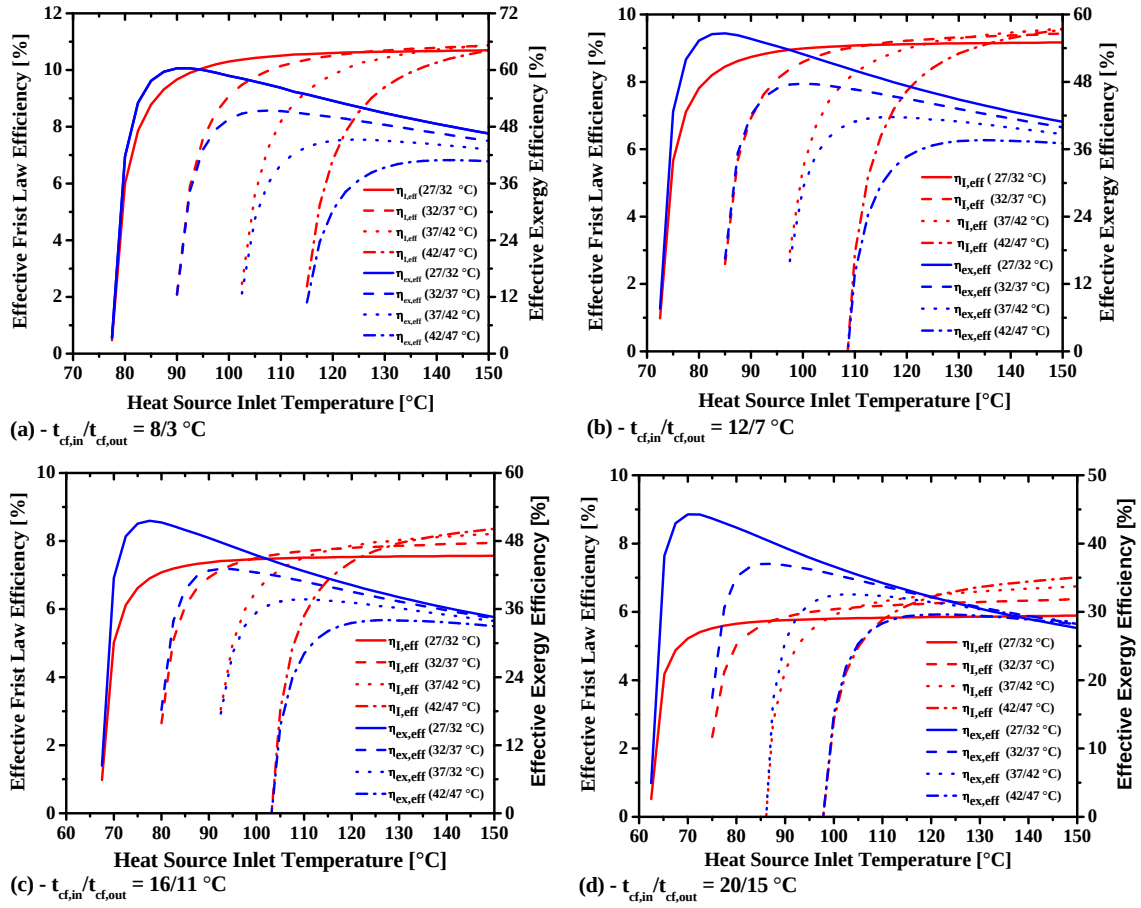

Figure 3.4: Effect of heat source inlet temperature on cycle efficiencies at several operating conditions for co-production of power and cold (SSAPRC-P).

The SSAPRC-P cycle configuration can function in different modes of operation depending on the cooling and power demand by varying its vapour split ratio (SR). The mix of power and cold production of the cycle with respect to *SR* is illustrated in Fig. 3.5 (a).

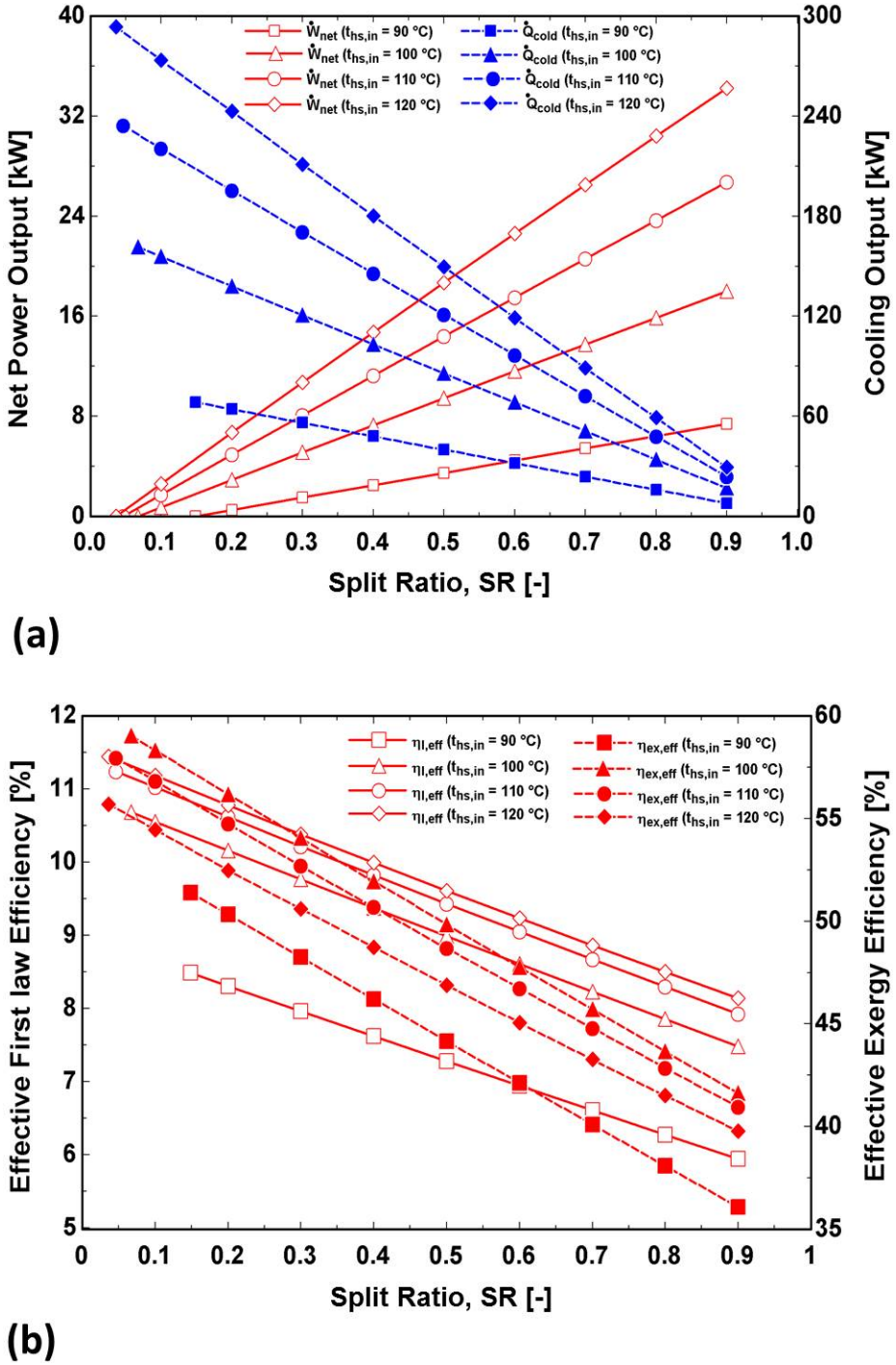

Figure 3.5: Cycle dual-outputs and efficiencies at different vapour split ratio for a typical operating conditions: (a) - power and cooling outputs; (b) - cycle efficiencies (SSAPRC-P, Fig. 3.1).

For the limiting cases, the cycle operates as pure absorption refrigeration cycle (only cold output mode) or pure absorption power cycle (only power output mode, with $SR = 1.0$). In cold mode of operation, the expander only produces the mechanical power necessary

for driving the solution pump which makes the cycle autonomous (independent of external work/electricity requirement for the solution pump). Thus, there is a corresponding split ratio to fulfil the power consumption of the solution pump (see Fig. 3.5 (a) when the net power output is null). When the cycle operates as a power cycle, the high pressure of the cycle is no longer dependent on the operating condition of the condenser and its value is between the bubble and dew pressures of the basic NH_3/H_2O solution at the desorber temperature. Therefore, a pressure that maximizes the effective exergy efficiency is taken as the optimum high pressure of the cycle. The performance indicators and useful output of the cycle at their corresponding optimum pressure are shown in Table 3.2. Another possible position for the vapour mass flow splitter is at the vapour outlet of the rectifier (at state 10 in Fig. 3.1). This means the vapour generated in the desorber is split into two portions by a split ratio (SR) for power and refrigeration sub-cyclic processes after purified in the rectifier. In this case the SR is defined as the ratio of the vapour mass flow rate that follows the power sub-cycle to the total purified vapour from the rectifier.

Table 3.2: Performance indicators and net power output of the SSAPRC-P operating as an absorption power cycle (SR=1.0) and the absorber at a heat sink inlet/outlet temperatures of 32/37 °C.

Parameter	**Value**				**Performance summery**	**Value**			
Heat source inlet temperature [°C]	90	100	110	120		90	100	110	120
Dew pressure [kPa]	111	162	232	324	Net power output [kW]	14.0	20.6	25.7	32.3
Bubble pressure [kPa]	1664	2067	2531	3060	First law efficiency [%]	6.1	7.1	8.1	9.0
Optimum cycle's high pressure [kPa]	1236	1403	1688	1948	Exergy efficiency [%]	37.9	39.5	41.0	42.0

Analogues to the Goswami combined power/cooling cycle, the rectified vapour of the power sub-cycle of the SSAPRC-P can expand to very low temperatures (below the ambient) consequently depending on the cycle's operating conditions sensible cooling output could be obtained by incorporating sensible heat exchanger (cooler) at the expander's exhaust (state 18 in Fig. 3.1). In this case, the superheater in the power sub-cycle has an adverse effect on the sensible cooling output of the cooler, the cycle preferably operates without superheating. Therefore, with this modification power and cold both sensible and latent at the same or different temperature levels (e.g. at 3 °C latent cooling and at 15 °C sensible cooling) could be obtained.

3.4 Single-Stage Combined Absorption Power and Refrigeration Cycle with Two Desorbers (SSAPRC-2D)

A new combined NH_3/H_2O absorption cycle is proposed for the co-production of mechanical power and cold. This cycle configuration is developed by introducing a second desorber at higher temperature in a single-effect NH_3/H_2O absorption refrigeration cycle. The second desorber is followed by a power sub-cycle with internal heat recovery. Fig. 3.6 shows the schematic diagram of the cycle configuration (SSAPRC-2D).

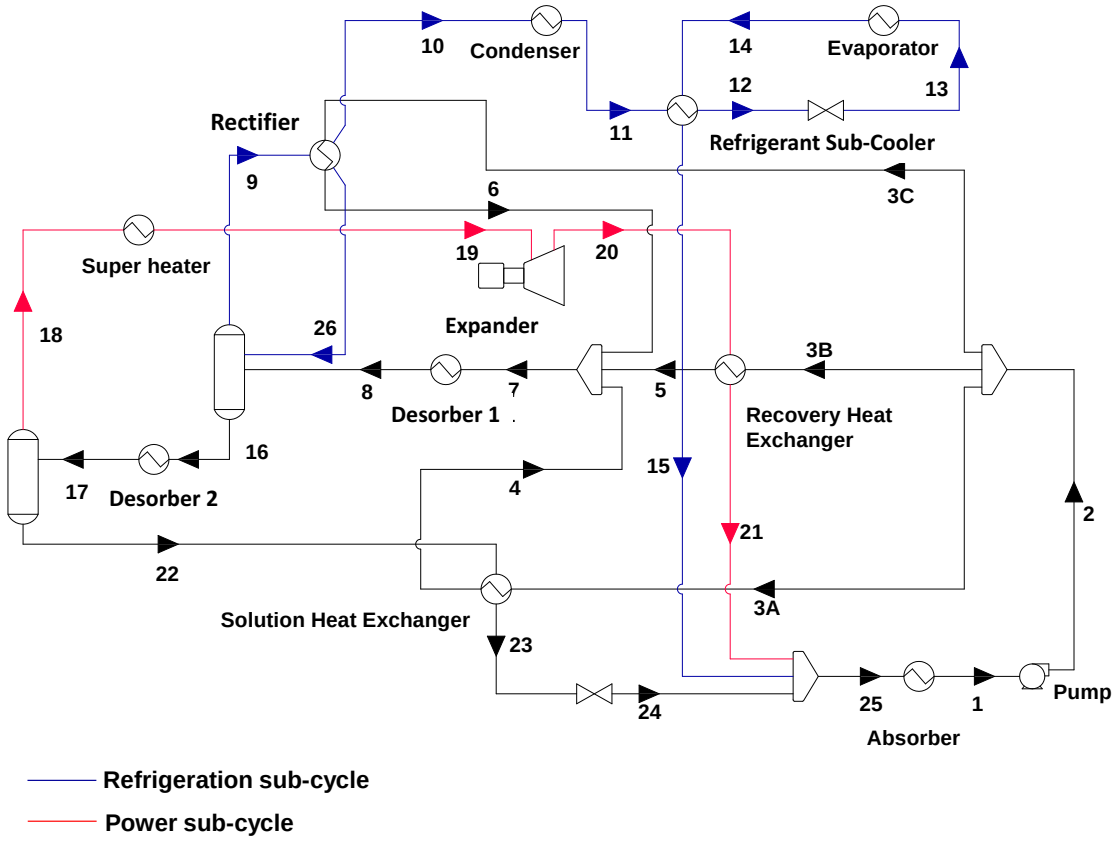

Figure 3.6: Flow schematic diagram of single-stage combined absorption cycle with two desorbers (SSAPRC-2D).

3.4.1 Process description of SSAPRC-2D

The cycle operates at two pressure levels, those given by the condenser at high pressure and the evaporator at low pressure. An NH_3/H_2O mixture, basic solution (state 1), is pumped from the absorber to the cycle high pressure (state 2) and split into three streams (states 3A, 3B and 3C). Stream 3B recovers heat internally before re-mixed (state 7) and enters

into the low-temperature desorber (Desorber 1, DES 1). The basic solution is partially boiled in Desorber 1 and separated into liquid (state 16) and vapour stream (state 9), which is further purified in the rectifier (state 10). The liquid condensate leaving the rectifier (reflux condenser, state 26) is re-mixed with the basic solution leaving desorber 1 (state 8) in the low temperature separator. Then, the liquid solution (state 16) is boiled in the high temperature desorber (Desorber 2, DES 2) and separated into vapour (state 18) and liquid (state 22) streams. The liquid solution (state 22) is throttled to the cycle low pressure (states 23-24) after exchanging heat with basic solution.

The vapour from the high-temperature separator (state 18) begins the power sub-cycle process (states 18-19-20-21) by being superheated to the highest temperature in the cycle (state 19). It then expands in the work developing expander to generate mechanical power (states 19-20). The expander exhaust is then cooled in recovery heat exchanger (states 20-21) by preheating the part of the basic solution (states 3B-5). The remaining basic solution (state 3C) is pre-heated by the recovered heat from the rectifier (states 3C-6) and weak solution in the solution heat exchanger (states 3A-4).

The purified vapour (state 10) begins the refrigeration sub-cycle process (states 10-11-12-13-14-15). After condensing in the condenser, the refrigerant is sub-cooled (states 11-12) by heating the vapour leaving the evaporator (states 14-15) and then throttled (states 12-13) in the expansion valve before it produces the cooling effect in the evaporator (states 13-14). The three streams (states 15, 21 and 24) mix to regenerate the basic solution (state 25), which is cooled in the absorber to state 1, and this completes the whole cycle process.

3.4.2 Operating characteristics and analysis of SSAPRC-2D

Pressurized hot water is used as a driving heat source fluid. In order to get a better temperature match between the heat source fluid and working fluid (NH_3/H_2O mixture) in the heat addition process, the superheater, and the high- and low-temperature desorbers are arranged in series according to their temperature levels. The external cooling water streams for the absorber and condenser are connected in parallel flow arrangement.

The thermodynamic performance evaluation of the proposed combined absorption cycle (SSAPRC-2D) is performed for a heat source inlet temperature ($t_{hs,in}$) between 125 °C and 160 °C. The effect of the cooling water (heat sink) inlet temperature on the cycle

performance is evaluated for a range of temperature between 22 °C and 42 °C. The chilled fluid outlet temperature is also varied between −10 °C to 10 °C. A unit (1 kg/s) of basic solution through the pump is taken as a bases for calculation. In addition to the assumptions considered for the generic combined absorption cycle modelling, the following additional assumptions were used in the thermodynamic model of the SSAPRC-2D cycle configuration:

- Temperature difference ($\triangle T$) between high-temperature desorber (DES 2) and low-temperature desorber (DES 1) is set to 10 K, $t_8 = t_{17} - 10$.
- Optimum split ratio of 0.277 is considered. The split ratio is defined as the ratio of the mass flow rate of the basic solution to the recovery heat exchanger to the mass flow rate of the basic solution from the absorber, $SR = \frac{\dot{m}_{2B}}{\dot{m}_1}$ see Fig. 3.6). And, it's value is obtained by minimizing the amount of the driving heat input of the cycle.
- State points (Fig. 3.6) at 1, 11, 16, 22 and 26 are saturated liquid at their corresponding pressures and temperatures.
- State points (Fig. 3.6) at 9, 10, and 18 are saturated vapour at the condenser pressure and their corresponding temperatures.
- A 10 K degree of superheating is considered in the superheater of the cycle.
- Minimum approach temperatures of 5 °C is considered at the inlet of superheater and low-temperature desorber (DES 1).
- Minimum temperature difference between the cold and hot streams at the warm end of the rectifier is 5 °C.

The influence of heat source inlet temperature on the cycle performance such as power produced, cooling capacity, effective first law efficiency and exergy efficiency and power/cold ratio is shown in Fig. 3.7 (a) and (b), respectively.

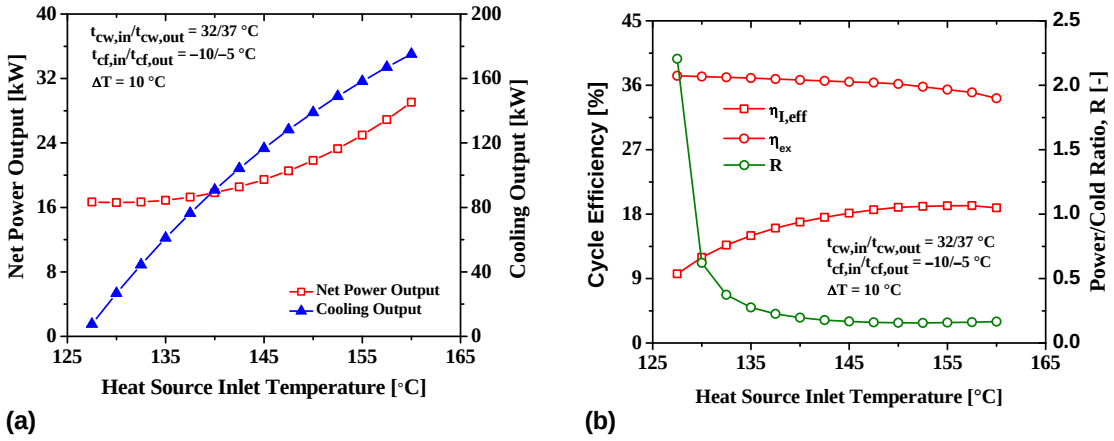

Figure 3.7: Effect of heat source inlet temperature on: (a) - cycle useful outputs; (b) - cycle efficiencies and power/cold ratio (SSAPRC-2D).

The cycle has an optimum value for the effective first law efficiency around the heat source inlet temperature of 148 °C at the baseline case considered in the cycle simulation ($t_{cw,in}/t_{cw,out}$ = 32/37 °C and $t_{cf,in}/t_{cf,out}$ =−5/−10 °C). The base-case performance summary for the proposed absorption cycle for power and cooling applications is shown in Table 3.3, and the corresponding stream characteristics is also provided in Table 3.4.

Table 3.3: Base-case performance summary for the proposed absorption cycle for power and cooling applications (SSAPRC-2D) ($\dot{m}_1 = 1$ kg/s basis for calculation).

Useful dual-output [kW]		**Mechanical power [kW]**	
Cooling output $\dot{Q}_{cold}$	130.39	Expander $\dot{W}_{exp}$	22.51
Net power output $\dot{W}_{net}$	20.78	Solution pump $\dot{W}_{sp}$	1.74
Thermal power [kW]		**Exergy flow [kW]**	
Absorber heat duty $\dot{Q}_{abs}$	374.27	Cooling exergy ($\dot{E}x_{cold}$)	15.96
Condenser heat duty $\dot{Q}_{con}$	131.13	Heat source exergy input ($\triangle\dot{E}x_{hs,in}$)	101.06
Low-temperature desorber heat duty $\dot{Q}_{des1}$	201.57	**Performance indicator**	
High-temperature desorber heat duty $\dot{Q}_{des2}$	191.95	Effective first law efficiency $\eta_{I,eff}$ [%]	18.69
Rectifier heat duty $\dot{Q}_{rec}$	114.81	Power/cold ratio R [-]	0.159
Refrigerant sub-cooler heat duty $\dot{Q}_{rsc}$	12.41	Exergy efficiency η_{ex} [%]	36.40
Recovery heat exchanger heat duty $\dot{Q}_{rhx}$	36.26		
Solution heat exchanger heat duty $\dot{Q}_{shx}$	277.35		
Superheater heat duty $\dot{Q}_{sh}$	2.27		

For a particular operating conditions, there is a minimum desorber temperature to operate the cycle. Accordingly, there is a corresponding minimum heat source temperature to fire the cycle. For the considered baseline case, the heat source temperature must be greater than 125 °C. When the heat source temperature increases from 127 °C to 160 °C,

the net mechanical power output and cooling capacity are also increased due to higher heat input (more vapour generated in both desorbers). The effective first law efficiency shows an optimum value however the exergy efficiency of the cycle is more or less steady until 150 °C. It is mainly due to the fact that the rate at which the exergy input ($\Delta\dot{E}x_{hs,in}$) of the cycle increases is more or less in the same rate as the useful exergy outputs ($\dot{W}_{net}$ and $\dot{E}x_{cold}$) of the cycle. But, above 150 °C the driving exergy input increases at a faster rate than the useful exergy outputs.

As expected, the cooling capacity of the cycle increases and net power out decreases with the increase in chilled fluid outlet temperature ($t_{cf,out}$) from 3 °C to 15 °C (see Fig. 3.8). Since the low pressure of the cycle increases as the $t_{cf,out}$ increases, the expander pressure ratio decreases as a result and the power output of the cycle decreases. Even though the specific enthalpy difference across the evaporator decreases the cooling capacity of the cycle increases because the mass flow rate of the rectified vapour increases at a faster rate than the decrease in the specific enthalpy difference across the evaporator.

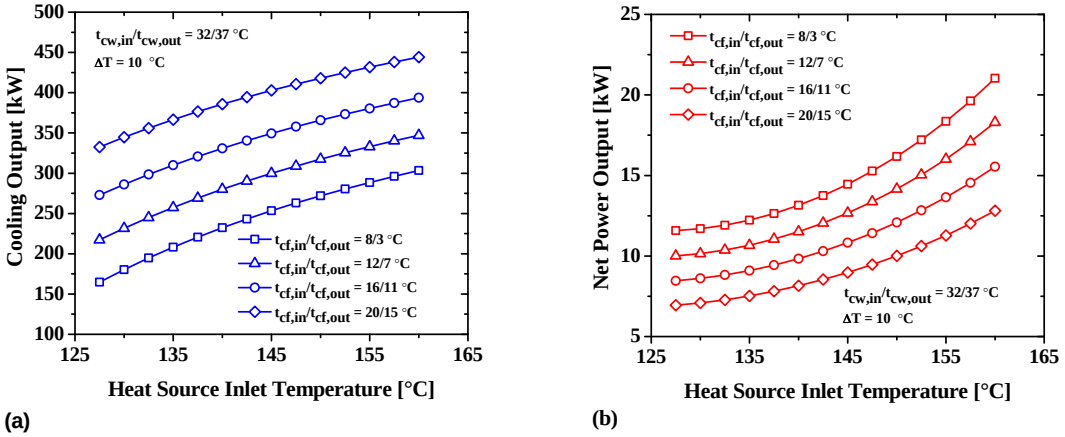

Figure 3.8: Effect of heat source inlet temperature on cycle useful outputs at several chilled fluid outlet temperatures: (a) - cooling capacity; (b) - net power output.

The effect of $\triangle T$ on cycle useful outputs, cycle efficiencies and power/cold ratio at the base-case condition is shown in Fig. 3.9. As the $\triangle T$ increases, the amount of heat supplied at high-temperature desorber also increases whereas the heat supplied in the low-temperature desorber decreases, leading to higher power output and lower cooling capacity. From the figures, it is observed that there is an optimum $\triangle T$ where both effective first law efficiency is maximum at the base-case condition.

Table 3.4: The base-case stream characteristics for the proposed SSAPRC-2D absorption cycle configuration (Fig. 3.6).

State point (i)	t_i[°C]	p_i[kPa]	z_i[kg/kg]	$\dot{m}_i$[kg/s]	h_i[kJ/kg]	s_i[kJ/kg K]	ex_i[kJ/kg]
1	37.0	236	0.3715	1	56.27	0.911	45.18
2	37.2	1427	0.3715	1	58.00	0.912	46.58
3A	37.2	1427	0.3715	0.4911	58.00	0.912	46.58
3B	37.2	1427	0.3715	0.2770	58.00	0.912	46.58
3C	37.2	1427	0.3715	0.2319	58.00	0.912	46.58
4	118.8	1427	0.3715	0.4911	622.72	2.480	143.79
5	65.9	1427	0.3715	0.2770	188.90	1.315	57.22
6	114.3	1427	0.3715	0.2319	553.17	2.301	127.46
7	109.9	1427	0.3715	1	486.42	2.128	112.37
8	123.0	1427	0.3715	1	688.00	2.645	159.68
9	119.3	1427	0.8954	0.1642	1938.77	6.445	277.63
10	54.4	1427	0.9980	0.1118	1689.05	5.840	208.42
11	37.0	1427	0.9980	0.1118	516.67	2.069	160.28
12	13.8	1427	0.9980	0.1118	405.68	1.697	160.15
13	-15.0	236	0.9980	0.1118	405.68	405.68	150.05
14	-12.0	236	0.9980	0.1118	1571.43	6.244	-29.70
15	24.7	236	0.9980	0.1118	1682.41	6.644	-38.14
16	119.3	1427	0.2926	0.8882	432.66	1.903	125.59
17	133.0	1427	0.2926	0.8882	648.77	2.445	180.35
18	133.0	1427	0.8233	0.0875	2027.00	6.573	327.60
19	143.0	1427	0.8233	0.0875	2052.99	6.637	334.74
20	74.6	236	0.8233	0.0875	1795.64	6.768	38.34
21	47.8	236	0.8233	0.0875	1381.19	5.534	-8.36
22	133.0	1427	0.2346	0.8007	498.18	1.993	164.26
23	57.0	1427	0.2346	0.8007	151.78	1.050	99.07
24	57.2	236	0.2346	0.8007	151.78	1.054	97.86
25	59.2	236	0.3715	1	430.54	2.077	71.63
26	54.4	1427	0.6760	0.0523	278.20	1.647	47.51
hs,in	148.0	451	-	2.27	623.56	1.821	85.05
hs,II	147.8	451	-	2.27	622.55	1.819	84.77
hs,III	128.0	451	-	2.27	537.99	1.613	61.55
hs,out	107.1	451	-	2.27	449.19	1.386	40.53
cw,in	32	101.325	-	24.19	134.18	0.464	0.34
cw,out	37	101.325	-	24.19	164.64	0.532	0.98
cf,in	-5	101.325	-	7.39	182.28	0.935	5.78
cf,out	-10	101.325	-	7.39	164.64	0.868	7.94

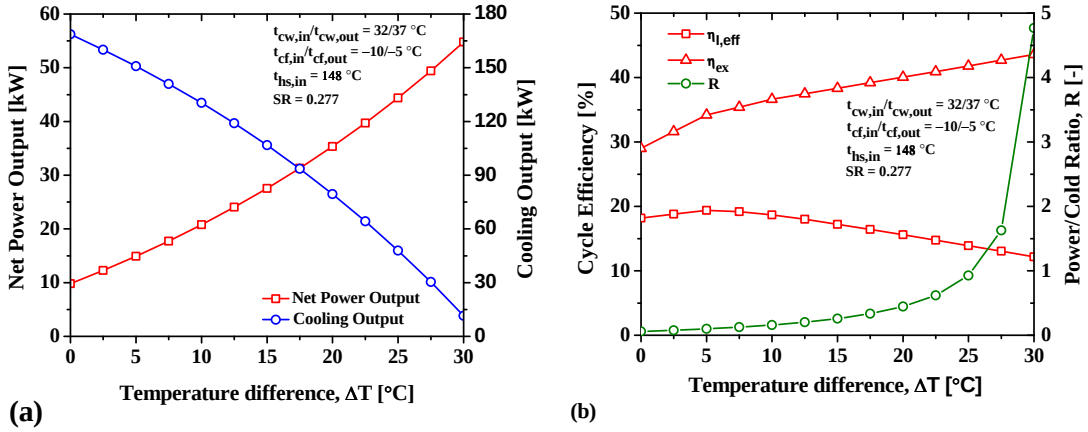

Figure 3.9: The effect of $\triangle T$ on: (a) - cycle useful outputs; (b) - cycle efficiencies and power/cold ratio at the base-case condition (SSAPRC-2D).

As seen from Fig. 3.10 (a), the cooling capacity of the cycle decreases significantly as the absorber (and condenser) cooling water temperature increases from 20 °C to 35 °C. Since the high pressure of the system increases as the cooling water inlet temperature increases, the amount of vapour desorbed (for constant desorber temperature) in both desorbers decreases. But, the specific enthalpy difference across the expander increases, consequently the net power output shows slight variation with high heat source temperatures (145 °C and 155 °C).

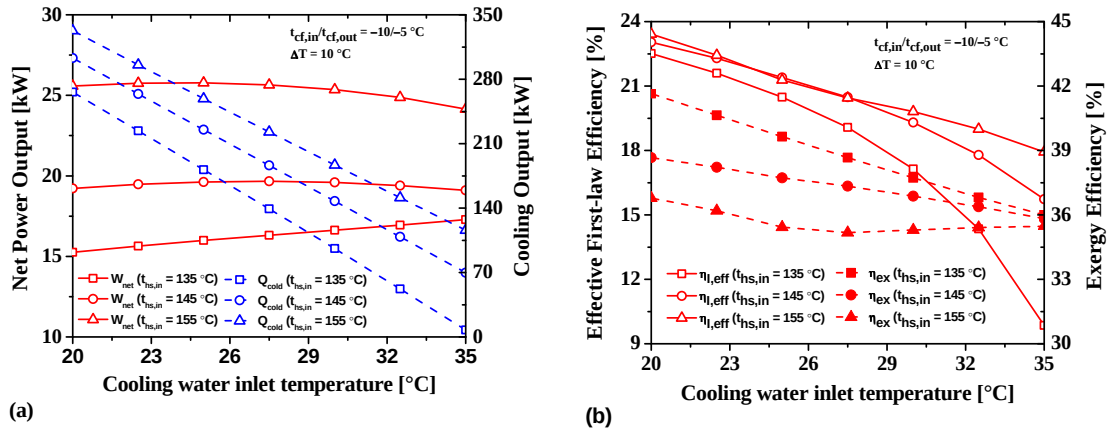

Figure 3.10: Effect of cooling water inlet temperature on: (a) - cycle useful outputs; (b) - cycle efficiencies at several heat source inlet temperatures (SSAPRC-2D).

For lower heat source inlet temperature (e.g. 135 °C), a decreasing trend is observed. The influence of cooling water inlet temperature on the cooling output is higher than that on the net power output of the cycle due to the marginal variation in the power produced

by the expander compared with the cooling capacity (Fig. 3.10 (a)). At lower heat source temperatures, the cycle efficiencies are highly sensitive to the variation of the cooling water inlet temperature (Fig. 3.10 (b)).

Fig. 3.11 illustrates the effect of the expander isentropic efficiency on cycle dual-outputs, efficiencies and power/cold ratio at the base-case condition. As expected, the expander efficiency has a higher impact on the net power output and power/cold ratio, exergetic efficiency compared with other performance parameters. It is found that at the optimum condition of heat source temperature about 148 °C, chilled fluid inlet/outlet temperatures of −5/−10 °C, a net power output of 24.6 kW and cooling capacity of 130.4 kW could be attained with effective first law and exergy efficiency of the cycle about 19.5% and 40.0%, respectively. The basic solution mass flow rate through the solution circulation pump was set at 1 kg/s.

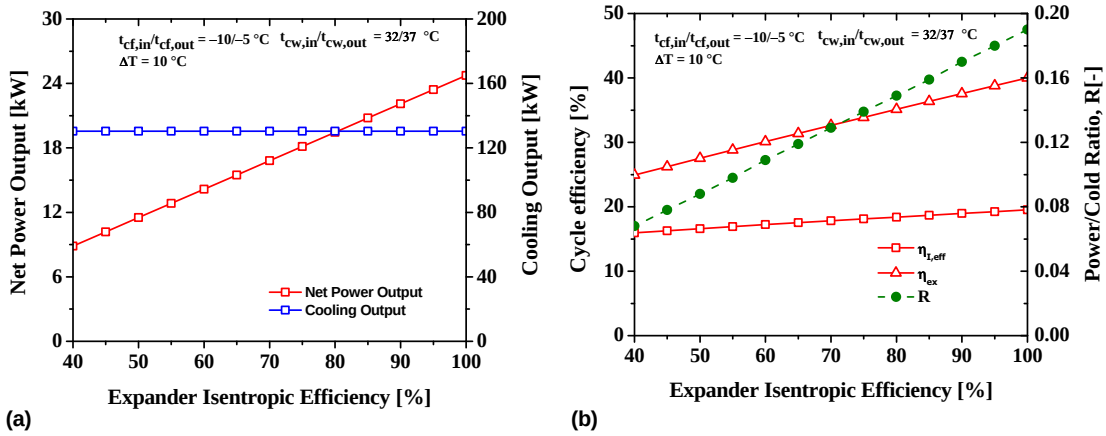

Figure 3.11: Effect of the expander (turbine) isentropic efficiency on: (a) - cycle useful outputs; (b) - cycle efficiencies and power/cold ratio at the base-case condition (SSAPRC-2D).

3.5 Single-Stage Combined Absorption Power and Refrigeration Cycle with Series flow arrangement (SSAPRC-S)

As discussed previously (in sections 3 and 4), apart from the advantages indicated, one of the limitations of the single-stage combined power and refrigeration cycles with parallel flow arrangement and the one with two desorbers (SSAPRC-P and SSAPRC-2D respectively) is that they cannot take the advantage of a relatively high temperature heat sources to achieve higher performance. It is quite obvious that the efficiency of a reversible cycle is sensitive to the driving heat input temperature, however the energetic efficiency of actual combined absorption system is essentially reached its maximum value and then no further efficiency gains despite the increase of the heat source temperature. Furthermore, the co-production of power using a SSAPRC-P system is obtained by sacrificing some of the refrigerant vapour which is otherwise be used to produce cold.

To achieve higher cycle performances, it is necessary to design a cycle that can take advantage of the higher exergy associated with a higher temperature heat input. A single-stage combined absorption cycle with series flow arrangement (SSAPRC-S) represents one of such combined absorption cycle variation. The present section is devoted to describing the operating characteristics and performance potential of the new SSAPRC-S at typical operating conditions. Other high-performance multi-stage combined absorption cycles are also possible and are presented in Chapter 5.

Fig. 3.12 depicts a single-stage combined absorption cycle with power and refrigeration sub-cycles connected in series flow arrangement. As it is seen in Fig. 3.12, the cycle configuration architecture can be viewed as the Goswami power/cooling cycle except the sensible refrigerant heat exchanger (cooler) is replaced by refrigeration sub-cycle, composed of several components, with a capability of producing latent cooling output. The refrigeration sub-cycle includes total condenser (CON), refrigerant sub-cooler (RSC), refrigerant expansion valve (REV) and evaporator (EVA). And also, the cycle becomes a triple-pressure levels cycle instead of dual-pressure levels as in the case of Goswami power/cooing cycle, SSAPRC-P and SSAPRC-2D. It is mainly due to the introduction of the total condenser. The same amount of vapour generated in the desorber of the cycle is used in both the

power and refrigeration sub-cycles to produce mechanical power and cold respectively.

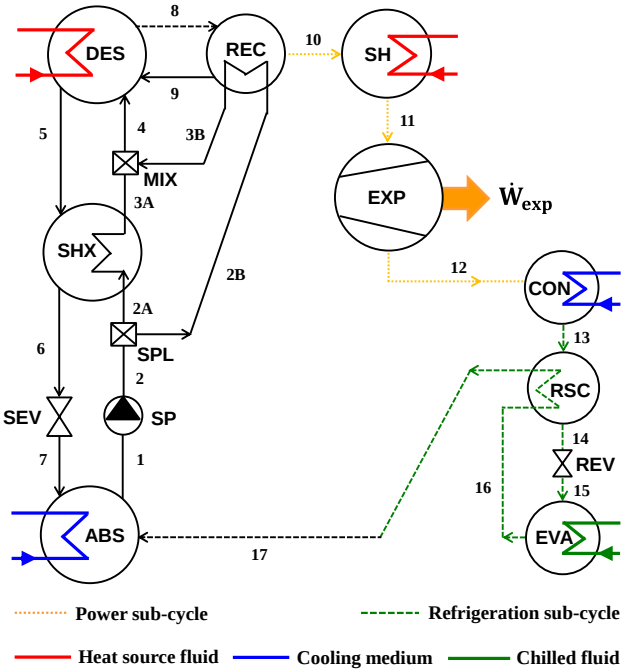

Figure 3.12: Flow schematic diagram of single-stage combined absorption cycle with series flow arrangement (SSAPRC-S).

3.5.1 Process description of the SSAPRC-S

The whole cycle essentially operates at three pressure levels, those given by the evaporator at low pressure, total condenser at intermediate pressure and desorber at high pressure. The desorber, superheater and rectifier operate at the same (high) pressure. An NH_3/H_2O mixture, the basic solution (state 1), is pumped to the cycle high pressure (state 2) and recovers heat internally before entering into the desorber (state 4). The internal heat recovery is done both in solution heat exchanger (states 2A-3A) and rectifier (states 2B-3B) as shown in Fig. 3.12.

After the heat recovery, the basic solution is then partially boiled in the desorber using external heat input $\dot{Q}_{des}$ and separated into liquid (state 5) and vapour (state 8) which is further purified in the rectifier (state 10). The liquid condensate leaving the rectifier is returned to the desorber (state 9). The rectified vapour follows the power sub-cycle process first superheated (states 10-11) by external heat input $\dot{Q}_{sh}$ and then expanded in the expander (states 11-12) to intermediate pressure for developing the mechanical power

output $\dot{W}_{exp}$. The exhaust of the EXP (state 12) is liquefied in the total condenser (states 12-13) at an intermediate pressure by rejecting heat $\dot{Q}_{con}$ to the cooling medium and then follows a similar refrigeration sub-cycle process (states 13-14-15-16-17) as of the SSAPRC-P. The weak, in ammonia, solution leaving the desorber (state 5) is throttled in the solution expansion valve (states 6-7) to the cycle low pressure after exchanging heat with the portion of the basic solution (states 5-6).

Finally, the vapour stream (state 17) is absorbed by a weak, in ammonia, solution from the desorber which then leaves the absorber as strong, in ammonia, solution (state 1). The heat of absorption $\dot{Q}_{abs}$ is rejected to the cooling medium.

3.5.2 Operating characteristics and analysis of SSAPRC-S

The energetic and exergetic performance evaluation of the SSAPRC-S is performed for a heat source inlet temperature between 150 °C to 200 °C in steps of 10 °C which corresponds to low-grade heat source range. In this analysis, the absorber and condenser heat rejection mediums are connected in parallel flow arrangement whereas the external heat source fluid circuit of the desorber and superheater are connected in series being the superheater first. A typical operating conditions are selected for the absorber (and condenser) and evaporator of the cycle: cooling water and chilled water inlet/outlet temperatures of 27/32 °C and 12/7 °C, respectively. A unit mass flow rate of basic solution is assumed for the extensive variables (quantities) calculation. The heat source fluid mass flow rate is determined by minimising the mismatch of thermal capacitance rates in the desorber: it is done by adjusting the heat source fluid outlet temperature in order to get similar temperature difference at the hot and cold end of the desorber [159].

The useful dual-outputs and cycle efficiencies of the SSAPRC-S at various heat source fluid inlet temperatures and expander pressure ratios ($pr_{exp} = p_{des}/p_{con}$) are illustrated in Fig. 3.13 (a and b) and Fig. 3.14 (a and b) respectively. As the expander pressure ratio increases, the amount of vapour desorbed in the desorber, at constant heat source inlet temperature, decreases consequently the cooling output of the cycle also decreases (Fig. 3.13 (b)). However, the power developed by the expander has an optimum value for each heat source temperature (see Fig. 3.13 (a)) it is mainly due to the trade-off between the change in specific enthalpy drop across the expander and amount of vapour flowing

through the power sub-cycle. It is obvious that the power consumption of the solution pump increases as the desorber pressure increases.

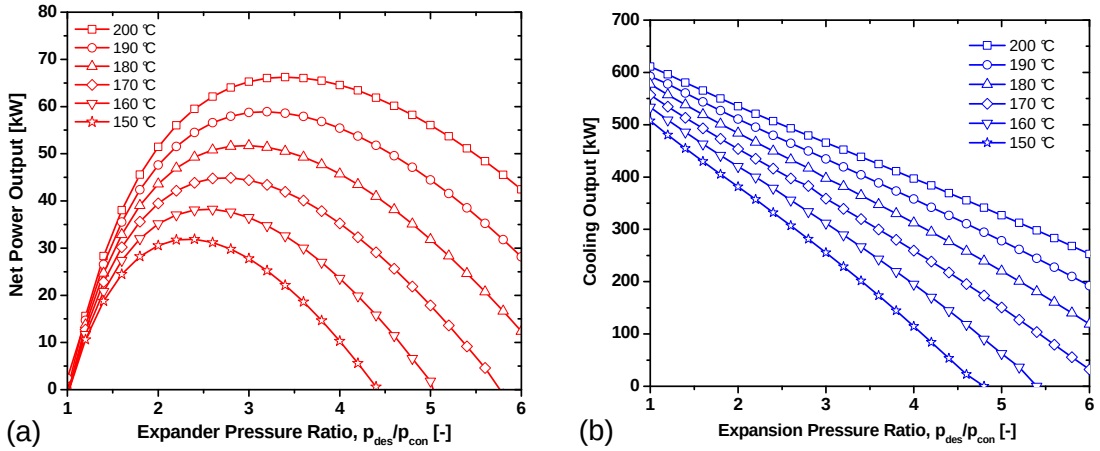

Figure 3.13: Effect of expander pressure ratio on cycle useful dual-outputs at several heat source inlet temperatures: (a) - net power output; (b) - cooling output (SSAPRC-S).

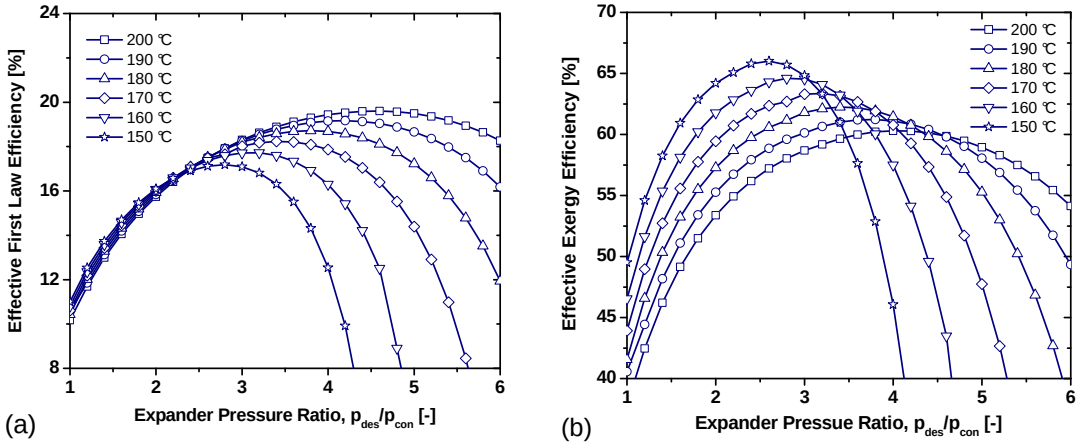

Figure 3.14: Effect of expander pressure ratio on the cycle efficiencies at several heat source inlet temperatures: (a) - effective first law efficiency; (b) - effective exergy efficiency (SSAPRC-S).

At constant heat source temperature, both the driving heat and exergy inputs (i.e. change in exergy of the heat source fluid) to the cycle decreases as the expander pressure ratio increases. The work contribution of the cooling output ($\frac{\dot{E}x_{cold}}{\eta_{II,ref}}$, in the effective first-law and exergy efficiency definitions) also decreases as the expander pressure ratio increases. The combined effect on the energetic and exergetic efficiencies of the cycle are illustrated in Fig. 3.14 (a) and (b) and, consequently, there is an optimum expansion pressure ratio for

each heat source inlet temperature that maximize the cycle efficiencies. It can be used as one of the criteria for the selection of a suitable expander for the system. When the cycle operates at $pr_{exp} = 1.0$, it produce only cold output, thus, it operates as a single-effect absorption chiller. The total exergy destruction is a quantitative measure of the lost work potential of the driving thermal energy being fed to the cycle, and it is the amount of this supplied energy which may no longer be used to produce mechanical work following the heat transformation process. It is generally used as a means of estimating the amount of irreversibility/exergy destruction within the system (a reversible cycle, has no exergy destruction), and thus it should be minimized at all times. It is simply quantified by summing the exergy destruction for each component. As shown in Fig. 3.15, the total exergy destruction rate of the cycle decreases with similar trend as the expansion pressure ratio increases for all heat source inlet temperatures considered.

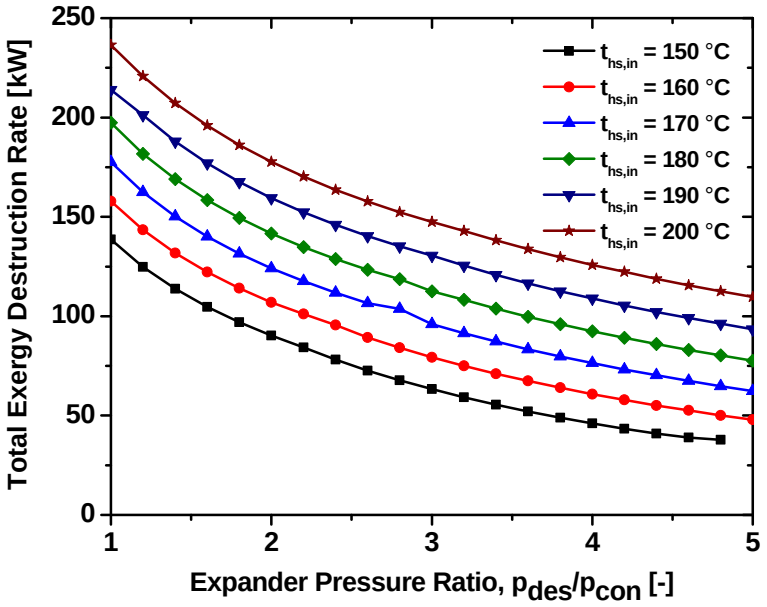

Figure 3.15: Effect of expander pressure ratio on the total exergy destruction rate of the cycle at several heat source fluid inlet temperatures (SSAPRC-S).

Since the cycle has an optimum expansion pressure ratio (to maximize the cycle efficiencies) for each heat source inlet temperature, a heat source temperature of 150 °C with its corresponding optimum expansion pressure ratio of about 2.5 is considered as a baseline case, and also, the typical cooling water and chilled water inlet/outlet temperatures are also

maintained: $t_{cf,in}/t_{cf,out}$ = 12/7 °C and $t_{cw,in}/t_{cw,out}$ = 27/32 °C respectively. The base-case performance summary for the SSAPRC-S is shown in Table 3.5 and its corresponding stream characteristics are provided in Table 3.6.

Table 3.5: Base-case performance summary for the proposed combined absorption cycle (SSAPRC-S) ($\dot{m}_1 = 1.0$ kg/s basis for calculation).

Useful dual-outputs [kW]		**Mechanical power [kW]**	
Cooling output $\dot{Q}_{cold}$	319.58	Expander $\dot{W}_{exp}$	35.67
Net power output $\dot{W}_{net}$	31.62	Solution pump $\dot{W}_{sp}$	4.05
Thermal power [kW]		**Exergy flow [kW]**	
Absorber heat duty $\dot{Q}_{abs}$	472.06	Cooling exergy ($\dot{E}x_{cold}$)	17.53
Condenser heat duty $\dot{Q}_{con}$	344.79	Heat source exergy input ($\triangle\dot{E}x_{hs,in}$)	136.57
Desorber heat duty $\dot{Q}_{des}$	468.75	**Performance indicators**	
Rectifier heat duty $\dot{Q}_{rec}$	46.61	Effective first law efficiency $\eta_{I,eff}$ [%]	17.03
Refrigerant sub-cooler heat duty $\dot{Q}_{rsc}$	19.77	Power/cold ratio R [-]	0.099
Solution heat exchanger heat duty $\dot{Q}_{shx}$	296.93	Effective exergy efficiency $\eta_{ex,eff}$ [%]	65.95
Superheater heat duty $\dot{Q}_{sh}$	60.15		

The total exergy destruction rate at the baseline case is about 75.28 kW, where the contribution of each cycle component to the total exergy destruction rate is illustrated in Fig. 3.16. This figure shows that the absorber and solution heat exchanger are the key components with the highest contribution to the total exergy destruction. The main reason for the higher exergy destruction rate observed in the absorber is because of the mass transfer between the internal streams and heat transfer takes place between the NH_3/H_2O working fluid and the external cooling water circuit.

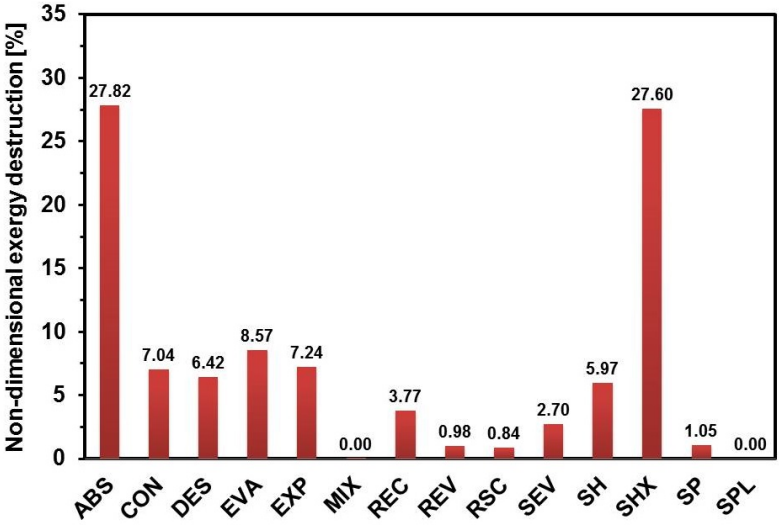

Figure 3.16: Exergy destruction for components at the baseline operating conditions.

Table 3.6: The base-case stream characteristics for the proposed combined absorption cycle (SSAPRC-S) shown in Fig. 3.12.

State point (i)	t_i[°C]	p_i[kPa]	z_i[kg/kg]	$\dot{m}_i$[kg/s]	h_i[kJ/kg]	s_i[kJ/kg K]	ex_i[kJ/kg]
1	32.0	496	0.5436	1	83.76	1.064	26.87
2	32.4	3089	0.5436	1	87.81	1.067	30.13
2A	32.4	3089	0.5436	0.8607	87.81	1.067	30.13
2B	32.4	3089	0.5436	0.1393	87.81	1.067	30.13
3A	103.4	3089	0.5436	0.8607	432.80	2.081	72.85
3B	101.4	3089	0.5436	0.1393	422.50	2.053	70.73
4	103.2	3089	0.5436	1	431.34	2.077	72.55
5	140.3	3089	0.3734	0.7275	548.49	2.269	132.48
6	55.0	3089	0.3734	0.7275	140.35	1.165	53.37
7	55.4	496	0.3734	0.7275	140.35	1.175	50.58
8	106.4	3089	0.9802	0.2836	1784.23	5.779	321.63
9	106.4	3089	0.5436	0.0111	447.82	2.121	76.03
10	75.9	3089	0.9980	0.2725	1667.78	5.459	300.51
11	145.0	3089	0.9980	0.2725	1888.53	6.039	348.36
12	75.6	1235	0.9980	0.2725	1757.61	6.106	197.44
13	32.0	1235	0.9980	0.2725	492.26	1.991	159.21
14	16.8	1235	0.9980	0.2725	419.73	1.747	159.4
15	4.0	496	0.9980	0.2725	419.73	1.756	156.7
16	7.0	496	0.9980	0.2725	1592.54	5.985	68.6
17	26.2	496	0.9980	0.2725	1665.08	6.236	66.2
hs,in	150.0	476.2	-	2.967	632.20	1.842	632.2
hs,int.	145.3	476.2	-	2.967	611.90	1.794	81.7
hs,out	108.2	476.2	-	2.967	453.90	1.398	453.9
cw,in	27	101.33	-	39.08	113.30	27	0.02792
cw,out	32	101.33	-	39.08	134.20	32	0.3382
cf,in	12	101.33	-	15.23	15.23	12	1.2
cf,out	7	101.33	-	15.23	15.23	7	2.4

Even though there is also a simultaneous mass and heat transfers in the desorber, its contribution to the total exergy destruction is relatively low. This is mainly due to the assumed perfect thermal capacitance match between the heat source fluid and NH_3/H_2O mixture in the desorber that minimize the exergy destruction. Regarding the solution heat exchanger, its higher exergy destruction rate is mainly attributed to the thermal capacitance miss-match between the strong and weak solutions as well as the assumed

effectiveness value (80%), it's exergy destruction rate can be reduced by assuming higher effectiveness values. There is no exergy destruction in the stream splitter (SPL) and insignificant exergy destruction is observed for the stream mixer (MIX) about 0.0035%.

The heat rejection medium (cooling water) inlet temperature and expander isentropic efficiency are varied in order to evaluate their effect on net power and cooling outputs, effective first law and exergy efficiencies, and total exergy destruction rate of the cycle. The cold produced by the combined absorption cycle (SSAPRC-S) is considered at a typical representative temperatures for refrigeration and air-conditioning applications which are given in Table 3.7 together with other parameters used for this sensitivity analysis.

Table 3.7: Input operating conditions and design parameters assumed for the sensitivity analysis of the proposed combined absorption cycle: SSAPRC-S.

Parameter	Value
Heat source inlet temperature, $t_{hs,in}$ [°C]	160, 170, 180
Cooling water inlet temperature, $t_{cw,in}$ [°C]	22–42
Typical chilled water inlet/outlet temperature, $t_{cf,in}/t_{cf,out}$ [°C]	8/3, 12/7, 16/11, 20/15
Expander isentropic efficiency, η_{exp} [%]	50, 75, 85, 100
Expander pressure ratio, $pr_{exp} = {}^{pr_{des}}/_{pr_{con}}$ [-]	3.0
Rectifier minimum temperature difference (at warm end), $\triangle T_{pinch}$ [°C]	5

3.5.2.1 Effect of heat sink inlet temperature

As seen from Fig. 3.17 (a-d), the useful dual-outputs of the cycle decrease significantly when the heat sink inlet temperature increases from 22 °C to 42 °C at constant heat source inlet temperature and expander pressure ratio. This is mainly because of the fact that when the heat sink inlet temperature increases the intermediate pressure of the cycle also increases, and therefore the high pressure of the cycle increases. Thus, less vapour is generated at constant heat source and chilled fluid inlet temperatures.

At the same heat sink and heat source temperatures, the concentration of ammonia in the basic solution (state 1, Fig. 3.12) increases as the chilled water inlet temperature increases: it is because the low pressure of the cycle increases and hence the absorption process is enhanced. As a result more power and cold are produced at high chilled water inlet temperatures. It is obvious that the power and cold production increases as the heat source temperature increases (see Fig. 3.17 (a-d)).

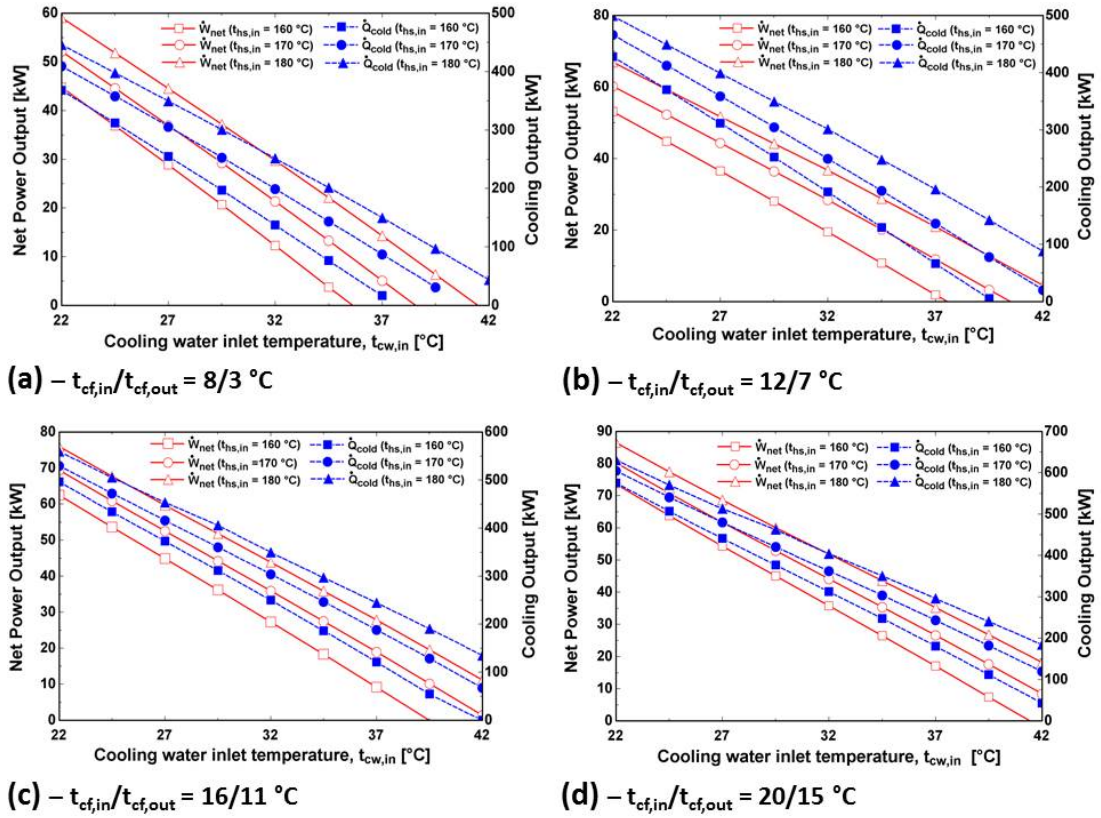

Figure 3.17: The effect of the cooling water inlet temperature on cycle useful dual-outputs at several heat source and chilled fluid temperatures (SSAPRC-S).

The variation of effective first law and effective exergy efficiencies, and power/cold ratio with respect to the cooling water inlet temperature at several chilled water inlet/outlet temperatures is shown in Fig. 3.18 (a-d). The effective exergy efficiency of the cycle is highly sensitive to the variation of the heat sink temperature in all the considered cases. However, the effective first law efficiency of the cycle is less sensitive to the variation of the heat sink temperature in particular at lower heat sink temperatures. The power/cold ratio of the cycle also shows a similar decreasing trend in all the cases with high sensitivity at high heat sink temperatures.

3.5.2.2 Effect of expander isentropic efficiency

The effect of expander isentropic efficiency on the cycle useful dual-outputs (power and cold) is shown in Fig. 3.19 (a) and (b) at two typical heat sink temperatures. In this sensitivity analysis, the chilled water inlet/outlet temperature is kept at 12/7 °C and the rest of the input parameters are according to their values given in Table 3.7.

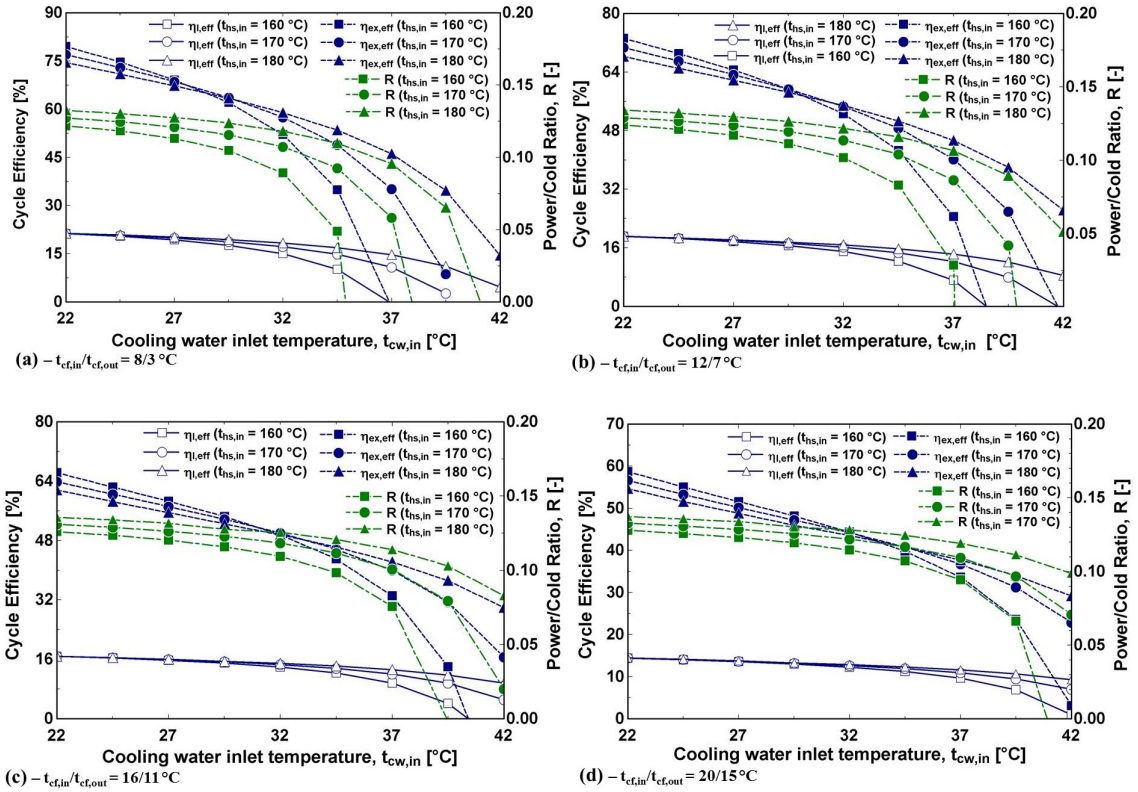

Figure 3.18: Effect of cooling water inlet temperature on cycle efficiencies and power/cold ratio at several heat source and chilled fluid inlet temperatures (SSAPRC-S).

The results show that there is a strong dependency between the expander efficiency and net power output of the cycle, however, as expected there is no effect on the cooling output of the cycle. Expander with high isentropic efficiency is more crucial for power production at high heat sink temperature conditions. For instance, the production of net mechanical power is null for expander efficiency less than 70% when the cycle operates at a heat sink medium inlet temperature of 37 °C and above at a heat source inlet temperature of 160 °C. Fig. 3.20 (a) and (d) depicts the variation of the effective first law and effective exergy efficiencies of the cycle with the expander isentropic efficiency. The chilled water inlet/outlet temperatures are maintained constant at 12/7 °C. Both efficiencies are sensitive to the variation of expander efficiency because of its effect on the co-produced power output.

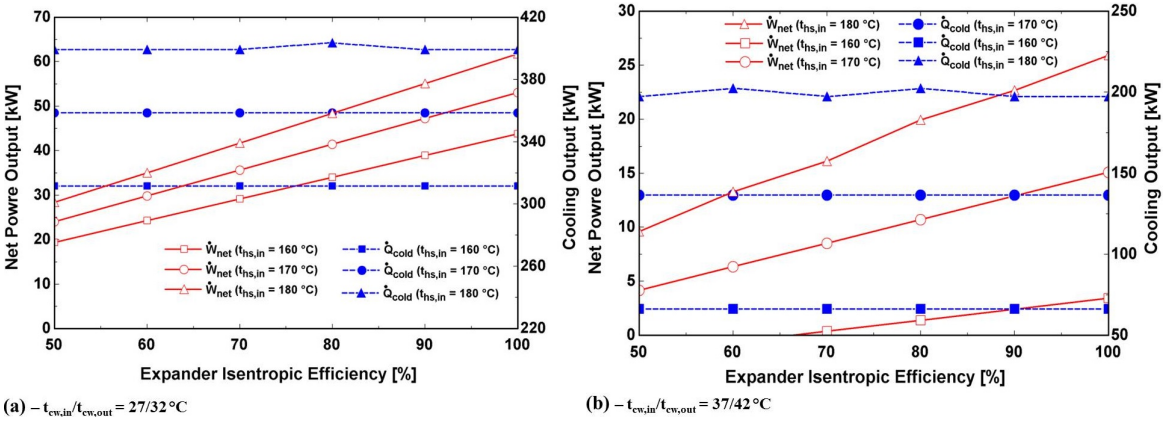

Figure 3.19: Effect of expander isentropic efficiency on cycle dual-outputs at several heat source and cooling water inlet temperatures (SSAPRC-S).

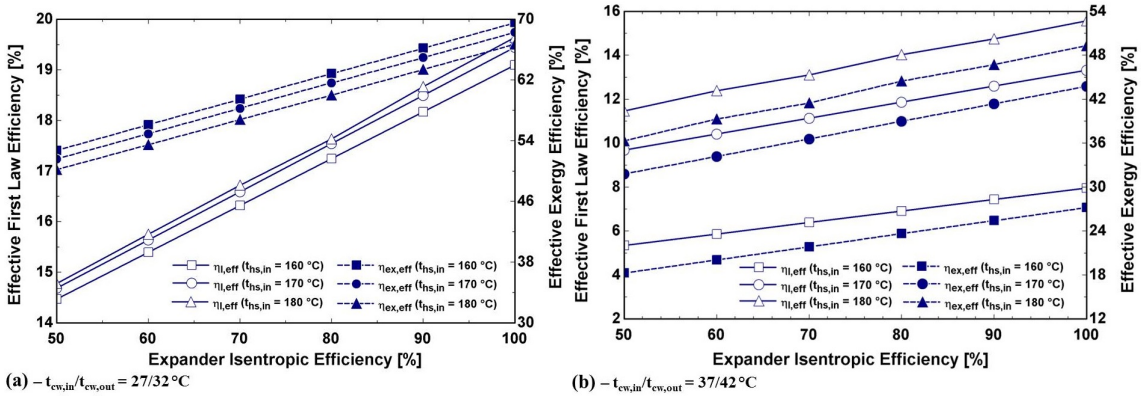

Figure 3.20: Effect of expander isentropic efficiency on cycle efficiencies at several heat source and cooling water inlet temperatures (SSAPRC-S).

3.6 Performance Comparisons

In this section, first the performance of the proposed single-stage combined absorption cycle (SSAPRC-2D) is compared with alternative systems for separate production of power and cold. The selected systems, for separate production, are organic Rankine cycle for power production whereas absorption chillers for cold production. The advantages of the other proposed combined absorption cycles (SSAPRC-P and SSAPRC-S) are clear from the energy consumption perspectives. Also, the main objectives of SSAPRC-P and SSAPRC-S configurations are: operational flexibilities in case of SSAPRC-P configuration, and in the case of SSAPRC-S configuration it is the production of more power and cold by using heat sources at relatively high temperature (150 °C to 200 °C). Then, secondly the performance

of the proposed single-stage combined absorption cycles (SSAPRC-P, SSAPRC-2D and SSAPRC-S) and the Goswami combined power/cooling cycle were compared at the same typical operating conditions.

The next subsection shows the comparison between energy consumption of separate production with co-production using SSAPRC-2D to produce equal amount of power and cold at the same thermal boundary conditions.

3.6.1 Comparison with systems that produce power and cold separately

The SSAPRC-2D cycle configuration is compared with other alternative systems for separate production of power (using regenerative ORC with n-Pentane as working fluid) and cold (single-effect NH_3/H_2O absorption refrigeration cycle) having the same power and cooling capacity. The regenerative ORC used in this analysis is shown in Fig. 3.21, and the input parameters and assumptions made are given in Table 3.8.

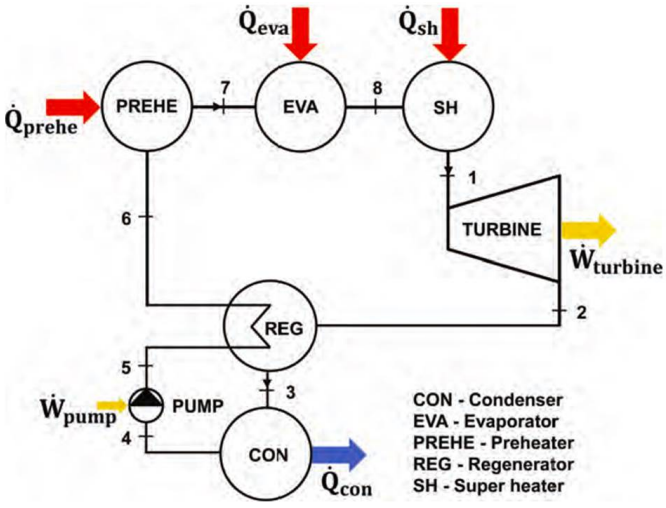

Figure 3.21: Schematic flow diagram of regenerative organic Rankine cycle used for comparison.

Other power cycles (steam Rankine, Kalina, ORC without superheating, and other working fluids) could be used for this comparison. But, the performance would be not very different and it was considered more interesting to show just one example to have an idea of the relative performance of the combined absorption power and refrigeration cycle with separate production of power and cold (refrigeration). The simulation result at the base line condition is presented in Table 3.9.

Table 3.8: Inputs and assumptions - for regenerative organic Rankine cycle.

Heat source inlet temperature [°C]	177
System high pressure [kPa]	1349
System low pressure [kPa]	285
Net mechanical power output [kW]	22.04
Working fluid: n-Pentene	
- Steady-state condition	
- No pressure change except through expander and pump	
- Degree of subcooling at the exit of the condenser (state point 4, Fig. 3.21) is 5 °C	
- State point 7 (Fig. 3.21) is saturated liquid	
- Minimum temperature difference at the cold end of the regenerator is 10 °C	
- Isentropic pump and expander efficiencies are 80 and 85%, respectively	

The driving heat input required for the ORC cycle to produce the same amount of power output, 22.0 kW, is around 160.0 kW yielding the thermal efficiency value of about 13.8%. For separate production of a cooling output of 180.8 kW at −10 °C evaporator temperature with a cycle COP of 0.48, the driving heat input required for single-effect NH_3/H_2O absorption refrigeration system is 376.7 kW. Thus, the total driving heat input required for the separate production of power and cold is about 536.7 kW. Therefore, the proposed combined absorption cycle (SSAPRC-2D) has an energy consumption that is lower by around 12% than when using the separate cycles (regenerative ORC and single-effect NH_3/H_2O absorption refrigeration cycle configurations) when it operates at a thermal boundary condition of $t_{des2} = 130$ °C, $t_{abs} = t_{con} = 35$ °C, $t_{eva} = -10$ °C and $t_{sh} = 177$ °C. Fig. 3.22 illustrates the energy flows in the separate production (power and cold) systems and co-production using SSAPRC-2D configurations.

Table 3.9: Simulation results of regenerative organic Rankine cycle.

Thermal power [kW]		**Mechanical power [kW]**	
Condenser heat duty $\dot{Q}_{con}$	137.9	Expander $\dot{W}_{exp}$	22.94
Evaporator heat input $\dot{Q}_{eva}$	93.9	Circulation pump $\dot{W}_{pump}$	0.9
Preheater heat input $\dot{Q}_{prehe}$	29.3	**Performance indicator**	
Regenerator heat duty $\dot{Q}_{reg}$	52.4	Thermal efficiency η_{th} [%]	13.8
Superheater heat input $\dot{Q}_{sh}$	36.8		

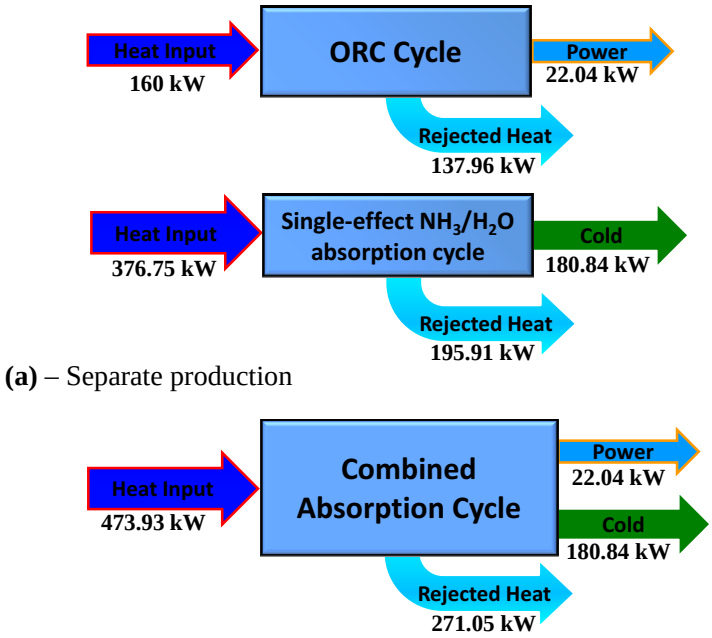

(a) – Separate production

(b) – Combined production using SSAPRC-2D configuration

Figure 3.22: Comparison of separate production of power and cold with combined production using SSAPRC-2D configuration.

3.6.2 Comparison between combined absorption cycles

The useful dual-outputs, energetic and exergetic efficiencies of the combined absorption cycles are compared with the variation of the heat source temperature at typical operating conditions (Fig. 3.23 to Fig. 3.26).

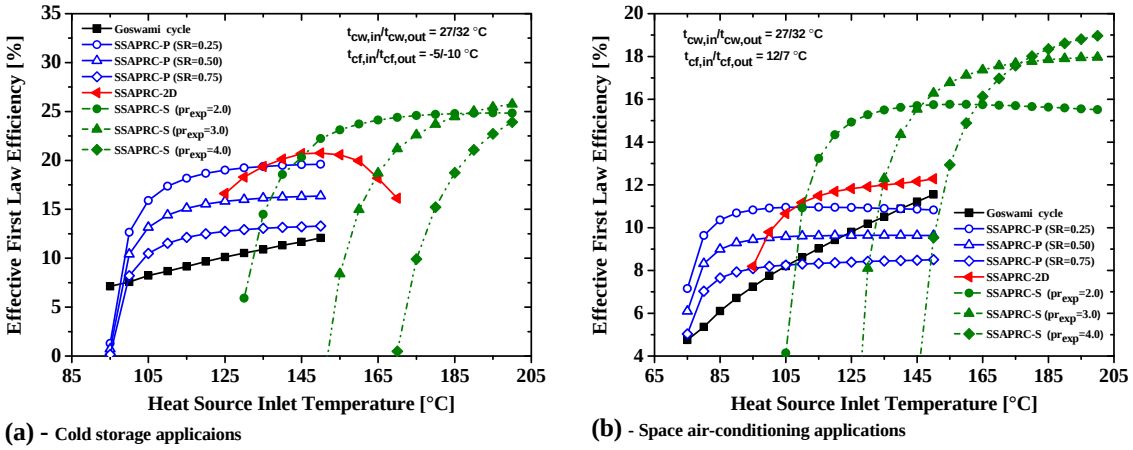

(a) - Cold storage applicaions

(b) - Space air-conditioning applications

Figure 3.23: Effect of heat source inlet temperature on effective first law efficiency of combined absorption cycles at typical operating conditions for: (a) - Deep-freezing (cold storage); (b) - Space air-conditioning applications.

Fig. 3.23 (a) and (b) shows the sensitivity of the effective first law efficiency of the combined absorption cycles with respect to the heat source temperature variations at the specified operating conditions: heat sink inlet/outlet temperatures of 27/32 °C and chilled fluid inlet/outlet temperatures of −5/−10 °C (cold storage) and 12/7 °C (space air-conditioning). The sensitivity of the useful dual-outputs (mechanical power and cold) of the combined absorption cycles with respect to the heat source temperature are depicted in Fig. 3.24 and Fig. 3.25.

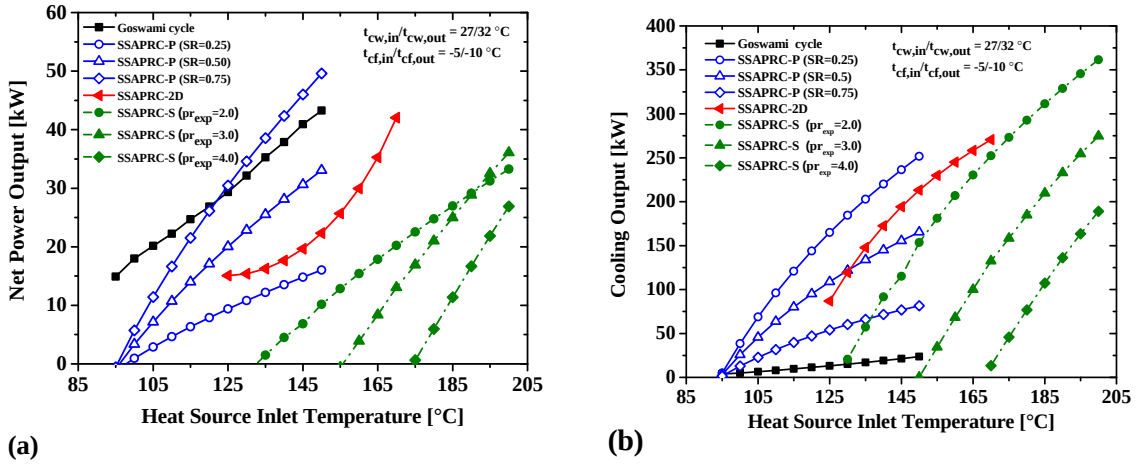

Figure 3.24: Effect of heat source inlet temperature on combined absorption cycles useful outputs at chilled fluid inlet/outlet temperatures of −5/−10 °C: (a) - net power outputs; (b) - cooling outputs.

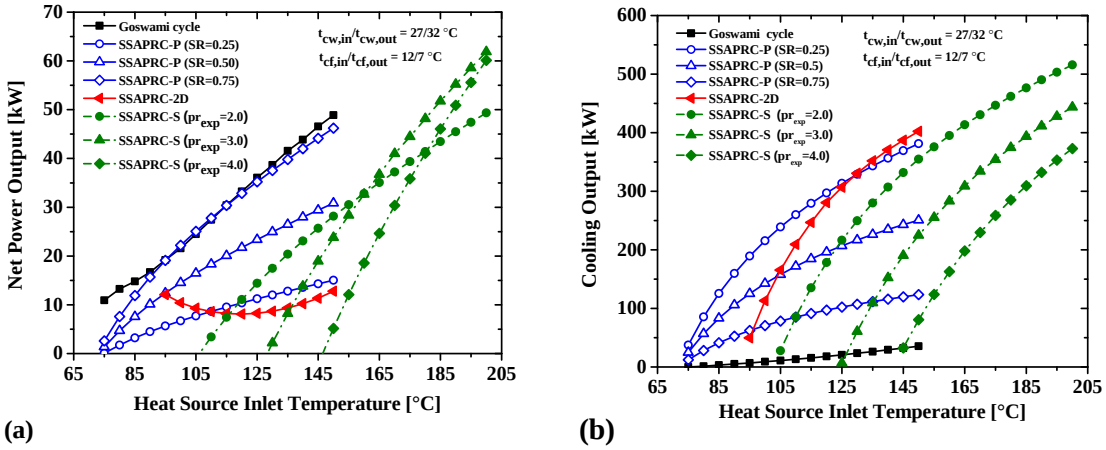

Figure 3.25: Effect of heat source inlet temperature on combined absorption cycles useful outputs for space air-conditioning applications: (a) - net power outputs; (b) - cooling outputs.

It is obvious that the cooling output of the Goswami combined power/cooling cycle is very low compared with the other proposed cycle configurations (SSAPRC-P, SSAPRC-2D and SSAPRC-S) however its power output is superior than the other cycles except with SSAPRC-P cycle configuration with high split ratios SR. And also the new cycle configurations are capable of producing a whole range of power and cooling capacities.

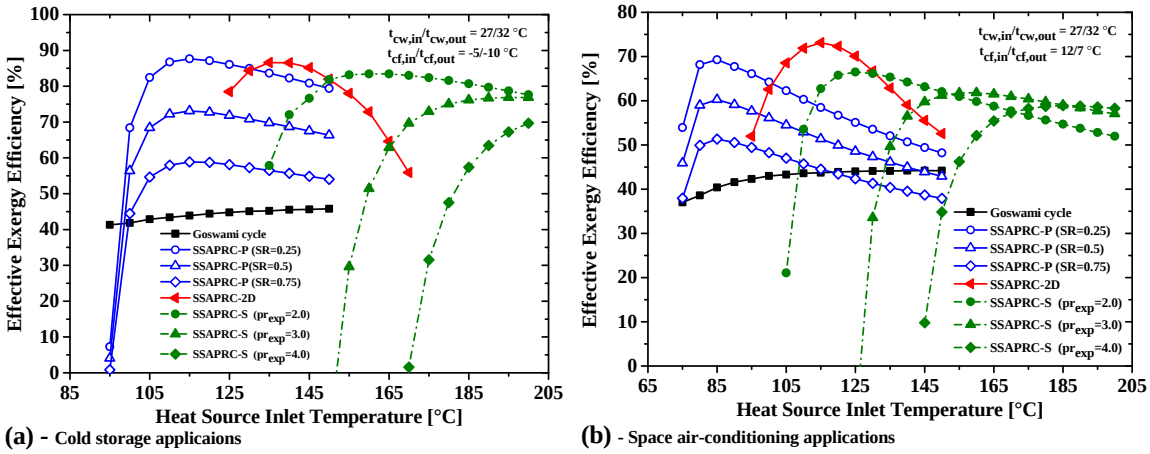

Figure 3.26: Effect of heat source inlet temperature on effective exergy efficiency of combined absorption cycles at typical operating conditions for: (a) - Deep-freezing (cold storage) applications; (b) - Space air-conditioning applications.

The effective exergy efficiency of the combined absorption cycles are shown in Fig. 3.26 and they show optimum value for SSAPRC-P, SSAPRC-2D and SSAPRC-S (except at $pr_{exp} = 3.0$ and 4.0 for cold storage applications) configurations at the heat source temperature range considered in the analysis.

Table 3.10 shows the performance summary of the proposed low-grade combined absorption cycles at typical operating conditions. The driving heat source inlet temperature ($t_{hs,in}$ in Table 3.10) is the optimum temperature that maximize the effective exergy efficiency of each cycles.

Table 3.10: Performance summary of low-grade heat driven combined absorption cycles at typical operating conditions for co-production mode.

Cycle Configuration	Operating Condition			Performance Parameter				
	$t_{hs,in}$	$t_{cw,in}/t_{cw,out}$	$t_{cf,in}/t_{cf,out}$	Useful Output [kW]		Performance indicator		
	[°C]	[°C]	[°C]	Mechanical Power	Cooling Capacity	$\eta_{I,eff}$ [%]	$\eta_{ex,eff}$ [%]	R [-]
SSAPRC-P ($SR = 0.5$)	85			7.6	83.20	8.99	60.24	0.091
SSAPRC-2D	115	27/32	12/7	8.20	246.9	11.49	73.10	0.033
SSAPRC-S ($pr_{exp} = 2.5$)	150			31.6	319.6	17.03	65.95	0.099

3.7 Conclusions

In this chapter, three new combined absorption cycle configurations derived from single-stage NH_3/H_2O absorption refrigeration cycle are presented and analysed from the energetic and exergetic viewpoints. They are suitable for efficient utilization of low-grade heat sources below 200 °C for the co-production of mechanical/electrical power and cold at several temperature levels intended for deep-freezing (cold storage), refrigeration or space air-conditioning applications. A physical-mathematical model has been developed for each cycle configuration for the purpose of analysis and performance simulation of the combined absorption cycles.

The first cycle presented, in this chapter, is a single-stage combined absorption power and refrigeration cycle with parallel flow arrangements (SSAPRC-P, Fig. 3.1). The main features of this cycle configuration is its operational flexibility that means its ability to operate in three different modes of operation: only cold-mode, co-production mode with variable power/cold ratio and only power-mode. The mix of power and cold in the co-production mode can be adjusted directly by varying the vapour split ratio at the exit of the desorber. For a thermal boundary conditions ($t_{hs,in}$ = 120 °C, $t_{cw,in}/t_{cw,out}$ = 32/37 °C and $t_{cf,in}/t_{cf,out}$ = 12/7 °C), the cycle produces 18.7 kW of mechanical power and 149.5 kW of cold with effective first law and exergy efficiencies of 9.6% and 46.9% respectively when the split ratio is 0.5. For the same thermal boundary conditions the cycle produces 32.3 kW of mechanical power with thermal and exergy efficiency of 9.0% and 42.0% when it operates in only power-mode. For only cold-mode of operation it produces 293.6 kW of cooling effect at a COP of 0.626.

The second cycle configuration presented and analysed is the single-stage combined absorption power and refrigeration cycle with two desorbers (SSAPRC-2D, Fig. 3.6). This cycle requires for its activation a relatively higher heat source temperature than the SSAPRC-P cycle configuration. The power output of the cycle is slightly sensitive to the variation of the heat sink temperature at the operating conditions analysed. And the co-produced cooling effect is highly sensitive for the heat sink temperature variation. The higher energy conversion efficiency is attained at conditions suitable for refrigeration and deep-freezing (cold storage) applications. It is found that at the optimum condition of heat

source temperature about 148 °C, $t_{cw,in}/t_{cw,out} = 32/37$ °C and $t_{cf,in}/t_{cf,out} = -5/-10$ °C, a net power output of 20.8 kW and cooling capacity of 130.4 kW could be attained with effective first law and exergy efficiency of the cycle about 18.7 and 36.4%, respectively.

Finally, a single-stage combined absorption power and refrigeration cycle with series flow arrangement between the power and refrigeration sub-cycles (SSAPRC-S, Fig. 3.12) is presented. The performance of this cycle was analysed for typical operating conditions. This cycle is more efficient and suitable for low heat sink temperatures conditions (water cooled absorber and condenser: e.g. 27/32 °C) and when heat sources are available at higher temperatures about between 150 °C to 200 °C. At the baseline case considered ($t_{hs,in} = 150$ °C, $t_{cw,in}/t_{cw,out} = 27/32$ °C, $t_{cf,in}/t_{cf,out} = 12/7$ °C and $pr_{exp} = 2.5$), the cycle produces 31.6 kW of mechanical power and 319.6 kW cooling effect with effective first law and exergy efficiencies of about 17.0% and 66.0%, respectively.

Chapter 4

Modification of the Basic Combined Absorption Cycle: Introduction of Pressure Devices and Other Working Fluid Mixtures

Major parts of this chapter are to be submitted to Energy the International Journal:

- *A single-stage combined absorption power and refrigeration cycle with an integrated compression booster: Part-I (Mechanical Compression) by* ***Dereje S. Ayou****, Joan Carles Bruno and Alberto Coronas.*
- *A single-stage combined absorption power and refrigeration cycle with an integrated compression booster: Part-II (Vapour Ejector) by* ***Dereje S. Ayou****, Joan Carles Bruno, Rajagopal Saravanan and Alberto Coronas.*

"This page intentionally left blank"

4.1 Introduction

In this chapter, the performance improvement and operational flexibility of a single-stage combined absorption cycle, SSAPRC-P, through the integration of mechanical compressor and vapour ejector into the cycle configuration are presented and discussed. The energetic and exergetic performance of these modified single-stage combined absorption cycles were analysed for typical operating conditions.

The performance of the modified combined absorption cycle configurations were compared with the basic combined absorption cycle configuration (SSAPRC-P) at the same operating conditions. Further, the performance potential of non-conventional Ammonia/Salt mixtures ($NH_3/LiNO_3$ and NH_3/NaSCN) were analysed using a single-stage combined absorption cycle configuration.

4.2 Integration of Compression Booster

The combination of absorption and vapour compression cycles for air-conditioning, refrigeration and heating applications is well-known and has a number of significant advantages reported in the literature. These advantages are from performance enhancement perspective as well as extending operational working range of the absorption cycles (low temperature applications, reduction of desorption temperature, etc.) ([168]-[177]). In these studies several working fluids were considered: NH_3/H_2O ([168]-[170]), $NH_3/LiNO_3$ ([171]-[173]), H_2O/LiBr [174] and organic refrigerant/absorbent combinations ([175]-[177]).

Kang et al. [168], developed an advanced hybrid GAX cycles named HGAX by combining absorption and vapour compression cycles. Four different types of HGAX cycles are proposed by the authors: type A for cycle performance improvement, type B for low temperature refrigeration applications, type C for reduction of desorber temperature and type D for hot water production using the heat rejected by the absorber and condenser. It is done by controlling the pressures of evaporator, absorber, condenser and desorber. A GAX absorption-compression hybrid cycle using NH_3/H_2O working pair has been studied for air-conditioning applications by Kumar et al. [169], the authors reported that about 30% performance improvements (COP) obtained than the basic GAX cycle at the analysed operating conditions.

Ventas et al. [171], developed and studied a detailed model for an hybrid single-effect absorption cycle with a mechanical compression booster between the absorber and evaporator. They found out that at the same COP and cooling capacity, the cycle allows the reduction of the driving heat source temperature up to 24 °C with a pressure ratio less than 2.0. They also claimed that mechanical work input to the cycle is more efficient than supplied to a separate ammonia vapour compression chiller with COP of lower than 4.0. Kim et al. [174] investigated four types of compressor assisted cycles based on basic series flow triple-effect H_2O/LiBr absorption cycle. The purpose of each type, due to different compressor position considered, of configuration is to lower the driving temperature of the cycle. They found out that to reduce the generator temperature by 40 °C about 3-4 % of the cooling capacity equivalent mechanical energies are required for the compression stage. And also the corrosion problem can also be avoided.

In conclusion, the above mentioned performance and technical improvements and other mentioned in the literature can only be realised at the expense of the electrical (or mechanical) power consumption for the compression process hybridised with the absorption (solution circuit) systems.

Several authors also proposed, in the literature, the integration of vapour ejector and liquid-vapour ejector with absorption refrigeration systems at different positions in the cycle configurations to improve performance and to extend operational working range ([178]-[182]). For instance, Vereda et al. [179] replace the solution expansion valve in a single-effect absorption chiller by a vapour-liquid ejector in order to recover the loss of high-pressure potential energy of the weak NH_3/H_2O solution in the throttling process which results in energy loss and consequently inefficiency. Recently, Li et al. [183] replace the throttle valve and the absorber of the Kalina cycle (KCS11) by a liquid-vapour ejector and consequently showed an increase in the mechanical power output and thermal efficiency of the cycle.

The aim of the next section is to study and analyse the performance improvement and operational flexibility of a single-stage combined absorption cycle for power and refrigeration applications (SSAPRC-P) same as the one presented in previous chapter through the integration of a mechanical compression process between the evaporator and absorber. This modified single-stage combined hybrid absorption cycle configuration is named hereafter as

"SSAPRC-COM". It is a triple-pressure levels cycle configuration. The cycle configuration is analysed based on energetic and exergetic viewpoint for a heat source temperature below 120 °C; this temperature level can be obtained from relatively low-cost solar thermal collectors (flat plate and evacuated tube solar thermal collectors) and other low-temperature thermal sources.

4.3 Basic Single-Stage Combined Absorption Cycle with Mechanical Compression

Fig. 4.1 shows a schematic representation of the single-stage combined absorption power and refrigeration cycle with an integrated mechanical compression booster (SSAPRC-COM) between the absorber and evaporator.

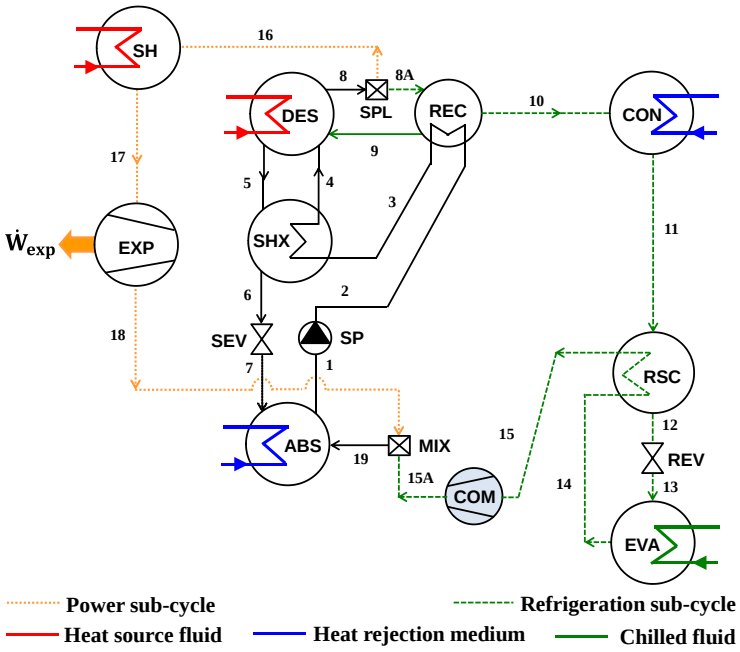

Figure 4.1: Schematic diagram of single-stage combined absorption power and refrigeration cycle with mechanical compressor (SSAPRC-COM).

The overall process of this cycle configuration is similar to the basic single-stage combined absorption cycle SSAPRC-P described in Chapter 3 (section 3.3) being the only difference is that the absorber is operating at a relatively higher pressure than the evaporator when the compression stage is in operation. The superheated vapour at low (evaporator) pressure (state 15, from the evaporator via the refrigerant sub-cooler) enters the mechanical

compression stage (COM) where its pressure is elevated by pr_{com}, compression booster pressure ratio, to intermediate (absorber) pressure. The power consumption of the mechanical compressor and solution pump $\dot{W}_{com}$ and $\dot{W}_{sp}$, respectively, can be supplied from the power developed by the expander which makes the system free, autonomous, from external electrical (or mechanical) power supply requirement.

4.3.1 Performance analysis and discussion

The energetic and exergetic analysis of the SSAPRC-COM was performed for several compression ratios, defined as $pr_{com} = p_{abs}/p_{eva}$, which are between 1.0 to 2.0 in steps of 0.2. It is also compared with the basic dual-pressure, SSAPRC-P, combined absorption cycle configuration (i.e. without the mechanical compression stage, $pr_{com} = 1.0$). Several vapour split ratios (0.2, 0.4, 0.6 and 0.8) are considered to investigate its effect on the cycle's useful dual-outputs (mechanical power and cold), cycle efficiencies and on the flexibility of its operational working range. The generic steady-state absorption cycle modelling approach and assumptions considered in Chapter 3 are followed to develop the thermodynamic model of the SSAPRC-COM cycle configuration. In this analysis, the heat source inlet temperature is varied between the minimum heat source temperature ($t_{hs,in,min}$) and 120 °C. The mechanical compression process is characterized by a constant isentropic efficiency of 75%.

4.3.1.1 Base-case analysis

The assumed input variables and design parameters for the base-case analysis are summarized in Table 4.1.

Table 4.1: Base-case input variables and design parameters for performance simulation of a combined absorption cycle with mechanical compression booster.

Input Variable/Design Parameter	Value
Cooling water (heat sink) inlet/outlet temperatures, $t_{cw,in}/t_{cw,out}$ [°C]	32/37
(parallel flow arrangement for absorber and condenser)	
Chilled fluid inlet/outlet temperatures, $t_{cf,in}/t_{cf,out}$ [°C]	$-5/-10^a$
Minimum approach temperature for absorber, condenser, evaporator and desorber, ΔT [°C]	5
Effectiveness of internal heat recuperators (SHX and RSC), ε_{IHX} [%]	80
Expander isentropic efficiency, η_{exp} [%]	85
Solution pump isentropic efficiency, η_{sp} [%]	80

[a] - Cold storage applications

For the purpose of analysing the energetic implication of the compression stage on the cycle's performance, the solution circulation ratio is fixed at 7 kg of basic solution per kg of vapour generated in the desorber. When the compression process is activated, $pr_{com} > 1.0$, the compression stage contributes for the heat transformation process in the cycle and it is presented below for different modes of operation of the cycle.

As the pressure ratio pr_{com} increases, the mechanical compression process enhances the heat transformation process. Consequently, the required heat source temperature $t_{hs,in}$ drops off as shown in Fig. 4.2 when the compression pressure ratio increases. The fraction of the vapour generated in the desorber which is necessary to make the system (cycle) autonomous, i.e. to cover the entire power consumption of solution pump and mechanical compressor, is also depicted in Fig. 4.2. This figure shows an important fact that the driving heat source temperature as well as the minimum temperature required to activate the cycle can be lowered at the expense of the compression power (by scarifying some of the potential for more cooling output). It makes it more interesting for effective utilization of solar thermal installations throughout the year since heat from such kind of thermal sources are characterized by intermittent nature.

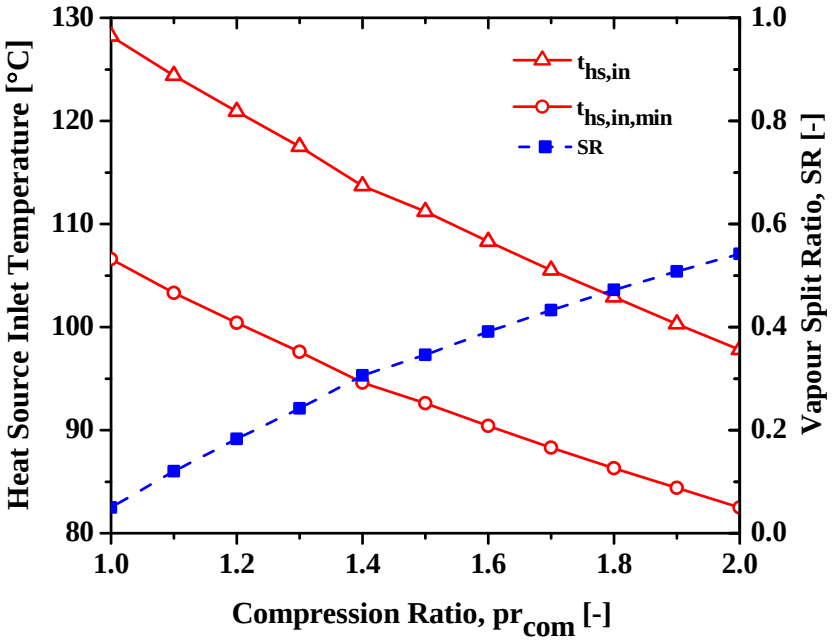

Figure 4.2: Influence of compression pressure ratio on the driving heat source temperature of the cycle (SSAPRC-COM, Fig. 4.1).

The energetic implications of the compression process on the cycle are demonstrated in Fig. 4.3. The driving heat input as well as the cooling output of the cycle decreases as the compression ratio increases. The driving heat input of the cycle decreases by 15.1% as the pr_{com} increases from 1.0 to 2.0. Thus, the compression effect has dual benefit: both the amount of heat input and its temperature level are reduced. But, it is at the expense of the cooling output reduction (see Fig. 4.3).

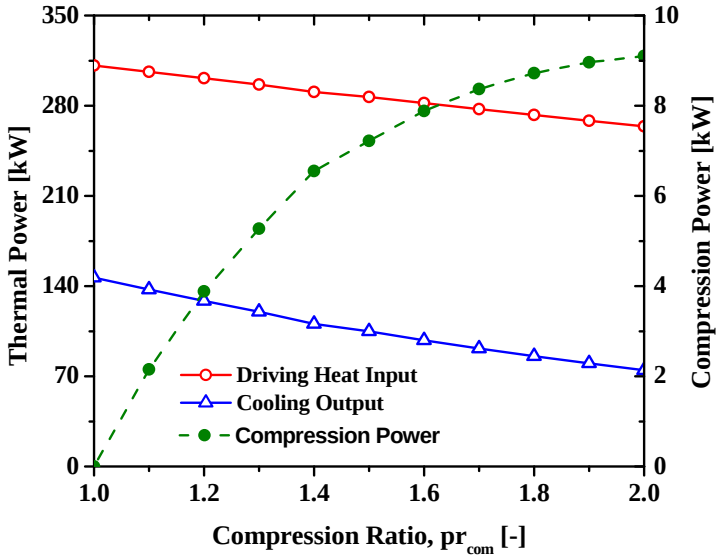

Figure 4.3: Driving heat input, cooling output and compression power consumption as a function of compression ratio of the cycle (SSAPRC-COM, Fig. 4.1).

When waste heat available at several temperature levels, this combined absorption cycle configuration (SSAPRC-COM) can be flexible to adjust its heat source temperature requirement to produce the same amount of cold. Fig. 4.4 illustrates this effect at several indicative fixed cooling capacities of the cycle. The corresponding power consumption of the compression process is show in Fig. 4.5.

Fig. 4.2 shows the minimum split ratio necessary to operate the cycle in autonomous mode of operation for compression ratio up to 2.0, thus, for $pr_{com} = 2.0$ co-production of power and cold are feasible at $SR > 0.54$. Consequently, the potential of the co-production of mechanical power and cold, after covering the power consumption of the compressor and solution pump are analysed for the baseline input conditions given in Table 4.1 at the vapour split ratio of $SR = 0.6$.

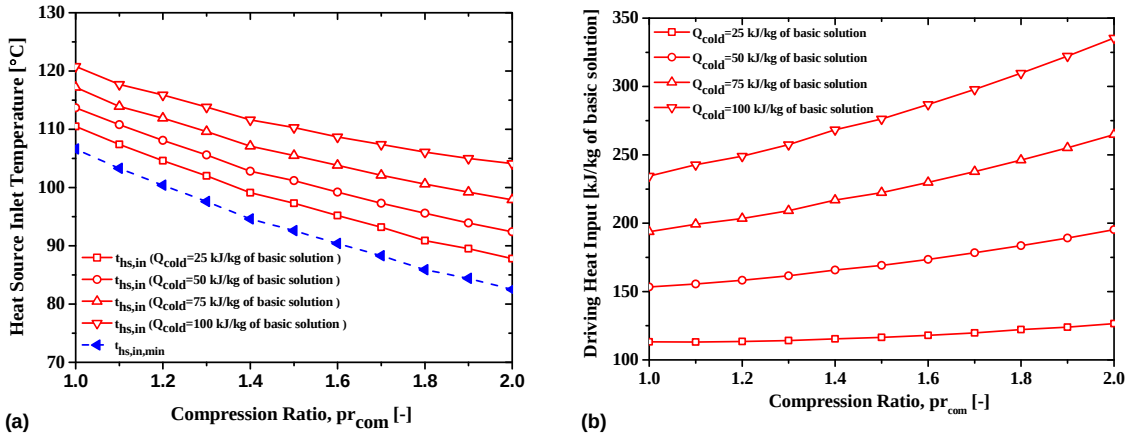

Figure 4.4: Effect of compression pressure ratio on: (a) - driving heat source inlet temperature; (b) - driving heat input for several constant cooling capacity of the cycle (SSAPRC-COM, Fig. 4.1).

The effect of mechanical compression process, pr_{com}, on the cycle useful dual-outputs (power and cold) and efficiencies at the co-production mode of operation ($SR = 0.6$) are illustrated in Fig. 4.6 (a) and (b), respectively. The extensive variables are based on a unit mass flow rate (1.0 kg/s) of NH_3/H_2O basic solution through the solution pump. The net power output of the cycle decreases from 19.0 kW to 2.3 kW while the driving heat source temperature drops by about 31 °C when the compression ratio increases from 1.0 to 2.0. But, the cooling output of the cycle increase slightly by about 5.2%.

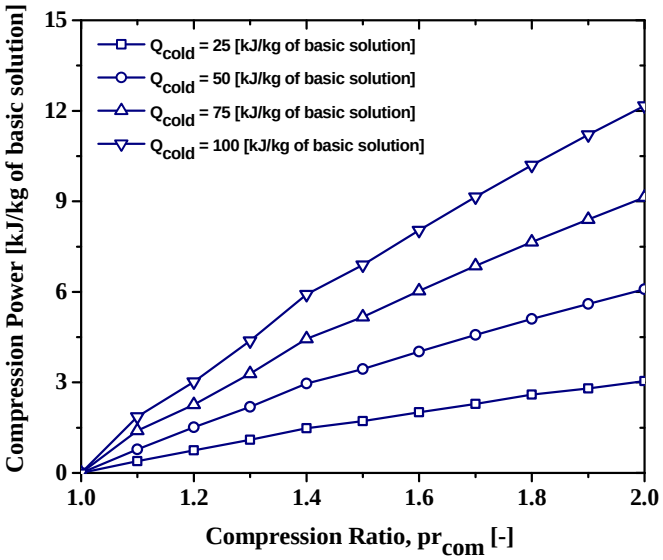

Figure 4.5: Power consumption for the compression process at several fixed cooling capacity of the cycle (SSAPRC-COM, Fig. 4.1).

As the compression ratio increases from 1.0 to 2.0, the driving heat input of the cycle decreases from 323.6 kW to 264.7 kW and the net power output of the cycle decreased by about 88%. The driving exergy input to the cycle also decreases from 75.1 kW to 46.7 kW when the compression ratio increased from 1.0 to 2.0. The work contribution of the cooling output of the cycle, in the effective first law and effective exergy efficiency definitions, increased slightly from 25.2 kW to 26.6 kW (at typical 30% second law efficiency for vapour compression refrigeration cycle). The combined effect on the energetic and exergetic efficiencies of the cycle are shown in Fig. 4.6 (b).

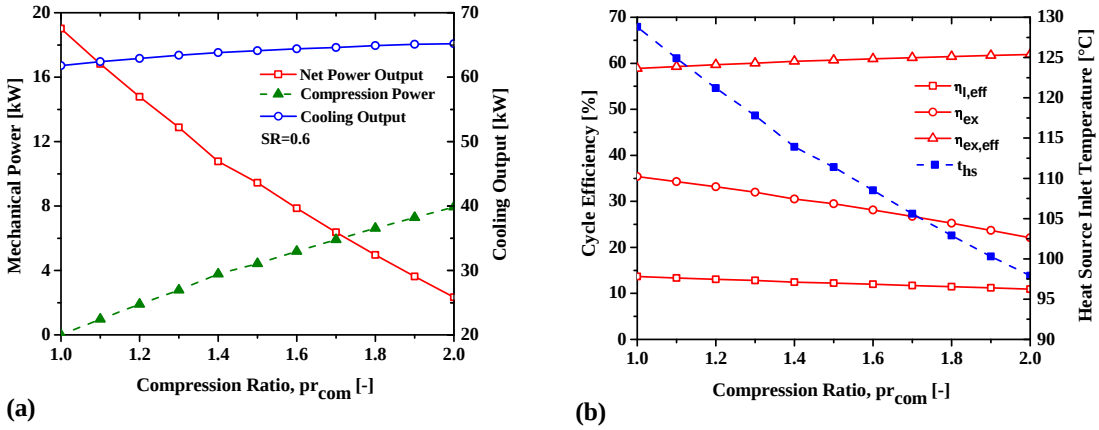

Figure 4.6: Effect of compression ratio on the cycle performances at the base-case of co-production mode: (a) - Dual-outputs and compression power; (b) - Cycle efficiencies and heat source temperature (SSAPRC-COM, Fig. 4.1).

4.3.1.2 Sensitivity analysis

Fig. 4.7 (a) and (b) shows the effect of pr_{com} on the cycle useful outputs (mechanical power and cold) and effective first law efficiency ($\eta_{I,eff}$) at several split ratios (SRs) in the range where there is net mechanical power output production. In this performance sensitivity analysis, the absorber and condenser exit temperatures (t_1 and t_{11} in Fig. 4.1) are set at 35 °C and 40 °C respectively. The evaporator exit temperature, t_{14}, is also set at -5 °C. The degree of purification in the rectifier is limited by an ammonia mass fraction of 0.999. The isentropic efficiency of the expander is set to 85%.

It is evident that the net power output of the cycle decreases with the increase of pr_{com}, at a fixed vapour split ratio, because the power consumption of the compressor increases with increasing of pr_{com}. In addition to this, the back pressure of the expander that

influences the expander power output is also increases with the increasing of pr_{com}. While the back pressure increases, the mass flow rate of the vapour in the power sub-cycle is constant. Consequently, the expander power output decrease.

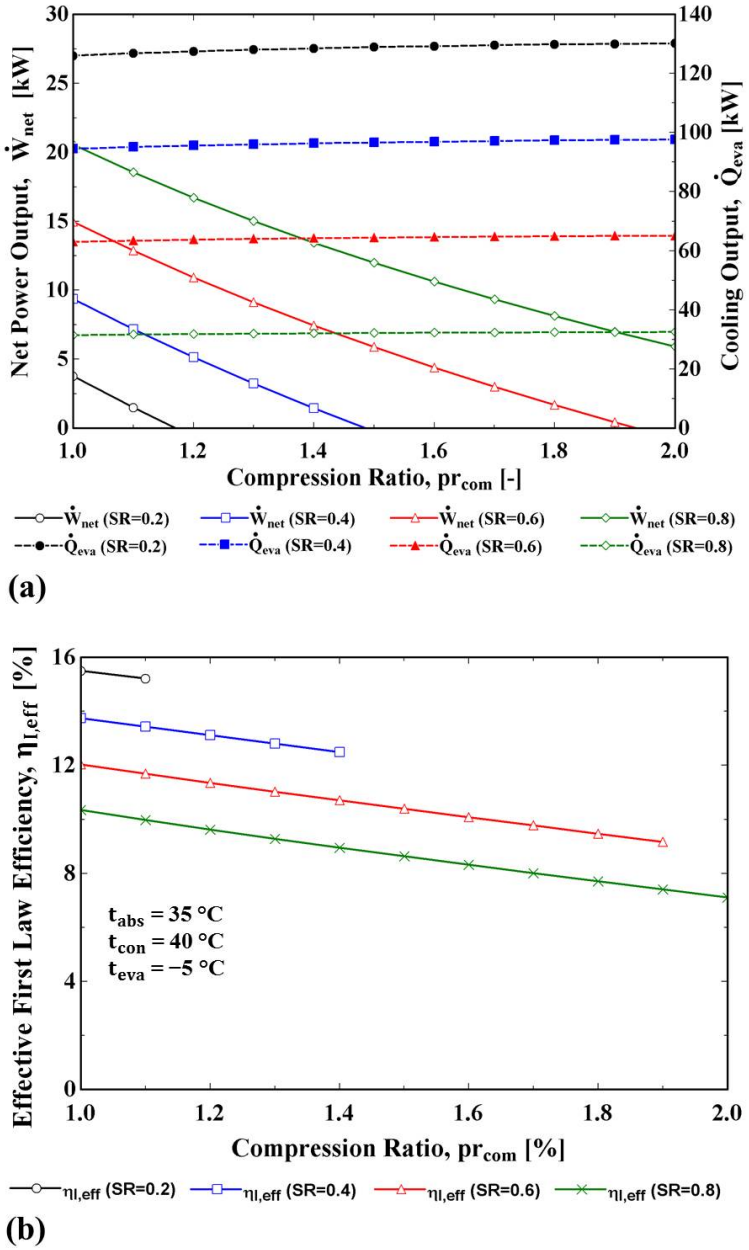

Figure 4.7: Effect of compression ratio on: (a) - cycle useful outputs; (b) - effective first law efficiency of the cycle at several SRs (SSAPRC-COM, Fig. 4.1).

The cooling output ($\dot{Q}_{eva}$) of the cycle is almost constant for the variation of pr_{com} at all vapour split ratios (SRs) as a result the work contribution of the cooling output on the $\eta_{I,eff}$ definition is almost insensitive to the variation of pr_{com}. Because of the combined

effects of the net power output and driving heat input, the values of the $\eta_{I,eff}$ decreases for at all split ratios considered.

Fig. 4.8 shows the effect of pr_{com} on the rectifier heat duty ($\dot{Q}_{rec}$). As the value of pr_{com} increases, the rectifier heat duty decreases for all the SRs considered. The reason for this effect is the increasing of the absorber pressure at constant temperature (t_1, in Fig. 4.1) increases the concentration of NH_3 in the basic solution. As a result, NH_3 rich vapour is generated in the desorber. Therefore, the rectification load on the rectifier is reduced due to the incorporation of the mechanical compressor between the absorber and evaporator.

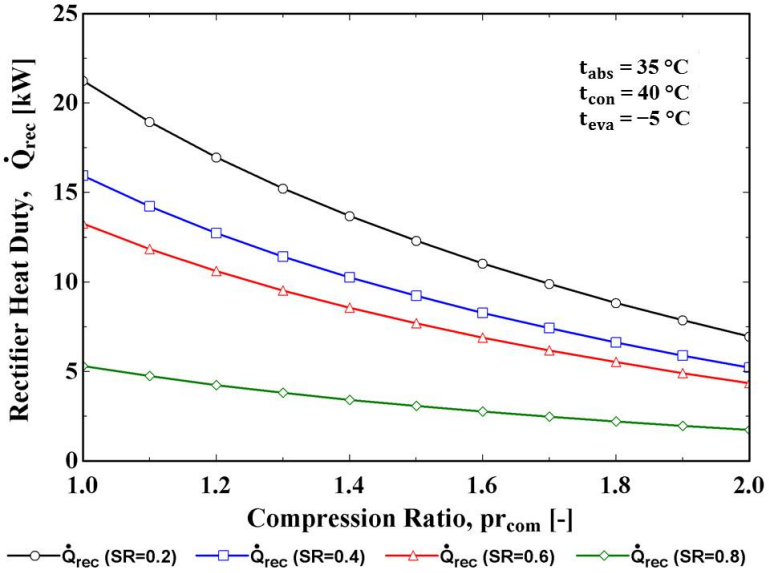

Figure 4.8: Effect of compression ratio on rectifier heat duty at several split ratios (SSAPRC-COM, Fig. 4.1).

A sensitivity analysis is performed to evaluate the effects of the desorber exit temperature t_{des} (t_5 in Fig. 4.1), which is related to the heat source inlet temperature, on the performance of the combined absorption cycle (SSAPRC-COM). Fig. 4.9 (a) and (b) shows the effect of t_{des} on the cycle's dual-outputs (mechanical power and cold) for different compression ratios considered. The cycle can operate in three different modes of operation: only cold-mode, only power-mode and intermediate co-production mode with different power/cold ratios R (i.e. by varying the SR). Fig. 4.9 (a) shows the net power output (when $\dot{W}_{net} > 0$, $\dot{W}_{net} = \dot{W}_{exp} - (\dot{W}_{sp} + \dot{W}_{com})$) of the cycle SSAPRC-COM with the variation of t_{des}. As it is depicted in the figure, the power generated by the expander increases with the increasing of the desorber temperature at all pr_{com} values considered.

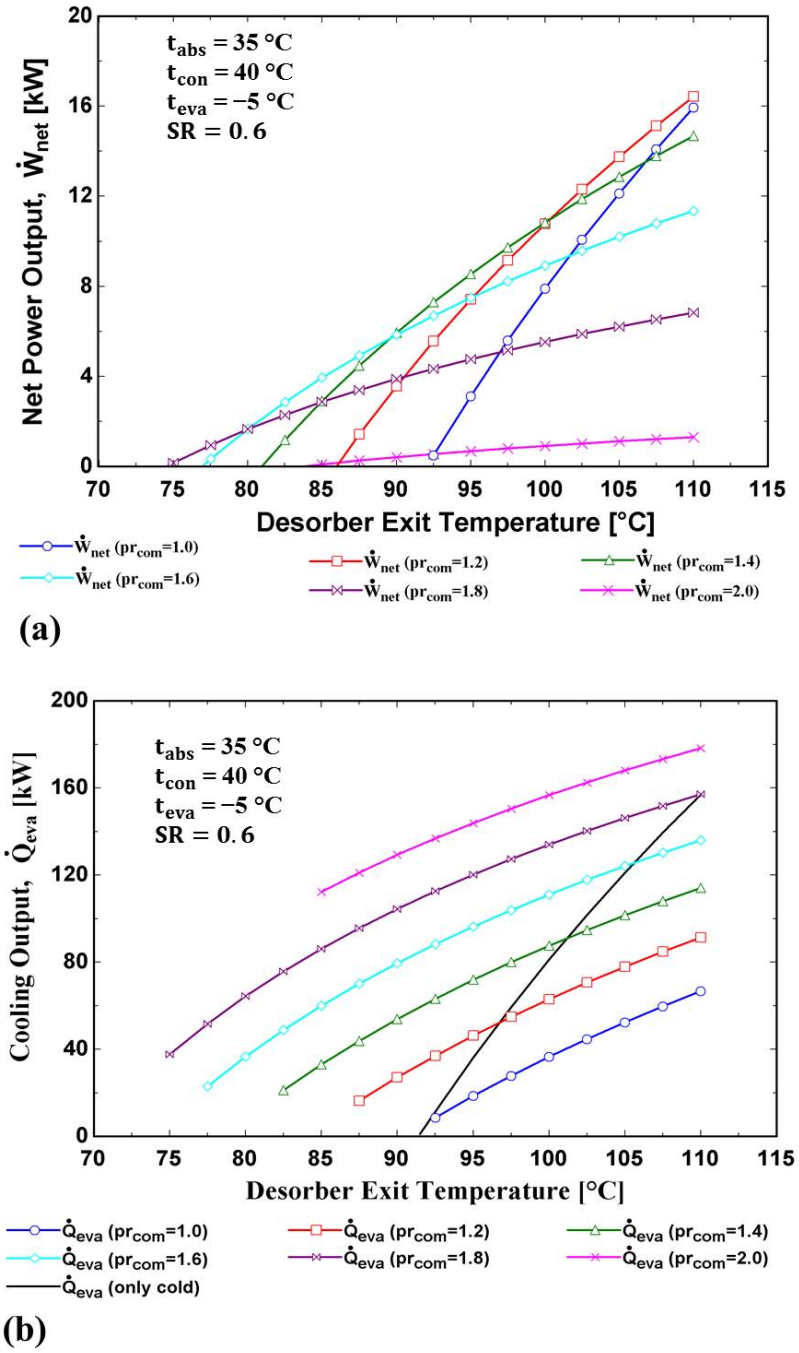

Figure 4.9: Cycle useful dual-outputs verses desorber exit temperature for different compression pressure ratios pr_{com}: (a) - net power output; (b) - cooling output (SSAPRC-COM, Fig. 4.1).

The power consumption of the compressor is also increases as t_{des} increases because the amount of the refrigerant flowing through the evaporator also increases. As illustrated in Fig. 4.9 (b), when the cycle operates in a cold producing mode only with $pr_{com} = 1$ the cooling output of the cycle increase from 1.1 kW to 157.0 kW with the increase in t_{des} from

91 °C to 110 °C. At this mode of operation, the expander only generates the mechanical power necessary to cover the power consumption of the solution pump (1.8 kW). For t_{des} lower than 91 °C there is no vapour production in the desorber of the cycle operating without the compression stage (it is the same as SSAPRC-P).

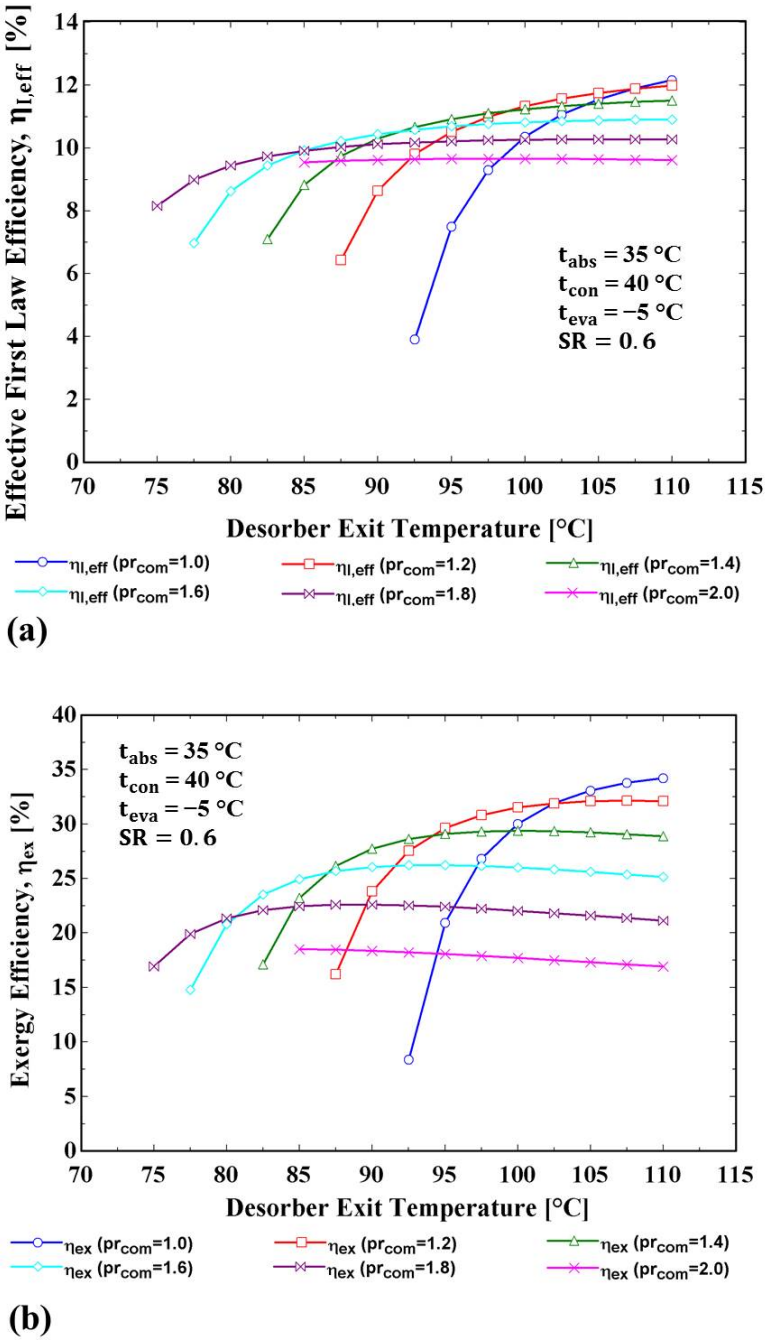

Figure 4.10: Cycle efficiencies versus desorber exit temperature for different compression ratios pr_{com}: (a) - effective first law efficiency; (b) - exergy efficiency (SSAPRC-COM, Fig. 4.1).

The cooling output of the cycle rises (for all pr_{com} considered) with increasing of t_{des}, and at the same t_{des} the cooling output is higher for higher pr_{com} values. This is mainly due to the fact that at constant absorber exit temperature (t_1 in Fig. 4.1), the NH_3 concentration of the strong liquid solution leaving the absorber increases as the absorber pressure raises as a consequence the amount of refrigerant flowing through the evaporator increases.

Fig. 4.10 (a) and (b) shows the effect of t_{des} on the effective first law ($\eta_{I,eff}$) and exergetic (η_{ex}) efficiencies of the cycle at several pr_{com}. The first law efficiency of the cycle is almost constant at compression ratio of 1.8 and 2.0. At the desorber exit temperature ranges considered in this analysis, the effective first law and exergy efficiencies of the cycle without compression stage (SSAPRC-P) is unstable. Whereas the cycle with compression stage shows a more stable efficiency curves. Since the net mechanical power output of the cycle is lower at higher pressure ratio and also the cooling output is undervalued in the exergy efficiency definition, the exergetic efficiency of the cycle is lower at higher pressure ratio. However, the effective exergy efficiency of the cycle is quite high in comparison with the exergy efficiency because in effective exergy efficiency definition the cooling output is weighted realistically, thus, its work contribution is quite high in comparison with the exergy associated with the cooling output.

4.4 Vapour Ejector

In the above section, the performance improvement and operational flexibility of SSAPRC-P configuration (Fig. 3.1) with the integration of mechanical compression booster is presented and discussed. In this cycle (SSAPRC-COM, Fig. 4.1), some of the developed mechanical power by the expander is used internally to drive the mechanical compression process.

When SSAPRC-P cycle configuration operates at high condenser temperature (for instance in air-cooled condenser operating conditions), the exhaust of the expander still can have significant pressure energy to be recovered after developing the mechanical power. With a proper pressure recovery device (e.g. vapour ejector), the exhaust, mostly superheated vapour, of the expander (state 18 in Fig. 3.1) can be used as a primary flow to entrain the vapour stream from the evaporator (state 15 in Fig. 3.1) and then the mixed vapour stream (state 19 in Fig. 3.1) at intermediate pressure between the evaporator and

expander exhaust pressures enters into the absorber. Consequently, the absorber operating pressure is boosted without mechanical power consumption (from both internal and external sources).

Therefore, a new modified single-stage combined absorption cycle configuration with vapour ejector hereafter refereed as SSAPRC-EJE is proposed: it is mainly suitable for systems operating in air-cooled conditions. The ejector replaces the vapour stream mixer in SSAPRC-P (MIX, Fig. 3.1) or vapour stream mixer and mechanical compressor in SSAPRC-COM (MIX and COM in Fig. 4.1). This cycle basically operates in four pressure levels those given by the condenser (high pressure), evaporator (low pressure), absorber operating pressure and pressure at exhaust of the expander. Fig. 4.11 shows a schematic flow diagram of a single-stage combined absorption power and refrigeration cycle with an integrated vapour ejector between the absorber and evaporator (SSAPRC-EJE).

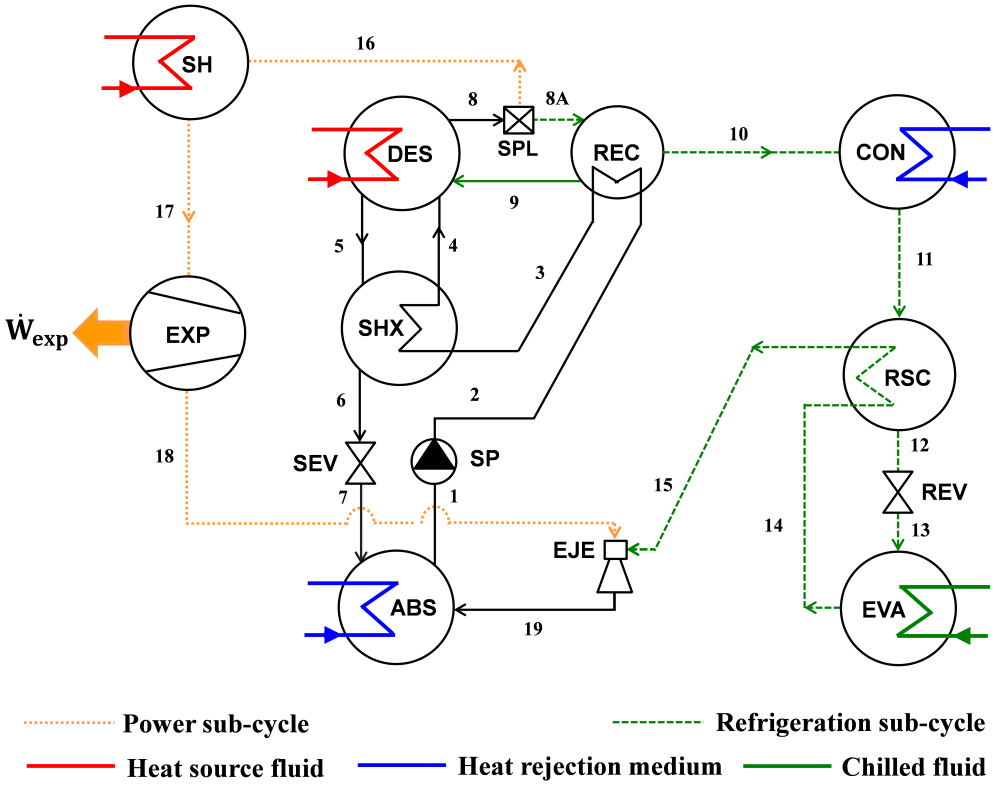

Figure 4.11: Schematic diagram of single-stage combined absorption power and refrigeration cycle with vapour ejector (SSAPRC-EJE).

The energetic and exergetic analysis of the SSAPRC-EJE configuration was performed for the operating conditions and design parameters given in Table 4.2. The performance of

the SSAPRC-EJE is also compared with the basic dual-pressure, SSAPRC-P, single-stage combined absorption cycle configuration (i.e. without the vapour ejector compression process, $pr_{eje} = 1.0$). The vapour ejector compression ratio is defined as $pr_{eje} = {}^{p_{abs}}/_{p_{eva}}$. The effect of heat source inlet temperature on the cycle's dual-outputs mechanical power and cold, and cycle efficiencies were evaluated for assumed typical operating conditions in Table 4.2. In this analysis, when a parameter ($t_{hs,in}$ in this case) is varied while the other parameters are kept constant at their values in Table 4.2 and model assumptions considered in Chapter 3.

Table 4.2: Input operating conditions and design parameters for single-stage combined absorption power and refrigeration cycle with vapour ejector (SSAPRC-EJE).

Input Variable	**Value**
Cooling water (heat sink) inlet/outlet temperature, $t_{cw,in}/t_{cw,out}$ [°C]	37/42
Chilled fluid inlet/outlet temperatures, $t_{cf,in}/t_{cf,out}$ [°C]	$8/3^{a}$
Heat source inlet temperature range, $t_{hs,in}$ [°C]	100–140
Mass flow rate of heat source fluid, $\dot{m}_{hs}$ [kg/s]	5.0
Vapour split ratio, SR [-]	0.6
Expander pressure ratio, pr_{exp} [-]	2.5^{b}
Effectiveness of internal heat recuperators (SHX and RSC), ε_{IHR} [%]	80
Expander and solution pump isentropic efficiencies, η_{exp} and η_{sp} respectively [%]	85, 80

[a] - Refrigeration applications; [b] - for SSAPRC-EJE (when $pr_{eje} > 1.0$)

Fig. 4.12 (a) illustrates the effect of heat source inlet temperature variation on the net power and cooling outputs of the cycle with and without the vapour ejector ($pr_{eje} = 1.5$ and $pr_{eje} = 1.0$, respectively). The driving heat source temperature of the cycle decreases by about 15 °C at the ejector compression ratio of 1.5. As a consequence, the operational working range of the cycle can be extended to produce both net power and cooling outputs for heat sources at temperature between 106 °C and 120 °C. Otherwise, without the ejector, it is not possible to produce any net power and cooling outputs in this temperature range for the operating conditions given in Table 4.2. For heat source temperatures between 120 °C and 138 °C, the net power out of the cycle with the vapour ejector (SSAPRC-EJE, $pr_{eje} = 1.5$) is higher than the power output of the cycle without the vapour ejector (SSAPRC-P). At a heat source temperature between 120 °C and 138 °C, the cooling capacity of the cycle can be increased by about 43% due to the introduction of the vapour ejector ($pr_{eje} = 1.5$)

in the cycle. Fig. 4.12 (b) shows the sensitivity of the cycle effective first law and effective exergy efficiencies with respect to the variation of the heat source inlet temperature. As can be seen in this figure, the cycle with the ejector has superior cycle efficiencies than the one without the ejector for heat source temperature lower than 132 °C.

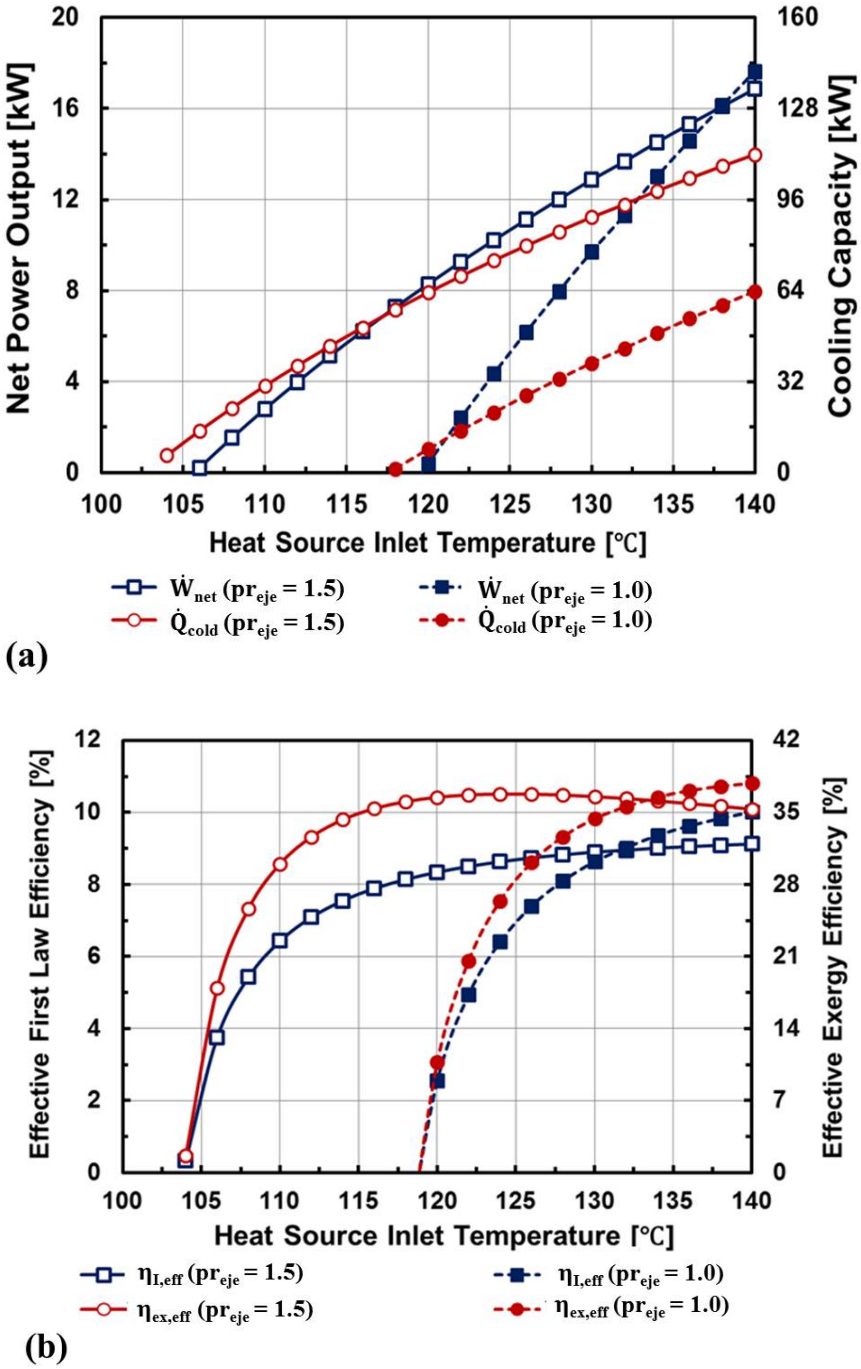

Figure 4.12: Effect of heat source inlet temperature on the performance of SSAPRC-EJE cycle configuration: (a) - Useful dual-outputs; (b) - Cycle efficiencies.

Fig. 4.13 illustrate the relative exergy destruction rate of the components of the cycle with respect to the heat source temperature variation. The absorber, solution heat exchanger and desorber have the most significant exergy destructions from all the components in the system. The solution heat exchanger performs better, less exergy destruction, at higher heat source temperature because of better thermal much between the hot and cold NH_3/H_2O solutions in the solution heat exchanger.

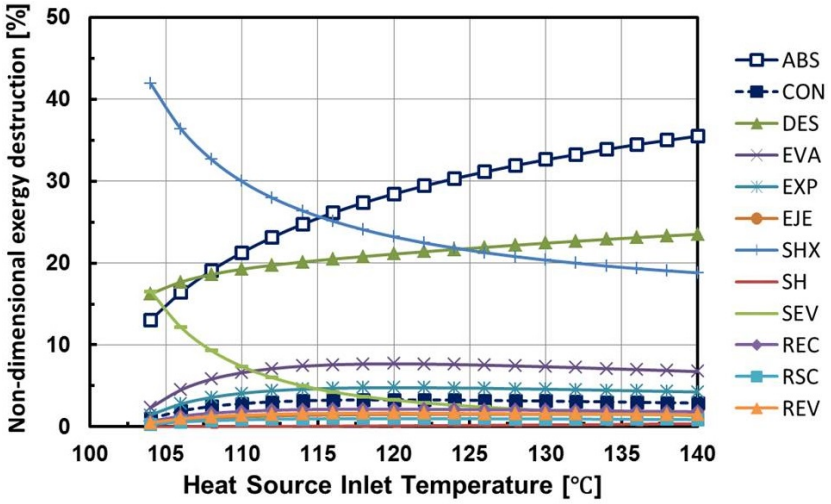

Figure 4.13: Effect of heat source inlet temperature on exergy destruction of SSAPRC-EJE components.

4.5 Performance Analysis of Ammonia based Working Fluid Mixtures

There are two cycle design configurations for the single-stage combined absorption cycle with parallel flow arrangement based on the type of absorbent (for NH_3 - refrigerant) in the working fluid mixture. Figs. 4.14 (a) and 4.14 (b) shows the cycle configurations using the volatile absorbent (H_2O) and non-volatile absorbents ($LiNO_3$ and NaSCN), respectively. These cycles process description and their features are similar to the SSAPRC-P configuration described in Chapter 3 with the main difference on the introduction of sensible heat exchanger (cooler, COL) in the power sub-cycles (see Figs. 4.14 (a) and (b)) and there is no rectifier in case of the $NH_3/(LiNO_3$ or NaSCN) based cycle. And also, the position of the vapour mass flow splitter for NH_3/H_2O based cycle is at the vapour exit of the rectifier (state 10 in Fig. 4.14 (a)). The cycles operation is described in detail elsewhere [184].

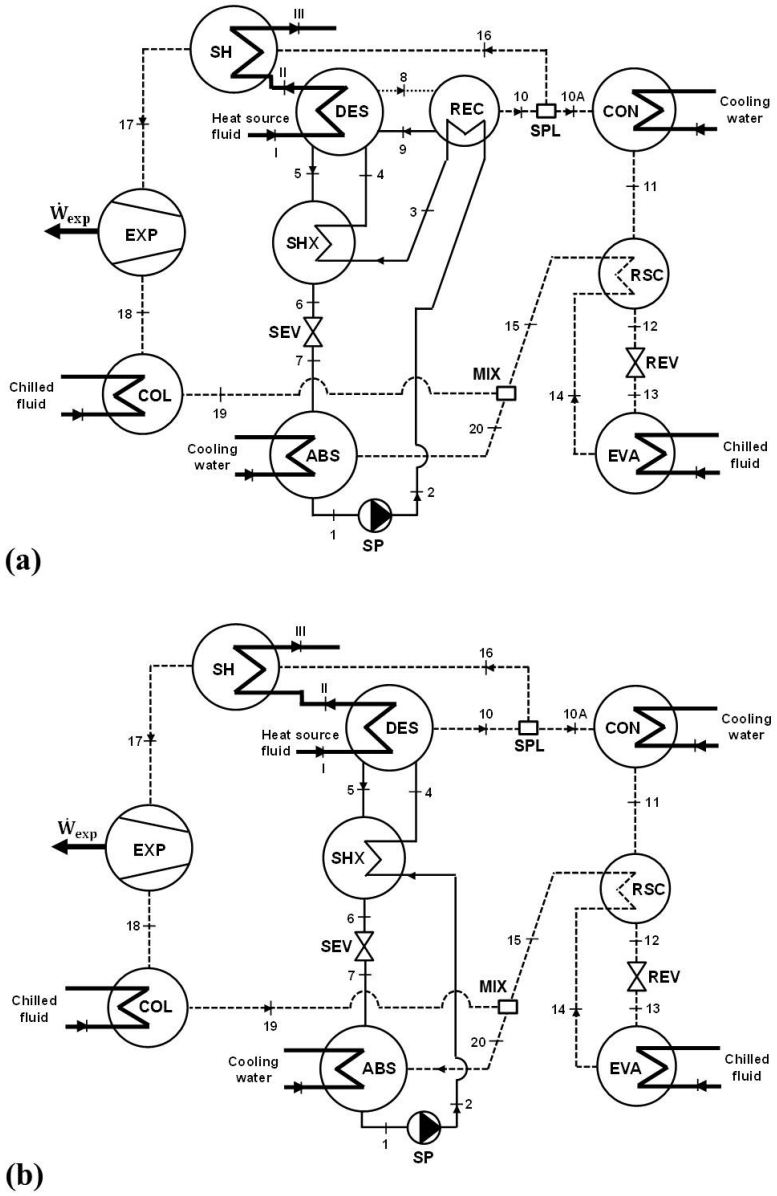

Figure 4.14: Schematic diagram of single-stage combined absorption cycles with cooler (sensible heat exchanger): (a) - NH_3/H_2O mixture; (b) - $NH_3/LiNO_3$ or NH_3/NaSCN mixture.

The thermodynamic performance of the single-stage combined absorption cycles with $NH_3/LiNO_3$, NH_3/NaSCN and the conventional NH_3/H_2O working fluids were evaluated for different modes of operation characterized by different vapour split ratios. The input conditions considered in the cycle simulation were heat source inlet temperatures from 100 °C to 130 °C, typical absorber and condenser cooling water inlet/outlet temperature of 30/38 °C, cycle low pressure of 300 kPa and chilled fluid inlet/outlet temperature of 10/3 °C. These input operating conditions were selected by considering the fact that: the cycle

with $NH_3/LiNO_3$ and $NH_3/NaSCN$ has to avoid crystallization during its operation, and the available property database correlation range. Since the sensible part of the cooling output decrease notably including a superheater, the cycle simulation was carried out without considering superheating.

The mix of power and cold production of the cycles with respect to the vapour split ratio is illustrated in Figs. 4.15 (a-d) at different heat source inlet temperatures.

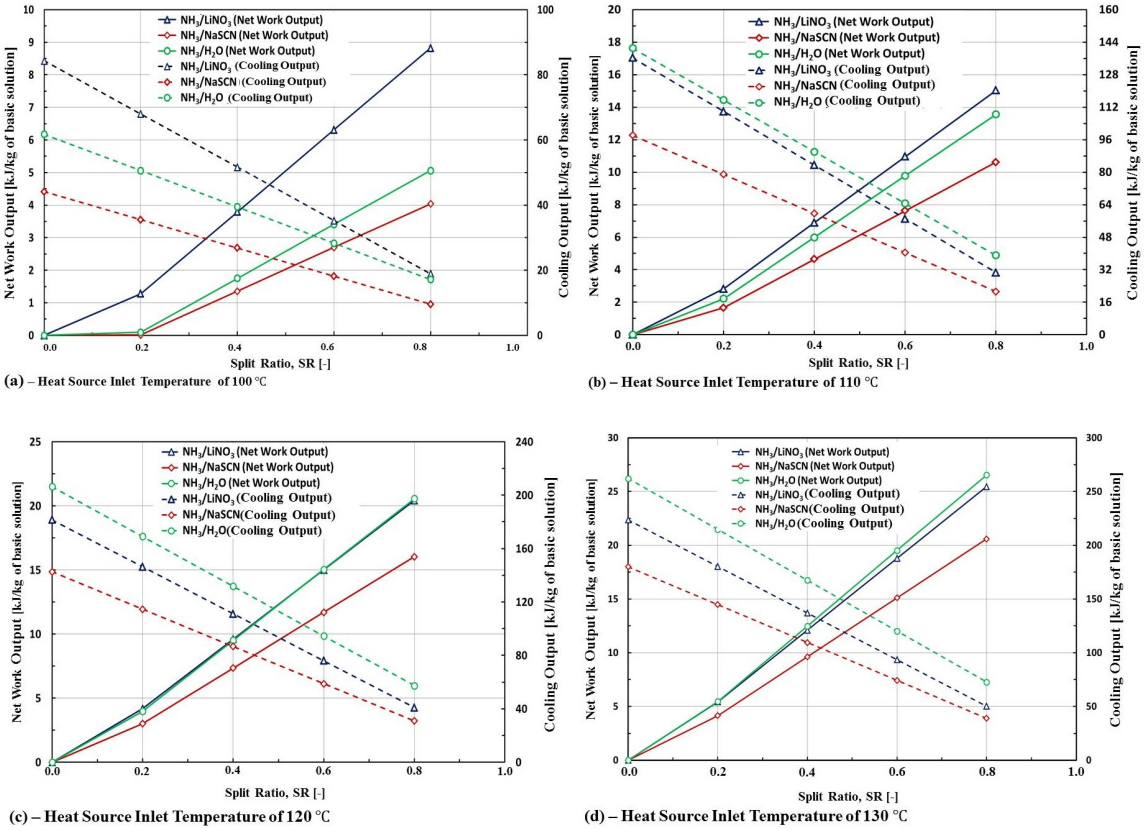

Figure 4.15: Cycle dual-outputs at different vapour split ratios for $NH_3/LiNO_3$, $NH_3/NaSCN$ and NH_3/H_2O working fluid mixtures.

Since the cycle operates as a Goswami cycle when the entire vapour flowing to the power sub-cycle (SR = 1.0), the high pressure of the system is no longer dependent on the operating condition of the condenser and its value is between the bubble and dew pressures of the basic solution at the desorber temperature. Therefore, a pressure that maximizes the effective exergy efficiency is taken as the optimum high pressure of the cycle. The performance indicators and useful outputs of the cycles at their corresponding optimum pressure are shown in Table 4.3.

Further detail analysis on the thermodynamic performance of the non-conventional working fluid mixtures ($NH_3/LiNO_3$ and NH_3/NaSCN) in a single-stage combined absorption cycle with parallel flow arrangements are described in Chapter 6 and 7 with the integration of scroll expanders and solar thermal collector technologies, respectively.

Table 4.3: Performance indicators and useful outputs of the single-stage combined absorption cycles (Fig. 4.14) operating as Goswami cycle (SR=1.0).

Parameter	Working fluid mixture											
	$NH_3/LiNO_3$				NH_3/NaSCN				NH_3/H_2O			
Heat source inlet temperature [°C]	100	110	120	130	100	110	120	130	100	110	120	130
Optimum cycle high pressure [kPa]	1260	1500	1760	2030	1150	1390	1660	1970	1020	1170	1320	1510
Effective first law efficiency [%]	9.6	10.5	11.3	12.0	6.9	7.8	8.6	9.4	6.4	7.1	7.7	8.2
Effective exergy efficiency [%]	48.4	48.9	48.8	48.5	35.1	26.1	36.6	36.8	32.9	33.4	33.6	33.5
Net power output [kW]	13.2	16.7	20.4	24.2	10.1	13.0	15.9	19.0	16.3	21.2	26.6	31.7
Sensible cooling output [kW]	2.7	4.1	5.6	7.0	1.0	2.0	3.1	4.3	11.4	15.6	20.2	25.0

4.6 Conclusions

A modified single-stage combined absorption power and refrigeration cycle is proposed by incorporating a relatively simple and well-known pressure booster, mechanical compressor, between the absorber and evaporator. This cycle configuration (SSAPRC-COM, Fig. 4.1) is more flexible in operation than the basic single-stage combined absorption cycle (SSAPRC-P) without electrical (or mechanical) energy consumption from external source to drive its mechanical compressor. The cycle can be activated by heat sources at very low temperatures (below 100 °C) and simultaneously produce power and cold with better energetic and exergetic efficiencies than SSAPRC-P cycle configuration.

In this chapter further cycle modification is presented, a vapour ejector is used to replace the mechanical compressor and stream mixer in the SSAPRC-COM cycle configuration. This new cycle configuration (SSAPRC-EJE, Fig. 4.11) is able to improve the co-production of power and cold under air-cooled absorber and condenser operating conditions. At a typical operating conditions for air-cooled case and refrigeration applications ($t_{cw,in}/t_{cw,out}$ = 37/42 °C and $t_{cf,in}/t_{cf,out}$ = 8/3 °C), the cycle refrigeration capacity increased by about 43% than the basic SSAPRC-P cycle configuration without reducing the co-produced mechanical power for a heat source inlet temperature range of 120 °C - 138 °C. The ejector compression ratio and expander pressure ratio were 1.5 and 2.5, respectively.

Finally, the effect of NH_3/H_2O, $NH_3/LiNO_3$ and $NH_3/NaSCN$ mixtures on the performance and operational working ranges of single-stage combined absorption cycle with a cooler (sensible heat exchanger) was analysed. The cycle operates in different modes of operation from only cold-mode (as an absorption refrigeration cycle) to Goswami cycle (mechanical power production with some sensible cold production, if any) and intermediate modes of operation. The intermediate modes of operation are for the co-production of mechanical power and cold (both latent and sensible) at different split ratios.

Chapter 5

Mid-Grade Heat Driven Combined Absorption Cycles

Major parts of this chapter are under review process in:

American Society of Heating, Refrigerating and Air-Conditioning Engineers (ASHRAE) Journal. Reference no. RSCH-00136-2014 to the HVAC&R Research. Combined Absorption Power and Refrigeration Cycles using Low- and Mid-Grade Heat Sources by ***Dereje S. Ayou****, Joan Carles Bruno and Alberto Coronas.*

"This page intentionally left blank"

5.1 Introduction

The aim of this chapter is to propose new combined absorption cycles that can be able to use the relatively high exergy of mid-grade heat sources (between 200 °C and 300 °C) for their efficient conversion into mechanical power and cold. The combined power and cooling cycle configuration proposed by Goswami can be driven by heat sources at temperature higher than 200 °C, however, mostly it requires multi-stage expansions. For desorber temperatures higher than 150 °C, at some operating conditions the vapour quality at the exit of the expander drops below 90% [156]. Thus, to eliminate lower vapour quality conditions the expansion stage should be increased and re-heaters have to be included. The need for using multi-stage expander, in the Goswami cycle, are crucial for desorber temperatures above 175 °C [156]. Further, the sensible cooling output of the cycle is relatively low or it may also be no cold production at all for mid-grade heat sources at typical operating conditions for air-conditioning and refrigeration applications. Other combined absorption cycles reviewed in Chapter 2 requires, relatively higher temperatures (above 300 °C) for their efficient conversion of thermal energy into mechanical power and cold.

In this chapter, a multi-stage multi-effect combined absorption cycle is proposed for the co-production of mechanical power and cold by using mid-grade heat sources. Later, this cycle configuration is modified through the use of pressure devices, like vapour-liquid ejector, to improve its performance and to extend operational working range of the cycle.

5.2 Two-Stage Combined Absorption Power and Refrigeration Cycle with Series flow arrangement (TSAPRC-S)

The single-stage combined absorption power and refrigeration cycle with series flow arrangement (SSAPRC-S) presented in Chapter 3, Fig. 3.12, leads to an important recognition that the cycle configuration can be modified into a two-stage double-effect combined absorption cycle that can utilize mid-grade heat sources for efficient conversion into mechanical power and cold. An important motivation in the development of this cycle configuration was the recognition that NH_3/H_2O working fluid mixture has a wide solution field to accommodate concentration staging, in addition to the possibilities of pressure staging.

The advantages of concentration staging is already exploited in absorption refrigeration cycles: two-stage double-effect and triple-effect absorption refrigeration cycles could be typical examples [48].

The cycle process description of the proposed mid-grade combined absorption cycle and its energetic and exergetic performance analysis are presented below.

5.3 Process Description of TSAPRC-S

Fig. 5.1 shows the schematic flow diagram of the proposed two-stage double-effect combined absorption power and refrigeration cycle based on NH_3/H_2O working fluid mixture.

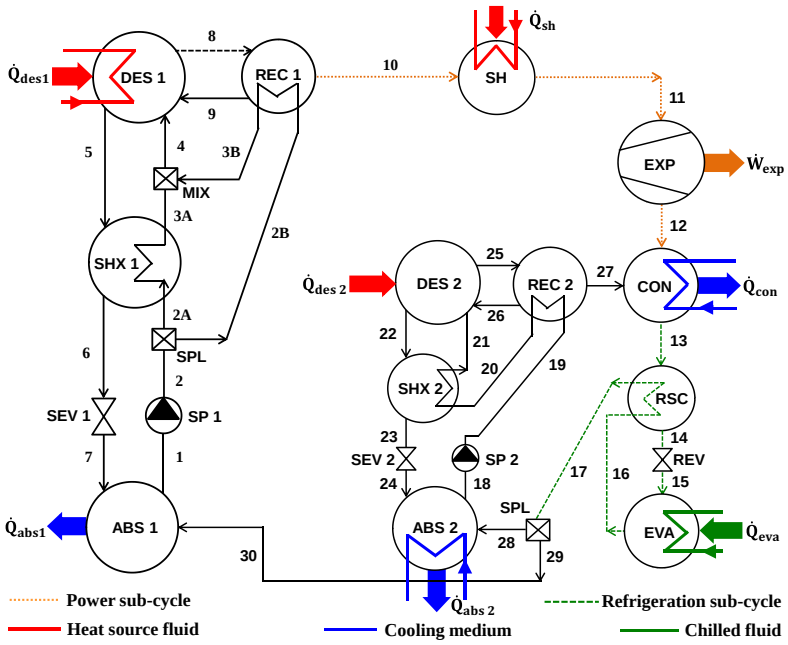

Figure 5.1: Schematic diagram of two-stage double-effect combined absorption power and refrigeration cycle with series flow arrangement (TSAPRC-S).

Basically, in this configuration (Fig. 5.1) two single-stage NH_3/H_2O absorption cycles can be recognized, one inside the other, larger one. The larger absorption cycle, hereafter referred to as first-stage absorption cycle, is same as the single-stage combined absorption cycle with series flow arrangement (SSAPRC-S, Fig. 3.12 in Chapter 3) except sharing its refrigeration sub-cycle process with the smaller absorption refrigeration cycle (second-stage absorption cycle). The second-stage absorption cycle is also similar to basic single-effect NH_3/H_2O absorption refrigeration cycle regarding its process flow and operating

conditions. However, its driving heat input is provided internally from the absorber of the first-stage (ABS 1 in Fig. 5.1) absorption cycle that operates at a relatively high temperature: enough to provide the necessary temperature level to activate the desorber (DES 2 in Fig. 5.1) of the second-stage absorption cycle. Similar to the SSAPRC-S combined absorption cycle configuration, the whole cycle operates at three pressure levels, those given by the evaporator at low pressure, total condenser at intermediate pressure and first-stage desorber at high pressure. The first-stage desorber and rectifier, and superheater operates at the same high pressure. The second-stage desorber and rectifier operates at the condenser, intermediate, pressure. The two absorbers (first and second-stage) operates at the same, low, pressure with the evaporator.

5.4 Operating Characteristics and Analysis of TSAPRC-S

The thermodynamic performance evaluation of the proposed mid-grade combined absorption cycle is performed for a heat source inlet temperature between 200 °C and 300 °C in steps of 20 °C. The second-stage absorber (ABS 2) and condenser (CON) heat rejection mediums are connected in parallel. The driving heat source fluid, "BP Transcal N" thermal oil is used in this study, it first enters into the superheater (SH) and then to the first-stage desorber (DES 1) of the cycle. A typical operating conditions are selected for the condenser (and second-stage absorber, ABS 2) and evaporator (EVA) of the cycle: cooling and chilled water inlet/outlet temperatures of 27/32 °C and 12/7 °C, respectively. The NH_3 concentration difference across the second-stage solution circuit is set at 0.04. A unit mass flow rate (1.0 kg/s) of NH_3/H_2O basic solution through the first-stage solution pump (SP 1) was taken as a basis for extensive variables calculation. In addition to the assumptions considered for the generic steady-state physical-mathematical modelling approach followed for combined absorption cycles in Chapter 3, the following additional assumptions were taken to develop the physical-mathematical model of the TSAPRC-S configuration:

- The lowest temperature in the first-stage absorber (t_1 in Fig. 5.1) is set 1 °C higher than the highest temperature in the second-stage desorber (t_{22} in Fig. 5.1).
- The portion of the heat rejected by the second-stage absorber (ABS 2) is used to heat the vapour entering the first-stage absorber (ABS 1, $t_{30} = t_{24}$ in Fig. 5.1).

- The mass flow rate of the NH_3/H_2O solution, strong in NH_3, leaving the second-stage absorber is determined by the energy balance between the first-stage absorber and second-stage desorber (i.e. $\dot{Q}_{abs1} = \dot{Q}_{des2}$).

- The degree of purification in the rectifiers (both in the first and second-stage absorption cycles) is specified by the concentration of the vapour leaving the rectifiers, and it is set at an ammonia mass fraction of 0.995.

- Minimum approach temperature of 5 °C is considered for the second-stage absorber, condenser, evaporator, first-stage desorber and rectifier, and superheater.

- Analogues to the low-grade heat driven combined absorption cycles analysis, the heat source fluid mass flow rate is determined by minimising the mismatch of thermal capacitance rates in the desorber of the first-stage absorption cycle (DES 1).

The net power output of the cycle is defined as the mechanical power output from the expander reduced by the mechanical power consumption of the solution pumps (SP 1 and SP 2 in Fig. 5.1). The cycle efficiencies, both effective first law and effective exergy efficiencies, are defined in the same way as given in Chapter 3 (Eq. 3.2.7 and Eq. 3.2.10).

Figs. 5.2 (a) and (b) show the sensitivity of the net power and cooling outputs of the mid-grade combined absorption cycle, TSAPRC-S, with the variation of the expander pressure ratio ($pr_{exp} = {}^{p_{des1}}/_{p_{con}}$) at several heat source inlet temperatures ($t_{hs,in}$). The amount of vapour generated in the first-stage desorber (DES 1) decreases as the expander pressure ratio increases (i.e. the high pressure of the cycle increases, at a fixed intermediate pressure), however, the value of specific enthalpy difference across the expander increases. When the expander pressure ratio increases, the mechanical power developed by the expander increases first and then decreases by showing a maximum value for each heat source inlet temperature considered in the performance analysis of the cycle. It is mainly because of the trade-off between the decreasing amount of vapour production in the first-stage desorber and increasing specific enthalpy difference across the expander. The power consumption of the solution pump of the first-stage absorption cycle (SP 1) increases as the expander pressure ratio increase whereas the second-stage absorption cycle solution pump (SP 2) power consumption decreases.

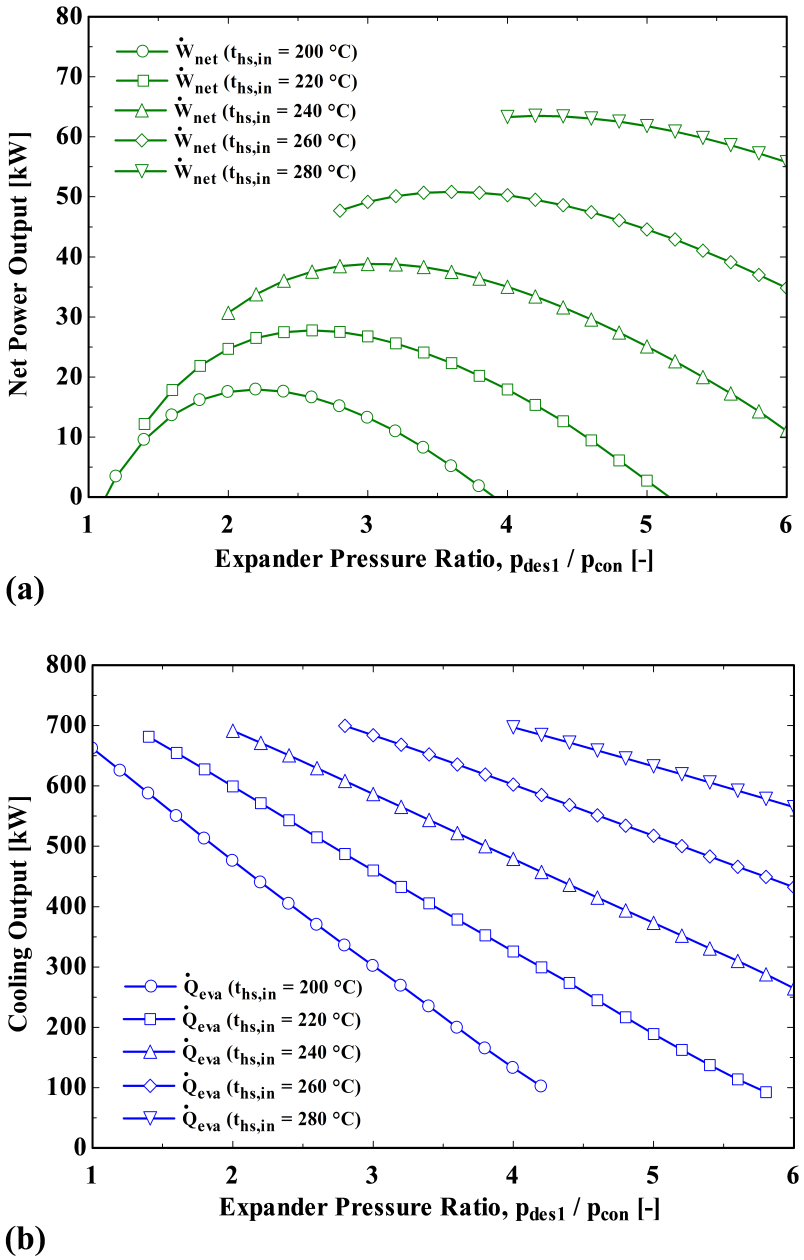

Figure 5.2: Effect of expander pressure ratio on cycle useful dual-outputs at several heat source inlet temperatures: (a) - net power output; (b) - cooling output (TSAPRC-S, Fig. 5.1).

The amount of refrigerant, both from the first and second-stage absorption cycle rectifiers, flowing through the evaporator decreases with the increase of the expander pressure ratio. However, the specific enthalpy difference across the evaporator remains constant (at 1169.63 kJ/kg) for the specified operating conditions. Thus, as expected the cooling output of the cycle decreases as the expander pressure ratio increases at constant heat source inlet temperature. For a constant heat source temperature, both the driving heat

($\dot{Q}_{in} = \dot{Q}_{des1} + \dot{Q}_{sh}$) and exergy ($\triangle \dot{E}x_{hs,in}$) inputs of the cycle decreases as expander pressure ratio increases. And also, the heat rejected by the first-stage absorber, i.e. driving heat input of second-stage desorber, decreases with the increase of expander pressure ratio.

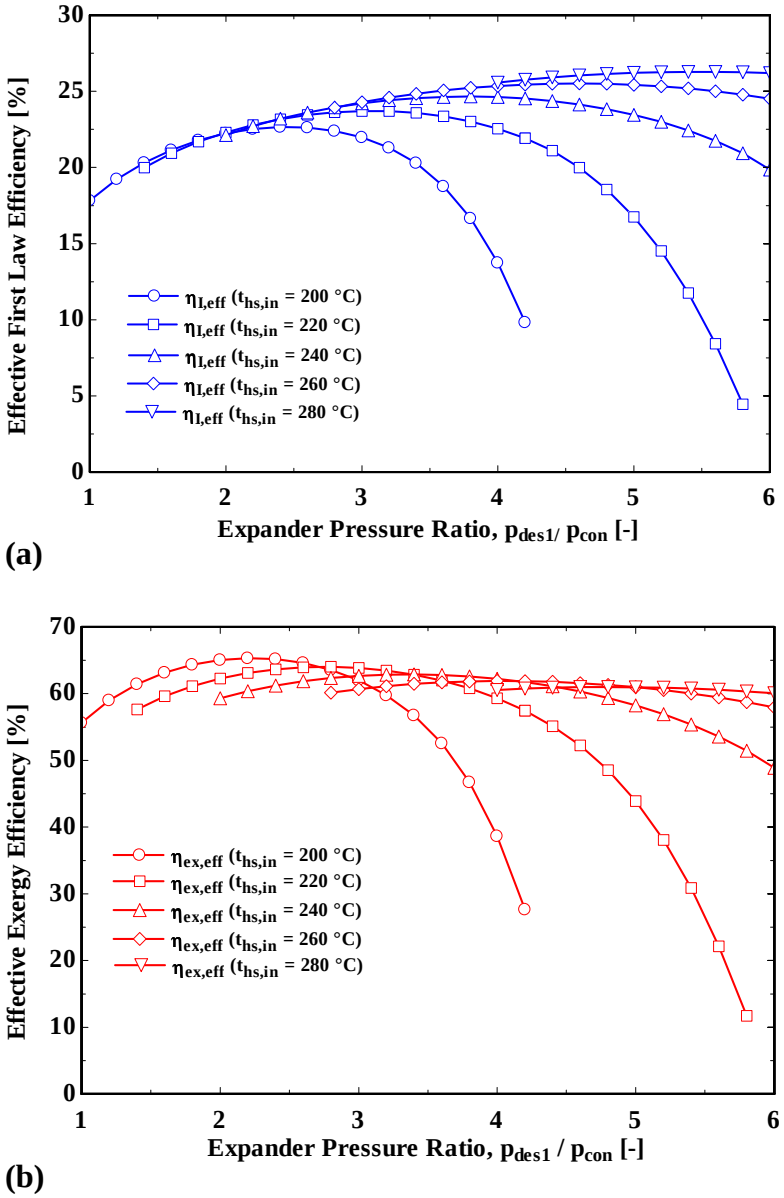

Figure 5.3: Effect of expander pressure ratio on the cycle efficiencies at several heat source inlet temperatures: (a) - effective first law efficiency; (b) - effective exergy efficiency (TSAPRC-S, Fig. 5.1).

The actual work contribution of the cooling output of the cylce, $\dot{E}x_{cold}/\eta_{II,ref}$ in both effective first law and effective exergy efficiency definitions, also decrease with the increase of expander pressure ratio. As a consequence for each heat source inlet temperatures,

the cycle has optimum expander pressure ratio that maximize the cycle efficiencies and depicted in Figs. 5.3 (a) and (b). Accordingly, a heat source inlet temperature of 220 °C with its corresponding optimum expander pressure ratio of about 3.0 is taken as a baseline condition. The cooling water and chilled water inlet/outlet temperatures considered at the base-case were: $t_{cw,in}/t_{cw,out} = 27/32$ °C and $t_{cf,in}/t_{cf,out} = 12/7$ °C respectively. The base-case performance summary for the TSAPRC-S cycle is shown in Table 5.1 and its corresponding stream characteristics are provided in Table 5.2.

Table 5.1: Base-case performance summary for the proposed mid-grade combined absorption cycle (TSAPRC-S, Fig. 5.1).

Useful dual-outputs [kW]		**Mechanical power [kW]**	
Cooling output $\dot{Q}_{cold}$	459.70	Expander $\dot{W}_{exp}$	34.66
Net power output $\dot{W}_{net}$	26.75	First-stage solution pump $\dot{W}_{sp1}$	4.72
Thermal power [kW]		Second-stage solution pump $\dot{W}_{sp2}$	3.19
First-stage absorber heat duty $\dot{Q}_{abs1}$	403.58	**Exergy flow [kW]**	
Second-stage absorber heat duty $\dot{Q}_{abs2}$	383.42	Cooling output exergy ($\dot{E}x_{cold}$)	25.22
Condenser heat duty $\dot{Q}_{con}$	517.06	Heat source exergy input ($\triangle\dot{E}x_{hs,in}$)	173.53
Second-stage desorber heat duty $\dot{Q}_{des2}$	403.58	**Performance indicators**	
First-stage rectifier heat duty $\dot{Q}_{rec1}$	162.32	Effective first law efficiency $\eta_{I,eff}$ [%]	23.71
Second-stage rectifier heat duty $\dot{Q}_{rec2}$	5.35	Power/cold ratio R [-]	0.058
Refrigerant sub-cooler heat duty $\dot{Q}_{rsc}$	39.16	Effective exergy efficiency $\eta_{ex,eff}$ [%]	63.87
First-stage solution HX heat duty $\dot{Q}_{shx1}$	404.26	Exergy efficiency η_{ex} [%]	29.95
Second-stage solution HX heat duty $\dot{Q}_{shx2}$	376.61		
Superheater heat duty $\dot{Q}_{sh}$	70.36		

The sensitivity of the useful dual-outputs (power and cold) and effective first law and effective exergy efficiencies with respect to the variation of the heat source inlet temperature at several expander pressure ratios ($pr_{exp} = 3.0$, 4.0 and 5.0) and heat sink medium, cooling water , inlet/outlet temperatures ($t_{cw,in}/t_{cw,out} = 27/32$ °C and 32/37 °C) are illustrated in Fig. 5.4 and Fig. 5.5 respectively. A similar increasing trend, at all operating conditions, for both net power and cooling outputs of the cycle are observed as the heat source inlet temperature increases. As the cooling water inlet temperature increases, the intermediate pressure of the cycle also increases as a result less vapour generated in both desorbers at the same expander pressure ratio, heat source and chilled fluid inlet temperatures. Consequently, as can be seen in Fig. 5.4 (a) and (b) the net power and cooling outputs of the cycle decreases as the cooling water inlet temperature increases.

Table 5.2: The base-case stream characteristics for the proposed mid-grade combined absorption cycle (TSAPRC-S, Fig. 5.1).

State point (i)	t_i [°C]	p_i [kPa]	z_i [kg/kg]	$\dot{m}_i$ [kg/s]	h_i[kJ/kg]	s_i [kJ/kg·K]	ex_i [kJ/kg]
1	74.1	460	0.2906	1.0000	222.13	1.335	84.65
2	74.6	3694	0.2906	1.0000	226.86	1.337	88.56
2A, 2B	74.6	3694	0.2906	0.6251, 0.3749	226.86	1.337	88.56
3A	181.8	3694	0.2906	0.6251	873.55	2.918	264.01
3B	165.4	3694	0.2906	0.3749	873.55	2.918	192.41
4	177.1	3694	0.2906	1.0000	793.43	2.741	236.66
5	209.4	3694	0.1303	0.8146	877.01	2.677	339.29
6	102.9	3694	0.1303	0.8146	380.75	1.518	188.57
7	103.5	460	0.1303	0.8146	380.75	1.528	185.71
8	170.4	3694	0.8068	0.2530	2065.38	6.228	469.05
9	170.4	3694	0.2906	0.0676	685.35	2.499	200.68
10	90.3	3694	0.9950	0.1854	1693.00	5.463	324.71
11	215	3694	0.9950	0.1854	2072.54	6.368	434.37
12	125	1231	0.9950	0.1854	1885.56	6.452	222.26
13	32	1231	0.9950	0.3949	488.76	1.988	156.58
14	11.1	1231	0.9950	0.3949	389.60	1.651	157.76
15	2	460	0.9950	0.3949	389.60	1.658	155.70
16	5	460	0.9950	0.3949	1553.73	5.884	59.87
17	24.8	460	0.9950	0.3949	1652.89	6.231	55.48
18	32	460	0.5259	2.6663	75.32	1.036	26.72
19	32.1	1231	0.5259	2.6663	76.51	1.037	27.69
20	32.6	1231	0.5259	2.6663	78.52	1.044	27.73
21	62.3	1231	0.5259	2.6663	219.77	1.485	37.55
22	73.1	1231	0.4859	2.4568	253.87	1.573	45.26
23	40.8	1231	0.4859	2.4568	100.57	1.109	30.50
24	38.4	460	0.4859	2.4568	100.57	1.112	29.54
25	66.7	1231	0.9924	0.2107	1737.85	6.051	194.26
26	66.7	1231	0.5259	0.0012	240.84	1.547	40.02
27	61.1	1231	0.9950	0.2095	1720.79	6.001	192.18
28	24.8	460	0.9950	0.2095	1652.89	6.231	55.48
29	24.8	460	0.9950	0.1854	1652.89	6.231	55.48
30	38.4	460	0.9950	0.1854	1702.05	6.392	56.58
hs,in	220.0	-	-	4.746	703.85	2.331	13.32
hs,int.	214.4	-	-	4.746	689.02	2.301	7.51
hs,out	182.1	-	-	4.746	605.34	2.124	−23.24
cw,in	27	101.323	-	43.09	113.28	0.3952	0.03
cw,out	32	101.323	-	43.09	134.18	0.4642	0.34
cf,in	12	101.323	-	21.91	113.28	0.1806	1.22
cf,out	7	101.323	-	21.91	134.18	0.1064	2.37

At a given heat source inlet temperature, the cooling output of the cycle decreases as the expander pressure ratio increases because the amount of vapour generated in the first-stage desorber decreases as the high pressure of the cycle increases at constant desorber temperature (t_5 in Fig. 5.1). The net power output of the cycle decreases as the expander pressure ratio increases at relatively lower heat source inlet temperatures. However, at higher heat source inlet temperatures the difference between the net power output at different expander pressure ratio is minimal since the decrease in the amount of vapour production is compensated by the increase in specific enthalpy drop across the expander when the expander pressure ratio increases.

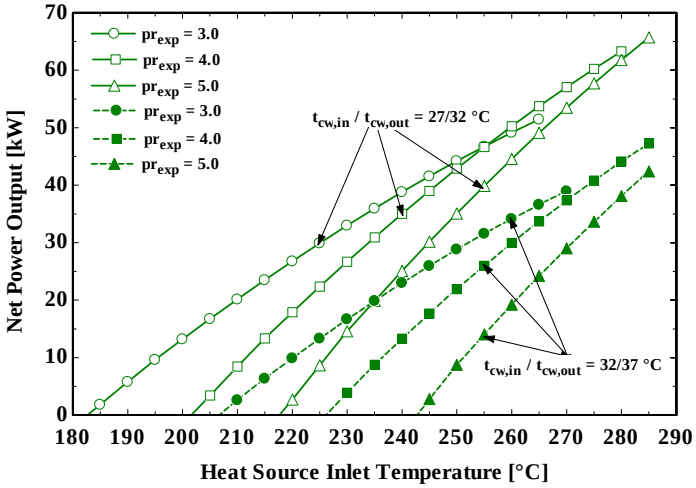

(a)

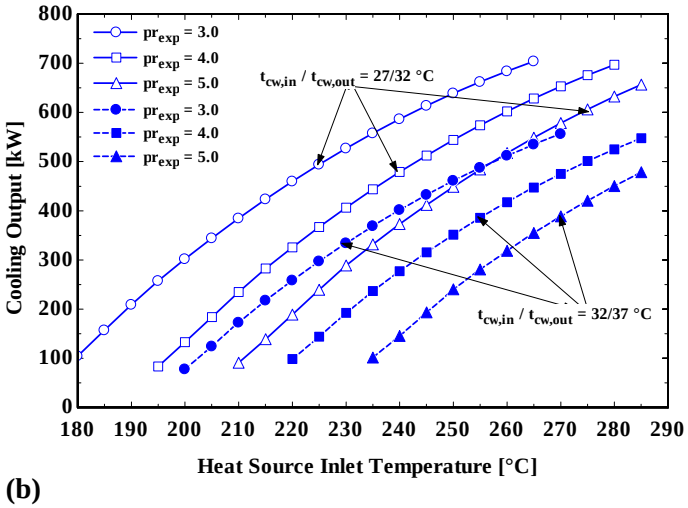

(b)

Figure 5.4: Effect of heat source inlet temperature on the cycle useful outputs at several expander pressure ratios: (a) - net power output; (b) - cooling output (TSAPRC-S, Fig. 5.1).

The effect of expander pressure ratio and heat sink temperature on the effective first law and effective exergy efficiencies are depicted in Fig. 5.5. As can be seen in these figures, when the heat source inlet temperature exceeds certain values the cycle efficiencies, at all operating conditions considered, are tends to be more flat. And, higher cycle efficiency values are obtained at lower heat sink temperatures. The influence of expander pressure ratio on effective first law and effective exergy efficiency values are reduced at higher heat source inlet temperatures.

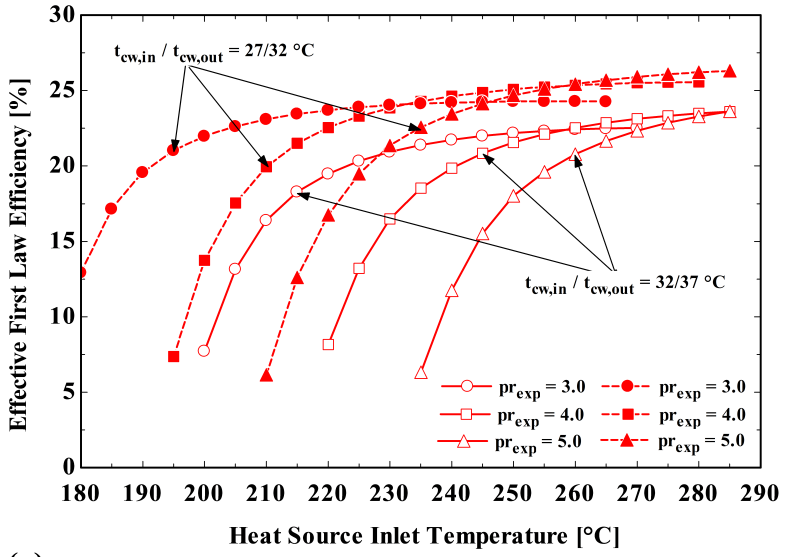

Figure 5.5: Effect of heat source inlet temperature on the cycle efficiencies at several expander pressure ratios: (a) - effective first law efficiency; (b) - effective exergy efficiency (TSAPRC-S, Fig. 5.1).

5.5 Cycle Modification for Performance Improvements

In a two-stage double-effect combined absorption cycle configuration (TSAPRC-S), it can be recognized that there is a significant pressure loss when the weak, in NH_3, solution in the first-stage solution circuit throttles from the high (first-stage desorber) pressure to low (evaporator) pressure (states 6-7 in Fig. 5.1). A pressure device such as vapour-liquid ejector can be used to recover some of the pressure energy in the weak solution from the first-stage desorber to entrain the vapour entering the first-stage absorber from the evaporator (state 30 in Fig. 5.1). And then, as a consequence, the first-stage absorber operate at a relatively higher pressure than the evaporator (and second-stage absorber) pressure. This effect enhances the absorption process in the first-stage absorber.

For a given thermal boundary conditions (heat source, heat sink medium and chilled fluid temperatures) and an expander pressure ratio, more vapour can be generated in the first-stage desorber by increasing the operating pressure of the first-stage absorber through the introduction of vapour-liquid ejector in place of the solution expansion valve in the weak solution stream (states 6-7). Thus, the triple-pressure levels TSAPRC-S configuration can be modified into quadruple pressure levels mid-grade combined absorption cycle configuration with increased amount of useful dual-outputs (mechanical power and cold) and cycle efficiencies than the triple-pressure levels TSAPRC-S configuration (Fig. 5.1) at the same operating conditions.

The thermodynamic performance comparison between the modified TSAPRC-S with the basic TSAPRC-S configurations is performed for a set of input operating conditions and design parameters given in Table 5.3.

Table 5.3: Input operating conditions and design parameters assumed for the thermodynamic performance comparison between the proposed mid-grade combined absorption cycle (TSAPRC-S) and the modified TSAPRC-S configuration.

Input Variable	**Value**
Heat source inlet temperature, $t_{hs,in}$ [°C]	200, 220, 240
Cooling water inlet/outlet temperature, $t_{cw,in}/t_{cw,out}$ [°C]	27/32
Chilled water inlet/outlet temperature, $t_{cf,in}/t_{cf,out}$ [°C]	12/7
Compression ratio, $pr_{com} = p_{abs1}/p_{eva}$ [-]	1.0, 1.5, 2.0
Concentration difference across the second-stage solution circuit, Δz_2 [kg/kg]	0.04

Fig. 5.6 (a) and (b) show the effect of compression ratio on the net power and cooling outputs of the cycle at several heat source inlet temperatures.

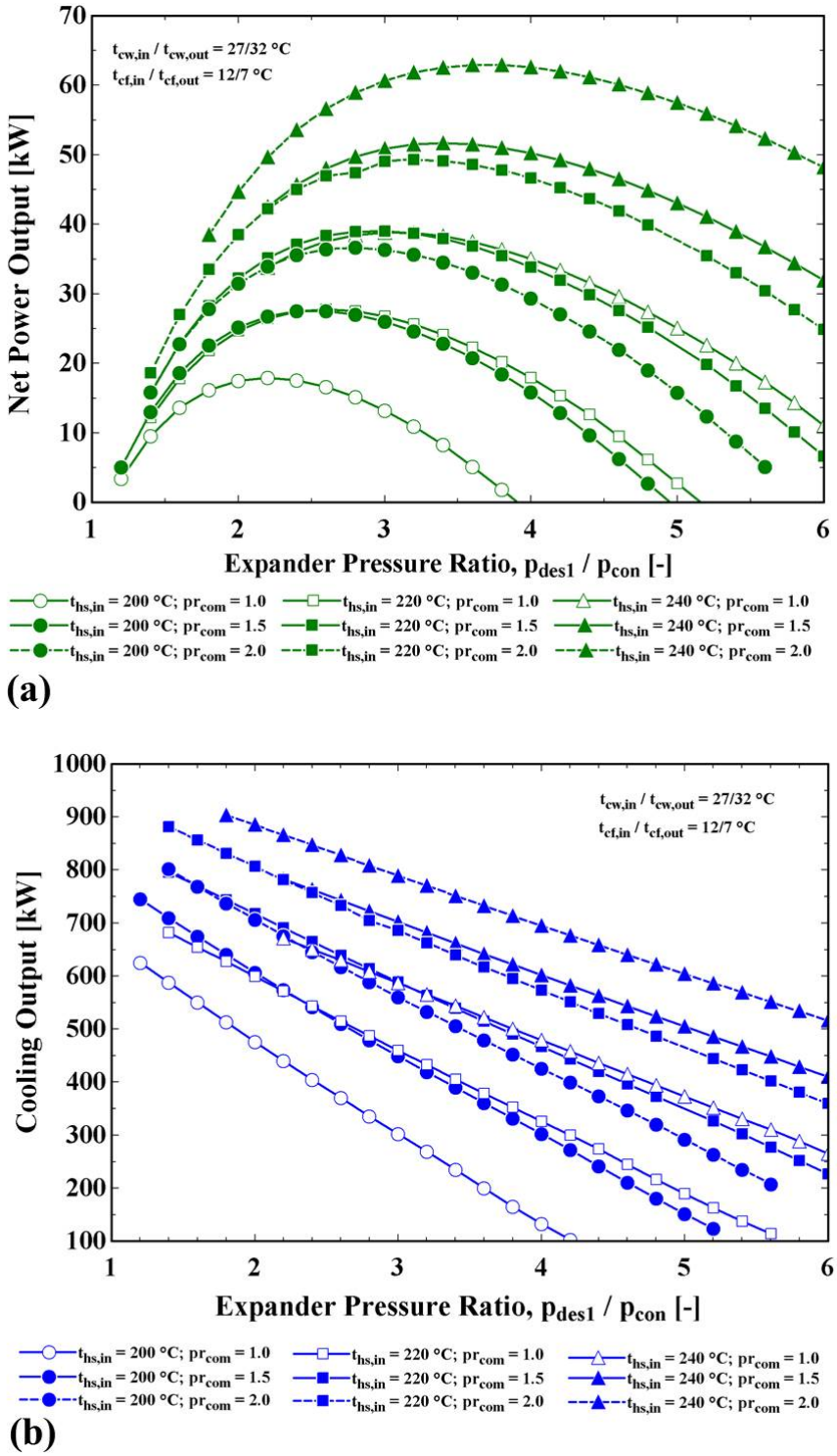

Figure 5.6: Effect of compression ratio on the cycle useful outputs at several heat source inlet temperatures: (a) - net power output; (b) - cooling output (TSAPRC-S and modified TSAPRC-S configurations).

It can be seen that the net mechanical power output of the cycle increases first to maximum and then decreases as the expander pressure ratio increases at all the cases considered in the performance analysis. It is obvious that the amount of vapour generated in the desorber decreases when the expander pressure ratio increases at constant desorber temperature. The specific enthalpy drop across the expander increases as the expander pressure ratio increases this is the main reason for the net power output to increase at first (Fig. 5.6 (a)). The power consumption of the first-stage pump (SP 1) increases as the expander pressure ratio increases whereas the power consumption of the second-stage pump (SP 2) decreases. When the compression ratio, pr_{com}, increases from 1.0 (without compression: a triple-pressure levels cycle) to 2.0, the maximum net power output of the cycle increase from about 18 kW to 37 kW, 28 kW to 49 kW and 39 kW to 63 kW for heat source inlet temperature of 200 °C, 220 °C and 240 °C, respectively. The optimum expander pressure ratio that maximize the net power output of the cycle also increase from 2.2 to 2.8 for 200 °C, 2.6 to 3.2 for 220 °C and 3.0 to 3.6 for 240 °C heat source temperatures.

As it is illustrated in Fig. 5.6 (b) as the expander pressure ratio increases, the cooling output of the cycle decreases in all the conditions considered during the simulation. The reason for this is that as the expander pressure ratio increases, less vapour flows through the evaporator. As it is depicted in Fig. 5.6 (b), at the same heat source inlet temperature and expander pressure ratio the cooling output of the cycle increases as the compression ratio pr_{com} increases.

Fig. 5.7 (a) and (b) show the effect of compression ratio on the cycle effective first law and effective exergy efficiencies at several heat source inlet temperatures. Similar to the net power output, both effective first law and effective exergy efficiencies of the cycle shows different optimum expander pressure ratio when the compression ratio changes from 1.0 to 2.0 at a constant heat source inlet temperature.

At the same operating conditions, for instance, $t_{hs,in} = 240$ °C, $t_{cf,in}/t_{cf,out} = 12/7$ °C, $t_{cw,in}/t_{cw,out} = 27/32$ °C and expander pressure ratio of $pr_{exp} = 3.5$ the cycle's effective first law efficiency and effective exergy efficiency values increases from about 24.6% to 27.1% and 62.9% to 72.9%, respectively, when the compression ratio of a pressure device incorporated in the cycle is changed from 1.0 to 2.0.

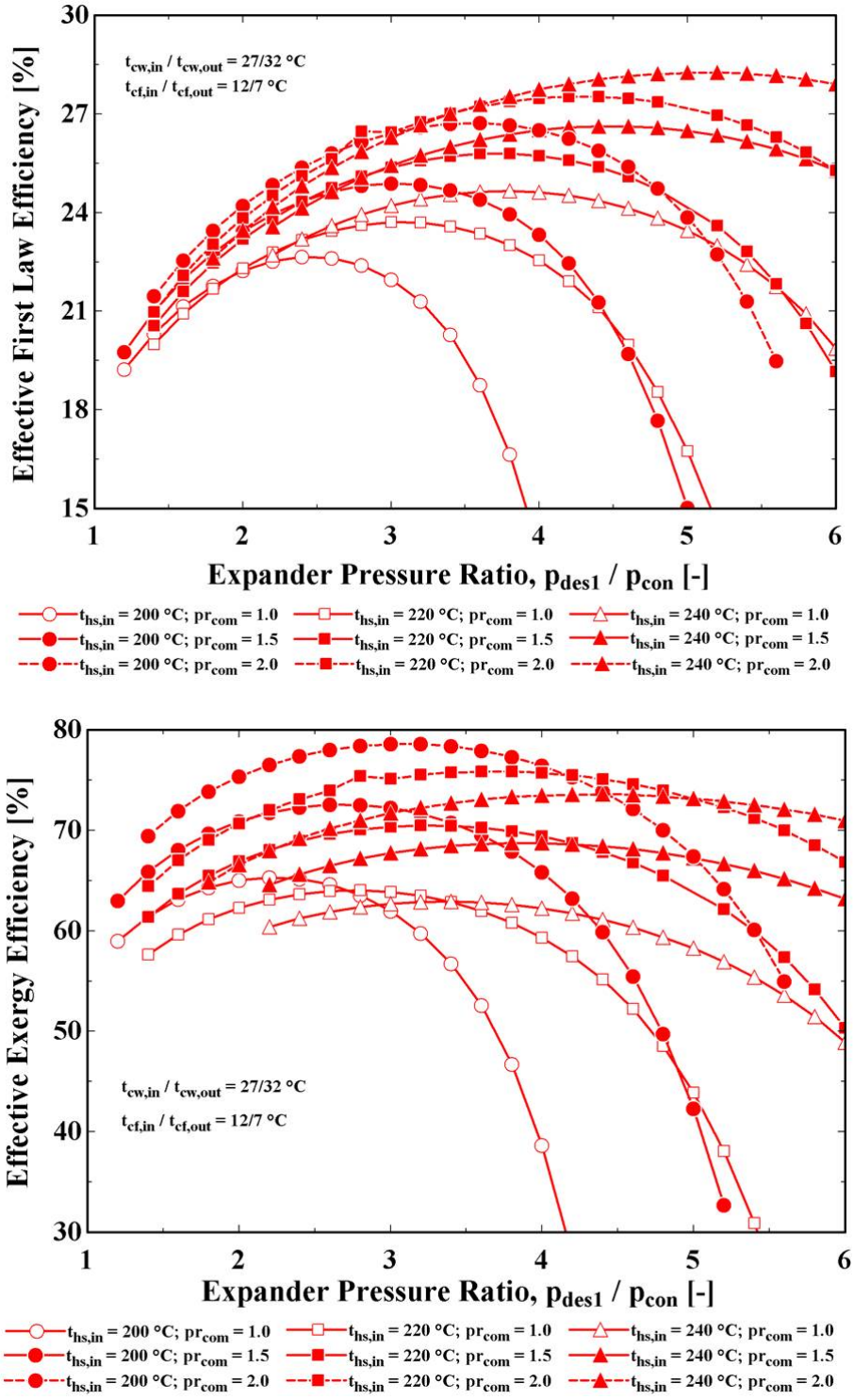

Figure 5.7: Effect of compression ratio on the cycle efficiencies at several heat source inlet temperatures: (a) - effective first law efficiency; (b) - effective exergy efficiency (TSAPRC-S and modified TSAPRC-S configurations).

5.6 Conclusions

In this chapter, a new two-stage combined absorption power and refrigeration cycle with series flow arrangement (TSAPRC-S) is proposed and analysed for the effective utilization of mid-grade heat sources at temperatures below 300 °C. A physical-mathematical model was developed, using NH_3/H_2O mixture as working fluid, for TSAPRC-S configuration and used to study the performance and operating conditions of the cycle. The performance improvement potential of the cycle by the introduction of pressure recovery device, such as vapour-liquid ejector, is also investigated from the energetic and exergetic point of view.

At the same operating conditions, the net mechanical power and cooling outputs of the combined absorption cycle TSAPRC-S configuration can be increased with the introduction of pressure recovery device. It operates the first-stage absorber at higher pressure than the low (evaporator) pressure of the cycle. The cycle also operates at higher energy and exergy efficiencies with the introduction of the pressure device. For thermal boundary conditions of $t_{hs,in}$ = 240 °C, $t_{cw,in}/t_{cw,out}$ = 27/32 °C and $t_{cf,in}/t_{cf,out}$ = 7/12 °C and pr_{exp} = 3.5, the effective first law and effective exergy efficiency values are about (24.6%, 62.9%), (26.1%, 68.6%) and (27.1%, 72.9%) when the compression ratio is set to 1.0, 1.5 and 2.0, respectively. The net power output and cooling capacity of the cycle increases from 37.9 kW to 72.9 kW and 532.7 kW to 741.4 kW respectively when the compression ratio of the pressure device increases from 1.0 to 2.0.

Chapter 6

Integration of Scroll-expanders into Combined Absorption Cycles

Major parts of this chapter has been published in:

- *The proceedings of International Sorption Heat Pump Conference ISHPC 2014, Maryland, USA, March 31 - April 2, 2014. Integration of scroll-expanders into combined absorption cycles for power and refrigeration applications by* ***Dereje S. Ayou****, Joan Carles Bruno, D. Yogi Goswami and Alberto Coronas.*

- *Applied Thermal Engineering, 72(2): 258-265, 2014. Small capacity absorption systems for cooling and power with a scroll expander and ammonia based working fluids by Luis Carlos Mendoza,* ***Dereje S. Ayou****, Joaquín Navarro-Esbrí, Joan Carles Bruno and Alberto Coronas.*

"This page intentionally left blank"

6.1 Introduction

In previous chapters several combined absorption cycles were proposed. In order to implement such types of cycles into practice, two interdependent questions need to be addressed regarding the expander technology: what types of expander would be suitable for given operating conditions and size of the system, and secondly what would be a cost-effective expander compatible with NH_3 particularly for small and micro-scale capacity systems. Scroll machines are one of the main candidates for such type of applications because of their good performance, reliability, and fewer moving parts. So far the least expensive scroll expanders are originally scroll compressors modified to operate as expanders. And also, compressors are used as expanders in ORC cycles.

This chapter presents the development of a semi-empirical model for a scroll expander with NH_3 or NH_3/H_2O mixture with high concentration of NH_3 as working fluids and its scale-up to higher size expanders in the same family series. The Sanden scroll compressor (TRSA05) was tested as an expander and used in this study. The other models of the same family considered in the scale-up process were TRSA09 and TRSA12. The semi-empirical model developed are characterized by good accuracy in predicting outputs (mass flow rate, shaft power and exhaust temperature), low computational time and robustness. The adjustable parameters of the model were estimated using experimental data obtained in a test bench (Mendoza, 2013) [204]. This semi-empirical model is integrated into a combined absorption cycle global model for the purpose of representing the performance of the work developing expansion device in the cycle.

6.2 Expander Technologies

The selection of a suitable work developing expansion device is crucial for designing and implementing power generating systems. For large-scale power generating systems (in MW), steam turbines (turbo type expanders) are well established technologies [156]. For NH_3/H_2O based power cycles like the Kalina cycle, medium and large-scale size turbine expander technologies are available. A typical example could be an 'Euler Turbine', shown in Fig. 6.1, developed for a geothermal project in Germany by Energent Corporation for Siemens AG [185]. The turbine operates with an NH_3/H_2O mixture in a Kalina cycle

to produce nearly 600 kWel (medium-scale capacity). It is characterized by low cost and erosion resistant design due to its robust blisk geometry with two-dimensional blades [185].

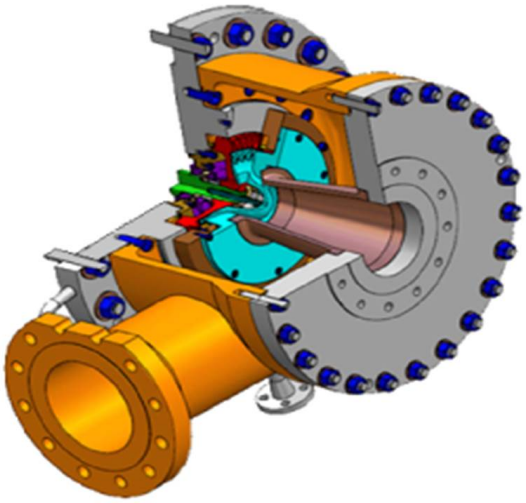

Figure 6.1: Euler Turbine – A patented high efficiency turbine developed for a geothermal project in Germany [185].

However, for small (10 kW - 100 kW) and micro-scale ($<$ 10 kW) applications for instance for buildings the development of a suitable expansion device is still necessary. This is mainly because of the following two main reasons: first it is difficult to find an off-the-shelf expander with high efficiency for such type of applications; second NH_3 is corrosive to copper and copper containing alloys therefore it presents a limitation on the selection and design of expanders.

Expanders, in general, can be categorized into two types: one is the velocity (dynamic) type, such as axial turbine expanders and radial-flow turbines; the other is the volumetric (positive displacement) type that includes typically the screw expanders, scroll expanders and reciprocating piston expanders and rotary vane type expanders. Their selection strongly depends on the operating conditions and the capacity of the system.

6.2.1 Dynamic type expanders

There are different types of velocity (turbo) expanders where the most common ones are axial and radial-inflow turbines. For systems with relatively high flow rates and low pressure ratios axial turbines are mostly used whereas for systems characterized by low flow rates and high pressure ratios like ORC systems radial inflow turbines are preferable.

There are several limiting factors on the performance of radial inflow turbines that includes tip speed, rotating speed, specific speed and maximum Mach number in the turbine nozzle and rotor [186]. Basically, a high tip speed is preferred because it increases the stage specific work. However, it is limited by the strength of the materials at the wheel periphery. Due to the effect of bearing capacity and loss, it exist an optimum rotating speed corresponding to the maximum efficiency. In order to obtain higher isentropic efficiency, specific speed varies between 0.3 to 0.9 [19]. In general, a maximum Mach number about 0.85 is recommended in order to avoid any local choking of the flow in the rotor [19]. The maximum Mach number in the turbine nozzle restrains the maximum allowable pressure/volume ratio over the turbine. A very high Mach number has adverse effect on the efficiency of the expander and should be avoided.

Turbo expanders are generally applied in power cycles with power outputs greater than 50 kWel because of their relatively high-expansion efficiency at high power outputs [187]. The performance of turbo expanders deteriorate for lower power outputs, especially below 50 kWel, and even it could reach to unacceptable efficiency levels for about 10 kWel [188]. Since the turbine rotational speed increases exponentially as the power output decreases, turbo expanders are not suitable for small-scale and micro-scale capacity systems otherwise reliability because of high rotational speed will be an issue. In addition to this, small-scale and micro-scale turbo expanders are more expensive and difficult to be commercially viable and also their efficiency is relatively low [188]. Nevertheless, some recent studies (both experimental and modelling) have also employed (turbo) turbine expanders in small-scale and micro-scale ORC systems ([188]-[192]). A typical example could be-Infinity Turbine Model IT10 with a capacity of 10 kWel manufactured by Infinity turbine LLC (USA) [188]. And also, recently GREEN TURBINE^{tm} [189] (a research and development company headquarters in the Netherlands) has developed a small, lightweight, steam driven turbo generator which generate electricity in the power range of 1 kW - 15 kW with a relatively high yield. It also operates silently with almost no vibration.

6.2.2 Volumetric type expander

The volumetric type expanders are more appropriate to the small-scale and micro-scale power generating systems (combined absorption systems) because they are characterized

by lower flow rates, higher pressure ratios (reciprocating piston expander) and much lower rotational speeds compared with the velocity-type expanders. In Table 6.1, different types of expander technologies are shown with their capacity and rotational speed ranges and Fig. 6.2 shows these different types of volumetric expanders. Moreover, they can tolerate two-phase conditions, which may appear at the end of the expansion in some operating conditions for wet working fluids like NH_3, H_2O and NH_3/H_2O mixtures.

Table 6.1: Comparison of various types of expander technologies [19].

Expander type	Capacity [kW]	Rotational speed [rpm]
Radial-inflow turbine	50–500	8000–80,000
Scroll expander	1–10	$<$ 6000
Screw expander	15–200	$<$ 6000
Reciprocating piston expander	20–100	-
Rotary vane expander	1–10	$<$ 6000

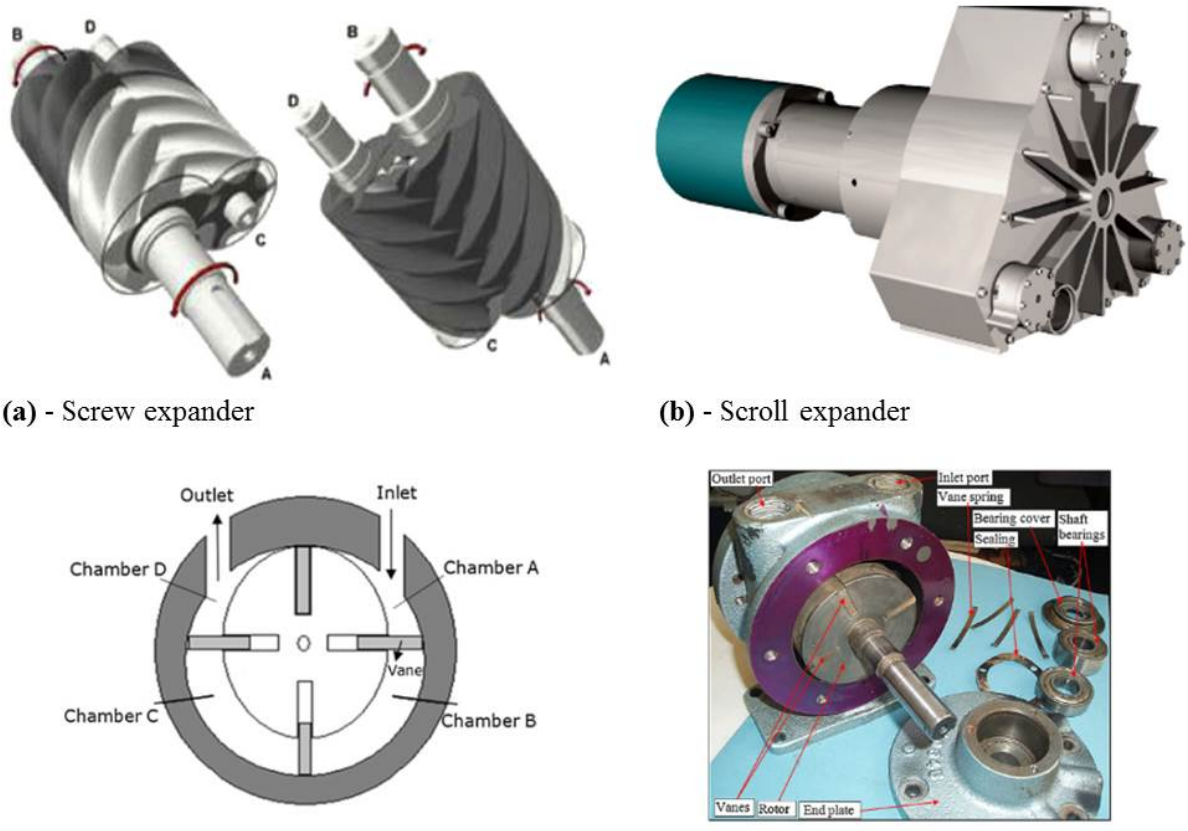

(a) - Screw expander **(b)** - Scroll expander

(c) - Vane- type air motor as expender

Figure 6.2: Volumetric type expander technologies ([188],[193]).

The two vital parameters that limit the performance of volumetric expanders are: internal built-in volume ratio and swept volume. The internal built-in volume ratio is the ratio between the expansion chamber volume at the end of the expansion process and that at the beginning of the expansion [186]. The maximum internal built-in volume ratio of positive-displacement expander is usually not higher than 5.0. It is mainly because of the limitation on the length of the rotor, in order to reduce bending stresses, for the case of screw expanders and by the number of spiral revolutions for scroll expanders. The swept volume is associated with maximum rotor diameter (about 400 mm) for screw expanders or the maximum spiral hight and diameter in the case of scroll expander. Nowadays, scroll expander technologies for micro-scale and small-scale power generation systems receive much attention worldwide. It is because of several reasons, to mention a few: wide use of scroll compressors in air-conditioning and refrigeration sectors, significant development in the manufacturing sector of scroll machines and no valves involved.

6.2.2.1 Scroll expanders

Scroll expanders are one of the main candidates for small-scale and micro-scale size capacity applications. It consists of two involute curves (mounted on base plates) in opposing directions which are called stationary and mobile scrolls. As its name stands, the stationary scroll dose not move and remains fixed to its position. The mobile scroll orbits around the shaft's centre by keeping its orientation. The working principle of a scroll expander includes three processes: suction, expansion and discharge. The expansion process (decrease of pressure) is accomplished by increasing the volume of the expansion chambers. Fig. 6.3 illustrates the working principle of a scroll expander. A high pressure and temperature working fluid enters at suction port (centre) of the scroll expander and is confined in a pocket that expands progressively, in crescent shaped form, while flowing towards the periphery where it is finally discharged at low pressure and temperature.

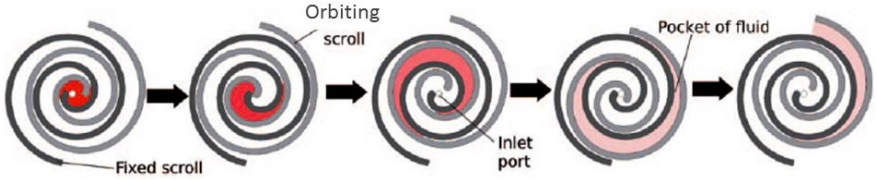

Figure 6.3: A scroll expander working principle [186].

The most common type of scroll machine (described in Fig. 6.3) is made of a stationary and orbiting scrolls (spirals). The main challenge associated with these scroll machines, in fact to any positive-displacement machine, is its lubrication requirements. The lubricating oil can prevent the clearance leakages and also lubricate the bearings consequently without the lubricant, performance of the expander will degrade. One possible solution to this challenge is installing an oil separator together with the oil pump at the expander exhaust and then pump back the oil to the expander suction.

Nowadays, novel scroll expanders are designed and developed for a specific applications and power output ranges and available commercially but not mass-produced. Air Squared Inc. (USA) [193] has developed micro-scale semi-hermetic scroll expanders for low-grade heat source utilization: the capacity of the expanders are 1 kW, 5 kW and 10 kW. They have the same built in volume ratio (3.5) but different swept volume with maximum rotational speed of 3600 rpm. A new scroll expander with a maximum capacity of 5 kW power output is developed by Eneftech Innovation [194] for its cogeneration (CHP) unit. This new developed scroll expander operates with rotational speeds of 1500-6000 rpm. Recently, a new group of oil free scroll machines based on co-rotating scroll concept [195] are under investigations. The main benefits of this design is easily decreasing of the internal clearances and less rubbing speed between the scrolls; according to the authors it is about one seventh less in the case of co-rotating scrolls compared with orbiting scrolls [195].

Several researchers suggested and have done experimental and numerical studies on the use of scroll expanders for ORC systems ([196]-[198]). Since custom designing and fabrication of scroll expander can be costly, they used commercially available scroll compressors by modifying it to work as expander. There are several type of commercially available mass-produced scroll compressors that can be converted to scroll expander and can be used in power cycles (e.g. ORC systems experimental set-up). It includes hermetic refrigeration scroll compressor, automotive air-conditioning compressor and open-drive air compressor (see Fig. 6.4). Depending on the type of scroll compressor the complexity of the modification process, to expander mode, are different - for instance, for hermetic scroll compressor the casing has to be cut and open to remove the check valve that prevents high pressure fluid backflow. Whereas semi-hermetic scroll compressors can be easily modified into expander mode by removing only the reed valve [203].

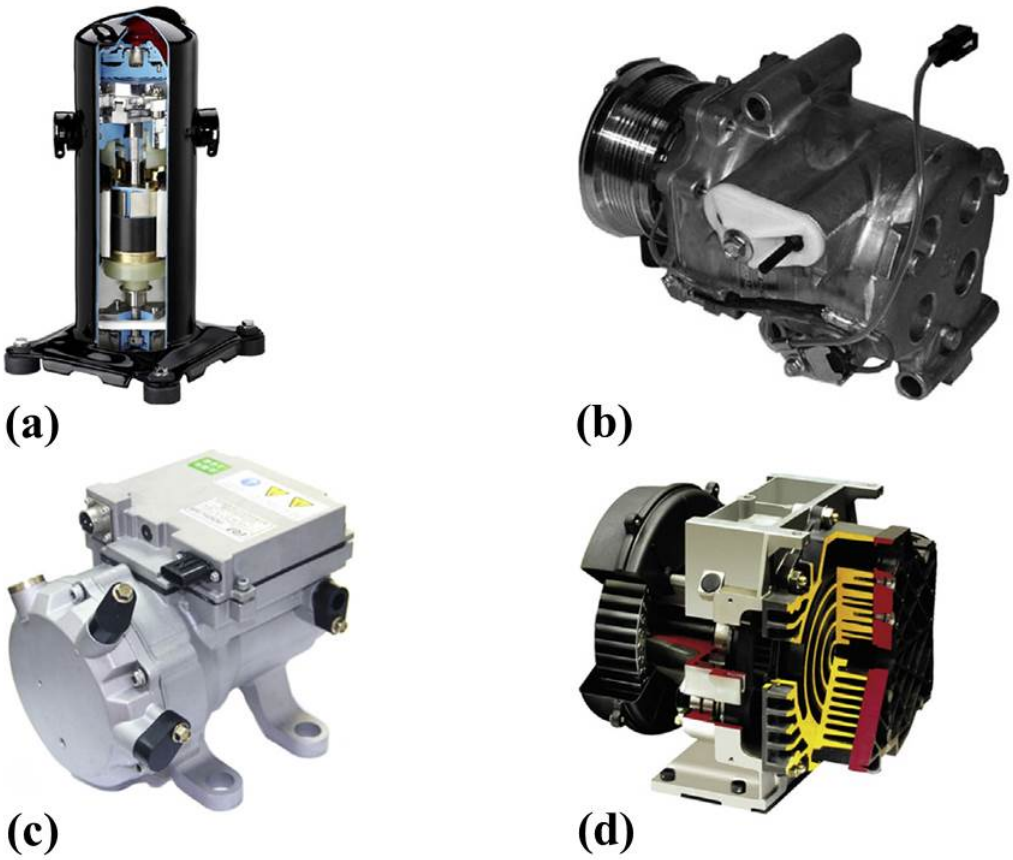

Figure 6.4: Different types of scroll compressors: (a) - Hermetic refrigeration compressor; (b) - Open-drive automotive Air-conditioning compressor; (c) - Semi-hermetic automotive Air-conditioning compressor; (d) - Air compressor ([199]-[202]).

The scroll expander selected for this study is the one tested and characterized by Mendoza [204]. It is originally an open-driven scroll compressor (shown in Fig. 6.5 (a)) that has been converted to operate in the expander mode. It is made with materials (aluminium and steel) that are compatible with NH_3 as a working fluid. According to the manufacturer, the volumetric displacement per revolution in compressor mode is 53.9 cm^3, and the maximum supply pressure and rotational speed are 3500 kPa and 10000 rpm, respectively. The built-in-volume ratio is 1.9, determined by measuring the cross section areas at the suction and exhaust chambers [205].

The next section of this chapter describes the development of a semi-empirical model of the scroll expander Sanden TRSA05, its validation and scale-up process to higher size scroll expanders in the same family series: model TRSA09 and TRSA12 which are shown in Fig. 6.5 (b) and (c), respectively.

Figure 6.5: Photos of scroll compressors employed as expanders in this study.

6.3 Scroll Expander Semi-empirical Model

The purpose of scroll expander modelling is to design, predict and/or improve the performance of scroll expanders applied in power generating systems. The most common theoretical, analytical, model for scroll expanders is the deterministic model. This model has been used by many researchers ([26],[206],[207]). It is highly dependent on an accurate geometrical modelling of the scroll machine in order to investigate the thermodynamic states of the working fluid, leakage, heat transfer, mechanical losses, supply pressure drop, etc. The geometric model determines the chamber volume and leakage area. A deterministic model is preferable for new scroll expanders design or existing scroll expander's design improvements. However, it is difficult, time consuming and cumbersome to implement deterministic expander models into a complete model of complex power generating systems; it is mainly due to complex scroll's geometry and internal transport mechanisms. Hence, empirical models and semi-empirical models are often applied to describe the thermodynamic behaviour of the scroll expanders in power generating system models.

Empirical models describe direct relationship between the operating conditions (parameters) and performance evaluating parameters. They skip the governing physical fundamental bases of the working process. As a consequence, empirical models mostly has no tolerance for extrapolation and restricted to a specific limited case. A semi-empirical model is based on a series of thermodynamic equations deduced mainly from mass, energy, momentum conservations and other thermodynamic and heat transfer relationships. Compared to scroll expander deterministic models, semi-empirical models have several advantages to incorporating the performance of a scroll expander into complex power generating systems such as combined absorption systems. These advantages include: lower

computational time, robustness and easiness for integration into global system models. Thus, a semi-empirical modelling approach for the expander is followed in this thesis.

The semi-empirical model developed in this work is deduced from the model proposed by Lemort [206] and has been validated with several working fluids including steam, R123 and R245fa in conventional Rankine and Organic Rankine Cycle applications ([206]-[209]). This model is based on a limited number of physically meaningful parameters that can be identified from the geometry and performance measurements on the scroll expander.

6.3.1 Model description

The conceptual scheme of the semi-empirical model is depicted in Fig. 6.6.

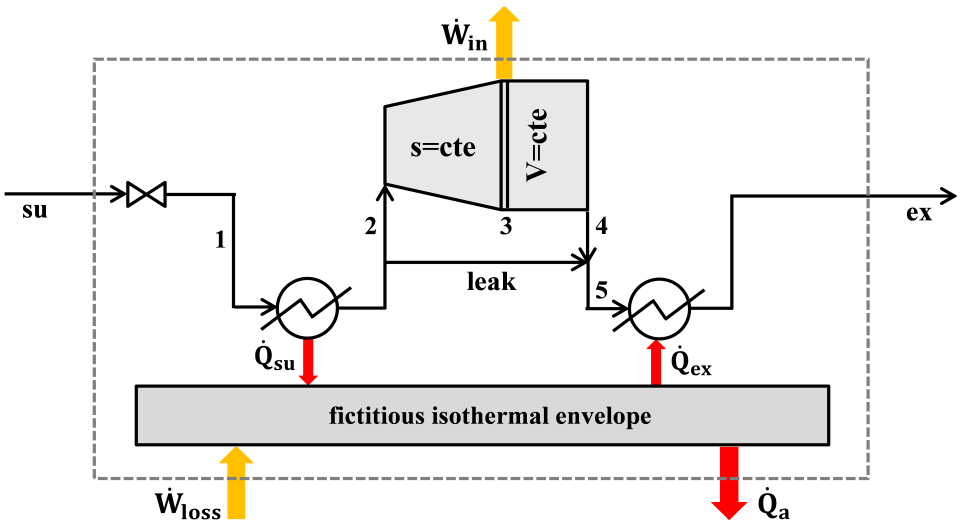

Figure 6.6: Conceptual diagram of the scroll expander semi-empirical model [206].

The evolution of the working fluid through the expander is divided into the following consecutive processes: adiabatic supply pressure drop (state: su to 1); an isobaric supply cooling down (state: 1 to 2); an adiabatic and reversible expansion to the internal pressure imposed by the built-in-volume ratio of the scroll expander (state: 2 to 3); a constant volume process (state: 3 to 4); adiabatic mixing between the displaced and leakage flows (state: 4 and leak to 5) and isobaric exhaust flow cooling-down or heating-up (state: 5 to ex). The displaced flow is the amount of working fluid directly involved in the expander work production. Detailed descriptions of these processes and their corresponding model equations are presented below.

Supply pressure drop: It includes all pressure losses associated with the working fluid as it flows from the suction line to the expander's suction chamber. The main causes of these pressure drops are explained in detail elsewhere [206]. In this model, all these pressure drops are lumped into one supply pressure drop process represented by an isentropic flow through an adiabatic convergent nozzle. The inlet of the nozzle corresponds to state point 'su' in Fig. 6.6. Therefore, using the steady-state mass and energy conservation laws, the mass flow rate $\dot{m}_{exp}$ of the working fluid entering the scroll expander can be expressed as:

$$\dot{m}_{exp} = \frac{A_{su}(\sqrt{2(h_{su}-h_1)})}{\upsilon_1} \tag{6.3.1}$$

where h_{su} and h_1 are specific enthalpies at the inlet and exit of the nozzle and υ_1 is the specific volume at the exit of the nozzle. The cross-sectional area A_{su} represents an average value of the effective suction port area over the entire suction process (corresponds to one shaft revolution). A_{su} is a parameter to be estimated experimentally. For completely specified inlet conditions (i.e. two independent intensive properties, $\dot{m}_{exp}$ and composition for multi-component working fluids), Eq. 6.3.1 can be used to determine the suction pressure drop: $\Delta p_{su} = p_{su} - p_1$.

Heat transfers: The external and internal heat flows associated with the flow of the working fluid through the expander are modelled by introducing three fictitious counter-flow heat exchangers that have an isothermal envelope at one-side. This envelope represents the metal mass associated with the expander shell, fixed and orbiting scrolls. The heat exchangers are characterized by their overall heat conductance: supply overall heat conductance (UA_{su}), exhaust overall heat conductance (UA_{ex}) and ambient overall heat conductance (UA_a). The first two are internal whereas the last one is an external heat flow. The heat transfer rates are computed as follows.

Ambient heat transfer ($\dot{Q}_a$):

$$\dot{Q}_a = UA_a(t_w - t_a) \tag{6.3.2}$$

where t_a and t_w represent the temperature of the ambient and uniform isothermal envelop.

Internal heat transfers ($\dot{Q}_{su}$ and $\dot{Q}_{ex}$):

$$\dot{Q}_{su} = \dot{m}_{exp}(h_1 - h_2) = (1 - e^{NTU_{su}})\dot{m}_{su}C_{p,su}(t_1 - t_w) \tag{6.3.3}$$

and

$$\dot{Q}_{ex} = \dot{m}_{exp}(h_{ex} - h_5) = (1 - e^{NTU_{ex}})\dot{m}_{ex}C_{p,ex}(t_w - t_5) \tag{6.3.4}$$

The supply and exhaust overall heat conductances (UA_{su} and UA_{ex}) are assumed to vary with the mass flow rate according to [208]:

$$UA_{su} = UA_{su,n}\left(\frac{\dot{m}_{exp}}{\dot{m}_{exp,n}}\right)^{0.8} \quad and \quad UA_{ex} = UA_{ex,n}\left(\frac{\dot{m}_{exp}}{\dot{m}_{exp,n}}\right)^{0.8} \tag{6.3.5}$$

where $UA_{su,n}$ and $UA_{ex,n}$ are the supply and exhaust nominal overall heat conductances at nominal mass flow rate ($\dot{m}_{exp,n}$), respectively.

Internal leakage: Basically, there are two different leakage paths in a scroll machine: radial and flank leakages. The radial leakage is due to a gap between the bottom or top base plates and the scrolls (fixed or orbiting). The flank leakage is the result of a gap between the flanks of the scrolls. For the purpose of modelling, these leakage paths are lumped into one unique fictitious clearance of a path that connects the supply and exhaust stream of the expander (Fig. 6.6). Its cross-sectional area A_{leak} is a parameter determined experimentally. Analogous to the supply pressure drop modelling: the leakage path is also modelled as an isentropic flow through a convergent nozzle. Hence, the leakage mass flow rate $\dot{m}_{leak}$ is expressed as:

$$\dot{m}_{leak} = \frac{A_{leak}(\sqrt{2(h_2 - h_{leak,t})})}{\upsilon_{leak,t}} \tag{6.3.6}$$

where $h_{leak,t}$ and $\upsilon_{leak,t}$ are the specific enthalpy and specific volume of the leakage flow at the nozzle throat. The pressure at the throat is computed as the maximum of the values of the exhaust and critical pressures: maximum (p_{ex}, p_{crit}). The critical pressure is calculated assuming a choked flow condition, Mach number, $Ma = 1.0$, at the throat of the nozzle using real fluid properties instead of considering the working fluid as a perfect gas as in the case modelled in Lemort et al. (2009) [208].

The internal flow rate $\dot{m}_{in}$ is the mass flow rate of the working fluid displaced by the expander for the work production. It is equal to the volume flow rate per specific volume of the working fluid determined after the supply pressure drop and cooling down (i.e. at state: 2 in Fig. 6.6). The volume flow rate $\dot{V}_{s,exp}$ is the swept volume multiplied by the expander rotational speed, N_{exp}. The swept volume in expander mode is equal to that in the compressor mode ($V_{s,com}$) divided by the built-in volume ratio, r_v, of the scroll machine. The internal mass flow rate can then be expressed as the difference between the mass flow rate entering the expander $\dot{m}_{exp}$ and the internal leakage mass flow rate. Thus, it can be given as:

$$\dot{m}_{in} = \frac{N_{exp} V_{s,com}}{\upsilon_2 r_v} = \dot{m}_{exp} - \dot{m}_{leak} \tag{6.3.7}$$

Internal expansion power: Volumetric expanders are characterized by the fixed built-in volume ratio. Thus, there may be a possibility of under-or over-expansion losses. It is due to the difference between the built-in volume ratio of the scroll machine and the volume ratio imposed by the operating condition of the system (combined absorption cycle). To account for the irreversibility associated with the under or over-expansion process, the whole expansion process in the expander is divided into two parts: isentropic and constant volume thermodynamic processes (Fig. 6.6). Therefore, the internal expansion power $\dot{W}_{in}$ is the sum of internal power associated to the isentropic and constant volume processes and equal to:

$$\dot{W}_{in} = \dot{m}_{in}[(h_2 - h_3) + \upsilon_3(p_3 - p_{ex})] \tag{6.3.8}$$

where h_3 and υ_3 are calculated at the internal pressure p_3 imposed by the scroll machine geometry.

For a scroll machine, the main sources of mechanical losses are friction between the scrolls and losses in the bearings [206]. All these losses are lumped into a single mechanical loss torque τ_{loss} and its value is determined by experimental measurements. Then, the shaft power $\dot{W}_{shaft}$ developed by the expander can be given as the difference between the internal expansion power and the total mechanical power loss $\dot{W}_{loss}$ and equal to:

$$\dot{W}_{shaft} = \dot{W}_{in} - \dot{W}_{loss} \tag{6.3.9}$$

6.3.2 Model parameters

The developed semi-empirical model requires eight parameters: three overall heat conductances, leakage area, supply port effective cross-sectional area, mechanical loss torque, built-in volume ratio and swept volume (either in compressor mode or expander mode). The latter two parameters can be obtained from the manufacturer's data (or geometry). The remaining parameters are identified on the basis of experimental performance measurements. The experimental data available in Mendoza (2013) [204] were used to identify the parameters. The parameters are obtained by minimizing a global deviation function (DEV, Eq. 6.3.10) accounting for the deviations of the main model outputs.

$$DEV = \frac{1}{3}\left(\sqrt{\sum_{1}^{n}\left(\frac{\dot{m}_{exp} - \dot{m}_{exp,meas}}{\dot{m}_{exp}}\right)^2}\right) + \frac{1}{3}\left(\sqrt{\sum_{1}^{n}\left(\frac{\dot{W}_{shaft} - \dot{W}_{shaft,meas}}{\dot{m}_{shaft}}\right)^2}\right) + \frac{1}{3}\left(\sqrt{\sum_{1}^{n}\left(\frac{t_{ex} - t_{ex,meas}}{t_{ex,meas,max} - t_{ex,meas,min}}\right)^2}\right) \tag{6.3.10}$$

The supply temperature and pressure, rotational speed of the expander and exhaust pressure are considered as inputs for the model whereas the mass flow rate, shaft power and exhaust temperature are the main outputs. The value of the parameters and correlations used for the total mechanical power loss and leakage area are given in Table 6.2. The coefficients of leakage area correlation are: $C_0 = -6.08 \times 10^{-6}$, $C_1 = 1.14 \times 10^{-9}$, $C_2 = 2.19 \times 10^{-8}$, $C_3 = -1.55 \times 10^{-8}$ and $C_4 = -1.81 \times 10^{-8}$ [204]. A nominal value of the mass flow rate entering the expander ($\dot{m}_{exp,n} = 0.07$ kg/s) is used to determine the nominal values of the supply and exhaust heat conductances.

Table 6.2: Parameters of the semi-empirical model for Sanden TRSA05 scroll expander with ammonia.

Parameter	Value
Supply overall heat conductance,$UA_{su,n}$ [kW/K]	0.03322
Exhaust overall heat conductance, $UA_{ex,n}$ [kW/K]	0.01621
Ambient overall heat conductance, UA_a [kW/K]	0.00138
Supply port cross-sectional area, A_{su} [mm^2]	23.1
Swept volume in compressor mode, $V_{s,com}$ [cm^3/rev]	53.9
Built-in-volume ratio, r_v [-]	1.9
Leakage area, A_{leak} [m^2]	$C_0 + C_1 p_{su} + C_2(t_{su} + 273.15) + C_3(\frac{N_{exp}}{60}) + C_4 pr_{exp}$
Total mechanical power loss, $\dot{W}_{loss}$ [kW]	$-0.127 + 0.00518(\frac{N_{exp}}{60})$

6.3.3 Model validation

Comparisons between the model estimation and the measurements for the main outputs of the model: expander mass flow rate $\dot{m}_{exp}$, shaft power $\dot{W}_{shaft}$ and exhaust temperature t_{ex} are given in Figs. 6.7, 6.8 and 6.9, respectively.

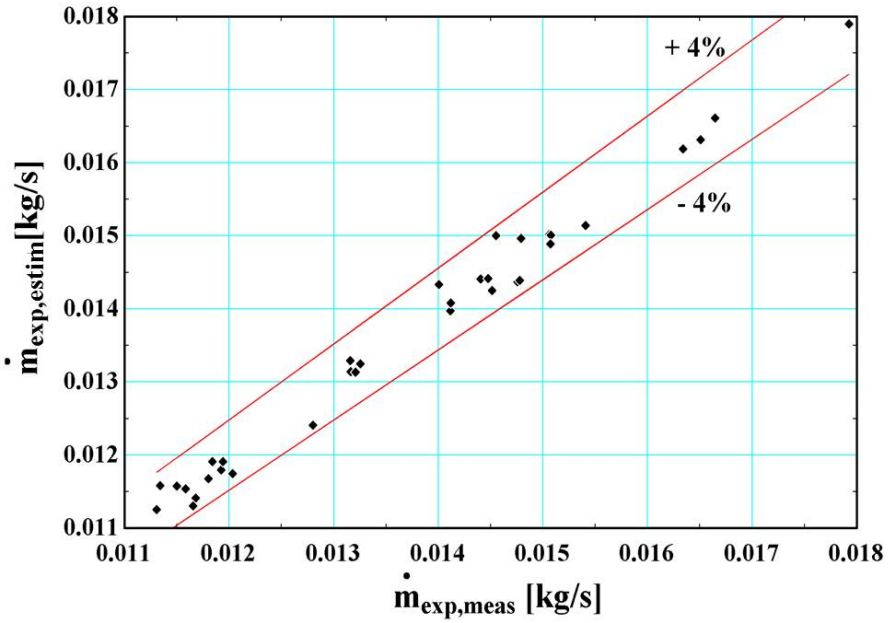

Figure 6.7: Estimation of mass flow rate entering the expander.

From these figures it can be observed that the estimation of the main outputs by the semi-empirical model is in good agreement with the experimental measurements. The model with the parameters and correlations listed in Table 6.2 is able to estimate the expander mass flow rate with ±4% deviation. The shaft power developed by the expander is also

estimated in the range of ±8% deviation. Fig. 6.9 compares the exhaust temperature estimation and it is within ±4 K.

The model parameters identification process and the model validation are conducted using the Engineering Equation Solver (EES) environment [210].

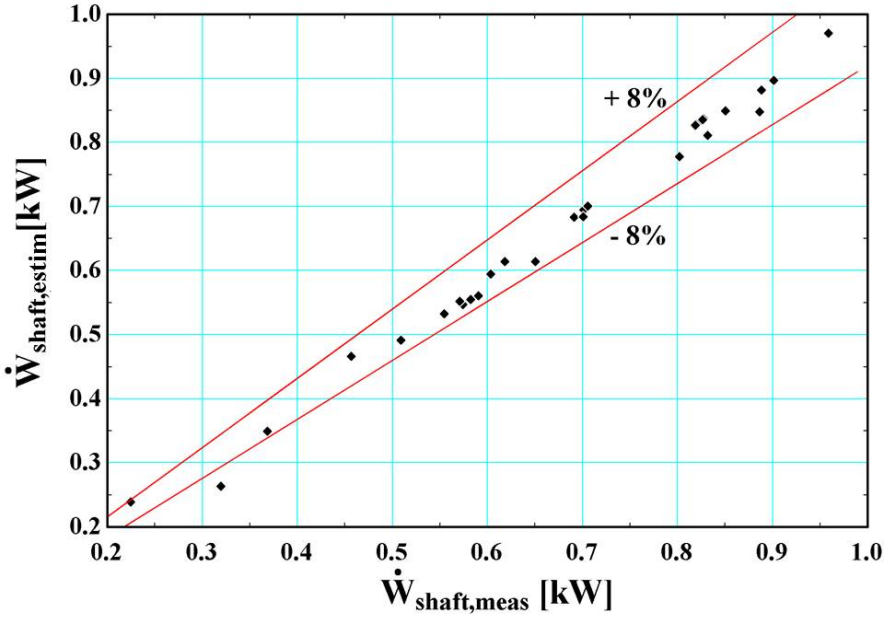

Figure 6.8: Estimation of the expander shaft power.

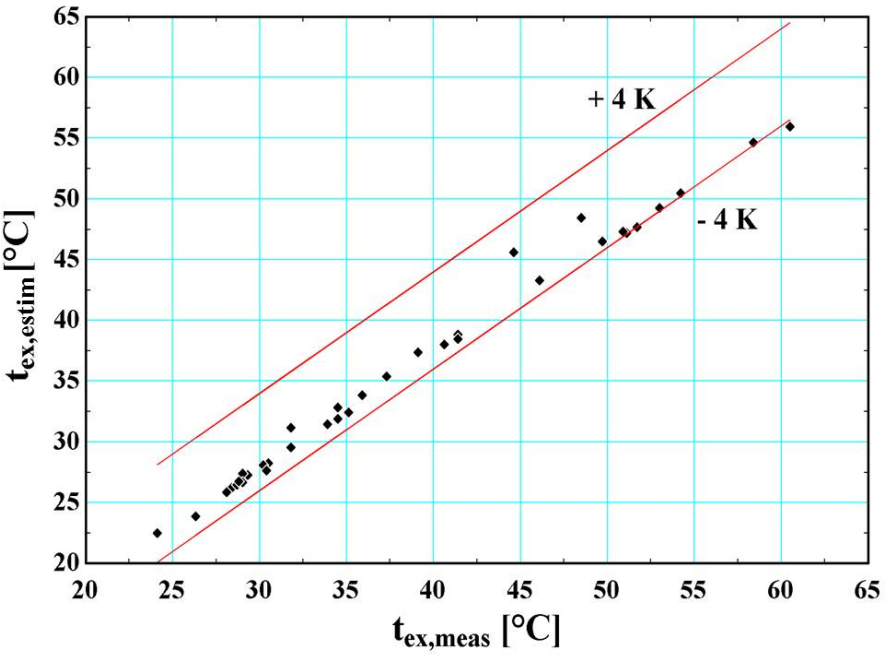

Figure 6.9: Estimation of the expander exhaust temperature.

6.3.4 Scale-up process

For scroll machines in the same family series like Sanden: TRSA05, TRSA09 and TRSA12, the geometry of the expander is simply scaled in order to modify its displacement (swept volume). The lamped parameters of the semi-empirical model can then be expressed as a function of the expander displacement [206]. Consequently, the leakage area and mechanical torque loss are given in Eqs. 6.3.11 and 6.3.12 respectively.

$$A_{leak} = A_{leak,n} \left(\frac{V_{s,exp}}{V_{s,exp,n}} \right)^{(4/9)} \tag{6.3.11}$$

$$\tau_{loss} = \tau_{loss,n} \left(\frac{V_{s,exp}}{V_{s,exp,n}} \right)^{(2/3)} \tag{6.3.12}$$

Similarly, the fictitious supply port cross-sectional area introduced in the semi-empirical model for accounting the supply pressure drop is assumed to vary proportionally with the displaced volume as follows:

$$d_{su} = d_{su,n} \left(\frac{V_{s,exp}}{V_{s,exp,n}} \right)^{(1/3)} \tag{6.3.13}$$

The supply and the exhaust overall heat conductances are given by:

$$UA_{su} = UA_{su,n} \left(\frac{V_{s,exp}}{V_{s,exp,n}} \right)^{(1/15)} \left(\frac{\dot{m}_{exp}}{\dot{m}_{exp,n}} \right)^{0.8} \tag{6.3.14}$$

$$UA_{ex} = UA_{ex,n} \left(\frac{V_{s,exp}}{V_{s,exp,n}} \right)^{(1/15)} \left(\frac{\dot{m}_{exp}}{\dot{m}_{exp,n}} \right)^{0.8} \tag{6.3.15}$$

In the following section, first the integration of the simplified semi-empirical model of Sanden TRSA05 [205] in single-stage combined absorption cycle configuration employing three ammonia based working fluid mixtures (NH_3/H_2O, $NH_3/LiNO_3$ and $NH_3/NaSCN$) is presented. Then, the integration of the developed semi-empirical models of Sanden TRSA05, TRSA09 and TRSA12 scroll expanders with an NH_3/H_2O combined absorption cycle for power and refrigeration applications is conducted using a steady-state thermodynamic model developed for the entire combined absorption cycle.

Three performance indicators are used to evaluate the performance of the scroll expanders: overall isentropic efficiency $\eta_{overall,ise}$, mechanical efficiency (η_{mech}) and volumetric efficiency (η_{vol}).

Overall isentropic efficiency is defined as the ratio between the shaft power $\dot{W}_{shaft}$ to the isentropic power:

$$\eta_{overall,ise} = \frac{\dot{W}_{shaft}}{\dot{m}_{exp}(h_{su} - h_{ex,ise})} \tag{6.3.16}$$

The isentropic power is the product of the mass flow rate entering the expander and the specific expansion work associated with an isentropic expansion from the supply condition to the exhaust pressure.

Mechanical efficiency is defined as the ratio between mechanical power output of the expander and the total mechanical power. The later is the sum of the mechanical power output and the mechanical losses caused by the moving parts of the expander.

$$\eta_{mech} = \frac{\dot{W}_{shaft}}{\dot{W}_{shaft} + \dot{W}_{loss}} \tag{6.3.17}$$

And the volumetric efficiency η_{vol} is defined by $\dot{m}_{in}/\dot{m}_{exp}$, where $\dot{m}_{in}$ is actual mass flow rate of the working fluid directly involved in work production and $\dot{m}_{exp}$ is the mass flow rate of working fluid displaced by the expander (i.e. entire mass flow rate entering the expander).

6.4 Expanders Integration into Combined Absorption Cycles

In this section, the scroll expander's semi-empirical model has been integrated into two combined absorption cycles proposed, in Chapter 3, for the co-production of power and cold. The cycle configurations used to study the integration of scroll expanders in them are single-stage combined absorption power and refrigeration cycles with parallel flow arrangement and the one with two desorbers: SSAPRC-P and SSAPRC-2D, respectively.

6.4.1 Expander integration into SSAPRC-P cycle configuration

The purpose of this sub-section is to present the integration of a scroll expander (Sanden TRSA05) in a cycle using three different working fluids that use NH_3 as refrigerant: NH_3/H_2O and $NH_3/LiNO_3$ and $NH_3/NaSCN$ mixtures. The scroll expander semi-empirical model, based on the simplified model of Mendoza et al.[205], is used to estimate (calculate) the mechanical power production, mass flow rate and exhaust temperature of the expander, and it is included in the proposed complete combined absorption cycle physical-mathematical model built using the EES software [210]. Figs. 6.10 (a) and (b) shows the schematic flow diagram of the cycle configurations used in the scroll expander integration.

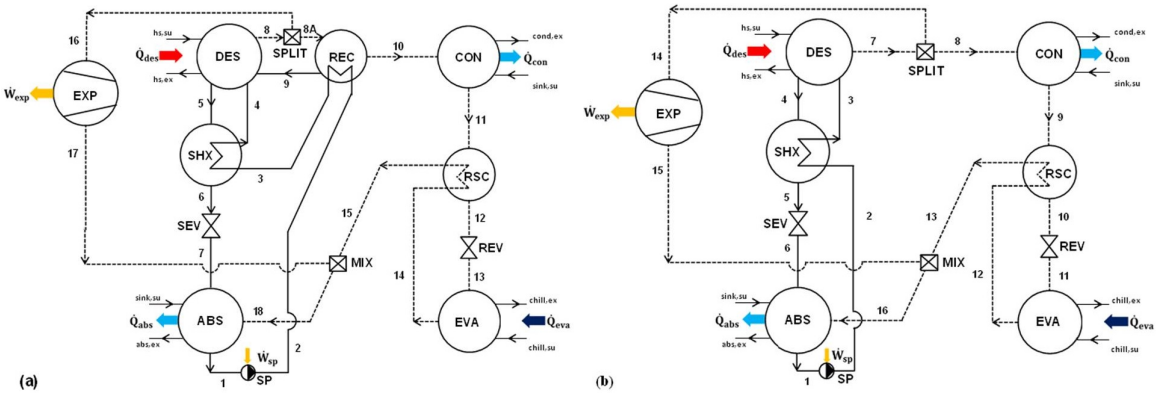

Figure 6.10: Schematic diagram of single-stage combined absorption cycles: (a) - for NH_3/H_2O mixture; (b) - for $NH_3/LiNO_3$ and $NH_3/NaSCN$ mixtures.

The main difference between the two cycle configurations is the rectification process (at the rectifier, REC) in the cycle based on NH_3/H_2O mixture Fig. 6.10 (a). In this cycle configuration, the heat of rectification is recovered and used internally to preheat the basic NH_3/H_2O solution entering the solution heat exchanger (SHX).

The thermodynamic performance evaluation of the proposed combined absorption system is executed for several working fluids (NH_3/H_2O, $NH_3/LiNO_3$ and $NH_3/NaSCN$ mixtures) in order to investigate their sensitivity to the variation of heat source, heat sink, and chilled fluid temperatures. The output of the global cycle model includes net mechanical power, cooling capacity, split ratio and energy and exergy efficiencies. The net mechanical power output is defined as the shaft power developed by the scroll expander reduced by the mechanical power consumption of the solution circulation pump.

The following assumptions were used in the developed global thermodynamic model of the system:

- The analysis is carried out under steady-state conditions.
- Liquid solutions leaving the absorber and desorber are saturated at the absorber and desorber temperatures and evaporator and condenser pressures, respectively.
- Effectiveness of the refrigerant sub-cooler is set at 80% and the temperature difference at the cold end of solution heat exchanger is set to 10 °C.
- The isentropic efficiency of the solution pump is 80%.
- The ammonia mass fraction of the vapour leaving the rectifier, in Fig. 6.10 (a), is set to 0.9995.
- Partial vaporization is allowed in the evaporator of the NH_3/H_2O system whereas complete vaporization, saturated vapour condition at the exit of the evaporator, is considered for the systems with $NH_3/LiNO_3$ and NH_3/NaSCN mixtures.
- Heat input to the desorber is set to 100 kW.
- The heat sink temperature is assumed to be 5 °C below the absorber and condenser exit temperatures.
- The heat source and chilled fluid inlet temperatures are assumed to be 5 °C above the desorber and evaporator exit temperatures respectively.
- The performances of the expander (it includes mechanical power output, mass flow rate and exhaust temperature) are obtained at a rotational speed of 166.6 Hz, except for the split ratio analysis.
- Hot water at pressure is considered as a heat source fluid with a constant mass flow rate of 5 kg/s.
- The reference temperature and pressure for exergy calculations were 20 °C and 101.325 kPa, respectively.
- Pressure drops and thermal losses in the components and pipes are neglected.

The effect of operating conditions (heat source, heat sink and chilled fluid temperatures) and split ratio on the performance and operational working range of the system are presented as follows.

6.4.1.1 Effect of heat source temperature

In Figs. 6.11 and 6.12, the effect of the heat source inlet temperature on the net power and cold produced and efficiencies are depicted for a heat sink temperature of 30 °C and a chilled fluid temperature of 0 °C and $N_{exp} = 166.6$ Hz.

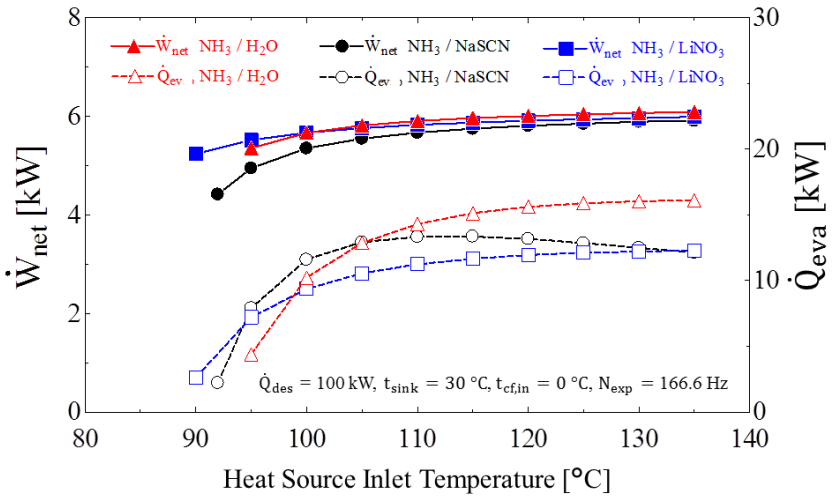

Figure 6.11: Effect of heat source inlet temperature on net power output and cooling capacity of the system using NH_3/H_2O, $NH_3/LiNO_3$ and NH_3/NaSCN mixtures.

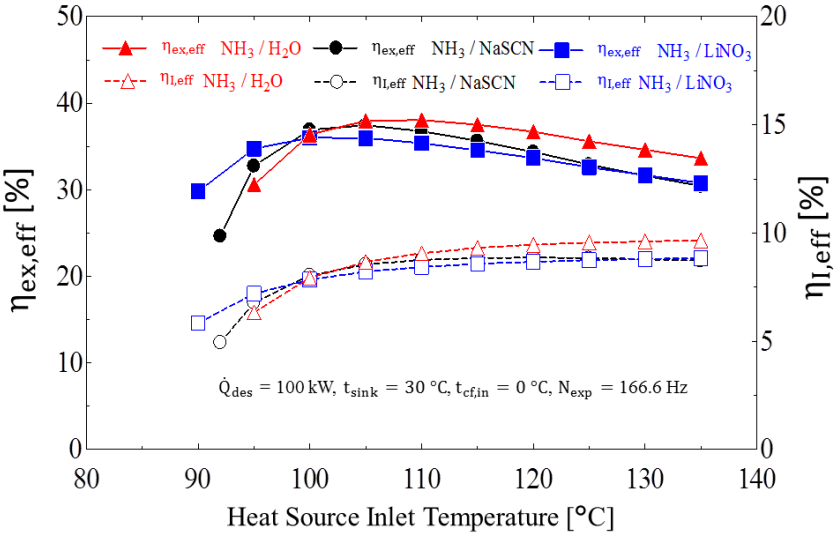

Figure 6.12: Effect of heat source inlet temperature on system energetic and exergetic efficiencies using NH_3/H_2O, $NH_3/LiNO_3$ and NH_3/NaSCN mixtures.

As shown in Fig. 6.11, the minimum activation temperature of the combined absorption system changes with the working fluid mixture used in the system: 90 °C for $NH_3/LiNO_3$, 92 °C for NH_3/NaSCN and 95 °C for NH_3/H_2O. For heat source temperatures between 90 °C and 100 °C, relatively higher system performance corresponds to the case using $NH_3/LiNO_3$ or NH_3/NaSCN as working fluid. However, the use of NH_3/H_2O for temperatures higher than 105 °C shows better performance. The average net mechanical power output and cooling capacity produced using a heat input of 100 kW at 120 °C, are nearly 6 kW and 15 kW, respectively. For temperatures higher than 110 °C, the net mechanical power output of the systems tends to be almost constant. The system working with $NH_3/LiNO_3$ and NH_3/NaSCN shows the better exergetic efficiency (30% to 38%) and energetic efficiency (5% to 9%) than NH_3/H_2O system for heat source temperatures lower than 100 °C. At higher temperatures the energetic efficiency changes slowly. The system working with NH_3/H_2O mixture has better efficiencies than the other working fluids for a desorber temperature higher than about 100 °C and could get values close to 40% and 10% for the exergetic efficiency and energetic efficiency, respectively.

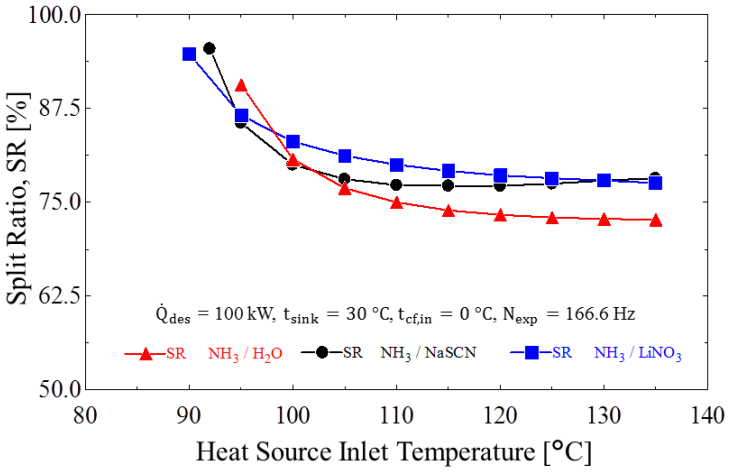

Figure 6.13: Effect of heat source inlet temperature on the split ratio for NH_3/H_2O, $NH_3/LiNO_3$ and NH_3/NaSCN mixtures.

The ammonia vapour produced by the desorber is split into two streams (see Fig. 6.10 (a) and (b)): first one flowing to the scroll expander (power sub-cycle) and the remaining flow goes to the evaporator (refrigeration sub-cycle). The mass flow rate of the power sub-cycle is fixed by the expander rotational speed. Then, the ammonia stream that goes to the evaporator, for cold production, increases with the increase of the heat source temperature.

In Fig. 6.13, it can be seen that the split ratio decreases (from 94% to 74%) when the heat source temperature increases from 90 °C and 110 °C. For temperatures higher than 110 °C, the split ratio tends to be constant about 72% for NH_3/H_2O and 77% for $NH_3/LiNO_3$ and NH_3/NaSCN.

6.4.1.2 Effect of sink temperature

In Figs. 6.14 (a) and (b), the effect of the sink temperature on the system dual-outputs and cycle efficiencies is illustrated at a heat source inlet temperature of 120 °C and chilled fluid inlet temperature of 0 °C.

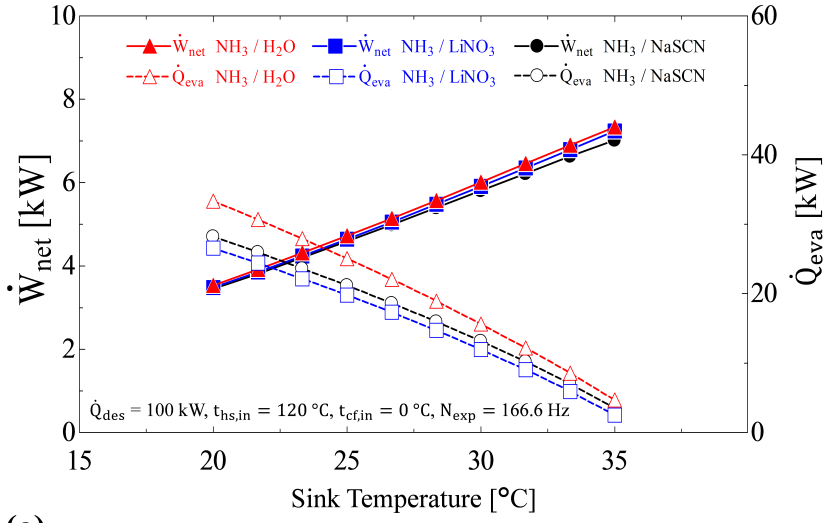

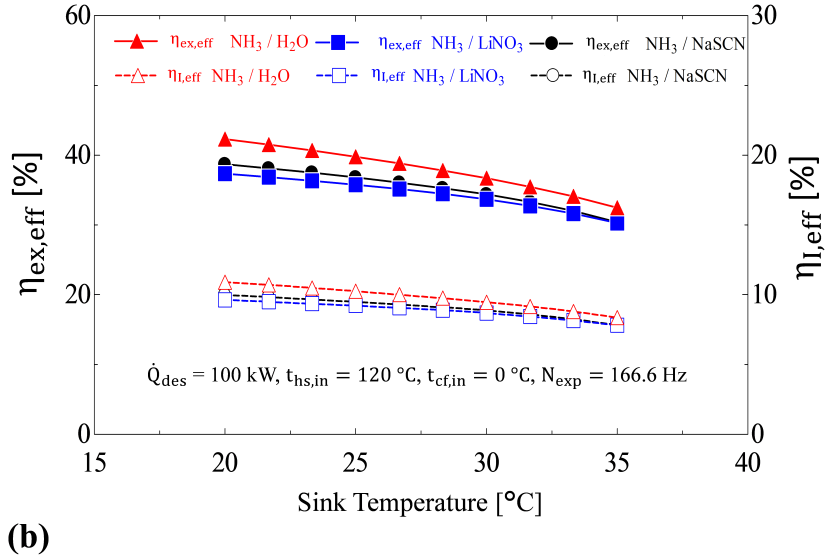

Figure 6.14: Effect of sink temperature on cycle: (a) - cycle useful dual-outputs; (b) - efficiencies for NH_3/H_2O, $NH_3/LiNO_3$ and NH_3/NaSCN mixtures.

As seen in Fig 6.14 (a), the cooling capacity of the system decreases significantly (from 33 kW to 4.6 kW) as the sink temperature increases from 20 °C to 35 °C. Since the high pressure of the system increases with the sink temperature, the low pressure kept constant, the expander pressure ratio increases. Consequently, the net mechanical power increases (from about 3.5 kW to 7.5 kW) with the sink temperature. Thus, in warm days when the ambient temperature start to rise and cooling capacity then declines, the system compensates this by providing a higher amount of power output due to an increase in the expander pressure ratio. For sink temperatures between 20 °C and 35 °C, it was observed that the system based on NH_3/H_2O has the highest cooling capacity. However, the power output of the system using the different working fluid pairs is quite similar.

In Fig. 6.14 (b) it can be seen that the system with NH_3/H_2O mixture shows a slightly better exergetic efficiency between 42% and 32% and also better energetic efficiency between 10% and 8.3%. The results for $NH_3/LiNO_3$ and $NH_3/NaSCN$ show very similar performance as a function of the sink temperature.

An increase of the sink temperature increases the high pressure of the system that in turn reduces the vapour production in the desorber. Since the mass flow rate that goes to the expander is fixed by the expander's rotational speed, the split ratio changes with the sink temperature. In Fig. 6.15 it can be seen that the split ratio changes between 51% to 93% for the different working fluid pairs with the sink temperature changing from 20 °C to 35 °C.

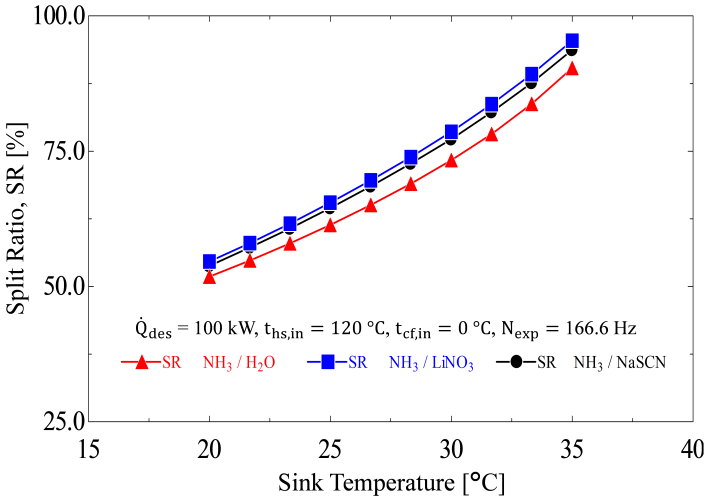

Figure 6.15: Effect of sink temperature on the split ratio for NH_3/H_2O, $NH_3/LiNO_3$ and $NH_3/NaSCN$ mixtures.

6.4.1.3 Effect of chilled fluid temperature

The effect of the chilled fluid inlet temperature on the cycle useful outputs and efficiencies at a heat source and sink temperatures of 120 °C and 25 °C is depicted in Figs. 6.16 (a) and (b) respectively.

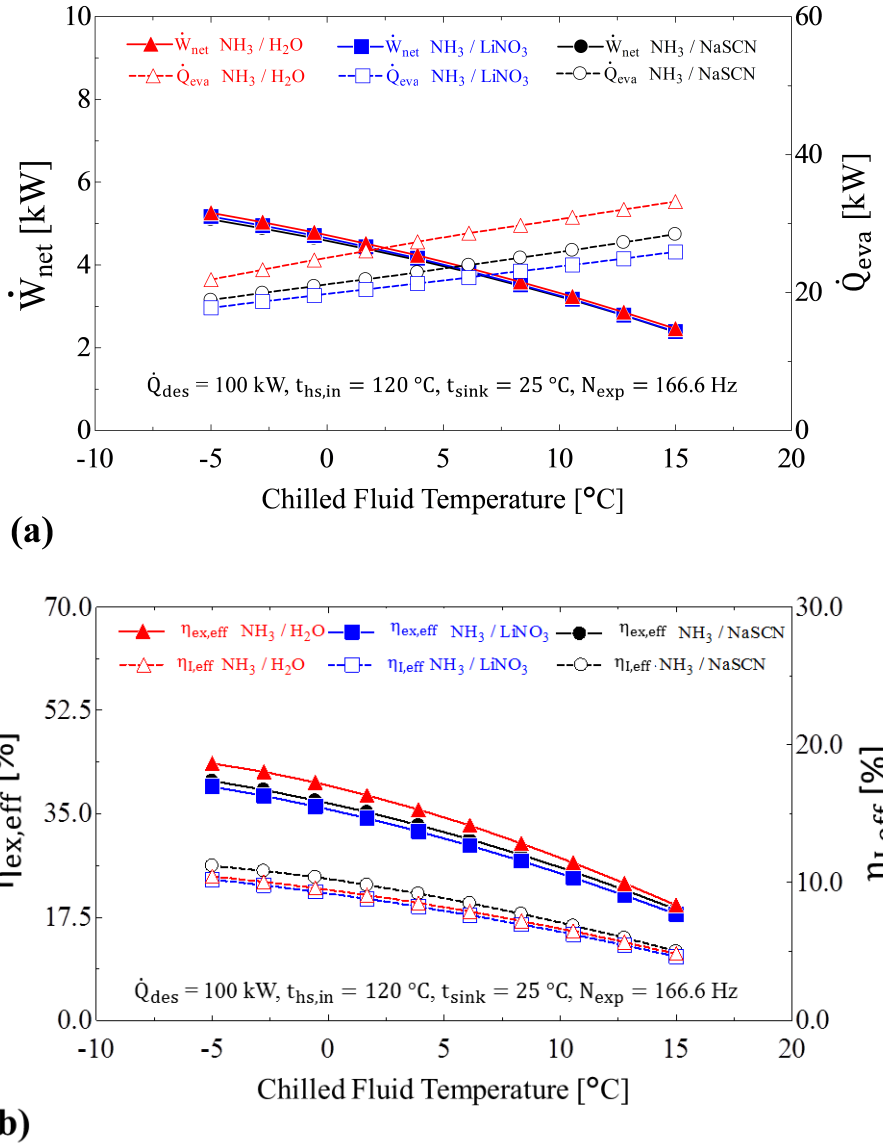

Figure 6.16: Effect of chilled fluid temperature on: (a) net mechanical power output and cooling capacity; (b) cycle efficiencies for system with NH_3/H_2O, $NH_3/LiNO_3$ and $NH_3/NaSCN$ mixtures.

As seen in 6.16 (a), the net mechanical power output of the system changes significantly with the chilled fluid temperature variation (from about 5.2 kW to 2.5 kW). Since the low pressure of the system increases with the chilled fluid temperature, being the cycle

high pressure constant, the pressure ratio decreases. Consequently, the net mechanical power decreases from around 5.2 kW to 2.5 kW. This is not the case at the lowest range of chilled water temperatures. And also, it is obvious that the cooling capacity increases with the chilled water temperature due to the increase of the low pressure of the system that improves the absorption process at constant heat sink temperature. The energetic and exergetic efficiencies of the cycle decrease as the chilled fluid temperature increases from 44% to 18% and 11% to 4%, respectively. When the chilled fluid temperature increases, low pressure of the cycle also increases consequently the absorption process is enhanced. As a result, more vapour is generated by the desorber. Since the amount of vapour flowing through the scroll expander is the same (fixed by the rotational speed of the expander), the vapour split ratio decreases as the chilled fluid temperature increases (see Fig. 6.17).

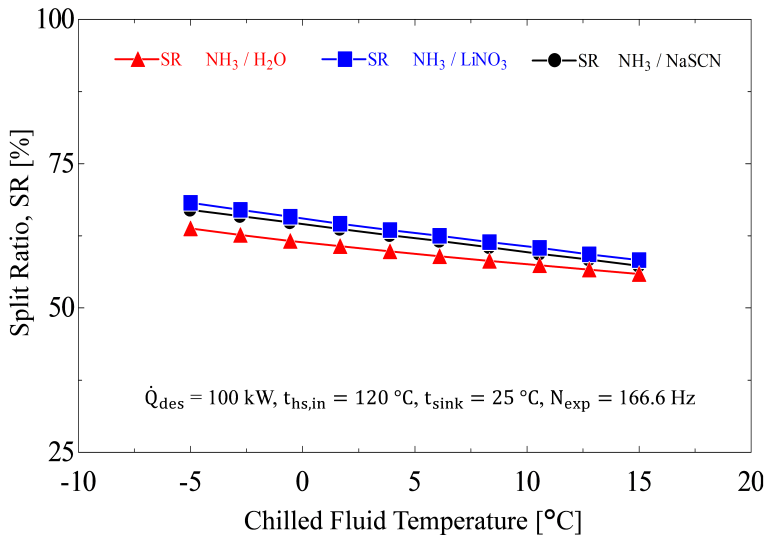

Figure 6.17: Effect of chilled fluid temperature on the split ratio for NH_3/H_2O, $NH_3/LiNO_3$ and NH_3/NaSCN mixtures.

6.4.1.4 Effect of split ratio

In Figs. 6.18 (a) and (b) it is shown the effect of the split ratio on the system performance and the cycle efficiencies with a heat source temperature of 120 °C, a sink temperature of 25 °C, chilled water temperature of 0 °C with a thermal energy input of 100 kW.

As seen in Fig. 6.18 (a), the mechanical power output of the system decreases significantly (from 8 kW to 0.5 kW) and the cold production increases (from 0.5 kW to 47 kW) as the split ratio increases from 20% to 90%. Therefore with the variation of the split

ratio, it is possible to fit the cycle with the desired energy demands. It can also be seen (Fig. 6.18 (b)) that cooling capacity has a higher weight on the exergetic efficiency than the power production, the maximum exergy efficiency achieved was about 44% and the energetic efficiency was about 11%.

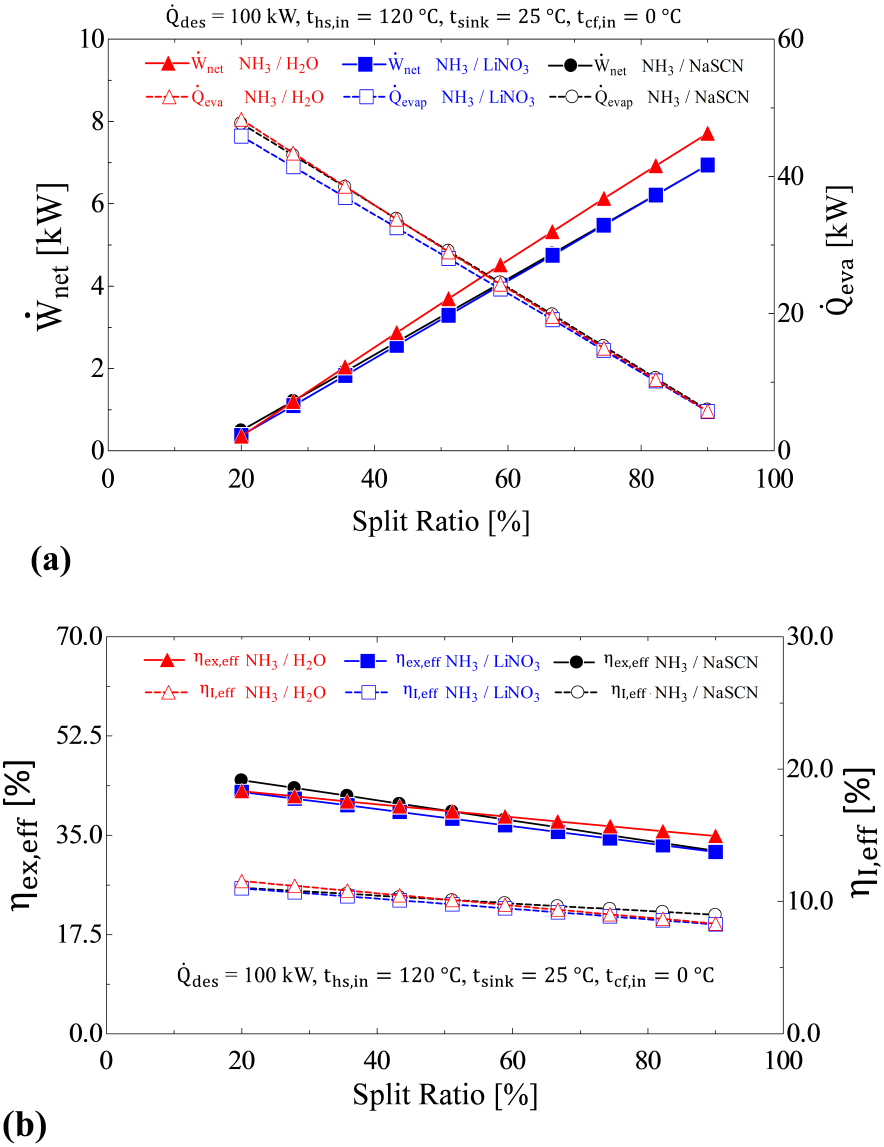

Figure 6.18: Effect of split ratio on: (a) - cycle dual-outputs; (b) - cycle efficiencies.

6.4.2 Expanders integration into SSAPRC-2D cycle configuration

Fig. 6.19 shows the schematic flow diagram of a single-stage combined absorption power and refrigeration cycle with two desorbers (SSAPRC-2D) proposed for the combined production of power and cold. Previously, the power generating unit of the cycle was modelled

by expansion process with an isentropic efficiency set at 85%. However, in order to obtain the real performance and size of this system, the semi-empirical model developed for scroll expanders in the previous section was used into the complete cycle thermodynamic model. The cycle process description, model assumptions, and global steady-state modelling approach followed can be found in detail in Chapter 3 of this thesis.

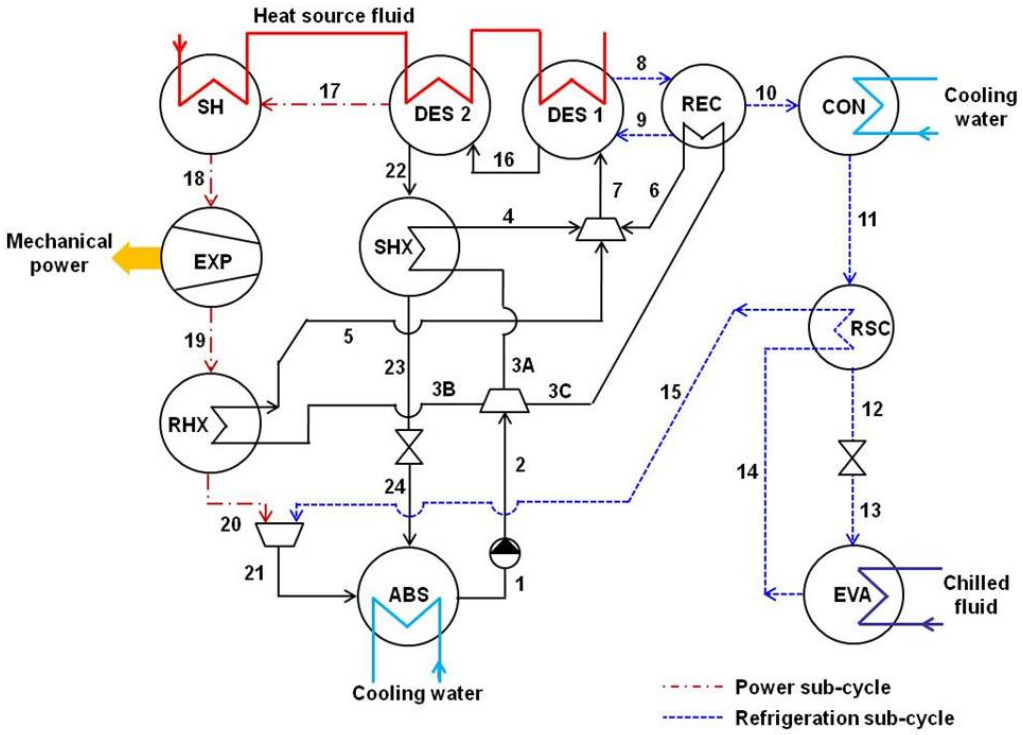

Figure 6.19: Schematic flow diagram of single-stage combined absorption power and refrigeration cycle with two desorbers (SSAPRC-2D) for power and cooling applications.

In general, thermal efficiency based on the first-law of thermodynamics is used to evaluate the energetic performance of a power generating system. However, as it is mentioned in Chapter 2 the dual-outputs of the system requires a thermodynamically consistent and appropriate way to account for the thermodynamic quality of the cooling output in the energy efficiency (it can also be in the exergy efficiency) definition. Accordingly, thermodynamically consistent and realistic first law efficiency definition is used to evaluate the energetic performance of the system and is given as follows:

$$\eta_{I,eff} = \frac{\dot{W}_{net} + (\dot{E}x_{eva}/\eta_{II,ref})}{\dot{Q}_{des1} + \dot{Q}_{des2} + \dot{Q}_{sh}} \tag{6.4.1}$$

where $\eta_{I,eff}$ is the effective first law efficiency and $\eta_{II,ref}$ is the second law efficiency for a vapour compression refrigeration cycle (which is assumed to be 30%). The net power output $\dot{W}_{net}$ of the system is the shaft power reduced by the power consumption of the solution circulation pump. $\dot{Q}_{des1}$, $\dot{Q}_{des2}$ and $\dot{Q}_{sh}$ are the desorbers (DES 1 and DES 2) and superheater (SH) thermal power inputs.

The exergy associated with refrigeration, $\dot{E}x_{eva}$, is calculated as the exergy change across the evaporator (in Fig. 6.19):

$$\dot{E}x_{eva} = \dot{m}_{13}[(h_{13}-h_{14})-T_0(s_{13}-s_{14})] \tag{6.4.2}$$

where T_0 is the reference (dead state) temperature and taken as 293 K.

The thermodynamic performance of combined absorption cycle (SSAPRC-2D) integrated with the scroll expanders is analysed for an expander inlet temperature (t_{18} in Fig. 6.19) varying between 105 °C and 130 °C. In all analysed cases, the absorber exit temperature and operating pressure were set to 30 °C and 350 kPa, respectively. The evaporator exit temperature is also set at −5 °C. In this analysis temperature difference between the high and low-temperature desorbers was kept at 10 K. A split ratio of 0.25 and 10 K degree of superheating in the superheater are considered in the global simulation of the system. The split ratio is defined as a ratio of the mass flow rate of the strong solution to recovery heat exchanger and the mass flow rate of the strong solution from the absorber: $\dot{m}_{3B}/\dot{m}_1$, in Fig. 6.19.

The expander inlet pressure p_{18} is controlled by the operating condition of the condenser, i.e. the temperature of the cooling medium of the condenser (ultimately the ambient temperature). Therefore, the condenser exit temperature is varied between 20 °C to 40 °C in order to investigate the influence of the inlet pressure on the performance of the expanders, useful dual-outputs of the system and its energetic efficiency ($\eta_{I,eff}$). Accordingly, the expander inlet pressure is varied in the range of 857 kPa to 1554 kPa, and its effect is illustrated in Figs. 6.20 (a) and (b) for the three expanders (Sanden model no.: TRSA05, TRSA09 and TRSA12) integrated into the combined absorption cycle. The swept volume (in compressor mode) of the two scroll machines TRSA09 and TRSA12 used in the model scale-up processes are 85.7 cm^3/rev and 121.1 cm^3/rev, respectively.

For the variation of the expander inlet pressure between 857 kPa to 1554 kPa, the mechanical efficiencies of the scroll expanders are in the ranges of 81% - 93% for TRSA05, 82% - 94% for TRSA09 and 84% - 94% for TRSA12. The volumetric efficiency of the expanders decreases with the inlet pressure from 80% to 75%, 84% to 80% and 86% to 83% for TRSA05, TRSA09 and TRSA12, respectively.

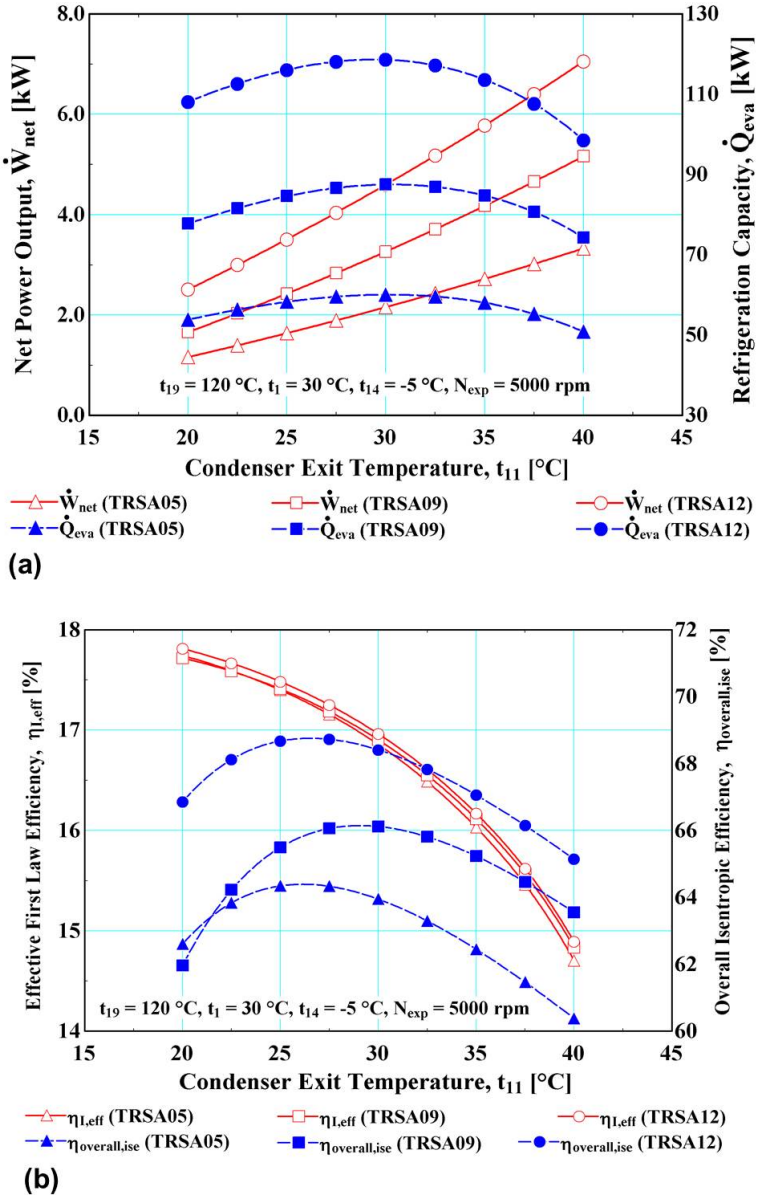

Figure 6.20: Effect of condenser exit temperature on: (a) - system dual-outputs; (b) - efficiencies.

As the inlet pressure increases the driving heat input of the system (the sum of thermal power inputs in the desorbers and superheater) also shows an increasing trend which tends

to be more flat at higher pressures in all the three expanders: (101 kW to 131 kW for TRSA05, 147 kW to 192 kW for TRSA09 and 204 kW to 255 kW for TRSA12). The thermal power input in the high temperature desorber and superheater increases as the expander inlet pressure increases whereas the low temperature desorber shows an optimum value at about 1255 kPa in all the three expander's integration cases: 83 kW for TRSA05, 121 kW for TRSA09 and 164 kW for TRSA12.

Figs. 6.21 (a) and (b) shows the effect of expander inlet temperature on the system useful dual-outputs and efficiencies.

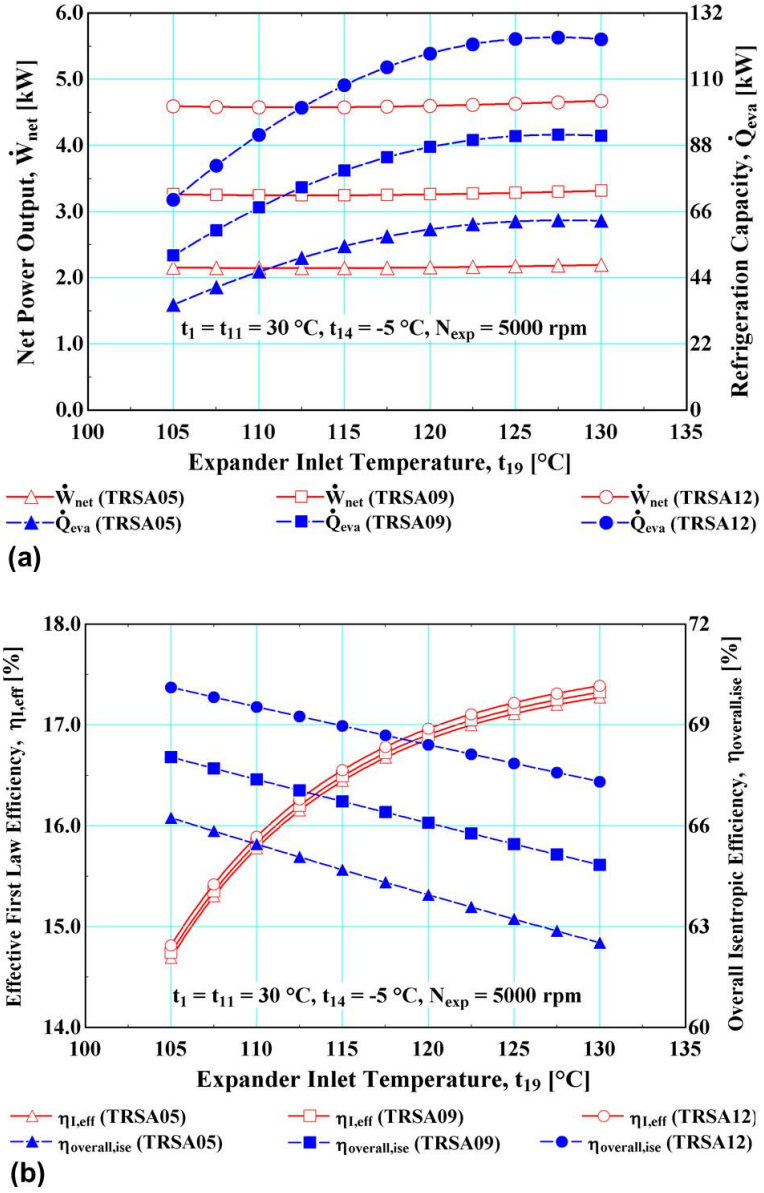

Figure 6.21: Effect of expander inlet temperature on: (a) - system useful dual-outputs; (b) - efficiencies.

The effect of inlet temperature on the overall isentropic efficiency is significant for all the three expanders considered. As the inlet temperature increases, a similar energetic performance is observed in all the three scroll expander integration cases.

When the inlet temperature increases, the driving heat input of the system increases as well in a similar trend for all expanders considered for the range of temperatures between 105 °C to 125 °C and becomes constant above 125 °C. The thermal power inputs in both desorbers (DES 1 and DES 2 in Fig. 6.19) increase as the expander inlet temperature increases. At the operating conditions considered, the thermal power input of the system using the TRSA12 expander is the highest (about 179 kW to 249 kW) for the temperature range of 105 °C to 130 °C and followed by the TRSA09 which is between 131 kW to 184 kW. The lowest driving thermal power input is for the system using a TRSA05 expander and it is in the range of 89 kW to 127 kW. This is mainly due to the amount of vapour expanded and its amount increases as the expander swept volume increases (i.e. more vapour has to be generated in the desorber by using the external driving thermal power input to the system). For instance, in this study about 0.019 kg/s, 0.028 kg/s and 0.038 kg/s of vapour are expanded in the TRSA05, TRSA09 and TRSA12 expanders respectively.

The mechanical efficiencies of the scroll expanders are almost constant as the expander inlet temperature increases with a value around 89%, 90% and 91% for TRSA05, TRSA09 and TRSA12 respectively. However, the volumetric efficiencies decrease from 80% to 75% for TRSA05, from 84% to 80% for TRSA09 and from 86% to 83% for TRSA12.

6.5 Conclusions

The semi-empirical model approach of Lemort [206] for scroll expanders was employed to develop a model for scroll expanders with ammonia (or ammonia/water mixture with high concentration of ammonia) as a working fluid. It is integrated into a combined absorption cycle for power and refrigeration applications. In this model real gas properties are used and therefore it is suitable for wet working fluid such as ammonia, water and ammonia/water mixtures. The model uses eight parameters (all are physically meaningful), determined from the geometry of the scroll expander and from the expander's performance measurements.

A comparison between the values of the developed model estimation and experimental results for the TRSA05 expander for the main outputs shows a good agreement: within ±4% for mass flow rate, ±8% for the developed shaft power and ±4 K for exhaust temperature. This model is later scaled-up to predict the performance of other scroll expanders, with higher swept volume, in the same family series (TRSA09 and TRSA12).

This semi-empirical model is integrated into a combined absorption power and refrigeration cycle (SSAPRC-2D) global model for the purpose of representing the real performance of the expansion device in the cycle. The energetic analysis of the combined absorption system (SSAPRC-2D) shows that it can be achieved 14.8% - 17.8% effective first-law efficiency with an overall isentropic efficiency of the expander in the range of about 61% - 71% for the operating conditions considered in this study (expander inlet temperature and pressure of 105 °C - 130 °C and 857 kPa - 1554 kPa respectively). The expander rotational speed of 5000 rpm, absorber and evaporator exit temperatures of 30 °C and −5 °C, respectively, were kept constant in the energetic analysis of the SSAPRC-2D system.

Although modifying commercially available scroll compressor to work as expander is the least expensive method to date way so far, such type of scroll machines have a fixed built-in volume ratio optimized for refrigeration or air-conditioning applications not for power generating systems therefore they may suffer significantly from under-expansion irreversibilities.

A new combined absorption system (based on SSAPRC-P cycle) using a scroll expander Sanden TRSA05 and three NH_3 based working fluid pairs are proposed for the co-production of mechanical power and cold. The systems using absorbent which are a soluble solid (non-volatile) as lithium nitrate ($LiNO_3$) and sodium thiocyanate (NaSCN) are very competitive in comparison with the NH_3/H_2O working fluid pair that uses a volatile absorbent (H_2O). Also in some operational conditions these working fluids have better performance than NH_3/H_2O system. For a heat source temperature of 120 °C, a sink temperature of 30 °C and a chilled fluid temperature of 0 °C, the net mechanical power obtained with these systems was about 5.9 kW with a heat input of 100 kW. The cooling outputs were in the range of 12 kW to 16 kW depending on the working fluid pairs employed in the system. The exergetic efficiency achieved was about 36% whereas the energetic efficiency was about 8.0%.

Chapter 7

Solar Thermal Collectors Integration: Methodology and Case Study

This chapter has been published in:

International Journal of Refrigeration, 39(March): 125-136, 2014. Modelling, simulation and analysis of solar absorption power-cooling systems by Jesus Lopez-Villada, ***Dereje S. Ayou****, Joan Carles Bruno and Alberto Coronas.*

"This page intentionally left blank"

7.1 Introduction

The aim of this chapter is to develop and demonstrate a representative case for the integration of combined absorption cycles with solar thermal collector technologies. Therefore, two combined absorption cycle configurations (the well-known Goswami cycle and the SSAPRC-P using NH_3/H_2O, $NH_3/LiNO_3$ and NH_3/NaSCN working fluid mixtures for latent cooling output) were considered and integrated with three type of solar thermal collector technologies. The solar thermal collectors selected in this study are: Evacuated Tube (ETC), Linear Fresnel (LFC) and Parabolic Trough (PTC) collectors. Then, a Solar Absorption Power and Cooling System (SAPCS) is proposed and developed using TRNSYS software as simulation tool. First, the energetic and exergetic performance of the Goswami cycle and SSAPRC-P cycle configuration were analysed. And then, a new component in TRNSYS for the combined absorption cycles was developed using the correlations obtained from the data generated by using the previously developed thermodynamic model of the combined absorption cycles.

Finally, a complete analysis of the proposed SAPCS is performed for a specific case located in Sevilla (Spain). Sevilla is selected because it is representative of the most suitable locations for solar power and cooling plants. Although only the Goswami cycle with NH_3/H_2O working fluid pair has been experimentally tested at a laboratory scale [156] and no other operational data was available to validate the model, the results presented in this chapter are representative of the potential application of these systems.

In the next section, the main components of the solar absorption power-cooling systems are presented.

7.2 Solar Absorption Power-Cooling Systems (SAPCSs)

This system consists of four main components: combined absorption subsystem (i.e. the thermodynamic cycles), the solar thermal subsystem, conventional heating subsystem and the recooling subsystem (Fig. 7.1). The SAPCSs considered in this thesis are based on the Goswami and SSAPRC-P cycles using NH_3 based working fluid mixtures. An NH_3/H_2O working fluid mixture is used for both cycle configurations whereas $NH_3/LiNO_3$ and NH_3/NaSCN working fluid mixtures are only used in SSAPRC-P cycle configuration.

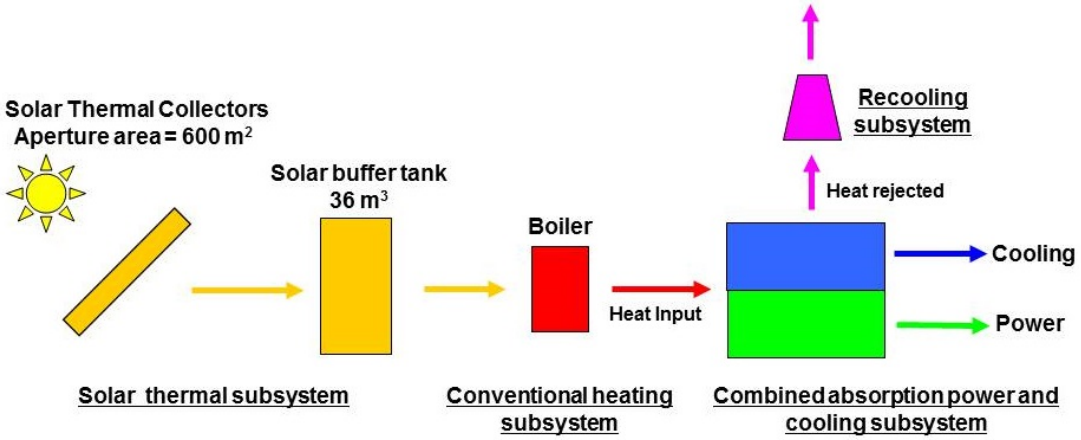

Figure 7.1: Block diagram illustrating the main components of the SAPCS.

The schematics of the cycle configurations, process descriptions and operational characteristics of the Goswami and SSAPRC-P cycles are described in detail in previous chapters. The external cooling water circuit (from the cooling tower) for the absorber and condenser of the SSAPRC-P cycles are connected in a series flow arrangement being first the absorber. In the case of NH_3/H_2O based SSAPRC-P cycle, a solution cooled rectifier is used. The maximum heat source fluid inlet temperature is limited by the thermodynamic property correlation range and the crystallization phenomena of $NH_3/LiNO_3$ and $NH_3/NaSCN$ working fluid mixtures.

Dealing with the solar thermal field, we considered three cases according to the technology evaluated: Evacuated Tube (ETC), Linear Fresnel (LFC) and Parabolic Trough (PTC) Collectors. We discarded flat-plate collectors (FPC) because of the relatively high temperatures needed to drive the combined absorption cycles. In this three configurations, some available commercial collectors suitable to be installed on the flat roof of the buildings with a total aperture area of 600 m^2, a tilt angle of 20° and an azimuth of 0° are considered. And also, as can be seen in Fig. 7.1 the solar subsystem is connected with a hot water buffer tank of 36 m^3. Finally, the recooling subsystem has a cooling tower of a maximum dissipation capacity of about 350 kW. The useful thermal power of the conventional heating system depends on the configuration and working fluid mixture employed in the combined absorption cycle, being 400 kW for Goswami cycle and 600 kW for NH_3/H_2O, 850 kW for $NH_3/NaSCN$ and 900 kW for $NH_3/LiNO_3$ SSAPRC-P cycles.

7.3 Modelling, Simulation and Performance Parameters

The SAPCS is simulated in Transient System Simulation Tool (TRNSYS, 2004) [211], a software commonly used to simulate solar thermal systems. Fig. 7.2 shows a schematic representation of the main components and the corresponding TRNSYS types with their description. It is important to remark that, a new type of solar collectors model (type 1288) was used to model the solar thermal collectors according to the quasi-dynamic model described in the standard EN-12975 [8]. The parameters of the solar collectors for the quasi-dynamic model are given in Table 7.1.

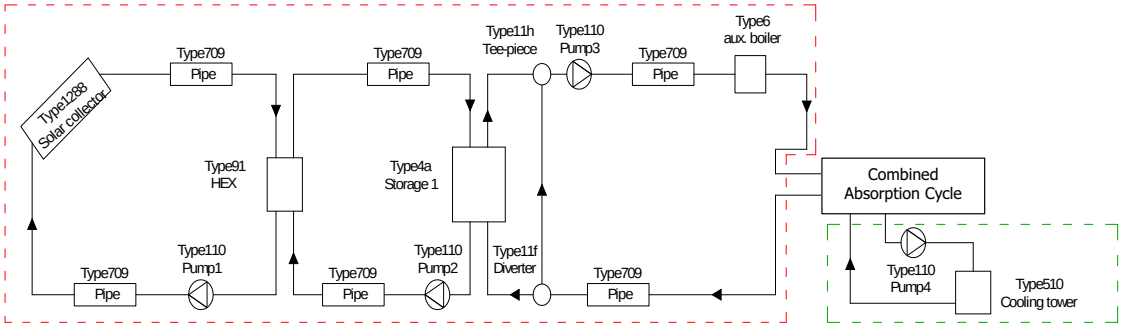

TRNSYS Model	Description
Type 1288	ETC, LFC or PTC solar thermal collectors (using new type of model according to the quasi-dynamic model in the standard EN-12975)
Type 709	Connecting pipe
Type 110	Variable speed pump
Type 91	Heat exchanger with constant effectiveness
Type 4a	Thermal storage/Stratified storage tank/Fixed inlets/Uniform losses
Type 11h	Pipe or duct tee-pieces/mixer/used for fluids except moist air
Type 11f	Flow diverter/used for fluids except moist air
Type 6	Auxiliary heater/boiler
Combined Absorption Cycle (CAC)	New type created: Combined absorption cycle for power and refrigeration cycle (e.g. Goswami or SSAPRC-P cycles)
Type 510	Cooling tower (for heat dissipation)

Figure 7.2: General schematic of the TRNSYS simulation studio models for the SAPCS.

For the simulation of the combined absorption cycles, in TRNSYS, a specific type unit was created based on linear correlations that could be obtained from the data generated using the steady-state thermodynamic performance simulation of the combined absorption cycles (Goswami and SSAPRC-P cycle configurations in this particular case). These correlations are used to provide the performance characteristics of the combined absorption

cycles in the system integration. The thermodynamic models of the cycles are developed in Engineering Equation Solver Software (EES) [210].

Table 7.1: Main parameters of the solar collectors for the quasi-dynamic model according to the European standard EN-12975.

Parameter	Solar thermal collector technology		
	LFC collector	PTC collector	ETC collector
Model	Chromasun MCT	SopoNova 4.1	Vario 2400-30
$F'(\tau\alpha)_{en}$	0.565	0.5897	0.774
$K_{\Theta d}$	0.12	0	1.015
c1[W $m^{-2}K^{-1}$]	0.54	0.9317	1.936
c2[W $m^{-2}K^{-2}$]	0.0032	0	0.006
c5[J $m^{-2}K^{-1}$]	7800	2459	12870
c6[sm^{-1}]	0	0.01248	n/a
Aap[m^2]	3.39	5.38	3.05
Azimuth [S = 0°]	0	0	0
Tilt angle [°]	20	0	20

The obtained correlations express the driving heat input, rejected heat, cooling capacity and net mechanical power output of the cycle as a function of the three temperatures namely: heat source fluid ($t_{hs,in}$), cooling water ($t_{cw,in}$) and chilled water ($t_{cf,in}$) inlet temperatures. The correlations are given in Eqs. 7.3.1 and 7.3.2.

$$\dot{Q}_x = a_x t_{hs,in} + b_x t_{cw,in} + c_x t_{cf,in} + d_x \tag{7.3.1}$$

$$\dot{W}_{net} = a_e t_{hs,in} + b_e t_{cw,in} + c_e t_{cf,in} + d_e \tag{7.3.2}$$

where: $\dot{Q}_x$ [kW] x = in driving thermal energy provided to the cycle (i.e. the heat supplied to the desorber and superheater (if any)), x = cw heat rejected in the absorber (and condenser in the case of the SSAPRC-P cycles), x = cold cooling capacity of the cycle; $\dot{W}_{net}$ [kW]: net mechanical power output of the cycle; a, b, c, d: (a, b and c in kW°C^{-1} and d in kW) are the correlation parameters given in Table 7.2.

Table 7.2: Correlation parameters for the driving heat, dissipated heat, cooling capacity and power output of the SAPCS according to Eqs. 7.3.1 and 7.3.2.

Goswami cycle								
Parameter	$\dot{Q}_{in}$		$\dot{Q}_{cw}$		$\dot{Q}_{cold}$		$\dot{W}_{net}$	
a	1.586		1.581		0.376		0.382	
b	−3.447		−3.372		−0.656		−0.730	
c	0		0		0.438		0	
d	154.362		146.572		−16.600		−2.385	
Adjusted R^2	0.9667		0.9711		0.9938		0.9910	
Parameter	$\dot{Q}_{in}$		$\dot{Q}_{cw}$		$\dot{Q}_{cold}$		$\dot{W}_{net}$	
	1	2	1	2	1	2	1	2
NH_3/H_2O SSAPRC-P cycle configuration ($a = a_1 + a_2 \cdot SR$, $b = b_1 + b_2 \cdot SR$, $c = c_1 + c_2 \cdot SR$)								
a	3.717	0.968	6.412	−2.076	2.702	−2.647	$4.765 \cdot 10^{-3}$	0.398
b	−9.704	−3.899	−18.355	5.168	−8.693	8.318	$-3.675 \cdot 10^{-2}$	0.754
c	6.895	4.252	14.896	−2.972	7.985	−7.284	$-1.539 \cdot 10^{-2}$	$-6.059 \cdot 10^{-2}$
d	0		0		0		0	
Adjusted R^2	0.9963		0.9956		0.9932		0.9937	
NH_3/NaSCN SSAPRC-P cycle configuration ($a = a_1 + a_2 \cdot SR$, $b = b_1 + b_2 \cdot SR$, $c = c_1 + c_2 \cdot SR$)								
a	6.356	1.601	10.752	−3.233	4.378	−4.217	$-2.078 \cdot 10^{-2}$	0.621
b	−16.928	−5.996	−30.329	8.182	−13.409	12.743	$7.765 \cdot 10^{-3}$	−1.454
c	8.579	5.999	18.170	−3.163	9.578	−8.823	2.000	0.346
d	0		0		0		0	
Adjusted R^2	0.9986		0.9981		0.9955		0.9943	
$NH_3/LiNO_3$ SSAPRC-P cycle configuration ($a = a_1 + a_2 \cdot SR$, $b = b_1 + b_2 \cdot SR$, $c = c_1 + c_2 \cdot SR$)								
a	6.234	0.968	10.027	−3.240	3.796	−3.699	$1.335 \cdot 10^{-3}$	0.511
b	−15.902	−2.946	−26.706	8.557	−10.873	10.523	$-6.250 \cdot 10^{-2}$	−0.989
c	8.234	2.720	15.768	−4.420	7.565	−7.181	$2.671 \cdot 10^{-2}$	$3.579 \cdot 10^{-2}$
d	0		0		0		0	
Adjusted R^2	0.9980		0.9975		0.9945		0.9942	

The thermodynamic modelling of the Goswami and SSAPRC-P cycle configurations used in the integration with the solar thermal subsystems is described in the next sub-section as follows.

7.3.1 Thermodynamic modelling of the Goswami and SSAPRC-P cycles

The steady-state modelling approach presented in Chapter 3 is followed to develop the thermodynamic model of combined absorption cycles used to generate the data for obtaining the correlations used in the system integration.

The models are based on the thermodynamic properties of the working fluid mixtures (NH_3/H_2O, $NH_3/LiNO_3$ and NH_3/NaSCN), steady-state mass and energy balances for each component of the cycle and some model assumptions. Apart from the common assumptions made in Chapter 3 for absorption cycle modelling, the following additional assumptions were taken in the thermodynamic modelling of the cycles:

- Isentropic pump and expander efficiencies are 80% and 85%, respectively.
- Minimum approach temperature of 5 °C is set for the absorber, condenser, cooler, desorber, evaporator and superheater.
- Minimum pinch temperature of 10 °C is set in the solution heat exchanger and refrigerant sub-cooler.
- Counter-current flow desorber for NH_3/H_2O SSAPRC-P cycle is considered whereas co-current flow desorber for Goswami and NH_3/Salt ($LiNO_3$ or NaSCN) SSAPRC-P cycles are considered.
- Concentration of the rectified vapour leaving the rectifier of NH_3/H_2O SSAPRC-P cycle is 0.999 and 0.996 for the Goswami cycle.
- Saturated pure NH_3 vapour leaving the evaporator of the $NH_3/LiNO_3$(or NaSCN) SSAPRC-P cycle.
- A constant mass flow rate of 5 kg/s is assumed for the external heat source fluid circuit of the Goswami and SSAPRC-P cycles. The mass flow rates of the external cooling and chilled water circuits are also assumed constant.

The constant mass flow rates of the external cooling and chilled water circuits of the Goswami cycle are calculated by operating the cycle at typical operating conditions: cooling water and chilled water inlet/outlet temperatures of 30/38 °C and 12/7 °C, respectively. A unit mass flow rate of the basic NH_3/H_2O solution through the solution pump is considered. Regarding the SSAPRC-P cycles, the constant mass flow rates of the external cooling and chilled water circuits are calculated by operating the cycle in cold-mode of operation (to obtain the peak cooling demand of the system, 175 kW) at the typical operating conditions. At this mode of operation the expander power output only cover the power consumption of

the solution pump. The heat source inlet temperature is fixed at the minimum acceptable heat source inlet temperature to achieve a steady COP. Accordingly, the cooling water, chilled water and basic solution mass flow rates are determined as follows.

- For NH_3/H_2O: $\dot{m}_{cw} = 13.33$ kg/s, $\dot{m}_{cf} = 8.34$ kg/s and $\dot{m}_1 = 0.55$ kg/s.
- For $NH_3/LiNO_3$: $\dot{m}_{cw} = 14.69$ kg/s, $\dot{m}_{cf} = 8.34$ kg/s and $\dot{m}_1 = 0.90$ kg/s.
- For NH_3/NaSCN: $\dot{m}_{cw} = 14.13$ kg/s, $\dot{m}_{cf} = 8.34$ kg/s and $\dot{m}_1 = 1.04$ kg/s.

7.3.2 Performance parameters

Energetic and exergetic efficiencies could be used to evaluate the performance of the SAPCS. In the first case, the energy balances in each component of the cycle need to be known in a defined time period. It is necessary also to calculate the energy received by the solar collectors, useful energy from the collector field and energy inputs and outputs of the combined absorption subsystem. In the second case, apart from the energy balances, it is necessary to perform exergy balances. A detailed explanation of this procedure could be found in Baghernejad and Yaghoubi [212] and details of combined absorption cycle's efficiency definitions and terminologies are given in Chapter 2. In this analysis Eq. 7.3.3 to Eq. 7.3.5 defines the energetic efficiencies and Eq. 7.3.6 and Eq. 7.3.7 defines the exergetic efficiencies.

$$\eta_{solar} = \frac{Q_{solar}}{E_{solar}} \tag{7.3.3}$$

$$\eta_{CAC} = \frac{W_{net} + {Ex_{cold}}/{\eta_{II,ref}}}{Q_{in}} \tag{7.3.4}$$

$$\eta_{SAPCS} = \frac{(W_{net} + {Ex_{cold}}/{\eta_{II,ref}}) \cdot \mathrm{SF}}{E_{solar}} = \eta_{solar} \cdot \eta_{CAC} \tag{7.3.5}$$

where E_{solar}: solar energy received by the solar collectors in a defined period (kWh). η_{solar}: energy efficiency of the solar subsystem. η_{CAC}: effective first law efficiency of the combined absorption subsystem. η_{SAPCS}: energy efficiency of the solar absorption power-cooling system. Ex_{cold}: exergy change in the chilled water circuit (kWh). $\eta_{II,ref}$: second law efficiency for the conventional vapour compression refrigeration cycle, which is assumed

to be 30% in this study. SF: solar fraction of the driving heat provided to the combined absorption subsystem. The exergetic efficiencies are defined as:

$$\eta_{ex,CAC} = \frac{W_{net} + Ex_{cold}/\eta_{II,ref}}{\triangle Ex_{hs,in}} \tag{7.3.6}$$

$$\eta_{ex,SAPCS} = \frac{(W_{net} + Ex_{cold}/\eta_{II,ref})\text{.SF}}{Ex_{solar}} \tag{7.3.7}$$

where $\eta_{ex,CAC}$: effective exergy efficiency of the combined absorption subsystem. $\eta_{ex,SAPCS}$: effective exergy efficiency of the solar absorption power-cooling system. Ex_{solar}: solar exergy received by the solar thermal collectors (kWh). $\triangle Ex_{hs,in}$: exergy change in the heat source fluid (kWh).

A controversial aspect of the exergy analysis is the reference temperature when the ambient temperature fluctuates during the studied period. According to Pons (2009) [213], the reference temperature must be kept constant in the whole period. However, other authors consider that it is better applying a dynamic reference environment (Angelotti and Caputo, 2007) [214]. In this study, it is decided to have a constant exergy reference temperature. The exergy analysis in this chapter covers only the entire system not the component exergy analysis.

7.3.3 Goswami and SSAPRC-P cycles performance modelling for the system integration

Using the developed thermodynamic models in the previous subsections, the energy balances and performance parameters for the Goswami NH_3/H_2O cycle and for NH_3/H_2O, $NH_3/LiNO_3$ and NH_3/NaSCN SSAPRC-P cycle configurations operating at a wide range of temperatures ($t_{hs,in}$, $t_{cw,in}$, $t_{cf,in}$) are determined.

Figs. 7.3 to 7.5 show the variation of the net mechanical power output and effective first law efficiency for the Goswami and SSAPRC-P cycles with the heat source, cooling water and chilled water inlet temperatures, respectively. For the SSAPRC-P cycles, it is observed that the variation of the vapour split ratio (SR, defined in subsection 3.3.2) has an effect on power output and effective first law efficiency.

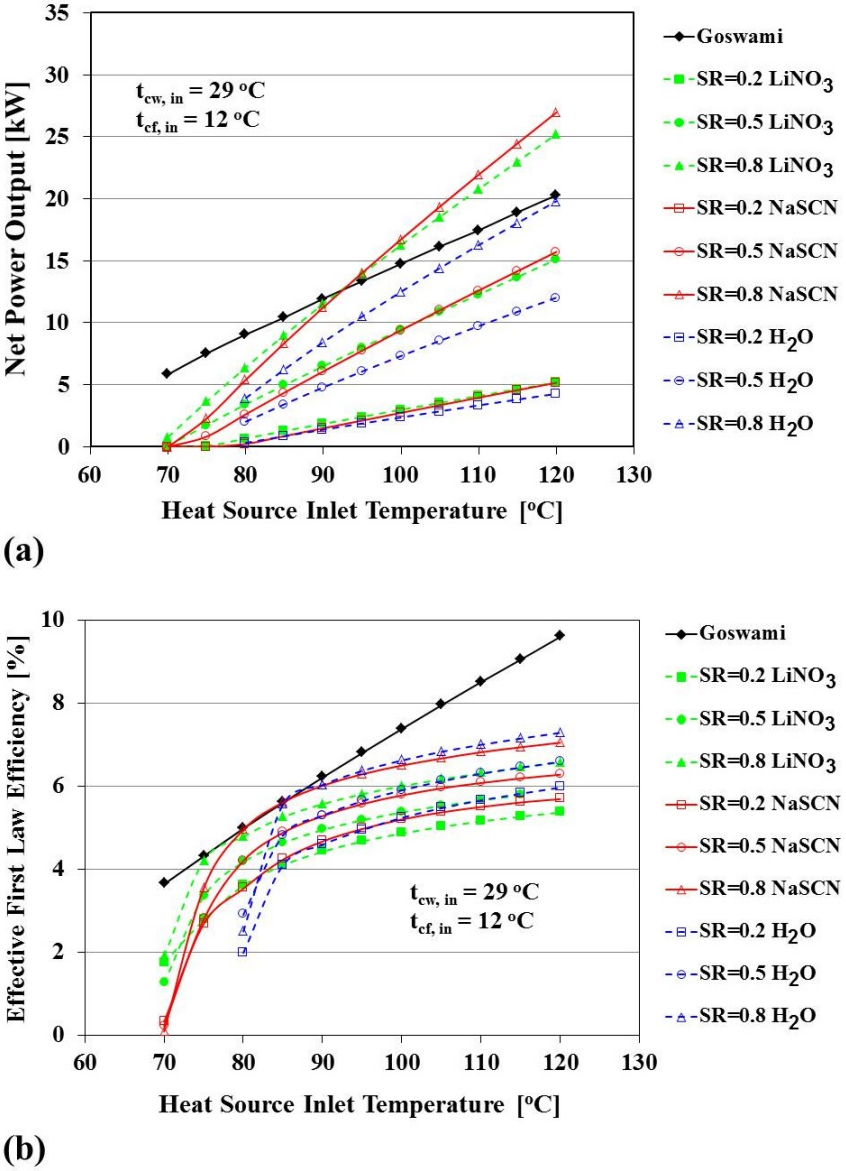

Figure 7.3: Variation of the net power output and effective first law efficiency with the heat source inlet temperature for the Goswami and NH_3/H_2O, $NH_3/LiNO_3$ and NH_3/NaSCN SSAPRC-P cycles: (a) - net power output; (b) - effective first law efficiency.

Since the amount of vapour generated in the desorber increases as the heat source temperature increases, the dual-outputs mechanical power (shown in Fig. 7.3 (a)) and cooling of the cycles also increases. Consequently, as illustrated in Fig. 3 (b), the effective first law efficiency of the cycle increases as the heat source temperature increases. It also shows clearly that when $t_{cw,in}$ = 29 °C and $t_{cf,in}$ = 12 °C, the Goswami cycle presents a better energetic performance and only when $t_{hs,in}$ ranges between 85 °C and 90 °C, the SSAPRC-P cycle with NH_3/NaSCN and NH_3/H_2O at SR=0.8 have a similar effective first

law efficiency values. The efficiency increases to more than 9.5% for the Goswami cycle and around 7.5% for the SSAPRC-P cycles at high values of SR and $t_{hs,in}$.

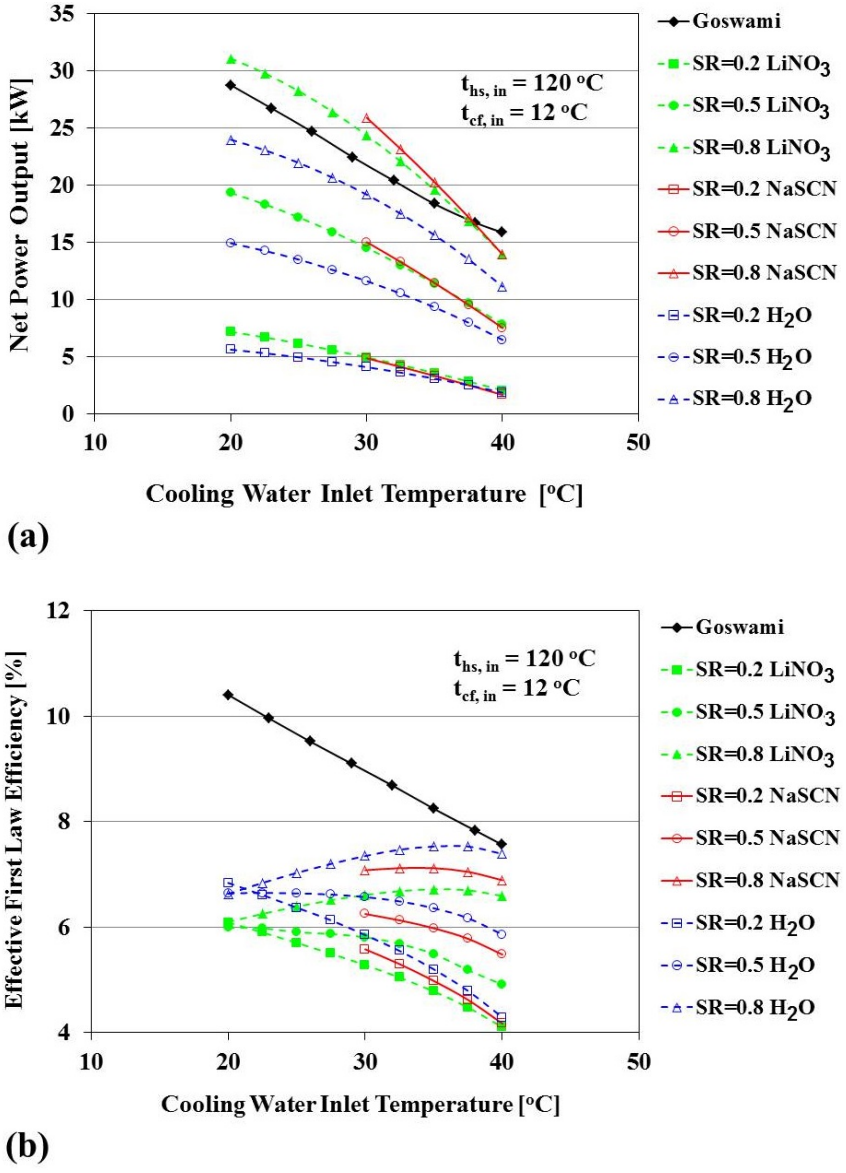

Figure 7.4: Variation of the net power output and effective first law efficiency with the cooling water inlet temperature for the Goswami and NH_3/H_2O, $NH_3/LiNO_3$ and NH_3/NaSCN SSAPRC-P cycles: (a) - net power output; (b) - effective first law efficiency.

Comparing the SSAPRC-P cycles using different working fluids, it could be seen that from 90 °C to 120 °C the NH_3/H_2O working fluid mixture is the best option followed closely by NH_3/NaSCN. However, $NH_3/LiNO_3$ and NH_3/NaSCN cycles are able to operate at relatively lower temperatures (70 °C to 80 °C) with a better efficiency than NH_3/H_2O

cycle. Therefore it makes sense to use these mixtures at lower temperatures. Similarly, we analysed the effect of the cooling water temperature on the cycle's net power output and energetic efficiency (Fig. 7.4). When cooling water inlet temperature ($t_{cw,in}$) increases from 20 °C to 40 °C, at constant $t_{hs,in}$ and $t_{cf,in}$, the net power output (see Fig. 7.4 (a)), the heat consumption (by the desorber) and the cooling capacity of the SSAPRC-P cycles decrease at all split ratios considered (SR=0.2, 0.5 and 0.8). The combined effect on the effective first law efficiencies of the cycles is illustrated in Fig. 7.4 (b).

The SSAPRC-P cycles present the same trend for SR between 0.2 and 0.8 with efficiencies in the range of 4% to 7%. Nevertheless, when $SR = 0.5$ the efficiency only drops slightly and even at $SR = 0.8$ it increases gently and peaks at 35 °C. In the case of the Goswami cycle, the effective first law efficiency value declines steadily from 10.5% to 7.6% when it operates between 20 °C and 40 °C. This is mainly due to the fact that when cooling water inlet temperature increases, the net power output (shown in Fig. 7.4 (a)) of the cycle decreases at a faster rate than the heat consumption of the desorber. It should be noticed that, at a heat source inlet temperature of around 120 °C and a chilled water inlet temperature of 12 °C, the NH_3/NaSCN SSAPRC-P could not operate at cooling tower temperatures lower than 29 °C to avoid risk of crystallization of the working fluid mixture.

Fig. 7.5 shows the variation of net power output and effective first law efficiency with the chilled water inlet temperature ($t_{cf,in}$). As the chilled water inlet temperature increases (at constant $t_{hs,in}$ and $t_{cw,in}$) the heat consumption of the desorber of the SSAPRC-P cycles increases but the net power output, shown in Fig. 7.5 (a), is almost constant. Even though the cooling capacity of the cycles increases with the chilled water inlet temperature, its work contribution ($Ex_{cold}/\eta_{II,ref}$) to the effective first law efficiency (in Eq. 7.3.4) is decreasing since it accounts both the quality and quantity of the cooling output of the cycles. Consequently, the effect of the variation of chilled water inlet temperature on effective first law efficiency is decreasing as illustrated in Fig. 7.5 (b) except the Goswami cycle where it is almost constant. For the Goswami cycle, the heat consumption and net power output is independent of the chilled water inlet temperature except the sensible (mainly) cooling output which has a low contribution on the effective first law efficiency values of the cycle. Therefore, the effective first law efficiency of the Goswami cycle remains practically constant at 9.1%.

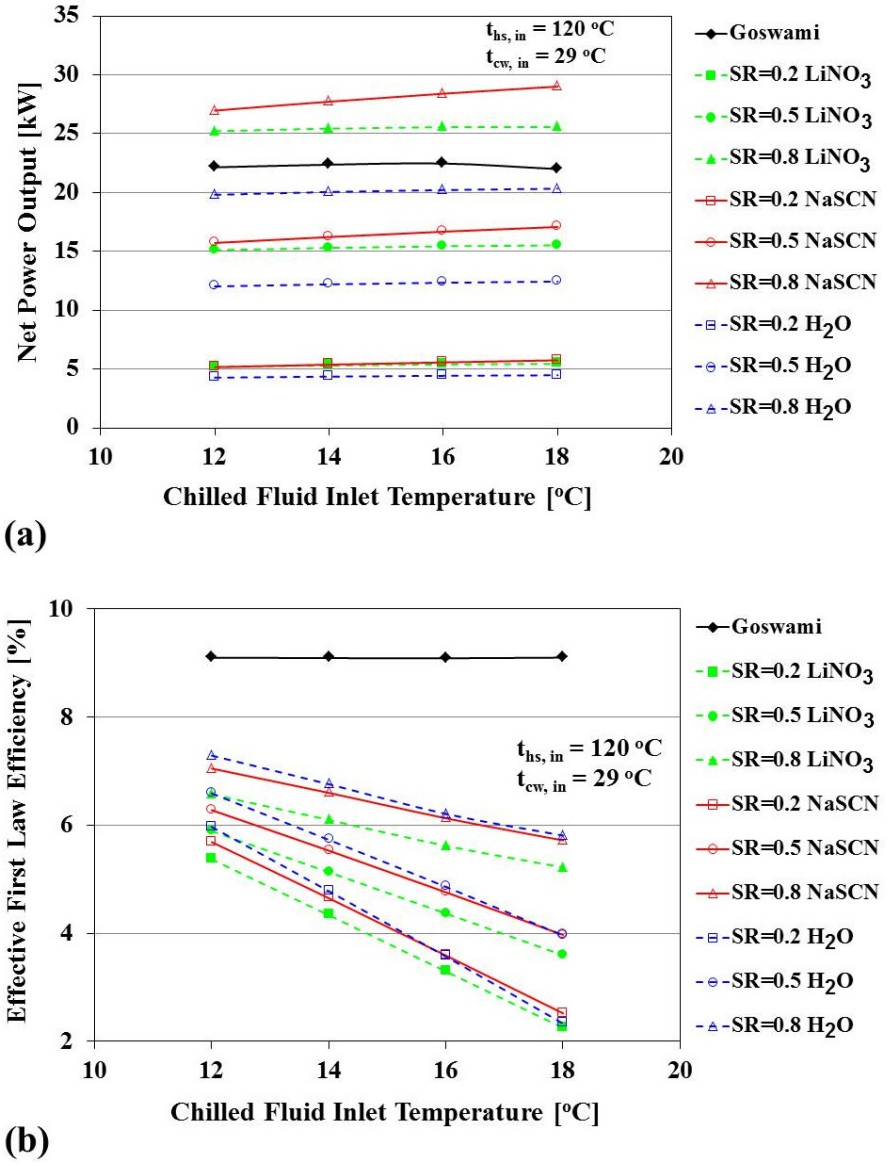

Figure 7.5: Variation of the net power output and effective first law efficiency with the chilled water inlet temperature for the Goswami and NH_3/H_2O, $NH_3/LiNO_3$ and NH_3/NaSCN SSAPRC-P cycles: (a) - net power output; (b) - effective first law efficiency.

For SSAPRC-P cycles, the effective first law efficiency decreases gradually at SR of 0.2 from 6% to 2%. At higher SR values the trend is similar with higher efficiencies and lower slope. Unlike Fig. 7.3 (b) and Fig. 7.4 (b), in Fig. 7.5 (b) is shown that NH_3/H_2O mixture has the highest efficiency in almost all the analysed cooling tower and chilled water temperatures followed closely by the NH_3/NaSCN.

In order to perform the TRNSYS simulations, first the parameters of Eqs. 7.3.1 and 7.3.2 for the Goswami and SSAPRC-P cycle configurations were estimated. The previous

Table 7.2 shows the parameter values for the different correlations as well as the value of the adjusted coefficient of determination R^2. As the obtained values of this coefficient are relatively high, the data could be considered to fit well in a linear model with the three external temperatures ($t_{hs,in}$, $t_{cw,in}$ and $t_{cf,in}$). It is also important to remark that a, b and c correlation parameters of the SSAPRC-P cycles depend linearly on the SR.

7.4 Simulation of Solar Absorption Power-Cooling System

The developed TRNSYS models for the Goswami and SSAPRC-P cycles were combined with ETC, LFC and PTC solar thermal models to build different SAPCSs (Fig. 7.2). Once these models were assembled, we carried out annual simulations considering the location of Sevilla city (Spain, coordinates 37°22´38˝N 5°59´13˝W) and assuming that SAPCS operates 24 h per day. Sevilla is selected because it is representative of the most suitable locations for these type of solar power and cooling plants.

For the exergy balances we considered a constant reference temperature of 290 K. One important issue to mention is that, as the heat source inlet temperature increases the effective first law efficiency of the combined absorption cycle also increases, the solar collector efficiency drops, thus it exists an optimum value for this temperature for each SAPCS. Additionally, for the specific case of SAPCS with SSAPRC-P cycles, the optimum temperature also depends on the value of the vapour split ratio SR. Consequently, the optimum heat source temperature was calculated by performing several simulations for each particular model using the TRNOPT application, which links TRNSYS (2004) with the optimisation software GenOpt (2011) [215].

Table 7.3 presents some optimal heat source temperatures values for the Goswami cycle for all the solar technologies and SSAPRC-P cycles with the ETC solar collector. For SSAPRC-P cycles Table 7.3 only shows the ETC cases because the optimum heat source temperature for these cycles is always below 100 °C for all the solar collectors considered in this study. At these temperatures, ETC collectors present by far the best energy performance and besides are more economical than LFC and PTC alternatives. As a consequence the ETC solar technology is the best option for SSAPRC-P cycles. On the other hand, regarding to Goswami cycle configuration, we found optimum temperatures of 138 °C for

ETC and LFC and 150 °C for PTC collectors. The main reason that explains these results is the relatively high effective first law efficiency of this cycle at high temperatures as could be seen in Fig. 7.3 (b).

Table 7.3: Annual energy values and energy efficiency rates for the SAPCS. In all cases we assumed a solar collector field facing to the South (azimuth angle 0°) with an aperture area of 600 m^2 and a tilt angle of 20°. For the SSAPRC-P cycles we considered several split ratios (SR) to change the power/cold production ratio.

	Goswami Cycle			SSAPRC-P cycles with ETC solar collectors								
	Solar Technology			NH_3/H_2O			$NH_3/NaSCN$			$NH_3/LiNO_3$		
	ETC	LFC	PTC	SR			SR			SR		
				0.2	0.5	0.8	0.2	0.5	0.8	0.2	0.5	0.8
Optimal annual heat source temperature [°C]												
	138.2	132.2	150.0	90.0	90.3	90.5	78.7	90.3	94.9	90.0	90.0	99.4
Annual energy [MWh]												
Solar heat	303	201	245	469	480	492	525	508	506	502	513	493
Q_{heat}	2448	2448	2594	1531	1683	1853	1517	2032	2423	1900	2076	2600
Q_{cold}	199	199	234	797	530	235	782	624	310	875	585	302
Power	267	267	302	23	70	118	12	71	139	19	68	142
Q_{cw}	2392	2392	2538	2305	2143	1970	2287	2586	2594	2756	2593	2760
Annual energy efficiency factors [%]												
SF	12.4	8.2	9.4	30.6	28.5	26.5	34.6	25.0	20.9	26.4	24.7	18.9
η_{solar}	26.1	17.3	21.1	40.3	41.2	42.2	45.1	43.6	43.5	43.1	44.1	42.3
η_{CAC}	14.9	14.9	16.3	5.3	6.3	7.2	4.5	5.6	6.6	4.4	5.2	6.2
η_{SAPCS}	4.1	2.8	3.4	2.1	2.6	3.0	2.0	2.4	3.0	1.9	2.3	2.6
$\eta_{ex,CAC}$	518	51.8	52.9	26.6	31.7	36.6	26.1	29.0	32.9	22.8	27.1	29.8
$\eta_{ex,SAPCS}$	4.1	2.8	3.6	2.2	2.7	3.2	2.2	2.6	3.0	2.0	2.4	2.8

Apart from the optimum temperatures, Table 7.3 also shows the total annual values of the heat consumption, solar heat, heat rejection, cooling and power production as well as some energy performance rates as solar efficiency and effective first law efficiency of the combined absorption cycles and SAPCSs. Furthermore, Fig. 7.6 offers monthly results for three of the more significant cases or the best possible combination of solar thermal collectors and combined absorption cycles:

- (a): Goswami – PTC.
- (b): NH_3/H_2O SSAPRC-P – ETC with SR = 0.2.
- (c): NH_3/NaSCN SSAPRC-P – ETC with SR = 0.8.

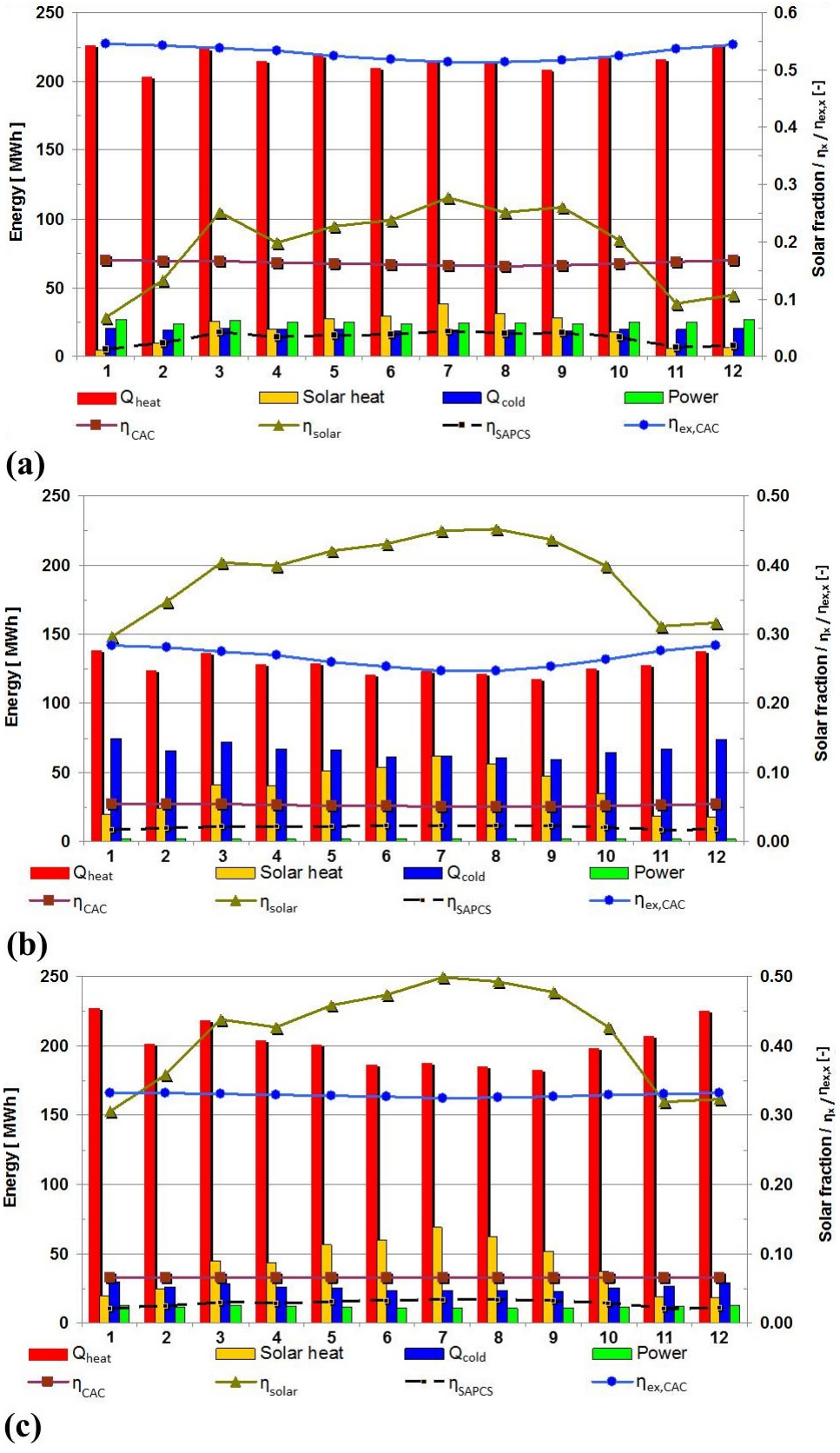

Figure 7.6: Monthly energy values and energy efficiency rates for some Solar Absorption Power-Cooling System: (a) - NH_3/H_2O Goswami cycle with PTC solar collector; (b) - NH_3/H_2O SSAPRC-P with ETC solar collector and SR=0.2; (c) - NH_3/NaSCN SSAPRC-P with ETC solar collector and SR = 0.8.

According to these results it is evident that Goswami cycle systems produce more power with an effective first law efficiency about twice the values obtained for the SSAPRC-P cycles. Nevertheless, when considering the different solar thermal technologies, it could be seen that, despite that Goswami-PTC and Goswami-ETC systems present higher values of η_{SAPC} and $\eta_{ex,SAPC}$, SSAPRC-P cycles operating at SR of 0.8 reach effective first law efficiencies in the same order of magnitude and even NH_3/H_2O-ETC and NH_3/NaSCN-ETC systems exceed the Goswami-LFC system. These results could be explained by the better performance of ETC solar collectors when coupled with the SSAPRC-P cycles. On the other hand, if the main interest is the cold production, SSARC-P cycles at lower SR are the best option because they produce more cold in spite of the lower values of η_{CAC}, η_{SAPCS}, $\eta_{ex,CAC}$ and $\eta_{ex,SAPCS}$.

Regarding the solar energy contribution, it ranges between 200 MWh and 300 MWh for Goswami and is around 500 MWh for SSAPRC-P systems. The higher contribution in the SSAPRC-P cases could be explained by three reasons. First of all, Goswami cycle operate at higher optimum temperatures resulting in an important reduction of the energy conversion efficiency of the solar thermal collectors. Secondly, ETC solar collectors capture the diffuse solar irradiation whereas concentrating collectors as LFC and PTC are unable to do it. Thirdly, ETC solar collectors also present a higher optic factor (Table. 7.1) and also higher incidence angle modifier factors. The differences in the energy performance between the three solar technologies analysed in this study are more evident if we look at the monthly charts of Fig. 7.6 in which we can observe that the ETC efficiency ranges from 30% in the winter months to almost 50% in summer with NH_3/NaSCN SSAPRC-P cycle. By contrast, PTC efficiency with the Goswami cycle is less than 10% in the colder months and only about 30% in the hotter period of the year. This better performance of the ETC collector leads to higher values of η_{SAPCS} when compared to the PTC collector despite the fact that the Goswami cycle presents higher effective first law efficiency. Even so, it has to be considered that some manufactures limit the operation temperatures of ETC collectors to 120 °C – 130 °C in order to protect some components from high temperatures. Therefore, from the point of view of SAPCS effective first law and exergy efficiencies, the best option is Goswami – ETC followed by Goswami – PTC. However, when working at

temperatures above 120 °C – 130 °C practical issues of some ETC manufactures have to be considered which means that PTC could be the best alternative. Alternatively, for SSAPRC-P cycles, as the optimum temperature is always below 100 °C, the solar ETC collectors are more suitable. Table 7.3 shows that NH_3/H_2O SSAPRC-P case has lower solar contribution due to its better thermal efficiency that leads to lower heat consumption and as a consequence to higher average temperature on the solar collectors. This is also the explanation of the change in the solar efficiency of the solar collectors when changing the SR factor.

The proposed absorption power and cooling systems are flexible enough to produce only power, only cold (in case of the SSAPRC-P) or power and cold simultaneously. However, the mode of operation considered in this study is the co-production mode: for SSAPRC-P with split ratios of 0.2, 0.5 and 0.8 and for Goswami cycle based on the operating conditions considered (no superheating in order to produce more sensible cooling output). Therefore, the suitable performance parameter to assess the energetic performance of the system is the first law efficiency instead of the COP. Consequently, the effective first law efficiency (which accounts the thermodynamic quality of the dual-outputs) is used to evaluate the energetic performance of the system. The variation of the power output of the proposed systems with the heat source, cooling water and chilled water inlet temperatures are presented in Fig. 7.3 (a), Fig. 7.4 (a) and Fig. 7.5 (a), respectively. In addition to this, we would like to comment that the best configuration cannot be decided just using a given set of operating conditions and run the three working fluids because the effect of the solar collector's efficiency and the partial load behaviour is also very important.

7.5 Conclusions

In this chapter, Solar Absorption Power-Cooling Systems (SAPCSs) based on representative new combined absorption cycles (SSAPRC-P, for latent cooling output) and the well-known Goswami cycle were developed and compared for the same operating conditions. The non-conventional ammonia/salt mixtures ($NH_3/LiNO_3$ and $NH_3/NaSCN$) were also employed in the SSAPRC-P cycle configuration. The cycles are partially activated by ETC, LFC and PTC solar thermal collectors. In order to perform the comparisons,

the SSAPRC-P and Goswami cycles were modelled with linear correlations obtained using performance data generated by using the developed thermodynamic models of the cycles. These correlations estimate the performance of the cycles as a function of the heat source, cooling water and chilled water inlet temperatures. The models were implemented in TRNSYS software to simulate SAPCSs for a whole year.

The SSAPRC-P cycle configuration with $NH_3/LiNO_3$ and NH_3/NaSCN working fluid mixtures are able to operate at relatively lower temperatures (between 70 °C and 80 °C) with better efficiency than NH_3/H_2O based cycle consequently it is recommended to use these mixtures at lower temperatures.

The results show that it exist an optimum heat source temperature for each SAPCS depending on the combined absorption cycle and solar thermal collector technologies. This optimum temperature is always below 100 °C for systems based on SSAPRC-P cycles, consequently it is concluded that ETC is the technology more suitable for systems with these cycles. On the other hand, although the Goswami-ETC also leads to the best efficiency at 138 °C, some ETC collectors may not work properly at these temperature levels and then the PTC collector could be a better alternative.

Finally, if the main interest of the SAPCS is power production, then the Goswami-ETC or Goswami-PTC combinations offer the best energetic and exergetic performances. On the other hand, if the interest is on chilled water production, the SSAPRC-P cycles at lower vapour split ratio are the best option in spite of the relatively lower values of energetic and exergetic efficiencies for both SSAPRC-P and SAPCS. To improve these efficiencies, other proposed latent cooling output based cycle configurations (see Chapter 3 and 4) could be used in the SAPCS. In addition to this, it is important to mention that the best configuration cannot be decided just using a given set of operating conditions and run the three working fluid mixtures because the effect of solar collector's efficiency and the partial load behaviour is also very important.

Chapter 8

General Conclusions and Future Outlook

"This page intentionally left blank"

8.1 Conclusions

Low and mid-grade heat sources ($<$ 300 °C), such as solar thermal, geothermal and waste heat from various thermal processes are abundantly available at different temperature levels. These heat sources through the use of efficient technologies have promising potential for conversion to highly valuable energy products as electricity, air-conditioning and refrigeration. However, the conventional power cycles, such as the steam Rankine cycles, has technical limitations to use these energy resources effectively. Moreover, the conventional vapour compression refrigeration cycle use high grade energy inputs (in the form of electricity or mechanical energy) to drive its compression stage (process) necessary to produce the refrigeration effect. Absorption chillers and refrigerators based on H_2O/LiBr and NH_3/H_2O working fluid mixtures are well-known technologies by using thermal energy from various thermal resources for air-conditioning and refrigeration applications.

In general, many end users need both cooling/heating and electricity for various purposes. In this sense, building applications can be typical examples. The cooling demand of a building fluctuates with the dynamic ambient condition in a year-round but the electrical power demand for other purposes is more or less constant. Therefore, systems capable of providing dual or more useful energy products simultaneously and/or alternatively have advantages from the technical and performance perspectives.

A wide variety of combined absorption cycle configurations has been studied and reported in the literature for the co-production of power and cooling (refrigeration). The literature review on combined absorption cycles reveals that greater emphasis is given to production of power than refrigeration. In this review, two general types of cycles have been identified: those producing cold using sensible heat (mainly the Goswami cycle) and those based on latent heat (mainly hybrid Rankine and absorption refrigeration cycle). Ammonia/water mixture is the most commonly used working fluid in combined absorption cycles, which is a natural working fluid. This mixture requires rectification of the vapour stream in the cold producing loop of the combined absorption cycles.

Some of the cycle configurations, available in the literature, are simple modifications of the Kalina absorption power cycle that produce cooling as sub product. In some cases these cycles are very complex and have a high number of splits and components. The most

suitable combined absorption systems for effective utilization of low and mid-grade heat sources such as from stationary or low-concentration solar thermal collectors seems to be those derived directly from such absorption chiller cycles as single or double-effect cycles or advanced GAX cycles. They are more suitable for solar applications in buildings which are characterised by small-to-medium power and cooling demands. The dual-output (mechanical/electrical energy and cold) nature of combined absorption systems needs care during the system performance evaluations in particular for its energetic performance evaluation. At least two independent parameters are required to evaluate the energetic performance of the combined absorption systems in our case the selected parameters are: effective first law efficiency and power/cold ratio.

In this thesis, three new combined absorption cycles derived from single-stage NH_3/H_2O absorption refrigeration cycle configuration are presented and analysed from the energetic and exergetic viewpoints. They are mainly suitable for the utilization of low-grade heat sources below 200 °C for the co-production of power and cold at different temperature levels intended for deep-freezing, refrigeration and space air-conditioning applications. A physical-mathematical model was developed for each cycle configuration for the purpose of analysing the performance of the proposed combined absorption cycles.

The first combined absorption cycle configuration presented is a Single-Stage combined Absorption Power and Refrigeration Cycle with Parallel flow arrangement (SSAPRC-P). The main feature of this cycle configuration is its operational flexibility that means its ability to operate in three different modes of operation: only cold-mode, co-production mode with variable power/cold ratio and only power-mode. For a thermal boundary condition ($t_{hs,in}$ = 120 °C, $t_{cw,in}/t_{cw,out}$ = 32/37 °C and $t_{cf,in}/t_{cf,out}$ = 12/7 °C), the cycle produce 18.7 kW of mechanical power and 149.5 kW of cold with effective first law efficiency and effective exergy efficiency values of about 9.6% and 46.9% respectively when the vapour split ratio is 0.5. For the same thermal boundary conditions the cycle produces 32.3 kW of mechanical power with thermal and exergy efficiency values of 9.0% and 42.0% when it operates in only power-mode. For only cold-mode of operation it produces 293.6 kW of cooling effect at a COP of 0.626.

The second cycle configuration presented and analysed is the Single-Stage combined Absorption Power and Refrigeration Cycle with two Desorbers (SSAPRC-2D). This cycle

requires, for its activation, a relatively higher heat source temperature than the SSAPRC-P configuration. The power output of the cycle is slightly sensitive to the variation of the heat sink temperature at the operating conditions analysed. And the co-produced cooling output is highly sensitive for the heat sink temperature variation. The higher energy conversion efficiency (effective first law efficiency) is attained at conditions suitable for refrigeration and cold storage (deep-freezing) applications. It is found that at the optimum condition of heat source temperature about 148 °C, $t_{cw,in}/t_{cw,out}$ = 32/37 °C and $t_{cf,in}/t_{cf,out}$ =−5/−10 °C, a net mechanical power output of 20.8 kW and cooling capacity of 130.4 kW could be attained with effective first law efficiency and effective exergy efficiency values of the cycle about 18.7% and 36.4%, respectively.

Finally, in the range of low-grade heat source utilization, a Single-Stage combined Absorption Power and Refrigeration Cycle with Series flow arrangement between the power and refrigeration sub-cycles is presented (SSAPRC-S). The performance and operating conditions of this cycle are reported for typical operating conditions. It is more efficient and suitable for low heat sink temperature conditions (water cooled absorber and condenser: e.g. 27/32 °C) and when heat sources are available at relatively higher temperatures about 150 °C to 200 °C. At the base-case considered ($t_{hs,in}$ = 150 °C, $t_{cw,in}/t_{cw,out}$ = 27/32 °C, $t_{cf,in}/t_{cf,out}$ = 12/7 °C and pr_{exp} = 2.5), the cycle produces 31.6 kW of mechanical power and 319.6 kW cooling effect with effective first law efficiency and effective exergy efficiency values of about 17.0 and 66.0%, respectively.

An improved single-stage combined absorption power and refrigeration cycle is proposed by incorporating a relatively simple and well-known compression booster, mechanical compressor, between the absorber and evaporator of the SSAPRC-P configuration. A sensitivity analysis was conducted to investigate the effect of heat source inlet temperature on the cycle useful dual-outputs and performance indicators. This cycle (SSAPRC-COM) configuration is more flexible in operation than the basic single-stage combined absorption cycle configuration (SSAPRC-P) to cope with the varying condition of heat source temperatures. The simulation results showed that the SSAPRC-COM configuration can be driven by heat sources at very low temperatures (below 100 °C) for power production and can be flexible to utilize solar thermal collectors (for instance flat-plate and evacuated tube collectors) in cloudy days, in morning and evening as well. For some operating conditions, the possibilit-

ies of producing net mechanical power and cold simultaneously is also demonstrated. The above indicated technical and performance improvements have benefits from the economic point of view. These benefits include reduction of investment cost (small size rectifier for NH_3/H_2O based systems), utilization of low cost solar thermal collectors such as flat-plate collectors. These benefits are obtained without external electrical (or mechanical) energy input to drive the compression process instead it is driven by the energy developed by the expander. Further, cycle modification was proposed through the introduction of a non-mechanical work consuming compression booster (pressure device like vapour-ejector) in place of the mechanical compressor. This modified cycle (SSAPRC-EJE) configuration extends the operational working range of SSAPRC-P configuration particularly for air-cooled absorber and condenser operating conditions. At the same thermal boundary conditions, it has also better performance than SSAPRC-P configuration.

A new Two-Stage combined Absorption Power and Refrigeration Cycle with Series flow arrangement (TSAPRC-S) is proposed for the effective conversion of mid-grade heat sources at temperature below 300 °C into mechanical power and cold. Energetic and exergetic performance analysis of the TSAPRC-S configuration were conducted using NH_3/H_2O mixture as a working fluid. Furthermore, the performance improvement potential and extension of operational working range of the cycle was analysed through the introduction of pressure recovering devices such as vapour-liquid ejector. A physical-mathematical model was developed for TSAPRC-S configuration as well as the modified TSAPRC-S configuration for the purpose of performance simulation and analysis of the cycle. The performance simulation shows that:

- At the same operating conditions (e.g. $t_{hs,in} = 240$ °C, $t_{cw,in}/t_{cw,out} = 27/32$ °C and $t_{cf,in}/t_{cf,out} = 12/7$ °C and expander pressure ratio $pr_{exp} = 3.5$), the net mechanical power output and cooling capacity of the combined absorption cycle TSAPRC-S increases with the introduction of pressure device to operate the first-stage absorber at higher pressure than the low (evaporator) pressure of the cycle. The cycle also operates at higher energetic and exergetic efficiencies with the introduction of the pressure device.

- For the thermal boundary condition of $t_{hs,in} = 240$ °C, $t_{cw,in}/t_{cw,out} = 27/32$ °C and $t_{cf,in}/t_{cf,out} = 12/7$ °C and expander pressure ratio $pr_{exp} = 3.5$, the effective first law efficiency and effective exergy efficiency values are about (24.6%, 62.9%), (26.1%, 68.6%) and (27.1%, 72.9%) when the compression ratio of the pressure recovery device is set to 1.0, 1.5 and 2.0, respectively. The net power output and cooling capacity of the TSAPRC-S increases from 37.9 kW to 72.9 kW and 532.7 kW to 741.4 kW respectively when the compression ratio increases from 1.0 to 2.0. These performances are higher than the single-stage combined absorption cycles.

In power generating systems (combined absorption systems); work developing expansion devices are crucial components that limit the capacity and performance of the system. Scroll expanders are suggested in the literature for micro and small-scale capacity applications. In this study, a commercially available scroll compressor (Sanden TRSA05) was used by modifying it to work as expander. A semi-empirical model approach of Lemort et al. (2008) for scroll expanders was employed to develop a model for scroll expanders working with NH_3 (or NH_3/H_2O mixture with high concentration of NH_3). It is integrated into a combined absorption cycle for power and refrigeration applications. In this model real gas properties are used and therefore it is suitable for wet working fluids such as NH_3, H_2O and NH_3/H_2O mixtures. The model uses eight parameters (all are physically meaningful) determined from the geometry of the scroll expander and the expander's performance measurements.

A comparison between the values of the developed semi-empirical model estimation and experimental results for the main outputs shows a good agreement: within ±4% for mass flow rate, ±8% for the shaft power developed by the expander and ±4 K for exhaust temperature. This model is later scaled-up to estimate the performance of other scroll expanders (Sanden TRSA09 and TRSA12), with higher swept volume, in the same family series. Then, this semi-empirical model is integrated into a combined absorption power and refrigeration cycle (SSAPRC-2D) global model for the purpose of representing the performance of the work developing expansion device in the cycle. The energetic analysis of the combined absorption system (SSAPRC-2D system) shows that it can be achieved 14.8% - 17.8% effective first law efficiency with an overall isentropic efficiency of the expander

in the range of about 61% - 71% for the operating conditions considered in this study (expander inlet temperature and pressure of 105 °C - 130 °C and 857 kPa - 1554 kPa respectively). The expander rotational speed of 5000 rpm, absorber and evaporator exit temperatures of 30 °C and −5 °C, respectively, were kept constant in the energetic analysis of the SSAPRC-2D system.

Further, a new combined absorption system (based on SSAPRC-P configuration) using a scroll expander Sanden TRSA05 and three NH_3 based working fluid mixtures (NH_3/H_2O, $NH_3/LiNO_3$ and NH_3/NaSCN) are compared for the co-production of mechanical power and cold. The systems using a soluble solid (non-volatile) absorbent such as $LiNO_3$ and NaSCN are very competitive in comparison with the conventional NH_3/H_2O mixtures. Also in some operating conditions these working fluids have better performance than NH_3/H_2O system. For a heat source temperature of 120 °C, a sink temperature of 30 °C and a chilled fluid temperature of 0 °C, the net power obtained with these systems was about 5.9 kW with a heat input of 100 kW. The cooling outputs were in the range of 12 kW to 16 kW depending on the working fluid pairs employed in the system. The exergetic efficiency achieved was about 36% whereas the energetic efficiency was about 8.0%.

Although modifying commercially available scroll compressor to work as expander is the least expensive method to date, such type of scroll machines have a fixed built-in volume ratio optimized for refrigeration or air-conditioning applications not for power generating systems therefore they may suffer significantly from under-expansion irreversibilities.

Finally, Solar Absorption Power-Cooling Systems (SAPCSs) based on representative new combined absorption cycle (SSAPRC-P, for latent cooling output) and the well-known Goswami cycle were developed and compared for the same operating conditions. The non-conventional ammonia/salt mixtures ($NH_3/LiNO_3$ and NH_3/NaSCN) were employed in SSAPRC-P configuration. The cycles are partially activated by ETC, LFC and PTC solar thermal collectors. The combined absorption cycles were modelled with linear correlations obtained using performance data generated by using the developed thermodynamic model of the cycles. The models were implemented in TRNSYS software, to estimate the performance of the cycles, and the SAPCSs were simulated for a whole year. Result of the simulations show that it exist an optimum heat source temperature for each SAPCS depending on the combined absorption cycle and solar thermal collector technologies. This

optimum temperature is always below 100 °C for systems based on SSAPRC-P configurations, consequently it is concluded that ETC is the technology more suitable for systems with these cycle configurations. On the other hand, although the Goswami-ETC also leads to the best efficiency at 138 °C, some ETC collectors may not work properly at these temperature levels and then the PTC collector could be a better alternative.

In conclusion the results of this PhD thesis will contribute to the development of new class of absorption systems able to provide mechanical (or electrical) power and cold at different temperature levels simultaneously and/or alternatively by utilizing low and mid-grade heat sources below 300 °C. One particular interesting application of such type of combined absorption systems could be the efficient utilization of solar thermal collector installations throughout the year to produce variable amounts of electricity and cooling according to a given building demand in order to minimize the consumption of primary energy. In this way, this technology could contribute to the concept of new Net Zero-Energy Buildings (NZEB).

8.2 Future Outlook

Even though several detail analysis are presented in this thesis regarding the development of new class of combined absorption systems, further research in practical (experimental) as well as theoretical aspects are crucial to realize these systems into practice. Therefore, some future works are indicated as follows.

8.2.1 Practical study

- The least cost approach to demonstrate the proof of concept for the co-production of power and cold (latent cooling) using a single-stage absorption chiller driven by a thermal energy source could be done by modifying a commercially available small capacity NH_3/H_2O absorption chiller. The modification could be done through the introduction of an expander in parallel with the refrigerant stream. It helps to demonstrate practical experience on corrosion, operating pressure and temperature ranges, control issues and performance estimation previous to the construction of a real combined absorption cycle designed specifically for this purpose.

- Then, the next step could be the development of a prototype for the relatively simple configuration analysed in this thesis SSAPRC-P configuration and study its performance characteristics and operational flexibility at several typical operating conditions.

8.2.2 Theoretical study

From the theoretical point of view the future lines of research could be the following:

- Autonomous system for remote locations: One of the interesting applications of combined absorption systems presented in this thesis could be off-grid remote area applicants for cold storage and lighting proposes. Therefore, integration and optimization of a complete solar absorption power and refrigeration system with backup source, e.g. biomass, for a specific off-grid remote area could be the first step to implement such types of integrated systems in the future.

- Design of an expander specific for combined absorption power and refrigeration cycles: The current approach followed regarding the expander is to modify commercially available scroll compressor to work as expander, however, this approach has inefficiencies. Therefore, one possible approach could be to design a scroll expander working with NH_3 using the deterministic modelling approach.

- Design of an ejector specific for combined absorption power and refrigeration cycles: Detail modelling and designing of the vapour ejector incorporated in the proposed single-stage combined absorption power and refrigeration cycle (SSAPRC-EJE).

Bibliographic References

[1] Redrawing the energy-climate map. World Energy Outlook Special Report. International Energy Agency, OECD/IEA, 2013.

[2] BP Energy Outlook 2035, January 2014. *http://www.bp.com/energyoutlook, accessed on August 11, 2014.*

[3] *http://www.worldbank.org/en/topic/energy/overview, accessed on August 5, 2014.*

[4] Y. Tian, C.Y. Zhao. A review of solar collectors and thermal energy storage in solar thermal applications. Applied Energy, 104(April): 538-553, 2013.

[5] *https://eosweb.larc.nasa.gov/sse/, accessed on June 2, 2014.*

[6] S.A. Kalogirou. Solar thermal collectors and applications. Progress in Energy and Combustion Science, 30(3): 231-295, 2004.

[7] D. Barlev, R. Vidu, P. Stroeve. Review, Innovation in concentrated solar power. Solar Energy Materials and Solar Cells, 95(10): 2703-2725, 2011.

[8] I.A. Montero. Modelización de sistemas de refrigeración por absorción con captadores solares de concentración. PhD Thesis (in Spanish), Department of Mechanical Engineering, Universitat Rovira I Virgili, Spain, 2012.

[9] D.S. Kim, C.A. Infante Ferreira. Review, Solar refrigeration options – a state-of-the-art review. International Journal of Refrigeration, 31(1): 3-15, 2008.

[10] *http://www.nrel.gov/csp/solarpaces/project_ detail.cfm/projectID=159, accessed on June 12, 2014.*

[11] *http://energy.gov/articles/celebrating-completion-worlds-largest-concentrating-solar-power-plant, accessed on June 12, 2014.*

Bibliographic References

[12] R. Bertani. Geothermal power generation in the world 2005-2010 update report. Geothermics, 41(January): 1-29, 2012.

[13] International Energy Agency. Technology roadmap bioenergy for heat and power. *http://www.iea.org/publications/freepublications/publication/bioenergy.pdf, accessed on June 15, 2014.*

[14] C. Somayaji. First and second law analysis of Organic Rankine Cycle. PhD Thesis, Department of Mechanical Engineering, Mississippi State University, USA, 2008.

[15] S. Quoilin, M. Van Den Broek, S. Declaye, P. Dewallef, V. Lemort. Techno-economic survey of Organic Rankine Cycle (ORC) systems. Renewable and Sustainable Energy Reviews, 22(June): 168-186, 2013.

[16] H. Chen, D.Y. Goswami, E.K. Stefanakos. A review of thermodynamic cycles and working fluids for the conversion of low-grade heat. Renewable and Sustainable Energy Reviews, 14(9): 3059-3067, 2010.

[17] F. Velez, J.J. Segovia, M.C. Martin, G. Antolin, F. Chejne, A. Quijano. A technical, economical and market review of organic Rankine cycles for the conversion of low-grade heat for power generation. Renewable and Sustainable Energy Reviews, 16(6): 4175-4189, 2012.

[18] A.I. Papadopoulos, M. Stijepovic, P. Linke. On the systematic design and selection of optimum working fluids for Organic Rankine Cycles. Applied Thermal Engineering, 30(6-7): 760-769, 2010.

[19] J. Bao, L. Zhao. A review of working fluid and expander selections for organic Rankine cycle. Renewable and Sustainable Energy Reviews, 24(August): 325-342, 2013.

[20] J.C. Bruno, J. López-Villada, E. Letelier, S. Romera, A. Coronas. Modelling and optimisation of solar organic Rankine cycle engines for reverse osmosis desalination. Applied Thermal Engineering, 28(17-18): 2212-2226, 2008.

[21] B. Saleh, G. Koglbauer, M. Wendland, J. Fischer. Working fluids for low-temperature organic Rankine cycles. Energy, 32(7): 1210-1221, 2007.

[22] M. Chys, M. van den Broek, B. Vanslambrouck, M. De Paepe. Potential of zeotropic mixtures as working fluids in organic Rankine cycles. Energy, 44(1): 623-632, 2012.

[23] S. Aghahosseini, I. Dincer. Comparative performance analysis of low-temperature Organic Rankine Cycle (ORC) using pure and zeotropic working fluids. Applied Thermal Engineering, 54(1): 35-42, 2013.

[24] H. Chen. The conversion of low-grade heat into power using supercritical Rankine cycles. PhD Thesis, Department of Chemical and Biomedical Engineering, University of South Florida, USA, 2010.

[25] S. Quoilin, M. Orosz, H. Hemond, V. Lemort. Performance and design optimization of a low-cost solar organic Rankine cycle for remote power generation. Solar Energy, 85(5): 955-966, 2011.

[26] M.S. Orosz, A.V. Mueller, B.J. Dechesne, H.F. Hemond. Geometric design of scroll expanders optimized for small organic Rankine cycles. ASME-Journal of Engineering for Gas Turbines and Power, 135(4): 042303(6 pages), Paper No: GTP-12-1018, 2013.

[27] V.E. Styliaras. A freon-ammonia comparison applied in a mixed power cycle. Heat Recovery Systems and CHP, 15(6): 601-603, 1995.

[28] S. Vijayaraghavan, D.Y. Goswami. Organic working fluids for a combined power and cooling cycle. ASME-Journal of Energy Resources Technology, 127: 125-130, 2005.

[29] H. Abed, K. Atashkari, A. Niazmehr, A. Jamali. Thermodynamic optimization of combined power and refrigeration cycle using binary organic working fluid. International Journal of Refrigeration, 36(8): 2160-2168, 2013.

[30] J.D. Maloney, R.C. Robertson. Thermodynamic study of heat power cycles. Oak Ridge National Laboratory Report. CF-53-8-43, 1953.

[31] A.I. Kalina. Generation of energy by means of a working fluid, and regeneration of a working fluid. United States Patent 4346561. Filed date: August 31, 1982.

[32] A.I. Kalina. Combined cycle and waste heat recovery power systems based on a novel thermodynamic energy cycle utilizing low-temperature heat for power generation.

ASME Proceedings, Joint Power Generation Conference, Indianapolis, Indiana, USA, Paper No. 83-JPGC-GT-3, pp. V001T02A003 1-5, 1983.

[33] A.I. Kalina. Combined-cycle system with novel bottoming cycle. ASME-Journal of Engineering for Gas Turbines and Power, 106(4): 737-742, 1984.

[34] X. Zhang, M. He, Y. Zhang. A review of research on the Kalina cycle. Renewable and Sustainable Energy Reviews, 16(7): 5309-5318, 2012.

[35] A.I. Kalina, M. Tribus. The Kalina power cycles, A progress report. In: Proceedings of the American Power Conference, Chicago, Illinois, USA, pp. 5-21, 1989.

[36] H.A. Mlcak. An introduction of the Kalina cycle. PWR-Vol. 30. In: Proceedings of the International Joint Power Generation Conference, Houston, Texas, USA, pp. 1-11, 1996.

[37] A.I. Kalina. Novel power cycle for combined systems and utility power plants. In: Proceedings of the Eighth Annual Industrial Energy Technology Conference, Houston, Texas, June 17-19, 1986.

[38] R.L. Bannister, G.J. Silvestri Jr., A. Hizume, T. Fujikawa. High-temperature supercritical steam turbines. Mechanical Engineering, February, 1987.

[39] H.D. Madhawa, M. Golubovic, W.M. Worek, Y. Ikegami. The performance of the Kalina cycle system 11 (KCS-11) with low temperature heat sources. ASME-Journal of Energy Resources Technology, 129(3): 243-247, 2007.

[40] A.I. Kalina, H. Leibowitz. Application of the Kalina cycle technology to geothermal power generation. Geothermal Research Council annual meeting, Santa Rosa, CA, October, 1989.

[41] P.K. Nag, A.V.S.S.K.S. Gupta. Exergy analysis of the Kalina cycle. Applied Thermal Engineering, 18(6): 427-439, 1998.

[42] S. Ogriseck. Integration of Kalina cycle in a combined heat and power plant, a case study. Applied Thermal Engineering, 29(14-15): 2843-2848, 2009.

[43] H.A. Mlcak. Kalina Cycle®Concepts for low temperature geothermal. Geothermal Resources Council Transactions, Vol. 26, September 22-25, 2002.

[44] *http://www.wasabienergy.com, accessed on May 28, 2014.*

[45] D.S. Kim. Solar Absorption Cooling. PhD Thesis, Technische Universiteit Delft, The Netherlands, 2008.

[46] P. Srikhirin, S. Aphornratana, S. Chungpaibulpatana. A review of absorption refrigeration technologies. Renewable and Sustainable Energy Reviews, 5(4): 343-372, 2001.

[47] X. Meng, D. Zheng, J. Wang, X. Li. Energy saving mechanism analysis of the absorption-compression hybrid refrigeration cycle. Renewable Energy, 57(September): 43-50, 2013.

[48] G. Alefeld, R. Radermacher. Heat Conversion Systems. Boca Raton, Florida: CRC Press, Inc., 1994.

[49] F. Ziegler. Recent developments and future prospects of sorption heat pump systems. International Journal of Thermal Sciences, 38(3): 191-208, 1999.

[50] F. Ziegler. State of the art in sorption heat pumping and cooling technologies. International Journal of Refrigeration, 25(4): 450-459, 2002.

[51] B.H. Gebreslassie, M. Medrano, D. Boer. Exergy analysis of multi-effect water–LiBr absorption systems: From half to triple effect. Renewable Energy, 35(8): 1773-1782, 2010.

[52] C.P. Jawahar, R. Saravanan. Generator absorber heat exchange based absorption cycle–A review. Renewable and Sustainable Energy Reviews, 14(8): 2372-2382, 2010.

[53] https://www.khi.co.jp/english/news/detail/20130221_1e.html., *accessed on August 17, 2014.*

[54] R.E. Critoph, Y. Zhong. Review of trends in solid sorption refrigeration and heat pumping technology. Proceedings of the Institution of Mechanical Engineers, Part E: Journal of Process Mechanical Engineering, 219(3): 285-300, 2005.

[55] D.W. Wu, R.Z. Wang. Combined cooling, heating and power: A review. Progress in Energy and Combustion Science, 32(5-6): 459-495, 2006.

[56] M.S. Fernandes, G.J.V.N. Brites, J.J. Costa, A.R. Gaspar, V.A.F. Costa. Review and future trends of solar adsorption refrigeration systems. Renewable and Sustainable Energy Reviews, 39(November): 102-123, 2014.

[57] J. Deng, R.Z. Wang, G.Y. Han. A review of thermally activated cooling technologies for combined cooling, heating and power systems. Progress in Energy and Combustion Science, 37(2): 172-203, 2011.

[58] R.Z. Wang, R.G. Oliveira. Adsorption refrigeration–An efficient way to make good use of waste heat and solar energy. Progress in Energy and Combustion Science, 32(4): 424-458, 2006.

[59] http://www.greenchiller.de*, accessed on August 17, 2014.*

[60] N. Enteria, K. Mizutani. The role of the thermally activated desiccant cooling technologies in the issue of energy and environment. Renewable and Sustainable Energy Reviews, 15(4): 2095-2122, 2011.

[61] Y. Yin, J. Qian, X. Zhang. Recent advancements in liquid desiccant dehumidification technology. Renewable and Sustainable Energy Reviews, 31(March): 38-52, 2014.

[62] X. Chen, S. Omer, M. Worall, S. Riffat. Recent developments in ejector refrigeration technologies. Renewable and Sustainable Energy Reviews, 19(March): 629-651, 2013.

[63] J.M. Abdulateef, K. Sopian, M.A. Alghoul, M.Y. Sulaiman. Review on solar-driven ejector refrigeration technologies. Renewable and Sustainable Energy Reviews, 13(6-7): 1338-1349, 2009.

[64] J.S. Brown, P.A. Domanski. Review of alternative cooling technologies. Applied Thermal Engineering, 64(1-2): 252-262, 2014.

[65] W.B. Gosney. Principle of refrigeration. Cambridge, United Kingdom: Cambridge University Press, 1982.

[66] *http://www.iea.org/publications/freepublications/publication/chp_report.pdf, accessed on June 4, 2014.*

[67] M. Liu, Y. Shi, F. Fang. Combined cooling, heating and power systems: A survey. Renewable and Sustainable Energy Reviews, 35(July): 1-22, 2014.

[68] G. Chicco, P. Mancarella. Distributed multi-generation: A comprehensive view. Renewable and Sustainable Energy Reviews, 13(3): 535-551, 2009.

[69] M. Jradi, S. Riffat. Tri-generation systems: Energy policies, prime movers, cooling technologies, configurations and operation strategies. Renewable and Sustainable Energy Reviews, 32(April): 396-415, 2014.

[70] COGEN Europe. A guide to cogeneration. *http://www.cogeneurope.eu/, accessed on June 4, 2014.*

[71] F. Ziegler. Novel cycles for power and refrigeration. In: Proceedings of the 1st European Conference on Polygeneration, Tarragona, Spain, October 16-17, pp. 169-181, 2007.

[72] ASHRAE, Handbook of Fundamentals. American Society of Heating, Refrigeration and Air-Conditioning Engineers, Inc., Atlanta (GA), 2009.

[73] S. Vijayaraghavan, D.Y. Goswami. On evaluating efficiency of a combined power and cooling cycle. ASME-Journal of Energy Resources Technology, 125(3): 221-227, 2003.

[74] O.M. Ibrahim, S.A. Klein. Absorption power cycles. Energy, 21(1): 21-27, 1996.

[75] Y. Amano, T. Suzuki, T. Hashizume, M. Akiba, Y. Tanzawa, A. Usui. A hybrid power generation and refrigeration cycle with ammonia-water mixture. In: Proceedings of the International Joint Power Generation Conference, Florida, USA, pp. 1-6, 2000.

[76] S. Dejfors, E. Thorin, G. Svedberg. Ammonia-water power cycles for direct-fired cogeneration applications. Energy Conversion and Management, 39(16-18): 1675-1681, 1998.

Bibliographic References

[77] E.D. Rogdakis, K.A. Antonopoulos. A high efficiency NH_3/H_2O absorption power cycle. Heat Recovery Systems and CHP, 11(4): 263-275, 1991.

[78] V. Hassani, J. Dickens, Y. Parent. Ammonia/water condensation test: plate fin heat exchanger (absorber/cooler). NREL, Golden CO. September, 2001.

[79] M. Jonsson. Advanced power cycles with mixtures as the working fluid. PhD Thesis, Department of Chemical Engineering and Technology, Energy Processes, KTH Royal Institute of Technology, Sweden, 2003.

[80] M. Jonsson, E. Thorin,G. Svedberg. Gas engine bottoming cycles with ammonia-water mixtures as working fluid. In: Proceedings of the world energy research symposium, Florence, Italy, pp. 1-11, 1994.

[81] A.I. Kalina, H.M. Leibowitz. Application of the Kalina cycle technology to geothermal power generation. Geothermal Resources Council Transactions, 13(October): 605-611, 1989.

[82] E.K. Olsson, E.B. Thorin, A.S. Dejfors, G. Svedberg. Kalina cycles for power generation from industrial waste heat. In: Proceedings of the world energy research symposium, Florence, Italy, pp. 39-49, 1994.

[83] Y.M. Park, R.E. Sonntag. A preliminary study of the Kalina power cycle in connection with a combined cycle system. International Journal of Energy Research, 14(2): 153-162, 1990.

[84] E. Thorin. Power cycles with ammonia–water mixtures as working fluid. Analysis of different applications and the influence of thermophysical properties. PhD thesis, Department of Chemical Engineering and Technology, Energy Processes, KTH Royal Institute of Technology, Sweden, 2000.

[85] M. Jonsson, J. Yan. Exergy and pinch analysis of diesel engine bottoming cycles with ammonia-water mixtures as working fluid. International Journal of Applied Thermodynamics, 3(2): 57-71, 2000.

[86] C.H. Marston, M. Hyre. Gas turbine bottoming cycles: triple-pressure steam versus

Kalina. ASME-Journal of Engineering for Gas Turbines and Power, 117(1): 10-15, 1995.

[87] Y.M. El-Sayed, M. Tribus. Thermodynamic properties of water-ammonia mixtures - Theoretical implementation for use in power cycles analysis. ASME-Analysis of Energy Systems–Design and Operation, The Winter Annual Meeting of the ASME, 1(November 17-22): 89-95, 1985.

[88] O.M. Ibrahim, S.A. Klein. Thermodynamic properties of ammonia-water mixtures. ASHRAE Transactions Symposia, 99: 1495-502, 1993.

[89] Y.M. Park. A Generalized equation of state approach to the thermodynamic properties of ammonia-water mixtures with applications. PhD Thesis, University of Michigan, USA, 1988.

[90] S.S. Stecco, U. Desideri. A thermodynamic analysis of the Kalina cycles: Comparisons, Problems and Perspectives. ASME-International Gas Turbine and Aeroengine Congress and Exposition, Vol. 4: Heat Transfer; Electric Power; Industrial and Cogeneration Toronto, Ontario, Canada, June 4-8, 1989.

[91] T.M. Smolen, D.B. Manley, B.E. Poling. Vapor-liquid equilibrium data for the ammonia-water system and its description with a modified cubic equation of state. Journal of Chemical and Engineering Data, 36(2): 202-208, 1991.

[92] M. Moshfeghian, A. Shariat, R.N. Maddox. Prediction of refrigerant thermodynamic properties by equations of state: vapour liquid equilibrium behaviour of binary mixtures. Fluid Phase Equilibiria, 80(November): 33-44, 1992.

[93] B. Ziegler, Ch. Trepp. Equation of state for ammonia-water mixtures. International Journal of Refrigeration, 7(2): 101-106, 1984.

[94] Y. Ikegami, T. Nishida, M. Uto, H. Uehara. Thermophysical properties of ammonia/water by the BWR Equation of State. In: Proceedings of the 13th International Japan Symposium on thermophysical properties, pp. 213-216, 1992.

[95] D.G. Friend, A.L. Olson, A. Nowarski. Standard thermophysical properties of the

ammonia-water binary fluid. In: Proceedings of the 12th international conference on the properties of water and steam, Orlando, Florida, 1994.

[96] J. Patek, J. Klomfar. Simple functions for fast calculations of selected thermodynamic properties of the ammonia-water system. International Journal of Refrigeration, 18(4): 228-234, 1995.

[97] R. Tillner-Roth, D.G. Friend. A Helmholtz free-energy formulation of the thermodynamic properties of the mixture water + ammonia. Journal of Physical and Chemical Reference Data, 27(1): 63-96, 1998.

[98] F. Xu, D.Y. Goswami. Thermodynamic properties of ammonia-water mixtures for power-cycle applications. Energy, 24(6): 525-536, 1999.

[99] P.C. Gillespie, W.V. Wilding, G.M. Wilson. Vapour–liquid equilibrium measurements on the ammonia–water system from 313 K to 589 K. AIChE Symposium Series, 83: 97, 1987.

[100] E. Thorin, C. Dejfors, G. Svedberg. Thermodynamic properties of ammonia–water mixtures for power cycles. International Journal of Thermophysics, 19(2): 501-510, 1998.

[101] A. Nowarski, D.G. Friend. Application of the extended corresponding states method to the calculation of the ammonia–water mixture thermodynamic surface. International Journal of Thermophysics, 19(4): 1133-1142, 1998.

[102] E. Thorin. Thermophysical properties of ammonia-water mixtures for prediction of heat transfer areas in power cycles. International Journal of Thermophysics, 22(1): 201-214, 2001.

[103] Kh. Mejbri, A. Bellagi. Modelling of the thermodynamic properties of the water–ammonia mixture by three different approaches. International Journal of Refrigeration, 29(2): 211-218, 2006.

[104] N.G. Polikhronidi, I.M. Abdulagatov, R.G. Batyrova, G.V. Stepanov. PVT measurements of water–ammonia refrigerant mixture in the critical and super-critical regions. International Journal of Refrigeration, 32(8): 1897-1913, 2009.

[105] T. Berlitz, H. Plank, F. Ziegler, R. Kahn. An ammonia-water absorption refrigerator with a large temperature lift for combined heating and cooling. International Journal of Refrigeration, 21(3): 219-229, 1998.

[106] W. Wu, B. Wang, W. Shi, L. Xianting. An overview of ammonia-based absorption chillers and heat pumps. Renewable and Sustainable Energy Reviews, 31(March): 681-707, 2014.

[107] M.K. Aggarwal, R.S. Agarwal. Thermodynamic properties of lithium nitrate-ammonia mixtures. International Journal of Energy Research, 10(1): 59-68, 1986.

[108] C.A. Infante Ferreira. Thermodynamic and physical property data equations for ammonia-lithium nitrate and ammonia-sodium thiocyanate solutions. Solar Energy, 32(2): 231-236, 1984.

[109] S. Libotean, D. Salavera, M. Valles, X. Esteve, A. Coronas. Vapour-liquid equilibrium of ammonia+lithium nitrate+water and ammonia+lithium nitrate solution from (293.15 to 353.15) K. Journal of Chemical Engineering Data, 52(3): 1050-1055, 2007.

[110] S. Libotean, A. Martin, D. Salavera, M. Valles, X. Esteve , A. Coronas. Densities, viscosities, and heat capacities of ammonia + lithium nitrate and ammonia + lithium nitrate + water solutions between (293.15 and 353.15) K. Journal of Chemical Engineering Data, 53(10): 2383-2388, 2008.

[111] L. Garousi Farshi, C.A. Infante Ferreira, S.M.S. Mahmoudi, M.A. Rosen. First and second law analysis of ammonia/salt absorption refrigeration systems. International Journal of Refrigeration, 40(April): 111-121, 2013.

[112] E.D. Rogdakis, K.A. Antonopoulos. Thermodynamic cycle, correlations and nomograph for NH_3–NaSCN absorption refrigeration systems. Heat Recover Systems and CHP, 15(6): 591-599, 1995.

[113] S.K. Chaudhari, D. Salavera, A. Coronas. Densities, viscosities, heat capacities, and vapor-liquid equilibria of ammonia + sodium thiocyanate solutions at several temperatures. Journal of Chemical Engineering Data, 56(6): 2861-2869, 2011.

Bibliographic References

[114] F.A. Al-Sulaiman, F. Hamdullahpur, I. Dincer. Performance assessment of a novel system using parabolic trough solar collectors for combined cooling, heating, and power production. Renewable Energy, 48(December): 161-172, 2012.

[115] M.D. Schicktanz, J. Wapler, H.-M. Henning. Primary energy and economic analysis of combined heating, cooling and power systems. Energy, 36(1): 575-585, 2011.

[116] A. Habibzadeh, M.M. Rashidi, N. Galanis. Analysis of a combined power and ejector-refrigeration cycle using low temperature heat. Energy Conversion and Management, 65(January): 381-391, 2013. Global Conference on Renewable energy and Energy Efficiency for Desert Regions 2011 "GCREEDER 2011".

[117] J. Wang, P. Zhao, X. Niu, Y. Dai. Parametric analysis of a new combined cooling, heating and power system with transcritical CO_2 driven by solar energy. Applied Energy, 94(June): 58-64, 2012.

[118] D.Y. Goswami. Solar thermal power – Status and future directions. In: Proceedings of the 2nd ISHMT-ASME Heat and Mass Transfer Conference, S. Murthy and Y. Jaluria, eds., Tata McGraw Hill, New Delhi, India, pp. 57-60, 1995.

[119] D.Y. Goswami. Solar thermal power technology: Present status and ideas for the future. Energy Sources, 20(2): 137-145, 1998.

[120] D.Y. Goswami and F. Xu. Analysis of a new thermodynamic cycle for combined power and cooling using low and mid temperature solar collectors. Journal of Solar Energy Engineering, 121(2): 91-97, 1999.

[121] S. Lu, D.Y. Goswami. Theoretical analysis of ammonia-based combined power/refrigeration cycle at low refrigeration temperatures. ASME-International Solar Energy Conference, Reno, Nevada, USA, June 15-20, pp. 117-125, 2002.

[122] S. Lu, D.Y. Goswami. Optimization of a novel combined power/refrigeration thermodynamic cycle. Journal of Solar Energy Engineering, 125(2): 212-217, 2003.

[123] C. Martin, D.Y. Goswami. Effectiveness of cooling production with a combined power and cooling thermodynamic cycle. Applied Thermal Engineering, 26(5-6): 576-582, 2006.

[124] S.M. Sadrameli and D.Y. Goswami. Optimum operating conditions for a combined power and cooling thermodynamic cycle. Applied Energy, 84(3): 254-265, 2007.

[125] Aspen Plus, Version 12.1. Ten Canal Park, Cambridge (MA) 02141: Aspen Technology, Inc.; 2004.

[126] C. Martin. Study of cooling production with a combined power and cooling thermodynamic cycle. PhD Thesis, Department of Mechanical and Aerospace Engineering, University of Florida, USA, 2004.

[127] G. Demirkaya, R.V. Padilla, D.Y. Goswami, E. Stefanakos, M.M. Rahman. Analysis of a combined power and cooling cycle for low-grade heat sources. International Journal of Energy Research, 35(13): 1145-1157, 2011.

[128] Chemcad. Version 6.1.2: Process flow sheet simulator. Chemstations Inc., 2008.

[129] F. Xu, D.Y. Goswami, S.S. Bhagwat. A combined power/cooling cycle. Energy, 25(3): 233-246, 2000.

[130] M. Pouraghaie, K. Atashkari, S.M. Besarati, N. Nariman-zadeh. Thermodynamic performance optimization of a combined power/cooling cycle. Energy Conversion and Management, 51(1): 204-211, 2010.

[131] A. Vidal, R. Best, R. Rivero, J. Cervantes. Analysis of a combined power and refrigeration cycle by the exergy method. Energy, 31(15): 3401-3414, 2006.

[132] A.A. Hasan, D.Y. Goswami, S. Vijayaraghavan. First and second law analysis of a new power and refrigeration thermodynamic cycle using a solar heat source. Solar Energy, 73(5): 385-393, 2002.

[133] S. Vijayaraghavan, D.Y. Goswami. A combined power and cooling cycle modified to improve resource utilization efficiency using a distillation stage. Energy, 31(8-9): 1177-1196, 2006.

[134] S. Vijayaraghavan. Thermodynamic studies on alternate binary working fluid combinations and configurations for a combined power and cooling cycle. PhD Thesis,

Department of Mechanical and Aerospace Engineering, University of Florida, USA, 2003.

[135] T.F. Edgar, D.M. Himmelblau, L.S. Lasdon. Optimisation of chemical processes. New York: MaGraw-Hill; 2001.

[136] V. Zare, S.M.S. Mahmoudi, M. Yari. Ammonia-water cogeneration cycle for utilizing waste heat from the GT-MHR plant. Applied Thermal Engineering, 48(December): 176-185, 2012.

[137] V. Zare, S.M.S. Mahmoudi, M. Yari, M. Amidpour. Thermoeconomic analysis and optimization of an ammonia-water power/cooling cogeneration cycle. Energy, 47(1): 271-283, 2012.

[138] G. Demirkaya, S. Besarati, R.V. Padilla, A.R. Archibold, D.Y. Goswami, M.M. Rahman, E.L. Stefanakos. Multi-objective optimization of a combined power and cooling cycle for low-grade and midgrade heat sources. ASME-Journal of Energy Resources Technology, 134(3): 032002-032002-8, 2012.

[139] R.V. Padilla, A.R. Archibold, G. Demirkaya, S. Besarati, D.Y. Goswami, M.M. Rahman, E.L. Stefanakos. Performance analysis of a Rankine cycle integrated with the Goswami combined power and cooling cycle. ASME-Journal of Energy Resources Technology, 134(3): 032001-032001-8, 2012.

[140] D.C. Erickson, G. Anand, I. Kyung. Heat activated dual function absorption cycle. ASHRAE Transactions, 110(1): 515-524, 2004.

[141] N. Zhang, R. Cai, N. Lior. A novel ammonia-water cycle for power and refrigeration cogeneration. In: Proceedings of the ASME advanced energy systems, Anaheim, California, USA, November 13-19, pp. 183-196, 2004.

[142] J. Wang, Y. Dai, L. Gao. Parametric analysis and optimization for a combined power and refrigeration cycle. Applied Energy, 85(11): 1071-1085, 2008.

[143] J. Wang, Y. Dai, T. Zhang, S. Ma. Parametric analysis for a new combined power and ejector-absorption refrigeration cycle. Energy, 34(10): 1587-1593, 2009.

[144] M. Liu, N. Zhang. Proposal and analysis of a novel ammonia-water cycle for power and refrigeration cogeneration. Energy, 32(6): 961-970, 2007.

[145] D. Zheng, B. Chen, Y. Qi, H. Jin. Thermodynamic analysis of a novel absorption power/cooling combined-cycle. Applied Energy, 83(4): 311-323, 2006.

[146] N. Zhang, N. Lior. Methodology for thermal design of novel combined refrigeration/power binary fluid systems. International Journal of Refrigeration, 30(6): 1072-1085, 2007.

[147] N. Zhang, N. Lior. Development of a novel combined absorption cycle for power generation and refrigeration. ASME. Journal of Energy Resources Technology, 129(September): 254-265, 2007.

[148] B. Kiani, A. Akisawa, T. Kashiwagi. Thermodynamic analysis of load-leveling hyper energy converting and utilization system. Energy, 33(3): 400-409, 2008.

[149] C.P. Jawahar, R. Saravanan. Generator absorber heat exchange based absorption cycle – A review. Renewable and Sustainable Energy Reviews, 14(8): 2372-2382, 2010.

[150] A.S. Mehr, M. Yari, S.M.S, Mahmoudi, A. Soroureddin. A comparative study on the GAX based absorption refrigeration systems: SGAX, GAXH and GAX-E. Applied Thermal Engineering, 44 (November): 29-38, 2012.

[151] C.P. Jawahar, R. Saravanan, J.C. Bruno, A. Coronas. Simulation studies on gax based Kalina cycle for both power and cooling applications. Applied Thermal Engineering, 50(2): 1522-1529, 2013.

[152] G. Tamm, D.Y. Goswami, S. Lu, A.A. Hasan. Theoretical and experimental investigation of an ammonia-water power and refrigeration thermodynamic cycle. Solar Energy, 76 (1-3): 217-228, 2004.

[153] G. Tamm, D.Y. Goswami. Novel combined power and cooling thermodynamic cycle for low temperature heat sources, Part II: Experimental investigation. Journal of solar energy engineering, 125(2): 223-229, 2003.

Bibliographic References

[154] G.O. Tamm. Experimental investigation of an ammonia-based combined power and cooling cycle. PhD Thesis, Department of Mechanical and Aerospace Engineering, University of Florida, USA, 2003.

[155] N. Goel. Theoretical and experimental analysis of absorption-condensation in a combined power and cooling cycle. PhD thesis, Department of Mechanical and Aerospace Engineering, University of Florida, USA, 2005.

[156] G. Demirkaya. Theoretical and experimental analysis of power and cooling cogeneration utilizing low temperature heat sources. PhD Thesis, Department of Mechanical Engineering, University of South Florida, USA, 2011.

[157] W. Han, Q. Chen, L. Sun, S. Ma, T. Zhao, D. Zheng, H. Jin. Experimental studies on a combined refrigeration/power generation system activated by low-grade heat. Energy, 74(September): 59-66, 2014.

[158] REFPROP. Version 9.0: Reference Fluid Thermodynamic and Transport Properties Database. National Institute of Standards and Technology (NIST), Gaithersburg, USA, 2010. *http://www.nist.gov/srd/nist23.cfm, accessed on March 12, 2013.*

[159] T.J. Kotas. The exergy method of thermal plant analysis. Malabar, FL: Krieger Publish Company, 1995.

[160] I. Dincer, M.A. Rosen. Exergy: energy, environment and sustainable development. 2nd Edition, Elsevier: Oxford, UK, 2013.

[161] P. Ahmadi, M.A. Rosen, I. Dincer. Multi-objective exergy-based optimization of a polygeneration energy system using an evolutionary algorithm. Energy, 46(1): 21-31, 2012.

[162] C. Dejfors, G. Svedberg. Second law analysis of ammonia-water power cycle for direct-fired cogeneration application. International Journal of Applied Thermodynamics, 2(3): 125-131, 1999.

[163] J. Aman, DS-K Ting, P. Henshaw. Residential solar air conditioning: Energy and exergy analyses of an ammonia-water absorption cooling system. Applied Thermal Engineering, 62(2): 424-432, 2014.

[164] L. Zhu, J. Gu. Second law-based thermodynamic analysis of ammonia/sodium thiocyanate absorption system. Renewable Energy, 35(9): 1940-1946, 2010.

[165] W. Wagner, A. Pruss. The IAPWS formulation 1995 for the thermodynamic properties of ordinary water substance for general and scientific use. Journal of Physical and Chemical Reference Data, 31(2): 387-538, 2002.

[166] H. Moser, R. Rieberer. First and second law analysis of a laboratory ammonia/water absorption heat pump. International Journal of Air-Conditioning and Refrigeration, 18(2): 117-129, 2010.

[167] A. Melinder. Thermophysical properties of liquid secondary refrigerants, tables and diagrams for the refrigeration industry, IIF/IIR, Paris, 1997.

[168] Y.T. Kang, H. Hong, K.S. Park. Performance analysis of advanced hybrid GAX cycles: HGAX. International Journal of Refrigeration, 27(4): 442-448, 2004.

[169] A.R. Kumar, M. Udayakumar. Simulation studies on GAX absorption compression cooler. Energy Conversion and Management, 48(9): 2604-2610, 2007.

[170] A.R. Kumar, M. Udayakumar. Studies of compressor pressure ratio effect on GAXAC (generator-absorber-exchange absorption compression) cooler. Applied Energy, 85(12): 1163-1172, 2008.

[171] R. Ventas, A. Lecuona, A. Zacarias, M. Venegas. Ammonia-lithium nitrate absorption chiller with an integrated low-pressure compression booster cycle for low driving temperatures. Applied Thermal Engineering, 30(11-12), 1351-1359, 2010.

[172] R. Ayala, C.L. Heard, F.A. Holland. Ammonia/lithium nitrate absorption/compression refrigeration cycle. Part I. Simulation. Applied Thermal Engineering, 17(3), 223-233, 1997.

[173] R. Ayala, C. L. Heard, F. A. Holland. Ammonia/lithium nitrate absorption/compression refrigeration cycle. Part II. Experimental. Applied Thermal Engineering, 18(8): 661-670, 1998.

[174] J.S. Kim, F. Ziegler, H. Lee. Simulation of the compressor-assisted triple-effect H_2O/LiBr absorption cooling cycles. Applied Thermal Engineering, 22(3): 295-308, 2002.

[175] D. Boer, M. Valles, A. Coronas. Performance of double effect absorption compression cycles for air-conditioning using methanol-TEGDME and TFE-TEGDME systems as working fluids. International Journal of Refrigeration, 21(7): 542-555, 1998.

[176] M. Bourouis, M. Nogues, D. Boer, A. Coronas. Industrial heat recovery by absorption/compression heat pump using TFE-H_2O-TEGDME working mixture. Applied Thermal Engineering, 20(4): 355-369, 2000.

[177] X. Meng, D. Zheng, J. Wang, X. Li. Energy saving mechanism analysis of the absorption-compression hybrid refrigeration cycle. Renewable Energy, 57(September): 43-50, 2013.

[178] G.K. Alexis, E.D. Rogdakis. Performance characteristics of two combined ejector-absorption cycles. Applied Thermal Engineering, 22(1): 97-106, 2002.

[179] C. Vereda, R. Ventas, A. Lecuona, M. Venegas. Study of an ejector-absorption refrigeration cycle with an adaptable ejector nozzle for different working conditions. Applied Energy, 97(September): 305-312, 2012.

[180] C. Vereda, R. Ventas, A. Lecuona, R. López. Single-effect absorption refrigeration cycle boosted with an ejector-adiabatic absorber using a single solution pump. International Journal of Refrigeration, 38(February): 22-29, 2014.

[181] R. Sirwan, M.A. Alghoul, K. Sopian, Y. Ali, J. Abdulateef. Evaluation of adding flash tank to solar combined ejector-absorption refrigeration system. Solar energy, 91(May): 283-296, 2013.

[182] X. Chen, S. Omer, M. Worall, S. Riffat. Recent developments in ejector refrigeration technologies. Renewable and Sustainable Energy Reviews, 19(March): 629-651, 2013.

[183] X. Li, Q. Zhang, X. Li. A Kalina cycle with ejector. Energy, 54(June): 212-219, 2013.

[184] D.S. Ayou, J.C. Bruno, A. Coronas. New power and cooling absorption cycles. Intentional Journal of Thermal and Environmental Engineering, 5(2): 135-143, 2013.

[185] *http://www.energent.net/technology/euler-turbine.html, accessed on September 19, 2014.*

[186] S. Quoilin. Sustainable energy conversion through the use of organic Rankine cycles for waste heat recovery and solar applications. PhD Thesis, Department of Aerospace and Mechanical Engineering, Université de Liège, Belgium, 2011.

[187] R.B. Peterson, H. Wang, T. Herron. Performance of small-scale regenerative Rankine power cycle employing a scroll expander. In: Proceedings of the Institution of Mechanical Engineers-Part A: Journal of Power and Energy, 222(3): 271-282, 2008.

[188] G. Qiu, H. Liu, S. Riffat. Expanders for micro-CHP systems with organic Rankine cycle. Applied Thermal Engineering, 31(16): 3301-3307, 2011.

[189] *http://www.greenturbine.eu/en/home.php, accessed on September 19, 2014.*

[190] T. Yamamoto, T. Furuhata, N. Arai, K. Mori. Design and testing of the organic Rankine cycle. Energy, 26(3): 239-251, 2001.

[191] G. Pei, J. Li, Y. Li, D. Wang, J. Ji. Construction and dynamic test of a small-scale organic Rankine cycle. Energy, 36(5): 3215-3223, 2011.

[192] S.H. Kang. Design and experimental study of ORC (organic Rankine cycle) and radial turbine using R245fa working fluid. Energy, 41(1): 514-524, 2012.

[193] *http://airsquared.com/products/expanders, accessed on September 19, 2014.*

[194] *http://www.eneftech.com/, accessed on September 19, 2014.*

[195] L.C. Mendoza, A. Iglesias, D. Favrat, J. Schiffmann. Experimental investigation of water injection in an oil-free co-rotating scroll machinery for compressed air energy storage. 22nd International Compressor Engineering Conference at Purdue, West Lafayette, Indiana, USA, July 14-17, pp. 13732 1-10, 2014.

[196] O. Badr, S.D. Probert, P. O'Callaghan. Performances of multi-vane expanders. Applied Energy, 20(3): 207-234, 1985.

Bibliographic References

[197] O. Badr, P.W. O'Callaghan, M. Hussein, S.D. Probert. Multi-vane expanders as prime movers for low-grade energy organic Rankine-cycle engines. Applied Energy, 16(2): 129-146, 1984.

[198] M. Mohd, N. Tahir, T. Hoshino. Efficiency of compact organic Rankine cycle system with rotary-vane-type expander for low-temperature waste heat recovery. International Journal of Environmental Science and Engineering, 2(1): 11-16, 2010.

[199]]*http://www.emersonclimate.com/en-ca/Products/*Compressors/Scroll_Compressors/*, accessed on September 25, 2014.*

[200]]*http://www.sanden.com.au/Consumer/Automotive-Air/ Compressor.php, accessed on September 25, 2014.*

[201] *http://zt.cnautonews.com/bjgys/qyzs/201312/t20131205_268028.htm, accessed on September 25, 2014.*

[202] *http://www.coaire.com/oil-less-scroll-air-end.html, accessed on September 22, 2014.*

[203] P. Song, M. Wei, L. Shi, S.N. Danish, C. Ma. A review of scroll expanders for organic Rankine cycle systems. Applied Thermal Engineering, 75(January), 54-64, 2015.

[204] L.C. Mendoza. Caracterización y modelización de un expansor scroll de pequeña-potencia. Integración en sistemas de absorción para producción de energíamecánica y refrigeración. PhD Thesis (in Spanish), Department of Mechanical Engineering, Universitat Rovira I Virgili, Spain, 2013.

[205] L.C. Mendoza, J. Navarro-Esbri, J.C. Bruno, V. Lemort, A. Coronas. Characterization and modelling of a scroll expander with air and ammonia as working fluid. Applied Thermal Engineering, 70(1): 630-640, 2014.

[206] V. Lemort. Contribution to the characterization of scroll machines in compressor and expander modes. PhD Thesis, Department of Aerospace and Mechanical Engineering, Université de Liège, Belgium, 2008.

[207] R. Dickes. Design and fabrication of a variable wall thickness two-stage scroll ex-

pander to be integrated in a micro-solar power plant. Master Thesis, Department of Aerospace and Mechanical Engineering, Université de Liège, Belgium, 2013.

[208] V. Lemort, S. Quoilin, C. Cuevas, J. Lebrun. Testing and modeling a scroll expander integrated into an Organic Rankine Cycle. Applied Thermal Engineering, 29(14-15): 3094-3102, 2009.

[209] S. Quoilin, V. Lemort, J. Lebrun. Experimental study and modeling of an Organic Rankine Cycle using scroll expander. Applied Energy, 87(4): 1260-1268, 2010.

[210] EES, Engineering Equation Solver, 1992-2014. F - Chart Software.

[211] TRNSYS, Transient System Simulation Tool, Program Manual. Solar Energy Laboratory, University of Wisconsin, Madison, USA, 2004.

[212] A. Baghernejad, M. Yaghoubi. Exergy analysis of an integrated solar combined cycle system. Renewable Energy, 35(10): 2157-2164, 2010.

[213] M. Pons. On the reference state for exergy when ambient temperature fluctuates. International Journal of Thermodynamics, 12(3), 113-121, 2009.

[214] A. Angelotti, P. Caputo. The exergy approach for the evaluation of heating and cooling technologies; first results comparing steady-state and dynamic simulations. In: Proceedings of the 2nd PALENC and 28th AIVC Conference, Crete Island, Greece, Vol. I, pp. 59-64, 2007.

[215] GenOpt, Generic Optimization Program, User Manual, Version 3.1.0. Lawrence Berkeley National Laboratory, Berkeley, 2011. *http://simulationresearch.lbl.gov/GO/index.html, accessed on October 14, 2013.*